Cardiff
Catalysis Institute

Sefydliad Catalysis
Caerdydd

CATALYTIC EXHAUST GAS REFORMING OF HYDROCARBON FUELS

Tim Dixon

Supervisors: Professor Stanislaw Golunski & Professor Stuart Taylor

December 2018

Thesis submitted in accordance with the requirements of Cardiff University
for the degree of Doctor of Philosophy

Acknowledgements

I'd like to begin by thanking a number of people for all their generous help and support throughout my time at Cardiff University, and during my PhD in particular.

Firstly, and most importantly, I'd like to thank my supervisor, Professor Stan Golunski, for both giving me the opportunity to study for my PhD in the first place, and for his continuous support and expert guidance throughout my project. Finally, I'd also like to thank him for his understanding when I informed him I had decided that I wanted to move on from academia and pursue an alternative career earlier than he was probably expecting. It really was appreciated, and without it, I'm not certain I'd have seen the work through. I wish him all the best in his retirement.

Secondly, I'd like to thank Dr. Dafydd Davies, who helped supervise my research in the initial stages while finishing up his own PhD studies – and has remained a good friend since.

I'd like to also thank all the staff, both academic and services, in the Cardiff Catalysis Institute (CCI) and the wider School of Chemistry for all their help throughout my time as an undergraduate and postgraduate at Cardiff University.

Particular thanks for their help during my PhD is due to Steve Morris, Lee Wescombe and Julian Young in the School of Chemistry workshop, and Chris Morgan in the CCI. I'm sure Steve in particular was sick of the sight of me waiting in his office at times, but I really do appreciate his patience, kindness and expertise.

I'd also like to thank the EPSRC for generously funding this project, and Solvay Rhodia for their generous provision, free of charge, of a number of their high quality catalytic support materials. Similarly, I'd like to thank Sono-Tec Corporation for their assistance in customizing the ultrasonic spray nozzle needed for this work.

Finally, I'd like to thank my friends and family. In particular, my parents, sister and girlfriend for their support and motivation throughout – especially during the harder than expected effort to finish writing up this thesis alongside starting my new career.

Thank you.

Abstract

Exhaust gas reforming is a technology that has the potential to serve as an intermediate technology between the current fossil fuel vehicle fleet, and future hydrogen-fueled and battery-powered systems, analogous to the role played by hybrid electric vehicles.

The technology involves reacting a portion of the primary fuel with the exhaust gases of an internal combustion engine, in the presence of a catalyst, yielding a reformed exhaust gas containing hydrogen that can be recirculated back into the engine of the vehicle. If operation is optimized, such a system can operate as an energy recover system, therefore improving miles to the gallon, while also improving engine emissions.

The barrier to entry for this technology is the availability of attractively priced, active and durable catalytic materials. The common catalytic candidates for exhaust gas reforming are precious metal based formulations, but their cost is often prohibitive if the loading of the precious metal is high. Base metal formulations have more competitive pricing, however can present issues with activity and durability.

This work was designed as a compare and contrast study of precious metal and base metal catalysts in the exhaust gas reforming of gaseous and liquid hydrocarbon fuels, under conditions typical of those found in the exhaust of a spark ignition internal combustion engine. The key aim was to determine whether base metal catalysts could show suitable catalytic activity and durability during exhaust gas reforming, both in absolute terms, but also relative to a commercial precious metal reforming catalyst, and hence whether such a formulation had the potential for use in a real vehicle.

A 10% Ni/CeO_2-ZrO_2 catalyst formulation was prepared via wet impregnation, as the first phase base metal formulation. Its performance was compared to a commercial precious metal based reforming catalyst, and a 1% Rh/CeO_2-ZrO_2 formulation, under a range of realistic exhaust conditions expected from spark ignition internal combustion engines. The testing was carried out using a reactor set up that required modification in order to be able to test with liquid hydrocarbon fuels. The surrogate fuels for gasoline used in this work were propane and iso-octane.

The key factors for consideration were activity, in terms of quantity of hydrogen in the reformed gas, and resistance to deactivation. Catalysts were characterized pre and post-testing using TPR, BET, TGA and XRD techniques.

The results presented here show that the activity, in terms of hydrogen production, of the nickel based catalyst was comparable to that of the precious metal catalysts with both gaseous and liquid fuels, and produced hydrogen in quantities sufficient to be of benefit when fed back into an internal combustion engine.

However, significant issues remained with the nickel catalyst with respect to its stability and durability. The rate of coking with the heavier feedstock was a significant issue. Additionally, the nickel catalyst showed sensitivity to the atmosphere it was exposed to during the post-operation cooling phase of

testing. Exposing the hot catalyst to an oxidizing atmosphere during this phase was found to be severely deactivating. This is important because this would be the situation expected in a real vehicle once the engine has been switched off and the exhaust is exposed to air while still hot. This was assigned to a thermal sintering effect, initiated by the oxidation of surface carbon deposited under reaction conditions, hence highlighting that the thermal stability of the catalyst was also inadequate.

The rate of coking with the heavier feedstock was found to be of lesser problem with the precious metal catalysts, and the sensitivity to the post-operation cooling conditions was not observed.

Three avenues of further work were therefore suggested, with particular focus on optimizing the nickel catalyst in an attempt to overcome the aforementioned durability issues, since as this work makes clear, these are the key roadblocks that need to be overcome for an exhaust gas reforming system to be competitive for use in real vehicles.

Contents

Declaration .....
Acknowledgements i
Abstract ii
Contents iv
Figures..... viii
Tables xiii
Chapter 1 - Introduction 1
Context 1
Climate Change 1
Hydrogen as a Fuel.....3
Literature Review.....5
Onboard Hydrogen Generation from Hydrocarbon Feedstock 5
Exhaust Gas Reforming 7
A Brief History of Exhaust Gas Reforming 9
The Exhaust Gas Reforming Process 14
The Catalysis of Exhaust Gas Reforming 21
The Techniques of Exhaust Gas Reforming Testing 33
Project Aims.....35
Chapter 2 - Experimental 37
Catalyst Preparation 37
The Nickel Catalyst.....37
The Rhodium Catalyst.....38
Johnson Matthey Commercial Reforming Catalyst 38
Catalyst Activation.....38
Catalyst Characterization 38
Brunauer-Emmett-Teller Surface Area (BET).....39
Temperature Programmed Reduction (TPR) 40
Thermogravimetric Analysis (TGA).....41
Powder X-ray Diffraction (XRD) 41
Catalyst Performance Testing 43
Initial Reactor Set Up.....43
Gas Chromatography 44
Reactor Modification for Liquid Fuel Testing 47
The Standard Performance Testing Regime.....49
Data Collection, Analysis, Errors and Presentation 54
Chapter 3 - Characterization of the Fresh Catalysts.....59
Introduction.....59

Results and Discussion 59
BET Surface Area 59
Temperature Programmed Reduction 60
X-ray Diffraction 61
Conclusions 63
Chapter 4 - Investigation of Post-Reactivity Testing, Atmosphere Induced, Catalyst Deactivation 64
Introduction 64
Additional Experimental Details and Observations 64
Results 65
The Effect of Atmosphere During the Cool-Down Phase of Reactivity Testing 65
Testing the Reversibility of the Observed Deactivation 72
Catalyst Characterization 74
Additional Observations 77
Discussion 77
Conclusions 85
Chapter 5 - Establishing the Baseline Exhaust Gas Reforming Performance of the Precious and Base Metal Catalysts with Gaseous and Liquid Fuels 86
Introduction 86
Additional Experimental Details 86
Results 86
Precious Metal Catalyst Performance for Exhaust Gas Reforming of Propane 87
Nickel Catalyst Performance for Exhaust Gas Reforming of Propane 93
Precious Metal Catalyst Performance for Exhaust Gas Reforming of Iso-octane 99
Nickel Catalyst Performance for Exhaust Gas Reforming of Iso-octane 104
Catalyst Characterization 108
Additional Observations 108
Discussion 109
Precious Metal Catalyst Performance for Exhaust Gas Reforming of Propane 109
Nickel Catalyst Performance for Exhaust Gas Reforming of Propane 114
Comparing the Performance of the Precious Metal and Nickel Catalysts for Exhaust Gas Reforming of Propane 117
Precious Metal Catalyst Performance for Exhaust Gas Reforming of Iso-octane 120
Comparing the Precious Metal Catalyst Performance for the Exhaust Gas Reforming of Propane and Iso-octane 123
Nickel Catalyst Performance for Exhaust Gas Reforming of Iso-octane 124
Comparing the Nickel Catalyst Performance for the Exhaust Gas Reforming of Propane and Iso-octane 126
Comparing the Precious Metal and Nickel Catalyst Performance for Exhaust Gas Reforming of Iso-octane 129
Comparing Propane and Iso-octane as Surrogate Fuels for Gasoline in Exhaust Gas Reforming 131

Conclusions & Further Work 133

Chapter 6 - Further Investigations into the use of Iso-octane as a Surrogate for Gasoline, and the Performance of the Precious Metal Catalyst 135

Introduction 135

Additional Experimental Details 135

Investigating the Effect of Reaction Conditions on the Rate of Carbon Deposition 135

Investigating the Poor Performance of the Precious Metal Catalyst in the Exhaust Gas Reforming of Iso-octane 135

Results 137

Nickel Catalyst Performance in the Exhaust Gas Reforming of 3 % Iso-octane at $\lambda = 1.5$ 137

Nickel Catalyst Performance in the Exhaust Gas Reforming of 7.5 % Iso-octane at $\lambda = 1.5$ 139

Nickel Catalyst Performance in the Exhaust Gas Reforming of 3 % Iso-octane at $\lambda = 1.5$, after Cooling in a Simulated Air Atmosphere 140

Nickel Catalyst Performance in the Exhaust Gas Reforming of Iso-octane at a H_2O/C of 2.1 under the $\lambda = 1.5$ Condition 142

Rhodium Catalyst Performance in the Exhaust Gas Reforming of Propane 144

Rhodium Catalyst Performance in the Exhaust Gas Reforming of Iso-octane 146

Catalyst Characterization 148

Additional Observations 151

Discussion 153

Nickel Catalyst Performance in the Exhaust Gas Reforming of Iso-octane: The Effect of Iso-octane Content 153

Nickel Catalyst Performance in the Exhaust Gas Reforming of Iso-octane: The Effect of Cool-Down Method 156

Nickel Catalyst Performance in the Exhaust Gas Reforming of Iso-octane: The Effect of the H_2O/C 159

Nickel Catalyst Performance in the Exhaust Gas Reforming of Iso-octane: The Effect of Temperature on the Rate of Carbon Deposition 162

Rhodium Catalyst Performance in the Exhaust Gas Reforming of Propane 163

Rhodium Catalyst Performance in the Exhaust Gas Reforming of Iso-octane 166

Rhodium Catalyst Performance in the Exhaust Gas Reforming: The Effect of Fuel Choice 168

Precious Metal Catalyst Performance in the Exhaust Gas Reforming of Iso-octane: Additional Experiments 169

Conclusions 170

Chapter 7 - Discussion, Further Work & Conclusions 172

Introduction 172

Discussion 172

Further Work 184

Probing the Chemistry of Exhaust Gas Reforming 184

Optimizing the Nickel Catalyst 186

Testing with Commercial Fuels 190

Conclusions 191

Chapter 3 Appendix 1 – XRD Reference data for the Ceria Zirconia Support 193
Ceria Zirconia 193
Chapter 4 Appendix 2 – XRD Reference Data for the Ni10CZ Catalyst 195
Nickel Oxide 195
Ceria Zirconia 197
Chapter 5 Appendix 3 – XRD Reference Data for the Rh1CZ Catalyst 200
Rhodium Oxide 200
Ceria Zirconia Support 203
Chapter 6 Appendix 4 – XRD Reference Data for nitrogen cooled Ni10CZ 206
Nickel Metal 206
Nickel Oxide 208
Ceria Zirconia Support 210
Chapter 7 Appendix 5 – Appearance of the Samples Tested in Chapter 4 213
References 214

Figures

Figure 1.1: Global greenhouse gas emissions in 2010 by sector [4] 2
Figure 1.2: Global transport greenhouse gas emissions in 2010 [5] 2
Figure 1.3: Improvements in vehicle emissions and efficiency [6] 3
Figure 1.4: An exhaust gas reformer inside the exhaust of a vehicle [29] 8
Figure 1.5: Exhaust gas emissions of a spark ignition engine as a function of λ [43] 18
Figure 1.6: LH and ER type mechanisms [71] 24
Figure 1.7: The effect of preparation method on a nickel reforming catalyst [83] 33
Figure 2.1: Type II adsorption isotherm 39
Figure 2.2: A basic powder X-ray diffraction set up [101] 43
Figure 2.3: The initial reactor set up 44
Figure 2.4: Schematic of the Bruker 450-GC system 45
Figure 2.5: Sono-Tek Microflow Ultrasonic Atomising Nozzle 47
Figure 2.6: The modified reactor set up 49
Figure 2.7: An illustrative plot of how the catalytic testing data from the GC will be presented in this work 56
Figure 2.8: Another illustrative example of how the data in this work will be presented, showing the comparison of three different catalysts in terms of hydrogen content of the dried product gas 56
Figure 2.9: Illustrative example of the direct relationship between concentration of hydrogen in the product gas and molar rate of hydrogen production 57
Figure 3.1: TPR data for the ceria zirconia support, Rh1CZ catalyst and Ni10CZ catalyst 60
Figure 3.2: XRD data for the ceriz zirconia support, Ni10CZ catalyst, and Rh1CZ catalyst 62
Figure 4.1: Nickel catalyst performance during exhaust gas reforming of propane at λ = 2.12, cooled under an oxygen rich atmosphere in-between tests. The concentrations of major components of the dried product gas are shown 67
Figure 4.2: Nickel catalyst performance during exhaust gas reforming of propane at λ = 2.12, cooled under a nitrogen atmosphere between tests. The concentrations of major components of the dried product gas are shown 69
Figure 4.3: Nickel catalyst performance during exhaust gas reforming of propane at λ = 2.12, cooled in an "air" atmosphere between tests. The concentrations of major components of the dried product gas are shown 71
Figure 4.4: Nickel catalyst performance in terms of hydrogen production in the exhaust gas reforming of propane at λ = 2.12, during the "deactivation phase" (cooling under an oxygen rich atmosphere between tests) 72
Figure 4.5: Nickel catalyst performance in terms of hydrogen production in the exhaust gas reforming of propane at λ = 2.12, during the "regeneration phase" (cooling in a nitrogen atmosphere between tests) 73
Figure 4.6: Nickel catalyst performance in the exhaust gas reforming of propane at λ = 2.12, in terms of oxygen consumption during the deactivation and regeneration phases 73
Figure 4.7: XRD data for the support and nickel catalyst samples tested in this chapter 75
Figure 4.8: Thermogravimetric analysis data for the nickel catalyst samples tested in this chapter 76

Figure 4.9: Nickel catalyst performance during the exhaust gas reforming of propane at λ = 2.12, and the effect of post-operation atmosphere control on the proportion of hydrogen in the product gas mixture 79

Figure 4.10: Nickel catalyst performance during exhaust gas reforming of propane at λ = 2.12, and the effect of post-operation atmosphere control on mol min^{-1} hydrogen produced per mol min^{-1} propane in the reactant feed..... 79

Figure 4.11: Nickel catalyst performance during exhaust gas reforming of propane at λ = 2.12, and the effect of post-operation atmosphere control on propane conversion..... 80

Figure 5.1: PM catalyst performance in the exhaust gas reforming of propane at λ = 1, in terms of the composition of the dried product gas as a function of bed temperature 88

Figure 5.2: PM catalyst performance in the exhaust gas reforming of propane at λ = 1.5, in terms of the composition of the dried product gas as a function of bed temperature 90

Figure 5.3: PM catalyst performance in the exhaust gas reforming of propane at λ = 2.12, in terms of the composition of the dried product gas as a function of bed temperature 92

Figure 5.4: Nickel catalyst performance in the exhaust gas reforming of propane at λ = 1, in terms of the composition of the dried product gas as a function of bed temperature 94

Figure 5.5: Nickel catalyst performance in the exhaust gas reforming of propane at λ = 1.5, in terms of the composition of the dried product gas as a function of bed temperature 96

Figure 5.6: Nickel catalyst performance in the exhaust gas reforming of propane at λ = 2.12, in terms of the composition of the dried product gas as a function of bed temperature 98

Figure 5.7: PM catalyst performance in the exhaust gas reforming of iso-octane at λ = 1, in terms of the dried product gas composition as a function of bed temperature 100

Figure 5.8: PM catalyst performance in the exhaust gas reforming of iso-octane at λ = 1.5, in terms of the composition of the dried product gas as a function of bed temperature 102

Figure 5.9: PM catalyst performance in the exhaust gas reforming of iso-octane at λ = 2.12, in terms of the composition of the dried product gas as a function of bed temperature 103

Figure 5.10: Nickel catalyst performance in the exhaust gas reforming of iso-octane at λ = 1, in terms of the composition of the dried product gas a function of bed temperature..... 105

Figure 5.11: Nickel catalyst performance in the exhaust gas reforming of iso-octane at λ = 1.5, in terms of the composition of the dried product gas as a function of temperature..... 106

Figure 5.12: Nickel catalyst performance in the exhaust gas reforming of iso-octane at λ = 2.12, in terms of the composition of the dried product gas composition as a function of temperature 107

Figure 5.13: Thermogravimetric data for the nickel catalyst samples tested in this chapter..... 108

Figure 5.14: Showing both the proportion of the dried product gas constituting carbon dioxide (vol. %), and the molar flow rate of carbon dioxide (mol min-1) as a function of catalyst bed temperature at λ = 1.5 in the exhaust gas reforming of propane..... 110

Figure 5.15: PM catalyst performance in the exhaust gas reforming of propane, in terms of hydrogen content of the dry product stream, as a function of λ and bed temperature 111

Figure 5.16: PM catalyst performance in the exhaust gas reforming of propane, in terms of hydrogen yield as a function of λ and bed temperature 111

Figure 5.17: Propane conversion as a function of bed temperature and -value for the PM catalyst in the exhaust gas reforming of propane..... 112

Figure 5.18: Nickel catalyst performance in the exhaust gas reforming of propane, in terms of hydrogen content of the dry product stream, as a function of λ and catalyst bed temperature..... 115

Figure 5.19: Nickel catalyst performance in the exhaust gas reforming of propane in terms of hydrogen yield as a function of λ and catalyst bed temperature..... 115

Figure 5.20: Propane conversion as a function of bed temperature and -value for the nickel catalyst in the exhaust gas reforming of propane 116

Figure 5.21: Comparing the exhaust gas reforming of propane performance of the PM and nickel catalysts, in terms of oxygen consumption as a function of bed temperature at λ = 1.5 117

Figure 5.22: Comparing the performance of the PM and nickel catalysts in the exhaust gas reforming of propane, in terms of hydrogen content of the product ga,s as a function of λ and bed temperature. ... 118

Figure 5.23: Comparing the performance of the PM and nickel catalysts in the exhaust gas reforming of propane in terms of hydrogen yield, as a function of bed temperature and λ. 118

Figure 5.24: Comparing the performance of the PM and nickel catalysts in the exhaust gas reforming of propane, in terms of propane conversion as a function of bed temperature and λ. 119

Figure 5.25: PM catalyst performance in the exhaust gas reforming of iso-octane, in terms of hydrogen content of the product gas as a function of λ and bed temperature 122

Figure 5.26: PM catalyst performance in the exhaust gas reforming of iso-octane, in terms of hydrogen yield as a function of catalyst bed temperature and λ. 122

Figure 5.27: Comparing the exhaust gas reforming performance of the PM catalyst with propane and iso-octane, in terms of hydrogen content of the product gas as a function of λ and bed temperature .123

Figure 5.28: Comparing the exhaust gas reforming performance of the PM catalyst with propane and iso-octane, in terms of hydrogen yield as a function of λ and bed temperature 124

Figure 5.29: Nickel catalyst performance in the exhaust gas reforming of iso-octane, in terms of hydrogen content of the product gas as a function of λ and bed temperature 125

Figure 5.30: Nickel catalyst performance in the exhaust gas reforming of iso-octane, in terms of hydrogen production as a function of λ and bed temperature 125

Figure 5.31: Nickel catalyst performance in the exhaust gas reforming of propane and iso-octane, in terms of oxygen consumption as a function of bed temperature at λ = 1.5 127

Figure 5.32: Comparing the exhaust gas reforming performance of the nickel catalyst with propane and iso-octane, in terms of the hydrogen content of the product gas as a function of λ and bed temperature 128

Figure 5.33: Comparing the exhaust gas reforming performance of the nickel catalyst with propane and iso-octane, in terms of hydrogen yield as a function of λ and bed temperature 128

Figure 5.34: Comparing the exhaust gas reforming performance of iso-octane of the PM and nickel catalysts, in terms of oxygen consumption as a function of bed temperature at λ = 1.5 130

Figure 5.35: Comparing the exhaust gas reforming of iso-octane performance of the PM and nickel catalysts, in terms of hydrogen content of the product gas as a function of λ and bed temperature 130

Figure 5.36: Comparing the exhaust gas reforming of iso-octane of the PM and nickel catalysts, in terms of hydrogen yield as a function of λ and bed temperature 131

Figure 6.1: Nickel catalyst performance in the exhaust gas reforming of 3 % iso-octane at λ = 1.5, in terms of the composition of the dried product gas as a function of temperature 138

Figure 6.2: Nickel catalyst performance in the exhaust gas reforming of 7.5 % iso-octane at λ = 1.5, in terms of the composition of the dried product gas as a function of bed temperature 139

Figure 6.3: Nickel catalyst performance in the exhaust gas reforming of 3 % iso-octane at λ = 1.5, and the effect of exposing the catalyst to air during the cooling phase, in terms of the composition of the dried product gas as a function of bed temperature 141

Figure 6.4: Nickel catalyst performance in the exhaust gas reforming of iso-octane at λ = 1.5, with a H_2O/C = 2.1, in terms of the composition of the dried product gas as a function of temperature 143

Figure 6.5: Rhodium catalyst performance in the exhaust gas reforming of propane at λ = 1.5, in terms of the composition of the dried product gas as a function of bed temperature 145

Figure 6.6: Rhodium catalyst performance in the exhaust gas reforming of iso-octane at λ = 1.5, in terms of the composition of the dried product gas as a function of bed temperature 147

Figure 6.7: Thermogravimetric data for the nickel catalyst samples tested at λ = 1.5, with varying iso-octane content of the exhaust gas reforming feed..... 148

Figure 6.8: Thermogravimetric data for the nickel catalyst samples exposed to the nitrogen and air cool down methods, after the exhaust gas reforming of iso-octane 149

Figure 6.9: Thermogravimetric data for the nickel catalyst samples tested at different H_2O/C ratios during the exhaust gas reforming of iso-octane..... 149

Figure 6.10: Thermogravimetric data for the nickel and rhodium catalyst samples tested in the exhaust gas reforming of propane and iso-octane at λ = 1.5..... 150

Figure 6.11: Thermogravimetric data for the nickel catalyst samples tested under exhaust gas reforming of iso-octane conditions at static temperature for two hours 151

Figure 6.12: Nickel catalyst performance in the exhaust gas reforming of iso-octane at = 1.5, in terms of oxygen consumption as a function of % of iso-octane and bed temperature 154

Figure 6.13: Nickel catalyst performance in the exhaust gas reforming of iso-octane at λ = 1.5, in terms of hydrogen content of the product gas as a function of iso-octane % and bed temperature 154

Figure 6.14: Nickel catalyst performance in the exhaust gas reforming of iso-octane at λ = 1.5, in terms of hydrogen yield as a function of iso-octane % and bed temperature..... 155

Figure 6.15: Nickel catalyst performance in the exhaust gas reforming of iso-octane, in terms of oxygen consumption as a function of H_2O/C of the feed and bed temperature 159

Figure 6.16: Nickel catalyst performance in the exhaust gas reforming of iso-octane, in terms of hydrogen content of the product gas as a function of H_2O/C of the feed and catalyst bed temperature 160

Figure 6.17: Nickel catalyst performance in the exhaust gas reforming of iso-octane, in terms of hydrogen yield as a function of H_2O/C of the feed and catalyst bed temperature..... 161

Figure 6.18: PM, nickel and rhodium catalyst performance in the exhaust gas reforming of propane at λ = 1.5, in terms of oxygen consumption as a function of bed temperature..... 164

Figure 6.19: PM, nickel and rhodium catalyst performance in the exhaust gas reforming of propane at λ = 1.5, in terms of hydrogen content of the product gas as a function of bed temperature..... 164

Figure 6.20: PM, nickel and rhodium catalyst performance in the exhaust gas reforming of propane at λ = 1.5, in terms of hydrogen yield as a function of bed temperature 165

Figure 6.21: PM, nickel and rhodium catalyst performance in the exhaust gas reforming of iso-octane at λ = 1.5, in terms of hydrogen content of the product gas as a function of bed temperature..... 167

Figure 6.22: PM, nickel and rhodium catalyst performance in the exhaust gas reforming of iso-octane at λ = 1.5, in terms of hydrogen yield as a function of bed temperature 167

Figure 6.23: Rhodium catalyst performance in the exhaust gas reforming of propane and iso-octane, in terms of hydrogen content of the product gas as a function of bed temperature..... 168

Figure 6.24: Rhodium catalyst performance in the exhaust gas refroming of propane and iso-octane, in terms of hydrogen yield as a function of bed temperature 169

Figure 7.1: Average exhaust gas reforming performance of the 10% Ni/CeO_2-ZrO_2 catalyst with both propane and iso-octane, in terms of hydrogen content of the product gas as a function of catalyst bed temperature..... 172

Figure 7.2: Average exhaust gas reforming performance of the 10% Ni/CeO_2-ZrO_2 catalyst with both propane and iso-octane, in terms of hydrogen yield as a function of catalyst bed temperature 173

Figure 7.3: Pathways to carbon deposition during reforming [69] 175

Figure 7.4: Formation of carbon deposits from hydrocarbon dissociation, via carbon intermediates [69] 176

Figure 7.5: Comparing the exhaust gas reforming performance of the PM catalyst with propane and iso-octane, in terms of the composition of the dried product gas composition as a function of bed temperature at λ = 1.....180

Figure 7.6: Comparing the exhaust gas reforming performance of the PM catalyst with propane and iso-octane, in terms of the composition of the dried product gas composition as a function of bed temperature at λ = 1.5.....180

Figure 7.7: Comparing the exhaust gas reforming performance of the PM catalyst with propane and iso-octane, in terms of the composition of the dried product gas composition as a function of bed temperature at λ = 2.12.....181

Figure 7.8: Average carbon balances for the PM, nickel and rhodium catalysts at λ = 1.5 with both propane and iso-octane.....182

Figure 7.9: Average carbon balance during propane and iso-octane exhaust gas reforming.....185

Figure 7.10: Preparation strategies for core-shell nickel reforming catalysts [148] 188

Tables

Table 1.1: Common reactions in exhaust gas reforming 14

Table 1.2: Other potential reactions during simulated exhaust gas reforming of iso-octane..... 15

Table 1.3: Example stoichiometric air to fuel ratios..... 17

Table 1.4: Exhaust gas compositions at different λ-values for gasoline and diesel engines (with nitrogen as balance) [36]..... 18

Table 2.1: Information & properties of gasoline and the surrogate fuels used in this project..... 50

Table 2.2: Synthetic exhaust gas and fuel mixtures..... 50

Table 2.3: Key reactant ratios with propane as the surrogate fuel..... 51

Table 2.4: Key reactant ratios with iso-octane as the surrogate fuel 51

Table 3.1: Average surface area values for the support, calcined support and fresh catalysts 59

Table 3.2: Scherrer calculation estimates of crystallite sizes for the ceria zirconia support, Ni10CZ catalyst, and Rh1CZ catalyst 63

Table 4.1: BET surface area data for the ceria zirconia support, and the nickel catalyst samples tested in this chapter..... 74

Table 4.2: Scherrer calculated estimates of NiO crystallite size 76

Table 5.1: Recorded post-testing weight gain, and observed appearance of the nickel catalyst samples tested in this chapter 109

Table 5.2: H_2/C ratios for the PM catalyst in the exhaust gas reforming of propane at λ = 1, λ = 1.5 and λ = 2.12..... 112

Table 5.3: Theoretical H_2O/C ratios for the main reactions in the exhaust gas reforming of propane 113

Table 5.4: H_2/C ratios for the nickel catalyst in the exhaust gas reforming of propane at λ = 1, λ = 1.5 and λ = 2.12 116

Table 5.5: H_2/C ratios for the PM catalyst in the exhaust gas reforming of iso-octane at λ = 1, λ = 1.5, and λ = 2.12 121

Table 5.6: Theoretical H_2/C ratios for the main reactions in the exhaust gas reforming of iso-octane121

Table 5.7: H_2/C ratios for nickel catalyst in the exhaust gas reforming of iso-octane at λ = 1, λ = 1.5, and λ =2.12..... 124

Table 6.1: Recorded weight gain and observations of appearance for the nickel and rhodium catalyst samples tested in this chapter under exhaust gas reforming conditions 152

Table 6.2: H_2O/C raitio in the exhaust gas reforming of 3%, 5%, and 7.5% of iso-octane..... 156

Table 7.1: Average maximum TGA weight loss and average sample weight gain of all powdered catalyst samples tested under exhaust gas reforming conditions of propane and iso-octane..... 176

Chapter 1 - Introduction

Context

Climate Change

As the Intergovernmental Panel on Climate Change has made clear in its most recent assessment [1], it is unequivocal that warming has occurred to both the atmosphere and the oceans, and that anthropogenic greenhouse gas emissions are the driving force for this warming. Though not the only greenhouse gas, carbon dioxide emitted from the burning of fossil fuels and industrial processes is by far the biggest contributor.

Given that it is cumulative stock of greenhouse gases in the atmosphere that is important, along with "locked in" warming from past emissions, sustained and substantial cuts in global emissions are required in order to have a good chance of limiting climate change and its resulting effects.

Under "business as usual" scenarios based on current emissions the amount of CO_{2e} (carbon dioxide equivalents - a measure of greenhouse gases in the atmosphere) will be around 750 ppm at the end of the century. Models of this scenario yield an associated median temperature rise of 4 °C (with substantial probabilities of well above 4 °C). The last time global greenhouse gas stocks and global temperatures were thought to be at this level was 35 million years ago, when the planet was entirely ice-free.

The effect on the environment, though highly unpredictable given the extreme nature of the warming, would be unprecedented. Global commitments like the Paris Climate Agreement [2], aim to keep the global temperature rise below 2 °C from pre-industrial levels at the end of the century. Global greenhouse gas levels will most likely need to be kept under 500 ppm CO_{2e}, just to have a 50-50 chance of keeping to this target.

This leads to an "emission space" (the prediction of what can be emitted between now and then, in order to keep below 500 ppm) of 1-1.5 trillion tonnes until 2100. At current rates that allocation could be used up within 40 years. It is therefore clear that to achieve these targets, emissions cuts would have to be sustained and substantial in all countries, and across all sectors [3].

The breakdown of global greenhouse gas (GHG) emissions by sector is shown below in Figure 1.1, taken from the IPCC report, with data from 2010 [4].

Though not the largest emitter, the transport sector is still a significant contributor to emissions, totaling around 14% globally - which equated to roughly 6.9 Gt of CO_{2e} in 2010. Therefore, emissions cuts in this sector are crucial.

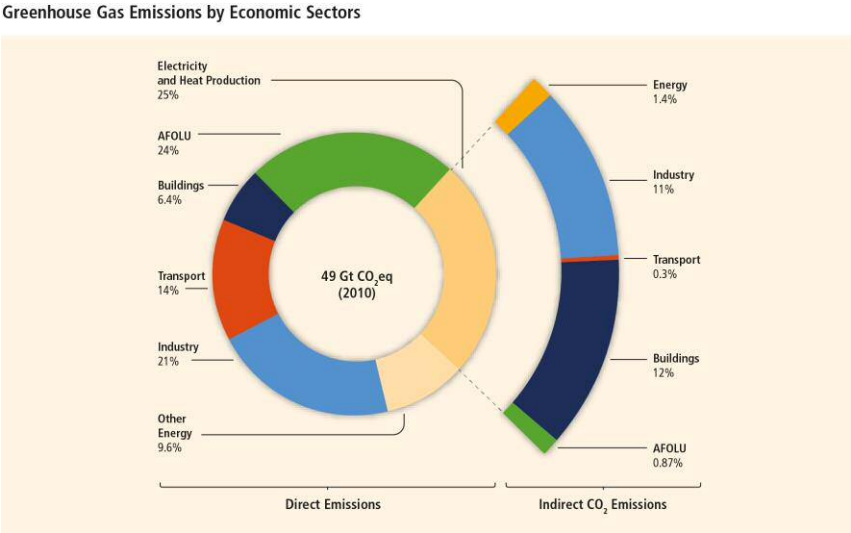

Figure 1.1: Global greenhouse gas emissions in 2010 by sector [4]

Figure 1.2 below shows the breakdown of emissions in the transport sector, and again is taken from the IPCC Fifth Assessment Report [5]. Though each sector has shown an increase since 1970, the largest rate of increase, and by a significant margin the biggest contributor, has always been road transport – the predominant propulsion technology of which has been the internal combustion engine.

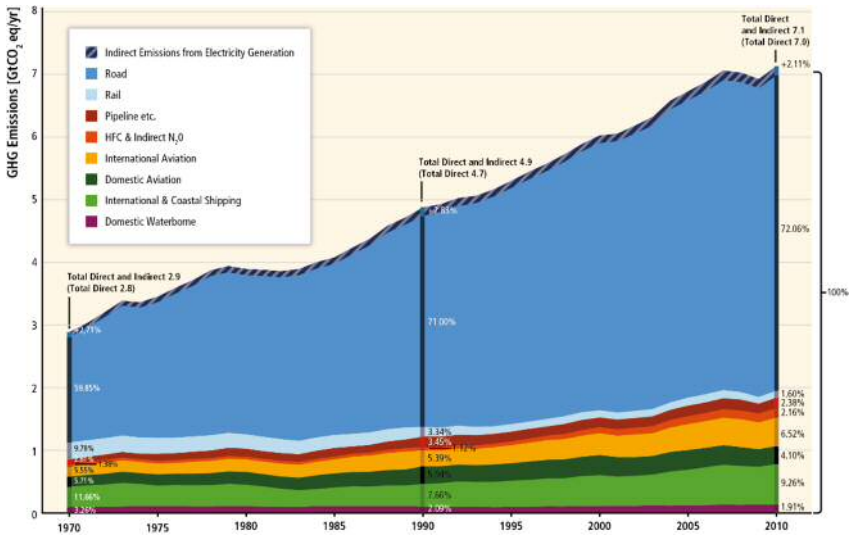

Figure 1.2: Global transport greenhouse gas emissions in 2010 [5]

Internal combustion engines, fueled by hydrocarbons (e.g petrol/diesel), have been the dominant form of vehicular transport since its invention. The reduction of emissions (both pollutants and greenhouse gases) from the burning of the hydrocarbon fuels has been a focus in the automotive industry as far back as the 1950's and 1960's, with attempts to clean up smog in cities (resulting from unburnt hydrocarbon and NO_x emissions). However, especially in recent years, driven by concerns over climate change, efforts to cut emissions have focused on two possible routes (1) gains in efficiency of the internal combustion engine and (2) the development of cleaner fuels for vehicle propulsion. Vehicle efficiency has been a particular focus, with governments forcing development here with regulation that has yielded

significant advances (see Figure 1.3, taken from the United States Environmental Protection Agency [6]). However, efficiency is almost certainly not enough alone, and therefore the development of cleaner fuels will also be needed.

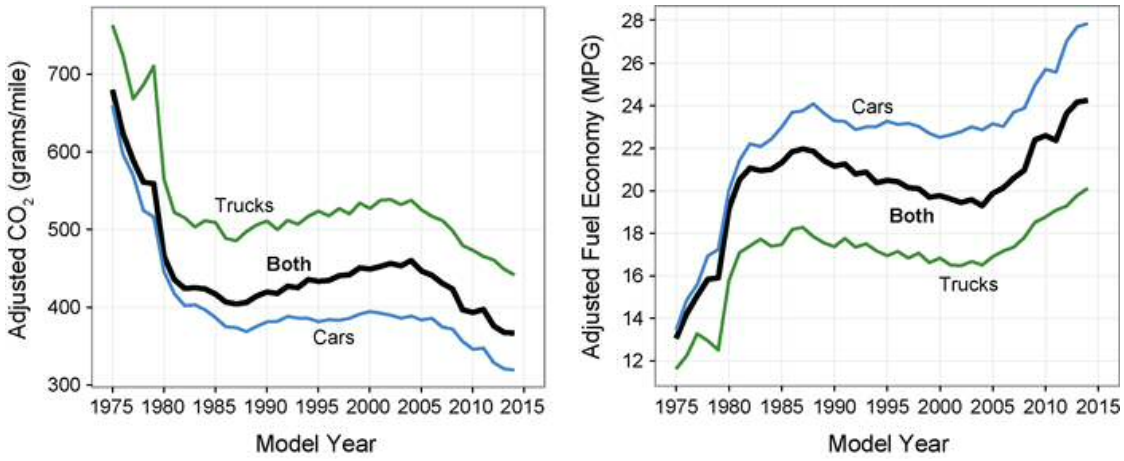

Figure 1.3: Improvements in vehicle emissions and efficiency [6]

The main attempts to develop cleaner transportation technology to replace fossil fuels have focused on (1) electric, (2) hydrogen, and (3) biofuel systems.

Though biofuels have been around for some time, and are playing a role in some locations (such as Brazil), their benefit with respect to GHGs is heavily dependent how the fuel was produced. The most significant advances in recent years on cleaner systems has been on electric vehicles, which have seen significant reductions in costs and significant gains in performance. In particular, the combination of electric motors with internal combustion engines (hybrid vehicles) can greatly improve fuel economy and therefore lower emissions. Full electric and hybrid vehicles will continue to become more competitive and attractive options for transport, and hence there use can be expected to increasingly widespread [7-11].

Progress on hydrogen fueled vehicles has been a more difficult technological challenge, and is therefore a much less developed technology, and is now significantly lagging behind electric/hybrid vehicles. However, given the importance of achieving emissions cuts, the development of a diverse range of likely energy sources and technologies is the most sensible path forward, and therefore hydrogen fuel for vehicles could still have a role to play.

Hydrogen as a Fuel

Using hydrogen as a fuel offers one route to cleaner, more sustainable transport. The energy it contains can be converted into chemical, mechanical or electrical energy, in order to drive motors. This results in two technologies, both of which yield water as the major waste product [12-14]:

1) Burning the hydrogen in an internal combustion engine, the energy released from which is then converted into mechanical energy to drive the motor. Simply analogous to fossil fueled vehicles with the hydrocarbon fuel exchanged for hydrogen.

2) Using the hydrogen to supply a fuel cell to convert its chemical energy into electricity, which in turn is then used to drive electric motors. The processes by which this occurs varies depending on the fuel cell type, but the electrochemistry can be summarized as follows: hydrogen is supplied at the anode, where it becomes ionized. The freed electrons are then able to provide a current, which can be used to do electrical work, in this case driving a motor. Oxygen is supplied at the cathode, and depending on the type of cell, combined with the electrons at the cathode or in the electrolyte, and then combined with hydrogen within the cell to produce water, which can then be removed through an exhaust. This is simply the reverse of the electrolytic process used to produce hydrogen from water [15].

Either method would require a source of the hydrogen. This could be from a compound of hydrogen, or molecular hydrogen gas, either to supply the fuel cell or the combustion chamber. Hydrogen is almost always found in a compound of some form (such as in water, minerals and hydrocarbons). Therefore, this raises several issues such as:

- Will the source be molecular hydrogen or from a compound containing hydrogen?
- How will the hydrogen source be produced at scale?
- How will the hydrogen source be stored onboard the vehicle?
- How will the vehicle be re-fueled with the hydrogen source?
- If in the compound form, how will the hydrogen be extracted for use?

Each of the above questions then needs to be considered against various criteria to assess the viability of the resulting vehicle.

For example, the considerations of consumers such as cost, convenience (like access to re-fueling infrastructure), performance, safety and longevity of the system might be a priority. For manufacturers technical complexity can increase engineering challenges and costs. Neither of the above questions and considerations is an exhaustive list – but the full list must obviously include the environmental impact of any set of choices, particularly on how the hydrogen source is produced, otherwise the choice of a "clean" fuel like hydrogen can be negated by environmental damage done before the hydrogen is even used in the vehicle.

For this reason, assessing the benefits and costs from any particular combination can be very complex. Parts of these enquiries are often the focus of so called "Well-to_Wheel", or "Life-Cycle" analyses (e.g [16, 17]), which are largely beyond the scope of this project, but which aim to consider the environmental impact of any particular technology, when all the processes leading to, and including its use, are considered.

However, a useful example of these tradeoffs, and the complexity involved, can be given by considering the issues that arise around storing various potential hydrogen sources onboard the vehicle, even with the assumption that the source has been produced in a desirable way.

Firstly, the hydrogen could be stored in its molecular form, as a gas or liquid. However, if the hydrogen is stored as a gas, it is difficult to ensure there is no loss of gas from the fuel tank by diffusion. This

therefore also raises safety concerns, and offers low energy storage density. Storing as liquid hydrogen can offer benefits such as higher storage density and easy re-fueling. However cryogenically storing hydrogen this way is prone to evaporative loss, and hence again safety. These concerns can be oversome by designing effective storage tanks, however this can add disproportionate weight, as well as increase costs.

Alternatively, the hydrogen could be stored in the form of a compound, such as a metal hydride, which is potentially simpler and safer than the above. However this method has low storage density, carries a significant weight penalty (therefore effecting fuel efficiency), requires elevated temperatures to release the hydrogen from its compound form, and could also pose problems around re-fueling [18].

The fact that there remain so many outstanding issues, means that it could be some time before hydrogen fueled vehicles are competitive in the market. This is not to say that efforts at hydrogen fueled vehicles are a fruitless pursuit, as mentioned previously, a key strategy to meeting environmental targets will be diversity in technology choice. Rather it is to suggest that until these hurdles are overcome, the use of an interim type technology could avoid some of the above considerations, while providing some of the desired environmental benefits.

Literature Review

Onboard Hydrogen Generation from Hydrocarbon Feedstock

One potential way of avoiding at least some of these hurdles is to obtain the hydrogen from hydrocarbon feedstock, since this would work within the existing infrastructure around producing and distributing the fuel. However, this would require the hydrogen to be stripped from its parent molecule (the hydrocarbon) onboard the vehicle during operation.

In industry, hydrogen generation from hydrocarbon feedstock is done primarily from two different processes [12, 19]:

1) Steam reforming – most commonly from natural gas or naphtha.

(1.1)

2) Partial oxidation – most commonly from oil.

(1.2)

The above reactivity can also be combined to yield autothermal reforming. Steam reforming of methane is the most common method of industrial scale hydrogen production, for example almost all (~95 %) hydrogen production in the United States is from steam reforming of methane [20].

There are clearly differences between the industrial applications of the above processes, and their use onboard a vehicle, however the technologies for onboard generation generally fall into two camps. The first looks to produce a feed of high purity of hydrogen gas which can be fed into a fuel cell. The second,

looks to feed a portion of the reformed gas, containing a quantity of hydrogen, back into the engine to be combusted alongside the primary fuel.

The demands of the first approach are obviously much higher, since a feed of pure hydrogen gas is required. For fuel cells, presence of gases like carbon monoxide can critically damage the fuel cell through its strong and fast bonding to the surface of the catalyst, causing deactivation through loss of active surface area [21, 22]. Though it is possible to remove these using a variety of follow up reactions and scrubbing techniques, this still adds complexity and hence cost to the resulting system.

The first attempt at onboard hydrogen generation was the Boston Reformed Fuel Car, by Newkirk and Abel in 1972 [23, 24]. They used non-catalytic, and therefore very high temperature (the condensed water from the engine was superheated to 1000 °C), steam reforming of gasoline. The product gas consisted mostly of hydrogen and carbon dioxide. However, portions of this fuel were then used to heat the reactor through combustion with air, and the rest fed into the engine, which made the processes too inefficient, and they experienced problems with carbon formation inside the reactor. They did however achieve a reduction in emissions through feeding the hydrogen into a spark ignition engine.

As mentioned, one line of enquiry has been to produce the hydrogen for fuel cells from hydrocarbon feedstocks, often referred to as onboard fuel reforming, or fuel processing. Both hydrocarbon and alcohol fuels have been used. This is an extensive topic in the literature, and the focus of several review papers, which describe the catalyzed processes used (steam reforming, partial oxidation and autothermal reforming), with a variety of feedstocks (gasoline, diesel, bioethanol and methanol) [25, 26].

An example of a complete fuel processing unit for use with a PEM fuel cell was produced by InnovaTek [14]. Using a proprietary catalyst formulation, they have tested the unit with various hydrocarbons such as natural gas, iso-octane (a surrogate for gasoline), retail gasoline and hexadecane (a surrogate for diesel). In order to tackle the issue of carbon monoxide produced during the reforming process, they used a version of their catalyst to remove carbon monoxide below 1 % of the product gas through water gas shift reactions. The authors state that in order to further remove carbon monoxide from the feed the selective oxidation of CO in air would be required.

Another development in onboard hydrogen generation was the HotSpot Reactor™, developed by Johnson Matthey [27, 28]. This offered an elegant solution to problems like that experienced with the Boston Reformed Fuel Car, where the heat for the reforming reactions was provided by burning fuel to heat a reactor, resulting in reduced system efficiency. It did this by using a precious metal catalyst (Pd/SiO_2) to catalyze exothermic oxidation reactions of the primary fuel, the heat from which then activated a reforming catalyst (Cu/SiO_2), which catalyzed the endothermic reforming reactions.

The catalysts were contained within a specially designed reactor. Preliminary models consisted of two layers, a reforming catalyst in the first layer, and the oxidation catalyst in the second layer, and the fuel was injected through a single point injector into the bed. Later designs improved performance by

injecting the fuel through a multipoint injector into a porous ceramic core, with the catalyst bed mixture deposited in concentric rings, allowing radial fluid flow through the reactor.

The work was mostly conducted with methanol as the fuel, and designed for use as a fuel processor to supply a fuel cell. The advantage of this development was the fact it required no input of energy, since the oxidation reactions, which occurred upon fuel injection at ambient temperatures, promoted the production of hydrogen via reforming reactions (i.e. autothermal reforming, the heat demand for the reforming reactions was met by the output of the oxidation reactions).

However, the absence of development and infrastructure required to use methanol as a fuel, along with other technical challenges associated with its toxicity and corrosiveness, meant the technology was not developed further. The focus for fuel processing switched to other fuels such as gasoline, diesel and bio-ethanol.

The HotSpot reactor made use of heat from exothermic reactions to power reforming reactions. But in a real vehicle there is one additional source of heat that could be utilized to promote reforming of hydrocarbon or alcohol fuels to generate hydrogen – that of the exhaust systems of internal combustion engines (ICE's). The exhaust gas from ICE's also contains some of the inputs required to generate hydrogen from reforming processes. Both of these could therefore be utilized.

Exhaust Gas Reforming

Though a less mature technology, Exhaust Gas Reforming is a development that arose from combining aspects of some of the efforts discussed above, with an adaptation of Exhaust Gas Recirculation, or EGR, which is used to reduce NO_x emissions from internal combustion engines (hence it is sometimes also called Reforming of Exhaust Gas Recirculation, or REGR).

In short, it is the process whereby a portion of the exhaust gas from an internal combustion engine, is combined with a small portion of the primary fuel, in the presence of a catalyst, to produce a quantity of hydrogen (but mostly nitrogen, along with other gases such as carbon monoxide).

The heat required to promote the production of hydrogen can be obtained from any exothermic reactions occurring, along with the heat of the exhaust gases themselves. This reformed exhaust gas, containing hydrogen, can then be fed back into the engine. A schematic of how this might be incorporated into a feedback loop onboard a vehicle is shown below in Figure 1.4 [29].

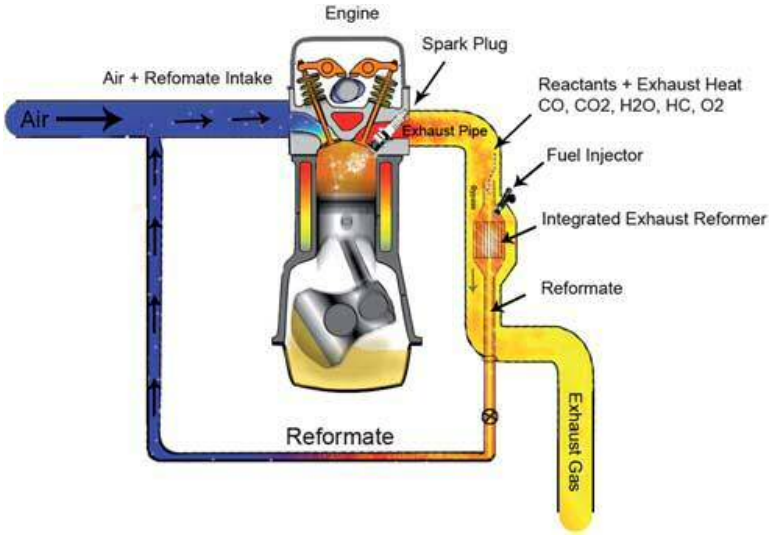

Figure 1.4: An exhaust gas reformer inside the exhaust of a vehicle [29]

This therefore is not a pure hydrogen powered propulsion system, rather it involves adding a quantity of hydrogen to the normal hydrocarbon fuel/air intake of an internal combustion engine. Supplementing the internal combustion engine feed with hydrogen in this way can bring several benefits such as improved fuel economy and efficiency and lower CO_2 and NO_x and particulate emissions. These benefits can apply to various engine fuels such as gasoline, diesel, bio-ethanol and natural gas [18, 28, 30-33].

There are benefits to be had from the addition of hydrogen into the combustion chamber as described above. However, the best use of the technology is as a heat recovery system, which yields a reformate with a higher heating value than the feed entering the reformer. This is called Thermochemical Recuperation (TCR) and results from the recovery of heat in the exhaust that would have otherwise been wasted, but instead is used to help promote hydrogen production via endothermic reforming reactions on the catalyst. Typically 30-40 % of the heat generated in combustion is utilized to do mechanical work, meaning 60-70 % can be wasted [34]. Exhaust gas temperatures depend on the type of combustion engine used, in the case of spark-ignition engines can be in the region of 400-700 °C, and as high as 950 °C upon leaving the engine [35, 36]. Hence a reformer operated in an optimized manner can bring efficiency gains to the vehicle.

Further heat could be provided from any exothermic reactions, and therefore overall efficiency improved, if like the HotSpot reactor, the reformer is appropriately designed, so that the reactions occurring in the reformer are as close to autothermal as possible. In other words, so that the demand of the endothermic reactions is met by the output of the exothermic reactions taking place. This is possible since under certain engine operating conditions, there can be oxygen present in the exhaust gas.

Since the reformed gas is fed back into the combustion chamber, unlike combining reformers or fuel processors with fuel cells, there is no requirement for additional processing to remove components like

carbon monoxide, which would poison a fuel cell. In other words, there is no demand for a high purity feed of hydrogen gas.

Furthermore, since it can be operated using the internal combustion engine and hydrocarbon/alcohol fuels, it works within the current technology and infrastructure of the global vehicle fleet, only with some modifications to optimize the running of the internal combustion engine, and the incorporation of the reforming unit into the exhaust pipe of the vehicle.

However, there are disadvantages – apart from controlling the quantity and timing of the primary fuel added to the reformer feed, the reformer is essentially a passive technology, and therefore its performance is controlled by the output of the internal combustion engine (which in turns depends on the driving inputs), so there is limited room to optimize reaction conditions. There are hurdles to be overcome in terms of catalyst price, performance and longevity, as found in industrial catalytic reforming. These aspects will be discussed further in later sections.

Although there are hurdles to overcome, if they prove more surmountable than those of fully hydrogen powered vehicles that have already been mentioned, then exhaust gas reforming offers a potential interim technology, extending the life of the internal combustion engine, while improving its environmental performance until the technology for more complete, cleaner vehicles is ready. This could be viewed as analogous to the function currently performed by hybrid petrol/diesel-electric vehicles, which improve the efficiency and emissions of ICE vehicles, while the technology and infrastructure for purely electric vehicles continues to develop.

A Brief History of Exhaust Gas Reforming

What follows is a brief discussion of some of the work on exhaust gas reforming found in the literature. Some aspects of the more recent work will be discussed in more detail in the relevant later sections, where the important concepts will be covered in greater depth.

The earliest attempt at exhaust gas reforming with gasoline was by Lindstrom [37], whose work led to a US patent in 1975. The technology used a reforming reactor, containing a reforming catalyst, which was situated between the fuel supply and the engine. The reactor was supplied with a portion (5-50 %) of the exhaust gases from the internal combustion engine, mixed with a quantity of gasoline fuel, and heat was supplied by the exhaust gases themselves. Samples of the reformed gas were used to supplement the intake of the engine and yielded reductions in unburned hydrocarbons, carbon monoxide and NO_x emissions.

More work on exhaust gas reforming of gasoline was done by Jamal et al.[38]. Interestingly the reformed fuel was actually fed into an internal combustion engine, specifically a single cylinder Ricardo E6 engine, to study its effects. This paper focused on performing the reforming at lower, and more realistic exhaust gas temperatures. This paper built on previous work [39, 40], which demonstrated optimized

reforming performance at temperatures of 950 °C, which would not be producible in a real exhaust system.

Their experimental set up used a propane burner to generate the simulated exhaust gases, and used an undisclosed catalyst in the reforming reactor. The fuel co-fed into the reactor to be reformed was European reference-grade unleaded gasoline (RF08). An excess of 3 % oxygen was added to the reactor feed through the addition of air, and the gas hourly space velocity (GHSV is a measure of reactant throughput, relative to the volume of the catalyst bed, more on this later) was 1,000 h^{-1}. Two different reactor conditions were tested, generating two different reformed fuel mixtures. Samples of the reformed fuels were collected and dry analysis of the composition was performed.

Then in a separate experiment, the Ricardo engine was run simultaneously with the reactor, where the reformed fuel from the reactor was mixed with the normal engine feed of gasoline and air, upon which the effect on engine performance was compared to the typical gasoline/air only feed. The first reformed fuel, called RF3 by the authors, was produced with a reactor inlet temperature of 650 °C, whereas the second reformed fuel, named RF4, was produced at 600 °C. Furthermore, RF3 was produced with a lower excess of oxidant in the reforming reactor feed than RF4. The results were compared to Gibbs function minimization equilibrium predictions of the reformed fuel compositions from the reactor. Significant differences between the predicted compositions of the reformed fuels and their actual composition were observed. Both fuels contained significantly lower hydrogen and carbon monoxide levels than predicted, and greater carbon dioxide levels (which was not found at the higher reactor inlet temperatures tested in their earlier work).

Despite this, when the reformed fuel was added to the Ricardo engine intake (with some changes in ignition timing and equivalence ratio to maintain constant load and speed), lower pollutant emissions, slightly higher overall efficiency and reduced cycle-to-cycle pressure variations were observed. The authors note that were the reformed fuel to have higher energy content, that these results could be better still, and that this would be achieved by a more active catalyst – allowing a rise in GHSV and better conversion of the feedstock fuel, as well as possible reduction in reaction temperature requirements.

The potential for exhaust gas reforming with fuels other than gasoline has also been studied. Tsolakis et al.[41], considered its application with compression ignition engines, which are fueled by diesel, as opposed to gasoline fueled spark ignition engines. At the time, diesel engines were in favor for passenger transport despite their high NO_x and particulate matter emissions, due to their better fuel economy. Their work consisted of two parts – first studying the effect of fuel replacement by biodiesel or hydrogen of diesel in the CI engine compared to exhaust gas recirculation, and secondly looking at the reforming of diesel fuels to produce hydrogen. They tested with Ultralow Sulfur Diesel (ULSD) and a mixture of 80 % ULSD with 20 % Rapeseed Methyl Ester (RME – a biodiesel), and used a Lister Petter TR1, single cylinder, direct injection diesel engine. The exhaust gas composition was monitored at different engine loads. The pelletized catalyst used in the mini reforming reactor was a prototype provided by Johnson Matthey. The liquid fuel was injected by a syringe pump and the GHSV was kept constant at about

90,000 h^{-1}, which is typical of those found across catalytic three way converters in car exhausts. The product gas analysis was performed by gas chromatography.

Their results on the effect to engine performance show that using 20 % by volume RME with the ULSD decreased smoke emissions, but increased NO_x emissions, and decreased the engine efficiency. The EGR (exhaust gas recirculation) process performed as expected, reducing NO_x but increasing smoke emissions and reducing engine efficiency. However, when hydrogen was combined with EGR in small quantities (10 % to 20 % of the EGR), in other words exhaust gas reforming, it was found to reduce both smoke and NO_x, as well as not adversely effecting engine efficiency and combustion quality. The results on the reforming of diesel in the mini reactor with the prototype Johnson Matthey catalyst show that a reformed fuel containing around 20 % hydrogen at 530 °C, and around 15 % at 470 °C (depending on fuel mix) was produced. In other words, it was possible to produce hydrogen at levels useful to achieve reductions in smoke and NO_x emissions, while maintaining engine efficiency.

However, the authors note that the reforming process still needs some optimization to function at all temperatures that are found in the exhaust stream. They suggest that since the H_2/CO ratio of the reformed fuel was around two, that the hydrogen was largely produced by steam reforming. They also show that the engine load has a significant effect on the exhaust gas composition, and hence reactant composition for the reformer, since at high loads the oxygen content is lower, while steam and carbon dioxide is higher, whereas at low loads oxygen content is higher, while carbon dioxide and steam content is lower. This in turn affects the balance of exothermic (oxidation) and endothermic (reforming) reactions occurring during the reforming processes in the reactor. Slightly more hydrogen was produced under the high load condition (lower oxygen and higher steam). They suggest that some complete or partial oxidation occurs in the reactor (shown by drop in oxygen content between exhaust gas and reformed gas and increase in carbon dioxide content), and that the second main reaction was steam reforming of the hydrocarbon fuel. The authors also note that further work is needed to assess the effects of carbon formation, sulfur poisoning, and sintering of the catalyst, in addition to the effect of lower exhaust gas temperatures. Optimizing the configuration of the reforming system is also suggested to bring further benefits.

Tsolakis and Megaritis followed up this work, by investigating the effect of water addition on hydrogen production, fuel conversion, and efficiency [42]. They varied the fuel and water flow rates into the reactor alongside the exhaust gas and found that the presence of additional water in the reactor feed could boost the hydrogen content of the reformed gas by an additional 15 %. Using an array of thermocouples throughout the catalyst bed, they also report a temperature profile existing in the bed. This profile consists of a hotter, or “exothermic area”, at the front part of the catalyst bed, and a cooler, or “endothermic area”, towards the rear of the bed. The sizes of these areas were determined mainly by the oxygen and steam content of the feed (higher oxygen = larger exothermic area, higher steam = larger endothermic area). Reforming without extra water added to the exhaust gas again yielded slightly more hydrogen in the condition with higher steam content in the exhaust gas (higher yielding steam reforming

promoted over oxidation reactions for consumption of the fuel. When the exhaust gas was rich in oxygen but low in steam, increasing water content resulted in increased hydrogen yield, lower carbon monoxide, and higher carbon dioxide, hence moving the H_2/CO ratio moved away from that expected from stream reforming. Equilibrium calculations suggested this was initially due to increased steam reforming, and later due to boosted water gas shift reactivity. Increasing the fuel in the reactant feed also increased hydrogen production. However, when the exhaust gas was lean in oxygen and already rich in steam, the effect of water addition was slightly different. Maximum hydrogen was observed with 15 mL h^{-1}, and then either plateaued or decreased with further water addition. This was prescribed to the fact that this condition already contained more steam in the exhaust gas, and therefore that the reactants (steam and fuel) were in excess of the requirements for maximum hydrogen production, and/or that the higher resulting GHSV negatively affected the reforming process.

The additional hydrogen produced by water gas shift is not necessarily always thermally beneficial, and the authors suggested that the optimum for system efficiency is just before water gas shift starts taking place – i.e when the increased hydrogen produced is down to steam reforming. Beyond this, hydrogen production by the exothermic water gas shift can reduce overall efficiency. The overall exhaust gas reforming process then involved complete oxidation of the fuel at inlet, followed by endothermic steam reforming. The addition of more water to the reactant stream initially promotes more steam reforming of the fuel, and later promotes water gas shift reactivity.

Peucheret et al.[43], at Johnson Matthey, in an initial screening tested over fifty potential reforming catalysts, using a synthetic exhaust gas mixture modelled on the actual output of a Ford V6 supercharged engine (as opposed to above studies which used burners to generate an exhaust gas). They report the most active catalyst was a Pt-Rh mix, which therefore was chosen as their prototype catalyst. They compare this prototype catalyst to two rhodium only catalysts. The composition of the synthetic exhaust gas was modelled on the output of the gasoline engine at three different air/fuel (λ) values (the λ-value will be discussed in more detail later), varying from lean in oxygen but rich in steam to rich in oxygen and leaner in steam. They chose propane as a surrogate for gasoline, which allowed experimental difficulties of using complex multicomponent fuels like gasoline to be avoided, but still giving reasonable modelling of reaction trends seen with more complex hydrocarbons. The quantity of propane was set to the theoretical value required for auto thermal reforming (i.e where heat generated through oxidation reactions is balanced by endothermic reforming reactions). A GHSV of 136,000 h^{-1} was used. They also investigated the effect of sulfur poisoning on the catalyst, using sulfur dioxide (since the organo-sulfur species in commercial fuel would be oxidized during auto ignition). They aim for a hydrogen content of the reformed gas to be in the region of 5-20 %, which would be beneficial to engine performance, and that this would occur at relatively low exhaust temperatures of 350-400 °C.

Their work shows that a Pt-Rh based catalyst can meet these requirements, particularly the low light off temperature when the oxygen levels were intermediate or high in the exhaust gas. However, at the low oxygen condition, only around 3 % hydrogen was produced. They suggest however that the addition of

air to the exhaust feed would be technically possible – allowing better performance under all engine operating modes. The effect of sulfur was found to be deactivating on the prototype catalyst, and irreversibly so, which led to the synthesis of the rhodium only catalysts (rhodium is immune to sulfur poisoning). The support of these catalysts was also poisoned by sulfur, though to a lesser extent, and the species were much more weakly held, therefore the activity of the rhodium catalysts could be recovered when the SO_2 feed was switched off. The rhodium catalysts showed greater hydrogen production than the prototype, however they did display higher light off temperatures (Pt was therefore beneficial to lower light off, but not for resistance to sulfur poisoning). Therefore, the authors suggest that, given the continuing presence of sulfur compounds in gasoline, that rhodium only formulations, with supports resistant to sulfur poisoning, be used in future.

More recent work by Ambroise et al.[44], studied exhaust gas reforming with a synthetic exhaust gas mixture lean in oxygen, but with another surrogate for gasoline – iso-octane. The tests were carried out at 520 °C. They prepared cobalt only, rhodium only, and cobalt-noble metal (Rh, Ru, Pd and Pt) bimetallic catalysts on ceria-zirconia. The catalysts were activated either under reactant flow or under a mixture corresponding to the predicted equilibrium composition ("equilibrium flow"). Choice of activation method was found to be very important in some cases. Cobalt only catalysts were found to be inactive regardless of activation method. Co-Rh and Co-Pt catalysts were found to be very active when activated under reactant flow, where as Co-Pd and Co-Ru were not. It was discovered that there was no great gain in hydrogen production with high loadings of rhodium (2.5 %) compared to lower loadings (1.0 %), and that given the cost savings associated with lower rhodium loadings, that this catalyst was the preferred option. When activated under the equilibrium mixture flow, the Co-Rh and Co-Pt catalyst showed no great change whereas that of the Co-Pd catalysts were slightly enhanced. However, the Co-Ru catalyst activity was greatly enhanced, and in fact showed the highest activity, approaching the predicted thermodynamic value of expected hydrogen production. The activity of the Co-Ru catalyst was also found be enhanced as if the catalyst was activated under reactive flow, but with the CO_2 removed, as much as when activated under equilibrium flow. The dependence on activation method was therefore assigned to the oxidative conditions present when activated under reactant flow with CO_2, which was lost when it was removed, and that the equilibrium flow was reductive enough to avoid these effects. All catalysts were found to deactivate over increasing time on stream – due to carbon deposition on the catalyst surface, which was found to increase in the order of Ru<Pt<Pd<Rh.

Hydrocarbon fuels are not the only fuels considered for this application, oxygenates such as bioethanol have also been investigated [29].

It will be made clear later, but these last two studies by Peucheret et al. and Ambroise et al. closely relate to the work in this project, since both are catalysis focused, as well as using propane and iso-octane as surrogates for gasoline.

The next section will now cover the concepts involved in greater detail, based on a discussion of the literature, both of reforming in general, and where possible, literature specific to exhaust gas reforming.

The Exhaust Gas Reforming Process

As mentioned previously, methods of onboard hydrogen production generally utilize either steam reforming, partial oxidation, or a combination of those known as autothermal reforming. These processes, particularly steam reforming are well studied industrial processes for the mass production of hydrogen from hydrocarbon feedstock. The reactions occurring during exhaust gas reforming can be complex combinations of these well-known processes and a number of side reactions. General equations and their broad heats of reaction, for some of these reactions are shown below in Table 1.1 [45-47]:

Reaction	Equation	ΔH
Steam Reforming 1 (SR1)	–	Endothermic
Steam Reforming 2 (SR2)	–	Endothermic
Dry Reforming (DR)	–	Endothermic
Partial Oxidation (POx)	– –	Exothermic
Complete Combustion	– –	Exothermic
Water Gas Shift (WGS)		Exothermic
Methanation 1		Exothermic
Methanation 2		Exothermic

Table 1.1: Common reactions in exhaust gas reforming

This is not an exhaustive list, among others there are also reactions occurring that can lead to the deactivation of the catalyst (more on these later), as well as other side reaction. Under certain conditions, there is both oxygen and steam in the exhaust gas, hence the reactions can be somewhat similar to auto thermal reforming (simply a combination of steam reforming and partial oxidation). The exact reaction enthalpies depend on the hydrocarbon in question, but generally speaking for steam reforming (SR) and partial oxidation (POx) the absolute reaction enthalpies increase with chain length of the hydrocarbon [46]. The composition of the reformed fuel will therefore depend on the balance of these reactions, which in turn is determined by the reaction conditions, the hydrocarbon, and catalyst activity/selectivity.

By way of example, Gomes et al.[31, 48], in two papers present a detailed study on the reactions involved when iso-octane was used as a surrogate fuel for gasoline in exhaust gas reforming. They use a rhodium catalyst, and simulated exhaust conditions where the gas is lean in oxygen (their feed was 71.3 % N_2, 1

% O_2, 12 % H_2O, 13.5 % CO_2 and 2.2 % iso-octane, by volume). They detail some additional reactions that could be occurring on the catalyst, shown below in Table 1.2 below, which yield methane:

Name	Equation
Decomposition	
Hydrogenolysis	

Table 1.2: Other potential reactions during simulated exhaust gas reforming of iso-octane

The studies present thermodynamic predictions, first to examine the effect of temperature and pressure, and later to further assess their experimental results. They predict hydrogen production to be optimal at 770 °C (an unrealistic exhaust temperature), and that hydrogen production can be negatively affected by higher pressures. They chose 580 °C as their preliminary test temperature, which was predicted to yield a product gas containing 13 % by volume of hydrogen according to equilibrium calculations, along with carbon monoxide as the major products, with methane, carbon dioxide, and water as lesser products.

An experiment with no catalyst present (a so called “blank”) showed some iso-octane consumption and close to total oxygen consumption, with a product gas containing ratios of carbon dioxide, carbon monoxide and hydrogen suggesting roughly equal parts total oxidation and partial oxidation of the fuel in the gas phase. This suggests that even when a catalyst is present, the oxidation reactions do not predominantly occur on the catalyst surface.

Initial testing found significantly lower iso-octane consumption (never exceeding 70 %) than predicted, while still obtaining predicted equilibrium yields of hydrogen. This was accounted for by much lower than predicted yield of methane. The consumption of some carbon dioxide also suggested a low level of dry reforming had occurred.

The reactions were probed further with experimental and thermodynamic investigations by varying the test temperature (450 °C, 520 °C and 580 °C), along with the mass of catalyst (which changes the GHSV, and therefore reactant contact time on the catalyst surface). These tests were first done under exhaust gas reforming conditions, followed by steam reforming conditions (removing carbon dioxide and oxygen) and then dry reforming conditions (removing steam and oxygen). Their thermodynamic calculations showed good agreement with their experimental results, and therefore allowed them to elucidate the likely reaction scheme. They found that iso-octane conversion increased with both temperature and contact time.

Their results from both studies, through product ratios, selectivities and yields, suggest that the exhaust gas reforming process of iso-octane on the rhodium catalyst occurs along the following lines (see Equations 1.3 to 1.6 below): Oxidation (partial and total) of fuel almost entirely in the gas phase, prior to the catalyst. This is then followed by steam reforming (1.3) of the fuel to carbon dioxide and hydrogen

(Steam Reforming 2) with an increasing, though still minor contribution from dry reforming (1.4) at higher contact times and higher temperatures (since it was found to be kinetically limited). Then carbon monoxide formation from the reverse water gas shift reaction (1.5), followed by methane formation, primarily by methanation (1.6) of carbon monoxide. The formation of methane directly from iso-octane (thermal decomposition or hydrogenolysis) is severely kinetically limited – hence the lower than predicted methane content of the reformed gas while obtaining close to the predicted equilibrium yield of hydrogen with lower than predicted iso-octane conversion. The methane yield was also thought to be further reduced via its consumption in reforming reactions.

(1.3)

(1.4)

(1.5)

(1.6)

Though the specific details and balance of the reactions occurring can depend on the combination of the identity of the hydrocarbon, the catalyst and the reaction conditions, a general scheme, similar to above can be concluded for exhaust gas reforming. When there is some oxygen present in the exhaust gas, the first step is the oxidation (partial or total) of the fuel, either on the catalyst or in the gas phase, which raises the catalyst bed temperature due to the exothermicity of these reactions. This is often referred to as light off. This is then followed by the reforming reactions, which is predominantly steam reforming, producing the hydrogen, and due to their endothermic nature, lowering the catalyst bed temperature. The result is consumption of some or all of the fuel, all of the oxygen, as well as up to a certain point, increasing yields of hydrogen and carbon monoxide as the temperature is increased further (since the reforming reactions are endothermic). The order of these reactions sets up a temperature profile along the catalyst bed, with maximum temperatures at the inlet side of the bed, and the temperature decreasing through the length of the bed [43, 49], which is also found in autothermal reforming applications [50, 51].

The reaction conditions are entirely dependent on the operating mode of the engine. In other words, the temperature, contents, and flow characteristics of the exhaust stream (the feed properties) of any potential exhaust gas reforming unit will depend on the output of the internal combustion engine at any moment, as in the case of the catalytic converter, currently used in vehicles. A vehicle engine takes in fuel and air, and combusts the fuel. If this were perfectly balanced, complete combustion, then the exhaust gas would only contain carbon dioxide, water, and nitrogen (un-reacted from the air). However, this is not the case, and the exhaust gas can contain un-consumed oxygen from the intake-air, along with low levels of carbon monoxide and unburnt hydrocarbon fractions. In engineering, the operating condition of the engine is measured by the equivalence ratio, or it's inverse the λ-value [52, 53]. This is a measure of the mass ratio between the actual air/fuel used in the engine, to the stoichiometric ratio for

the fuel in question. The stoichiometric air/fuel ratio for any hydrocarbon can be calculated using the expressions below:

(1.7)

Modelling air as 21 % oxygen, and 79 % nitrogen by volume, and assuming Avagadro's law, then the molar fraction of oxygen in air is 0.21, and that of nitrogen is 0.79 (a 1:3.77 ratio). The mass of air per mole of oxygen is therefore roughly 137.6 g/mol (using molar masses as 32 $gmol^{-1}$ and 28 $gmol^{-1}$ for oxygen and nitrogen respectively). Using the molar mass of carbon as 12 $gmol^{-1}$, and that of hydrogen as 1 $gmol^{-1}$, then the stoichiometric air to fuel ratio (AFR_{st}) for any hydrocarbon (C_aH_b) can be calculated by:

(1.8)

Some example stoichiometric fuel ratios are given below:

Fuel	**AFR_{st}**
Gasoline (assuming $C_nH_{1.8n}$)	14.5
Iso-octane	15.1
Propane	15.6

Table 1.3: Example stoichiometric air to fuel ratios

The λ-value is then calculated by the ratio of the actual air/fuel ratio (AFR_{actual}) used to the stoichiometric air/fuel ratio:

(1.9)

Hence a λ=1 would represent stoichiometric conditions, λ>1 would be an air rich mixture, λ<1 would be a lean mixture.

Depending on the load demand, the engine will either operate under stoichiometric conditions (λ=1) or under non-stoichiometric conditions (λ≠1). This can vary between excess fuel and excess air operation of the engine intake. The higher the engine load the higher the λ-value [43].This will then determine the composition of the exhaust gas.

Additionally, the operating condition of the engine will determine the temperature of the hot exhaust gas stream moving through the exhaust pipe, as well as the flow rate of the gases. Table 1.4 [36] and

Figure 1.5 [43] below, present a summary, taken from the literature, of how the exhaust gas characteristics can vary as the operating condition of the engine is changed.

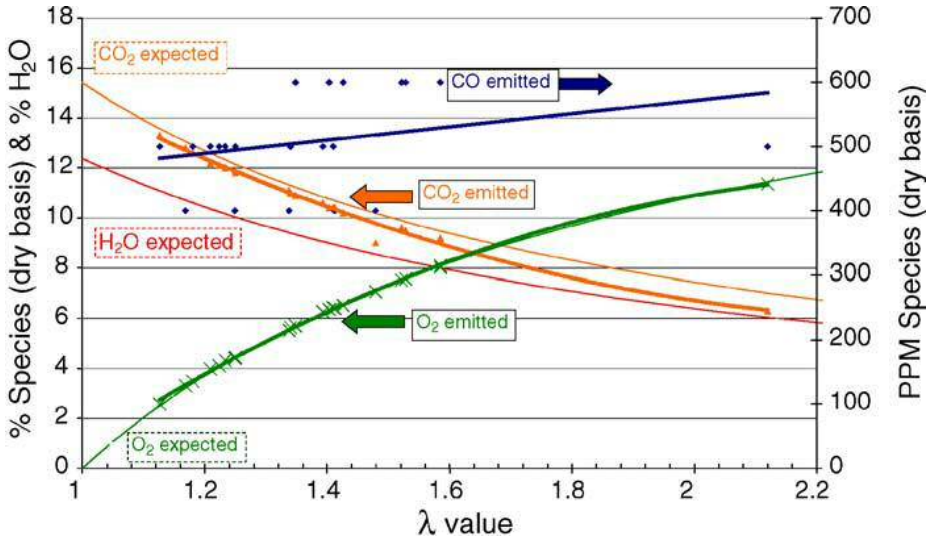

Figure 1.5: Exhaust gas emissions of a spark ignition engine as a function of λ [43]

Fuel	λ	T /°C	% O_2	% CO	% CO_2	% H_2O
Gasoline	1.00	400	0.40	0.30	12.90	12.50
	1.50	350	6.80	0.14	9.30	8.30
	2.12	350	10.70	0.14	5.90	5.60
Diesel	2.01	370	9.10	0.01	6.40	6.20
	2.83	288	11.90	0.01	4.80	4.70
	3.25	240	14.30	0.01	4.30	4.10
	4.25	200	15.80	0.01	3.30	3.30

Table 1.4: Exhaust gas compositions at different λ-values for gasoline and diesel engines (with nitrogen as balance) [36]

It can be seen from the table that as the engine is operated in a richer air mixture, that the quantity of oxygen present in the exhaust gas stream increase. It can also be seen that diesel engines are typically operated at richer air mixtures than gasoline engines. Finally, the higher the λ-value, the lower the temperature of the exhaust gases exiting the engine. It should also be noted that the temperatures shown here are lower than the maximum quoted previously as possible temperatures in the exhaust stream. This shows the importance of both the reforming unit proximity to the engine, as well as the role played by exothermic reactions to further raise the catalyst bed temperature.

Since the engine mode determines the composition of the exhaust gas, and therefore the feed for a potential reforming unit, it is also important to consider what effect this changing composition of reactants can have on the reactions taking place. Generally, the two most important factors to consider are the feed molar steam to carbon (H_2O/C) and oxygen to carbon (O_2/C) ratios. The quantity of fuel added into the exhaust gas stream prior to the reformer can obviously be controlled, however unless additional changes are made to the exhaust system, the steam and oxygen contents of the exhaust gas are controlled by the engine operation. It has already been mentioned that higher steam content (greater H_2O/C) of the feed can promote stream reforming reactions and therefore improve hydrogen yields [42]. In a similar manner, the greater the presence of oxygen, the more oxidation reactions will be favored [49]. There is a balance to be struck, since the more fuel consumed in oxidation reactions, then the less there will be available for reforming reactions. However, as Peucheret et al. [43] found when testing at λ-values of 1, 1.5 and 2.12, with propane as the fuel, the λ=1 condition displayed the worst yield of hydrogen, which was because of the negligible oxygen content of the exhaust gas. This meant that the exotherm from the low level of oxidation reactions occurring was not great enough to promote the endothermic reforming reactions to the same extent as the conditions with higher oxygen levels. In other words, the ideal operation of the reform is somewhat autothermal – where the endothermic reactions producing hydrogen are promoted by the exothermic oxidation reactions to the greatest extent possible, and that the exhaust gas temperature makes up for any short fall.

Therefore, the presence of both oxygen and steam are required for best hydrogen yields. There is some room for optimization of H_2O/C and O_2/C ratios through controlling the fuel flow rate into the exhaust stream, however in cases such as those at λ=1 where little/no oxygen is in the exhaust gas, such optimization is difficult.

Another important reaction condition is the rate at which the reactants (exhaust gases and fuel) are flowing over the catalyst bed in the reforming unit. This is often measured by the Gas Hourly Space Velocity, or GHSV:

(1.10)

GHSV has units of reciprocal hours, h^{-1}, therefore, if the volumes of gas flow and catalyst were in mL, the GHSV would be:

(1.11)

The GHSV is a measure of the rate of reactant flow over the catalyst bed, per unit volume of catalyst. It is therefore related to other catalytic terms such as contact time, in that if the GHSV is increased the contact time would be expected to decrease. Typical GHSV values of potential exhaust gas reforming systems in the works discussed so far were in the range of 10^4 to 10^5 h^{-1}.

The effect of GHSV on exhaust gas reforming can depend on the system in question (fuel, catalyst and exhaust composition). As already discussed previously from the work of Gomes et al.[31, 48] in the case of iso-octane, the greater the contact time (resulting from a lower rate of reactant flow over the catalyst bed volume), the greater the iso-octane conversion. The authors also report that optimum hydrogen was obtained at intermediate levels of iso-octane conversion, in other words that the contact time, and its effect on iso-octane conversion had an impact on the selectivity of the products.

Sen et al.[36], simulated the effect of GHSV on exhaust gas reforming (with both gasoline and diesel exhaust conditions), and propane as the surrogate fuel. They find that increasing feed flow rates, and hence higher GHSV's, initially results in better hydrogen yields, due to increased propane total oxidation raising the bed temperature (promoting endothermic reforming). However, at the highest flow rates they tested (corresponding to a GHSV of $6.6x10^4 h^{-1}$), the hydrogen yield was found to be negatively affected.

A similar result was found by A.Tsolakis and S.Golunski [49], when ultra-low sulfur diesel was used for exhaust gas reforming. Increasing space velocities raised the maximum temperature obtained in the bed, and shifted the position of peak temperature further along the bed. This assigned to the mass transfer-limited nature of exothermic reactions, that their rate can be increased with increasing reactant flow rate since this increases the rate at which reactants are delivered to active sites. Over the GHSV range tested, they also found that increasing the GHSV led to hydrogen yields approaching predicted equilibrium yields.

Recent work by Chang et al.[54] underlines the importance of operating an exhaust gas reformer as a heat recovery, or thermochemical recuperation (TCR) device – through the favoring of steam reforming over partial oxidation. Though POx may be effective at producing high levels of hydrogen, there is a cost in terms of the quantity of the primary fuel required to maintain such levels. On the other hand, the endothermic nature of SR makes it possible to recover the waste heat of the exhaust. The authors display this preference of SR over POx in terms of the energetics by reference to the "Enthalpy Ratio", which is the enthalpy of combustion of the products over that of the reactants. An enthalpy ratio < 1 would show chemical energy loss during a reaction, and a ratio > 1 would show a gain – in other words TCR. They first show that for a range for a series of alkanes, olefins and aromatics that the enthalpy ratio for partial oxidation is < 1. However, for steam reforming (and dry reforming) the ratio is > 1. When all the fuels are considered, energy increase in the region of 15 %- 25 % can be obtained by steam reforming relative to partial oxidation. The authors then show that this favorable outcome in terms of the energetics is possible in exhaust gas reforming if the feed of the reformer is balanced so as to favor SR over POx, by keeping the oxygen content of the feed low (though not to such an extent that CH_4 becomes a favored product which negatively impacts the energetics) – while still producing hydrogen levels in the reformate (15 vol%) that would be beneficial to engine performance.

In a follow up work [55] the authors demonstrate that when operated as described above, exhaust gas reforming be used to extend the exhaust gas recirculation dilution limit. The combination of the extension of this limit and the inclusion of reformate (containing hydrogen) in the engine intake can

yield significant efficiency gains, resulting in 8 % lower fuel consumption relative to baseline operation in a multi-cylinder, stoichiometric SI engine.

Another recent paper by Leung et al. [35] shares these conclusions, showing that when optimized, exhaust gas reforming in combination with exhaust gas recirculation can bring the efficiency of gasoline fueled SI engines in line with those of diesel engines. This is an attractive prospect since if used in combination with the catalytic converter technology already used in SI engine vehicles promises the strong fuel economy of diesel vehicles, with the accompanying lower CO_2 emissions, and the low NO_X, hydrocarbons, CO and particulate emissions typical of SI-engine vehicles.

The next section will now consider the catalytic elements of exhaust gas reforming. Despite the potential of the technology to bring efficiency gains to spark ignition engine, as shown in the three works described above, the passive nature of the technology does mean that in order for it to be successful a highly active and durable catalyst is required. It is these catalytic elements that the next section considers.

The Catalysis of Exhaust Gas Reforming

The reaction processes discussed above for producing hydrogen are most effectively carried out with the assistance of a catalyst. A catalyst is a substance that facilitates a reaction not by changing the thermodynamic favorability, but rather improving the favorability of the kinetics, and is not itself consumed in the reaction [19].

In order for an exhaust gas reforming system to be incorporated into a real vehicle the catalyst must meet certain targets. Physical criteria could include weight and size. Catalytic criteria such as activity (especially at low temperature), selectivity for hydrogen, and resistance to deactivation (and hence longevity of use, which for automotive catalysts is in the range of 160,000 km of driving [53, 56, 57]) are also vital. It must also meet certain application specific criteria such as versatility and durability to enable good performance under variable reaction and environmental conditions given the operating situations a reforming unit is likely to be exposed to in a vehicle. Given the similar chemistry between exhaust gas reforming and other hydrogen generating techniques, such as steam and auto thermal reforming used in industrial processes or for use with fuel cells, the catalysts used in these applications are often similar in terms of their structure and component parts. However, exhaust gas reforming catalysts must of excellent dynamic response to changes in reaction conditions, as well as coping with repeated startup/shutdown cycles. This is unlike most industrial catalysts operate under optimized, steady-state conditions,

Reforming catalysts normally consist of supported precious (Pt, Pd, Rh etc.) and/or base metals (Ni, Co, Fe etc.), along with any other beneficial metals (called dopants, or promoters). The support materials are often carefully engineered alumina/metal oxides [58]. For example, industrial steam reforming of methane, the source of most bulk hydrogen production, is normally catalyzed using a supported nickel catalyst [59]. Generally speaking, precious metals tend to show higher activity, and higher resistance to

deactivation pathways than base metals [60, 61]. For example, in the case of ethanol steam reforming (often for fuel cell applications), rhodium and nickel are proposed as the most active reforming catalysts (amongst Rh, Pt, Pd, Ni, Co and Cu), and though the choice of support can help, nickel is more susceptible to deactivation due to carbon formation than rhodium [62]. However, they are significantly more expensive than base metals, by way of example as of November 2018, the rhodium spot price was around \$78 /g [63], whereas nickel was at around \$0.01 /g [64]. This cost of precious metals is certainly a limiting factor for exhaust gas reforming.

Not only do the components of the catalyst matter, but so do the preparation techniques used. These can have great influence on the performance characteristics of the resulting catalyst. The careful design of catalysts, their components, structure and preparation, is a formalized process in industry. In the case of exhaust gas reforming where supported metal catalysts are used, the general procedure can be summarized as follows (i) introduction of the active metal precursor onto the support, (ii) drying and calcination, and finally in some circumstances, (iii) activation/pre-reduction.

Factors such as the quantity of active metal loading, its dispersion, the surface area of the catalyst, the nature of the surface species, and the components interactions with each other, can all be somewhat controlled for at each stage. There are several methods of impregnating the support with the active metal varying from simple wet-impregnation to more involved techniques such as co-precipitation or sol-gel methods. Wet impregnation does not provide much control, but does generally provide fairly homogeneous dispersions of the active metal, whereas the more involved techniques can provide more control of certain aspects such as particle size.

The removal of solvent in the drying stage, and the calcination stage (exposure of catalyst to temperatures as high or higher than encountered during reactions, in order to decompose the metal precursor and fixing the resulting metal oxide to the support surface), must be controlled – specifically the maximum temperature, ramp rate (how quickly the temperature is raised), and duration of heating. Sustained exposure to high temperatures can cause loss of surface area due to sintering. Sintering is an agglomeration process which occurs as the melting point of a solid is approached and the mobility of the atoms in the solid increases. These processes often begin around the Huttig and Tammann temperatures ($0.35T_{MP}$ and $0.5T_{MP}$ respectively) [65].

Finally, whether the catalyst is best activated before use, and by what method must also be considered. Base metals tend to require reduction before use, whereas precious metals often do not since they are often easily reduced at low temperatures in-situ during operation. The reduction can be carried out under different conditions, which can alter the structure and species of the catalyst.

The catalyst can also be prepared in powdered or pelletized form and then used in a packed bed reactor, or the catalyst formulation can be coated onto structured substrates such as monoliths. Monoliths present certain advantages in some situations, for example they result in much lower pressure drop than packed beds due to their large open frontal area. Due to the high space velocities present in the exhaust of a

vehicle, an exhaust gas reforming catalyst will almost certainly use a monolith substrate. However, they can have disadvantages for some reactions, resulting from aspects like the more laminar flow through the monolith channels (which can result in large residence time distributions, which can negatively impact conversion levels), and sometimes poor radial heat conductivity.

Hence it is clear that there any many variables at each stage, and that the effect of these on the end nature of the catalyst have to be considered for each application [66-68].

As mentioned already, any catalyst used in a real vehicle must be able to cope with a wide range of operating conditions over long periods of time. However, as in other applications, catalyst deactivation is an issue. Deactivation of catalysts generally falls into three categories: (i) chemical deactivation, such as poisoning of active sites, (ii) thermal deactivation, such as degradation and sintering, or (iii) mechanical deactivation such as attrition/crushing and fouling [69]. The nature of the processes involved in the application will determine which of these are more of a risk. In the case of exhaust gas reforming (as well as other reforming techniques) the main cause of catalyst deactivation is often the deposition of carbon species onto the catalyst surface. Poisoning of catalyst active sites can also be an issue, particularly if the fuel used contains sulfur species (as gasoline and diesel still do). Thermal sintering, though less of a problem given exhaust temperatures don't tend to exceed 600 °C, is still a possibility. Therefore, it is vital that any catalyst designed shows strong resistance to these deactivation pathways.

Each of these possibilities are affected by the reaction conditions. In the case of sulfur poisoning for example, the continuing improvement on the removal of sulfur from fuels would certainly be beneficial. However, in the case of carbon deposition and thermal deactivation, since exhaust gas reforming is largely a passive process, there is limited scope for the optimization of reaction conditions to minimize these possibilities.

The details of what occurs on the catalyst surface during operation is the focus of mechanistic and kinetic studies. Adesina, Trimm and Cant [70] present a detailed mechanistic and kinetic study for the steam reforming of iso-octane over a nickel based catalyst, which was pre-reduced before testing. They determined the kinetic order of reactions with respect to iso-octane and steam by following their rate of consumption at various combinations of partial pressures, and at three different temperatures (585, 603 and 623 K). They found that the activation energy for iso-octane was 44 kJ mol^{-1}, which is inline with a trend they report to be present in the literature of how activation energy varies with hydrocarbon chain length (activation energy decreases with increasing chain length). They find that the order of reaction with respect to iso-octane partial pressure is low (they report the order with respect to higher hydrocarbons often approaches zero), and so ascribes to a power-law fit, and is symptomatic of strong adsorption of the hydrocarbon. However, increasing steam partial pressure (and hence steam: carbon ratio) improved activity. This suggests either increased gas phase steam attack of the surface carbon, or chemisorption of steam on sites different from those containing the carbon species leading to a surface reaction. This suggested Langmuir-Hinshelwood (LH) and Eley-Rideal (ER) type mechanisms (see Figure 1.6 below [71]).

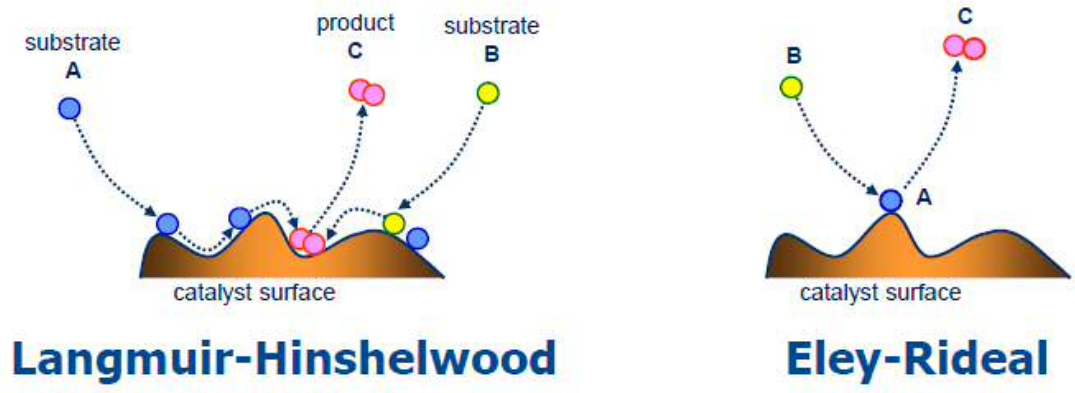

Figure 1.6: LH and ER type mechanisms [71]

These two mechanistic categories logically suggested six different possible mechanisms (by varying single/dual site and molecular/associative/dissociative adsorption of the reactants) for steam reforming of iso-octane by nickel. Four of these fitted the LH-type and two fitted the ER-type. Once defined, each models expected kinetic parameters could be derived.

The kinetic parameters of each model were then compared to those obtained in the experimental testing described above. The two ER-type mechanisms showed negative values for one or more of the kinetic coefficients, and were therefore ruled out (since this suggests the reaction would not happen).

Of the remaining LH-type mechanisms, the most suitable model was found to be a dual-site mechanism, with dissociative adsorption of iso-octane and steam, and a bimolecular surface reaction as the rate determining step. They therefore suggest the following mechanism, where S_1 and S_2 represent the active sites; m_1, m_2, x and y are integers; and the dotted lines represent adsorption to the active site:

(1.12)

(1.13)

(1.14)

(1.15)

(1.16)

(1.17)

Where steps (1.12) and (1.13) are the dissociative adsorption. The reaction of the dissociated hydrocarbon and steam species (1.14) is the rate determining step. The main reforming products of hydrogen and carbon monoxide (red) are then released from the active sites (1.16) and (1.17), with

further hydrogen production and associated carbon monoxide consumption from the water gas shift reaction.

A similar mechanism was reported by Hou and Hughes [72], for the steam reforming of methane over a Ni/Al_2O_3 catalyst, where the nickel atoms are cited as the active sites. As above the mechanism followed an LH type pathway, with dissociative adsorption of steam and methane, and the reactions between the surface species was again the rate determining step.

In the case of ethanol reforming, rather than a hydrocarbon fuel, two studies on a Ni/CeO_2 [73] and Rh/ZrO_2 [74], give a detailed theoretical understanding of the reactions occurring on the catalyst surface, as well as serving to highlight the importance of not just the active metal, but the support and the interaction between the two. In both cases, the detailed analysis of surface species is enabled through the use of techniques like DRIFTS, in-situ XRD, and GC/MS.

In the former study, they identify the metallic nickel (Ni^0) in close contact with the CeO_2 (specifically Ce^{3+}) as the active phase during the steam reforming reactions – and that either component by itself was not sufficient to begin the decomposition of the ethanol until much higher temperatures. They identified ethoxy, acetate, carbonate and hydroxyl as intermediates. The nickel promotes the adsorption of the ethanol and cleavage of its C-C bond, while the support facilitates the decomposition of water, which then facilitates the reactions of the surface species.

In the latter study, they find that the dissociative adsorption of water occurs on a stepped Rh(211) surface. Dissociation happens via sequential O-H bond breaking, the first of which is an exothermic process, the second is endothermic (the first H abstraction is easier than the second). They also find that recombination of the adsorbed H species is then favored on this catalyst over recombination with hydroxyl species to form hydrogen over water. The ethanol interacts with the Rh step in various ways: Rh-C, Rh-O or an Rh-C-O-Rh organometallic cycle. They find that with the aid of water ethanol decomposition occurs via a hydroxyl dehydrogenation, followed by sequential α-dehydrogenation. The generated acetyl then undergoes direct C-C bond breaking, producing carbon monoxide and a CH_3 fragment, which then undergoes sequential decomposition, resulting in the formation of carbon and carbon monoxide. The carbon monoxide reacts with steam in water gas shift reactions, producing the carbon dioxide and hydrogen. Interestingly it was the WGS that produces the hydrogen, and was rate limiting, not the ethanol decomposition. This also highlighted the source of catalyst deactivation – the buildup of carbon residue on the catalyst.

From each of the above papers, what is clear is that both the metal, support and their interaction are crucial in reforming reactions, since both can be involved. It is also clear, as discussed in the previous section on the reactions occurring during reforming, that these can be complex systems, with a number of decomposition products, alongside the main reforming products. Furthermore, as already touched on, there are additional reactions to consider - those leading to the deactivation of the catalyst.

Carbon formation is the most common issue in processes like reforming. It leads to catalyst deactivation generally via three pathways: (1) fouling of the metal surface, (2) blockage of catalyst pores/voids, and (3) physical disintegration [75]. In industrial processes prone to carbon formation, thermodynamic studies can be used to create "boundary" data – the thermodynamic calculation of how carbon formation is affected by various operating parameters, allowing optimization of processes conditions (steam to carbon ratios, temperature etc.) to operate the processes outside of the likely range of carbon formation. As already mentioned, this sort of process optimization isn't as possible in a passive technology like exhaust gas reforming.

D. L. Trimm [76] shows some of the likely reactions leading to carbon formation during reforming of methane:

(1.18)

(1.19)

(1.20)

(1.21)

Reactions (1.18) to (1.20) are reversible, and therefore offer routes towards carbon formation since according the Le Chatelier's Principle they can be driven in reverse direction (away from carbon formation).

This is often done by gasification, which involves operating at higher steam to carbon ratios, therefore driving reaction (1.20) in reverse. The bulk of carbon formation occurs on the catalyst surface, but is also possible in the gas phase, with the carbon species formed then condensing downstream on the catalyst surface.

The intermediates involved in carbon formation are found to be the same intermediates as the reforming reactions – hence the same active sites (in this case for a nickel catalyst) active in steam reforming are also those prone to promote carbon formation. As already mentioned, during steam reforming, the hydrocarbons dissociatively adsorb to the nickel surface, and it is these dissociation products that can then lead to carbon formation.

The carbon once deposited could be gasified, or it could encapsulate the surface, or may dissolve into the nickel crystallite. This last process can lead to carbon whisker formation, which can actually lift the nickel crystallite from the catalyst surface, resulting in fragmentation of the catalyst. It is suggested, that since the intermediates are the same/similar, the way to suppress carbon formation is to control the kinetics of the intermediate reactions.

This can be done by controlling reaction conditions such as steam to carbon ratios, but also by catalyst modifications such as using dopant/modifying metals, and through beneficial metal-support interactions.

Noble metals are more resistant to carbon formation – particularly since metals like Rh and Ru don't dissolve the carbon into their crystallites in the same way as nickel does. The addition of sulfur to the feed can also suppress carbon formation, though this can then poison the catalyst also.

More recent work by Parmar et al. [77], considers carbon formation during diesel reforming, where the diesel fuel contains 50ppm of sulfur. They emphasize the complexity and range of reactions between surface species that can occur during the reforming process. They also point out that the nature of the carbon species formed can depend not only on the catalyst and conditions, but also on the hydrocarbon fuel being used, and that elemental carbon can take various forms such as whisker or filamentous carbon. Carbon forming reactions include the Boudouard reaction, reverse gasification reactions, and thermal cracking of hydrocarbons. They point out that carbon formation normally occurs in the following sequence:

(1.22)

Amorphous carbon is favored at temperatures below 600 °C, and graphitic carbon at greater temperatures. There is also the possibility for carbon formation in the gas phase via the Boudouard and reverse gasification reactions, which are favored at low temperatures. This often can lead to blockages and pressure build up in reactors, prior to the catalyst.

The authors also look at the effect of sulfur in the fuel feed (as it would be present in commercial diesel and gasoline). The likely species present in the reformer are SO_2 and H_2S, with the potential for SO_3 and H_2SO_4. H_2S in particular can adsorb to the catalyst surface (blocking active sites), or cause metal sulfide formation. Often resulting in loss of catalytic activity.

The effect of and nature of sulfur poisoning was beyond the scope of this work, so will not be looked at in any more detail other than to say that the strength of the adsorption of sulfur species can determine the extent to which any resulting deactivation is reversible. The strength of any adsorption can depend on reaction conditions, the nature of the sulfur species in the fuel feed and their decomposition products, as well as the catalysts resistance/preference towards specific species [78, 79].

Given the passivity of an exhaust gas reforming technology, the best route to avoiding deactivation is in the optimization of the catalysts – making them as resistant to these pathways as possible (as well as the continuing removal of sulfur from gasoline and diesel). In the following examples from the literature, this aspect will be considered, along with the reforming performance of various catalysts, and how these can be affected by the catalytic components, preparation method, and activation method.

In a paper previously discussed in the section on exhaust gas reforming, Ambroise et al. [44], synthesized and tested a range of different exhaust gas reforming supported metal catalysts, allowing comparison between the base metal cobalt, and selected precious metals (rhodium, ruthenium platinum and palladium). Iso-octane was used as the surrogate fuel for gasoline. The ceria-zirconia supported metal compositions were: cobalt only (5 %), 0.5 % rhodium only, cobalt-rhodium formulations with 0.5 %,1

% and 2.5 % rhodium, cobalt and 0.5 % ruthenium, cobalt and 0.5 % palladium, and finally a cobalt and 0.6 % platinum formulation (the total metal weighting of the bi-metallics was kept at 5 %).

All the samples showed surface areas in the region of 49-67 m^2g^{-1}, though the mixed metal oxides showed much smaller particle sizes (3.7-4.4 nm) compared to the cobalt only sample (16-29 nm), which showed some signs of sintering during preparation. Temperature programmed reduction analysis showed characteristic peaks for the surface and bulk species of the ceria-zirconia support (around 600 °C and 900 °C respectively). Cobalt insertion lowered these temperatures, with noble metal insertion lowering these temperatures further. Increasing the rhodium content led to lower reduction temperatures for both the support and Rh^{3+} to Rh^0. Reduction temperatures for the noble metals (in cobalt-NM mixed oxides) was found to be in the order of Pd<2.5% Rh<Ru<Pt<Pd<1%Rh<0.5%Rh. Noble metal doping also resulted in much deeper reduction. This enhanced reducibility of the support by insertion of the metal ions was ascribed to a spillover process.

The cobalt only catalyst was found to be largely inactive, regardless of whether pre-treatment under reactant flow or equilibrium flow was used. However, the exhaust gas reforming performance of the remaining catalysts was found to depend on the activation method chosen.

When activated under reactant flow the best catalysts were the Co-Rh bimetallic catalysts, which also performed well when activated under equilibrium flow. The Co-Ru catalyst showed significant dependence on the activation method, showing poor performance when activated under reactant flow, but it showed the strongest performance when activated under equilibrium flow. The Co-Pt catalyst showed no significant change between activation methods, and the Co-Pd catalyst showed a slight enhancement when activated under equilibrium flow. The change in Co-Ru catalyst performance was assigned to the fact the presence of high CO_2 levels in the activation flow was hindering its reduction. All the catalysts showed varying degrees of deactivation over time. The catalysts were characterized post-reactivity tests by temperature programmed oxidation, temperature programmed desorption and scanning electron microscopy – in order to study the extent and nature of carbon deposited on the catalysts, and hence explain the deactivation. The results show that the degree of deactivation was related to the quantity of carbon deposited on the surface. All catalysts showed some level of carbon deposition, though the quantity was dependent on the activation method, and the identity/weighting of the noble metal. The only stand out was the Co-Ru catalyst activated under equilibrium flow, which showed almost no deposited carbon.

This work therefore demonstrates the often superior performance of noble metal based reforming catalysts (in terms of activity and stability), as well as the benefits of doping base metal catalyst with noble metals. In addition, it also shows how choosing the correct activation method can often be very important in optimizing catalyst performance.

Another work by Ambroise et al. [80], again on exhaust gas reforming with iso-octane, looks at the effects of preparation method on cobalt only, and cobalt-rhodium catalysts. The preparation methods chosen

were a sol-gel method, and an impregnation method. They again used a ceria-zirconia support, this time in two different formulations (58:42 and 80:20 by weight Ce:Zr respectively). The cobalt catalysts contained 5 %wt. cobalt, and then Co-Rh catalysts contained 0.5 % or 1 % rhodium, with the cobalt loading adjusted so that metal loading was kept constant at a total of 5 %.

The pseudo sol-gel method used was based on the thermal decomposition of propionate precursors – this involved the dissolution of the precursor salts in hot propionic acid, which were then mixed and boiled for 1h, before the solvent was evaporated and a resin obtained. This was then heated at 2 °C min^{-1} in air, up to 500 °C, and maintained for 6 h at this temperature.

The impregnated cobalt catalysts were prepared by wet impregnation, where the salt was dissolved in a volume of water corresponding to the porous volume of the support, with the support added and left to mature for 1 h. The sample was then dried at 120 °C for 2 h, and calcined at 500 °C, using the same ramp rate as before, and then held at that temperature for 2h. The Co-Rh bimetallic catalysts prepared by wet impregnation were obtained by performing a subsequent impregnation of the rhodium, in the same manner as above, to the relevant samples of cobalt catalyst. The ceria-zirconia support used in the sol-gel method had a lower surface area than those used in the impregnation samples. However after metal deposition both groups (sol-gel and impregnated catalysts) had similar surface areas, showing a fall in surface area associated with the metal addition in the impregnation method. XRD data showed that the ceria rich support displayed unit cell expansion associated with the increase in ceria content.

When the sol-gel method was used, cobalt insertion into the ceria-zirconia matrix results in some contraction of the unit cell, likely associated with the incorporation of smaller 6-coordianted Co^{2+} ions. Rhodium co-insertion had no additional effect since Rh^{3+} is of similar size to Co^{2+}. On the other hand, the impregnated catalysts showed no change in the lattice parameter, suggesting no metal-insertion had occurred. The bimetallic catalysts prepared by each method showed particles sizes in the nanoparticle range (3.8-5 nm for sol-gel, and 6.4-7.3 nm for impregnation). However, the cobalt only samples showed much larger particles sizes, indicating some cobalt sintering (5-15.8 nm), and some Co_3O_4, cobalt oxide cubic phase (i.e resulting from some rejection of cobalt from the lattice). Transmission electron microscopy showed good homogeneity of the Co-Rh distribution in samples prepared by sol-gel, and some heterogeneity for those prepared by impregnation. This was linked to the detection of Co_3O_4 particles in the XRD. Temperature programmed reduction, as in the previous work, showed a decrease in reduction temperatures with metal insertion into the ceria-zirconia support. The TPR data also suggested stronger metal-support interactions in the sol-gel prepared samples, and suggested that in the impregnation prepared samples the metal was just deposited onto the surface, hence showing a weaker metal-support interaction.

In terms of exhaust gas reforming performance, the tests were again carried out with iso-octane as the surrogate fuel, at conditions corresponding to an exhaust gas lean in oxygen, at 520 °C. Iso-octane was added in a quantity predicted to yield 10 % hydrogen, by volume of the product gas. Though they don't present the data for the cobalt-only catalysts, all the bimetallic samples showed close to equilibrium

predicted levels of hydrogen production, particularly those with 1% rhodium, which were so close as to make comparison difficult. Of the other samples, the bimetallic samples using the stoichiometric (as opposed to ceria rich) support, prepared by impregnation, exhibited higher activity than their sol-gel equivalents. However, the ceria rich bimetallic sample prepared by sol-gel, and containing 0.5 % rhodium, showed higher activity than its equivalent impregnation-prepared catalyst. The ceria rich supported samples showed better performance than the stoichiometric when prepared by sol-gel (assigned to the higher oxidation properties associated with higher content of the ceria). Interestingly for the ceria rich samples, the impregnated samples showed higher methane in the product gas than the sol-gel samples, which showed higher isoC_4 products. The isoC_4 is likely the primary product of iso-octane activation by β-scission as a redox process, therefore favored by catalysts with high oxygen mobility (as opposed to α-scission for further C-C bond breaking occurring on metallic sites), therefore suggesting slightly different activation mechanisms for the impregnated and sol-gel prepared catalysts (i.e the impregnated catalyst showed stronger metallic behavior).

The effect of sulfur poisoning on a Pt-Rh and Rh only (on a support containing CeO_2, ZrO_2 and Al_2O_3 for the bimetallic catalyst, and silica and ceria enriched alumina for the Rh only formulations) exhaust gas reforming catalyst was studied in the work by Peucheret et al.[43], discussed previously. They found that when they included SO_2 in the simulated exhaust gas/fuel feed, sulfur poisoning (through SO_3 and H_2S species) deactivated both the bimetallic and rhodium only catalysts. Though the deactivation was more severe, and somewhat irreversible, for the Pt-Rh catalyst, the rhodium only samples were able to recover their activity after the sulfur was removed from the reactant feed. This was largely assigned to rhodium's immunity to sulfur poisoning, and platinum's tendency to form S^{2-} species on its surface from H_2S. Though both catalysts showed deactivation resulting from sulfur species blocking the metal-support interface (a crucial site in reforming reactions as already discussed), these sulfur species were more weekly bound in the rhodium only catalysts, likely due to both the rhodium and the presence of silica. The silica increases the surface acidity of the support (by increasing ceria-zirconia dispersion) and therefore depressed SO_x adsorption. So again it is clear that choice of both active metal and support can greatly affect the stability of the catalyst.

The literature specific to exhaust gas reforming is not extensive, however comparisons between different active metals (precious and base) can instead be found in the literature relating to other steam reforming applications. For example Frusteri et al. [81], studied the performance of MgO supported Pd, Rh, Ni and Co catalysts in the steam reforming of ethanol for fuel cell applications. All the catalysts were prepared by the same impregnation procedure, only the loadings were varied: 21 % Ni, 21 % Co, 3 % Rh, and 3 % Pd. Ethanol conversion was in the order of Rh>Co>Ni>Pd, whereas hydrogen selectivity was in the order of Ni>Rh≈Co>Pd. Hydrogen selectivity for the nickel, cobalt and rhodium catalysts remained fairly constant over time on stream, whereas the Pd catalyst was somewhat inconsistent. In contrast, ethanol conversion decreased over time for the Co, Ni and Pd catalysts (significantly so for the Co and Pd), whereas the Rh catalyst conversion remained fairly stable. The authors explain the differences

observed in product distributions (H_2, CO_2, CO, CH_4, CH_3HO, C_2H_4), in terms of each catalysts preference for certain reactions in the general reaction scheme of ethanol reforming. The Rh catalyst for example is very active towards acetaldehyde decomposition and water gas shift reactions, but not so active in steam reforming. Co and Ni are very active for steam reforming, but not in acetaldehyde decomposition. The Pd catalyst on the other hand showed average activity to acetaldehyde decomposition only. Post-reaction tests showed that the Pd, Ni and Co catalysts were affected by metal sintering, whereas the Rh was not. This was assigned as the main cause of the causing the decrease in ethanol conversion over time for these catalysts. Carbon formation was found to be drastically inhibited on the Rh catalyst, and modest on the Ni and Co catalysts. The authors note that modest coke formation on the nickel and cobalt catalysts was less than expected, and assign this to the inhibition of ethylene formation by the MgO support resulting from its basic nature. They also suggest that the support advantageously modifies the electronic properties of the metal, further suppressing carbon formation. Though not on exhaust gas reforming or hydrocarbon fuels specifically, this serves as another example of the often superior performance of the precious metal rhodium in reforming applications (in terms of activity and stability), relative to base metals, as well as the important role played by the support.

Work by Sánchez-Sánchez et al. [82], also shows the importance of the support, again in the context of ethanol steam reforming. They prepared Ni-reforming catalysts, supported on metal oxide modified alumina, where the metal oxides were either of Ce, La, Zr or Mg. The catalysts alumina support was doped with the metal oxides via impregnation from the metal nitrate salts, to achieve a constant metal/Al ratio. The nickel was then added via impregnation as well. Through various techniques the authors found that the addition of the different metal oxides had an effect on the structure and properties of the support, the deposition of the nickel on the support, and the resulting metal-support interactions. They note that since both metal and support play an essential role in steam reforming of ethanol, that this therefore could explain differences in their catalytic performance. This is because the ethanol can absorb on the alumina support and dehydrate on acidic sites to ethylene, the nickel activates the organic molecule through O-H, C-C and CH_2 bond breaking, and promotes reactions between organic fragments and OH groups from the water. The addition of the metal oxides was found to lower the alumina acidity in the order of Ce≈La>Zr>Mg.

The nature of the nickel phases present also effects the selectivity, particularly towards ethylene. The presence of Mg led to the largest drop in the surface acidity of the alumina support, and that its presence inhibited the incorporation of nickel into the alumina, therefore improving nickel dispersion. This lower acidity and better nickel dispersion explained the low initial ethylene production, and stable total ethanol conversion and stable hydrogen production. The addition of Zr to the alumina decreased the surface acidity and decreased the dispersion of nickel phases because of strong Ni-ZrO_2 interactions. This is suggested as the cause of the promotion of reforming activity through enhanced water activation seen for the Zr-supproted catalyst. This was also found to be the case with the Ce modified support. The addition of La to the alumina enhanced nickel dispersion, but also lead to some nickel phases partly

covered by lanthana. This dilution of the nickel lead to a decrease in intrinsic activity of the catalyst for ethanol steam reforming. In all cases, carbon deposition was found to be the cause of changes in selectivity over time on stream, through changes to the catalyst surface. This was found to be particularly quick and significant on the alumina only, Zr, and Mg modified catalyst (due to significant quantities of filamentous carbon covering the nickel particles), whereas it was much more moderate and progressive for the Ce and La samples (due to suppressed formation of carbon filaments). The high carbon formation on the Zr modified catalyst was assigned to the higher particle size of the Ni^0 crystallites. The suppression of carbon formation on the La and Ce samples was assigned to the interaction between nickel and lanthana for the La-supported sample, and the enhanced gasification of carbon due to enhanced water absorption on the Ce-supported sample. In both the La and Ce-supported samples, good contact between nickel and metal oxide, and ceria and lanthana entities on top of of nickel crystallites also helped suppress carbon formation.

The interaction between the support and the active metal (as already touched on in the work of Ambroise) is also important, and can be heavily influenced by the preparation method as shown in the work of Achouri et al. [83], who investigated the effect of two different preparation methods on the performance of nickel aluminate catalysts for diesel steam reforming. The preparation methods used were wet-impregnation and co-precipitation. The catalysts were tested for 12h under diesel steam reforming conditions. Both fresh catalysts showed a $NiAl_{10}O_{16}$ phase supported on the alumina. However, the sample prepared by impregnation showed a $NiAl_2O_4$ "spinel" phase also. Both showed the γ-Al_2O_3 phase of the support, however the impregnated sample also showed some κ-Al_2O_3 phase. The lack of this phase in the co-precipitated sample was assigned to the homogeneity of the transformation of the precursor used in this method from κ-Al_2O_3 to γ-Al_2O_3 during calcination. After reforming the content of both $NiAl_2O_4$ and κ-Al_2O_3 on the impregnated catalyst were found to have increased. Reduced nickel (Ni^0) was found in both of the used catalysts, but to a much greater extend in the co-precipitated catalyst. The impregnated sample showed a more homogeneous (narrower) particle size distribution than the co-precipitated sample, which showed a wide range of 10 to 100μm. The authors state that catalytic activity is related to the reducibility of the catalyst, the surface area and the active metal dispersion. The co-precipitated catalyst showed unstable activity during the time on stream. Hydrogen production increased during the first 2h, suggesting an activation under reaction conditions, moving into a "stable" stage for approximately 4h, with high activity, assigned to the presence of metallic Ni, formed during the activation step in the presence of hydrogen:

(1.23)

This was perhaps more prevalent in the co-precipitated catalyst, due to the higher γ-Al2O3 content, the more acidic nature of which promotes the reduction. The final stage was deactivation of the catalyst, shown by decreasing hydrogen and increasing methane yields. In contrast the impregnated catalyst showed very stable performance. Studies on the used catalyst showed much greater carbon deposition

(carbon filaments, whisker carbon and carbon nano-filaments) on the co-precipitated catalyst. This carbon deposition blocked the active sites, making them inaccessible for reforming. The presence of higher quantities of metallic nickel was determined to be the cause of the increased carbon deposition on the co-precipitated catalyst. The performance of the impregnation prepared catalyst was assigned to the presence of the more active and more stable nickel spinel phase, present in low amounts in the fresh catalyst, but also formed under reforming conditions by:

(1.24)

The increase of the spinel phase was thought to be promoted by the presence of it in the fresh catalyst acting as seeds for further growth. The presence of the spinel phase in the fresh catalyst was assigned to the higher local concentrations of nickel for the impregnated catalyst, compared to the co-precipitated catalyst. In the case of the latter, this results in the nickel forming the stable $NiAl_{10}O_{16}$ phase dispersed amongst the bulk alumina support, which is then reduced during reforming to metallic nickel. Whereas in the former, the nickel is only deposited on the surface of the alumina, and forms a mixture of the same phase, along with the spinel phase, which then acts as the seeds for more spinel growth during reforming. This difference is displayed in Figure 1.7 below [83].

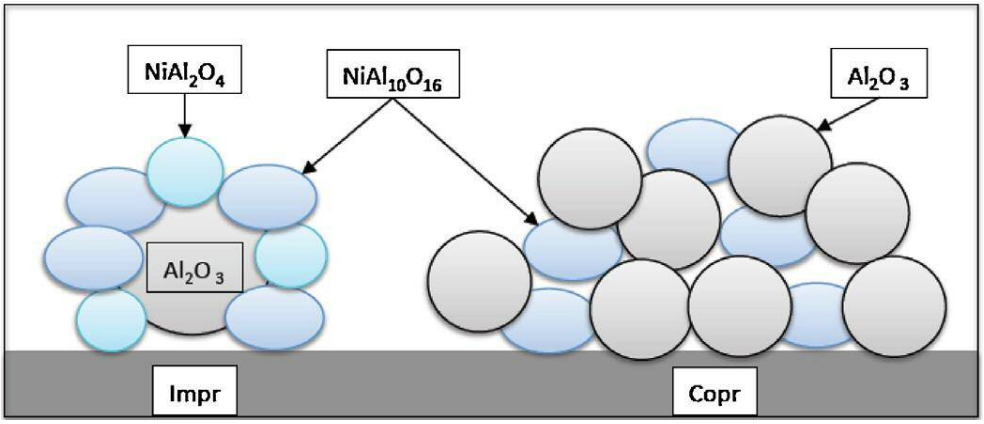

Figure 1.7: The effect of preparation method on a nickel reforming catalyst [83]

Despite the co-precipitation method producing a more homogeneous, higher surface area catalyst, the difference in metal-support interactions resulting from the choice of preparation method meant that the impregnation catalyst showed superior performance and stability.

The discussion in this section regarding the stability of exhaust gas reforming catalysts has been centered around the stability under reaction conditions. There is a lack of information in the literature regarding the effect of repeated startup/shutdown cycles of an exhaust gas reformer. As Chapter 4 in this work will show this aspect is also important to consider.

The Techniques of Exhaust Gas Reforming Testing

The specific methods and techniques used in this work will be discussed in more detail in the Experimental chapter, but as seen in the discussion on the literature above, efforts to experiment with

exhaust gas reforming often fall in to two categories. The first creates real exhaust gas, either from an internal combustion engine or fuel burner (e.g. [38] and [41]). The second, is analogous to techniques used to test other reforming applications, where the reactants are all provided from pure supplies, and used to create a synthetic exhaust gas (e.g.[43, 44, 80]), the composition of which is modelled on the real output of internal combustion engines under certain operating conditions (λ-values). This latter method is therefore similar to techniques used to test steam and autothermal reforming, where gaseous reactants come from cylinder supplies and their flow is controlled by mass flow controllers. Any liquid reactants are pumped into the reactant feed usually via syringe or HPLC pump. Liquid reactants are also sometimes sprayed into the gas mixture to achieve better mixing and a more continuous supply of the vaporized liquid reactants [50, 51]. The reactant mixtures are then pre-heated (to ensure vaporization of any liquid components), and sometimes mixed. Some set ups use specially built reactors encompassing the reactant feed lines, heating and catalyst bed [84] in one unit. The catalyst bed is sometimes a simple packed bed between quartz wool layers, but in some cases, more complex set ups are used that allow the incorporation of thermocouples throughout the catalyst bed, to monitor temperature profiles [47, 50, 85-87]. Post-reforming, if the reformed fuel is not to be passed into an engine to test engine performance and the effect of the reformed fuel on that performance, then the product gases are usually analyzed using gas chromatography. Sometimes, in-situ analysis via techniques such as in-situ XRD and DRIFTS are performed to study the reaction processes on the surface [73, 74].

In terms of the types of hydrocarbon fuels used – gasoline [38, 84] and diesel [41, 42, 49-51, 83, 84] are sometimes used in their commercial form. However to avoid experimental difficulties, surrogate fuels are often used to model these complex hydrocarbon mixtures. Issues can arise from the complex mixtures of fractions present in gasoline and diesel – which can cause difficulties in cleanly vaporizing all the fractions, as well as bring in complications associated with impurities in the fuels such as sulfur containing compounds. Both gasoline (C_5-C_{12} fractions) and diesel (C_{13}-C_{25} fractions), can be complex mixtures mostly of paraffinic, but also of olefin and aromatic compounds. The precise composition can depends on its production [84, 88].

In the case of using surrogate fuels, the choice of surrogate can influence the results from activity tests. In general, the longer the hydrocarbon chain – the lower the activation energy for reforming [70], the lower the ignition temperature for oxidation (at a set air/fuel ratio) [89], and the increased likelihood of carbon formation [76]. In addition, both aromatics and olefins are harder to reform and more prone to carbon formation than paraffinic hydrocarbons [85, 90]. The use of surrogate fuels for activity testing generally fall into three categories: (1) choosing just a single compound, that either has desirable properties, is the most common fraction present in gasoline or diesel, or matches the average molecular weight of gasoline/diesel, (2) using a combination of paraffinic, olefin and aromatic compounds, in similar proportions to those found in the commercial fuels, or finally (3) similar to 2, but where the mixture is chosen on the basis of showing similar reforming results to the commercial fuel (so matching

combustion/reforming properties). In addition, some efforts will also try to model the effect of sulfur compounds by including such compounds in the reactant feed.

In the case of single compound modelling of gasoline, which was the initial focus of this work, iso-octane is often used as a surrogate [14, 31, 44, 48, 80], since it is an important component of commercial gasoline (it is the standard used to create the octane rating of various fuels). Propane has also been used as a surrogate, since it avoids the need for vaporization of the fuel [36, 43], and due to its short chain length is more difficult to reform. However due to its shorter chain length, it is also less prone to carbon forming reactions, if not actually immune [91]. More complex mixtures of hydrocarbon compounds, more closely matching the properties of commercial gasoline and diesel have also been reported [46, 61].

Analysis of the catalyst itself, both pre- and post- reforming is carried out using a range of techniques. Amongst those used in the works discussed in previous sections are: X-Ray Diffraction, X-Ray Photoelectron Spectroscopy, Scanning Electron Microscopy, Tunneling Electron Microscopy, Temperature Programmed Reduction/Adsorption/Desorption/Oxidation, Thermo Gravimetric analysis, and BET surface area analysis. Combinations of these techniques are used to probe the physical nature, and chemical composition of the catalyst, both pre and post reactivity testing.

Project Aims

As discussed in this introduction, exhaust gas reforming has the potential to improve fuel economy and emissions from internal combustion engine vehicles, particularly in the gas of gasoline fueled spark ignition engines as shown in the recent works of Chang et al. [54, 55] and Leung et al. [35] discussed in this chapter.

The key challenge is to develop suitable catalysts that show high activity, producing hydrogen in quantities that would be beneficial (5-20 % by volume of the reformed gas), over a lifetime equivalent to existing automotive catalysts (>100,000 km), and doing so using materials that do not come at a punitive cost. Such a catalyst would ideally also show flexibility in fuel choice (gasoline, diesel and bio-fuels for example). If this can be achieved, then the technology has the potential to be a useful interim technology in the transport sector while more comprehensive systems for renewable and clean transport mature.

The aim of this study therefore was to investigate and provide insights into these catalytic aspects of exhaust gas reforming, with particular focus on:

- Producing an exhaust gas reforming catalyst with base metals as the active components, and compare this catalysts performance in terms of activity and durability to a commercial reforming catalyst based on precious metals.
- To compare the performance of these catalysts with both gaseous and liquid hydrocarbon fuels. Initially this would be done using single component surrogates for gasoline, but then to build up the complexity of the model fuels, culminating in the testing of commercial gasoline.

- The above would require modifications to a laboratory testing rig, and a suitable procedure to be developed, in order to allow the testing of liquid hydrocarbon fuels.

It was hoped that the work in this study would develop a solid understanding of the potential of base metal catalysts for exhaust gas reforming of various hydrocarbon fuels. Such catalysts, though popular in other industrial reforming applications (such as methane steam reforming), are not often chosen for applications like exhaust gas reforming due to their inferior resistance to deactivation and lower activity, instead expensive precious metal formulations are used. This study therefore aims to determine whether cheaper base metal formulations can meet the demands of exhaust gas reforming, a positive result would enhance the attractiveness of the technology.

Chapter 2 - Experimental

This chapter covers the core techniques and methods used throughout the work. Additional details, specific to individual chapters, will be described in the relevant sections.

Catalyst Preparation

Note: All percentage values with respect to catalyst formulation refer to percentage by weight.

The Nickel Catalyst

The base metal catalyst prepared for this work was 10 % nickel supported on ceria-zirconia, and was prepared by standard wet impregnation. For this method, the appropriate amount of nickel nitrate salt ($Ni(NO_3)_2.6H_2O$ – Alfa Aesar), to achieve 10 % by weight of the resulting catalyst, was dissolved in a minimal quantity of HPLC grade deionized water (VWR) to dissolve the salt in a round bottomed flask. The appropriate quantity of ceria zirconia support (58.2% CeO_2 – 41.2% ZrO_2, Solvay Rhodia), was then added to the solution, which was then left gently stirring overnight. The water was then removed via rotary evaporation, at a pressure of <200 bar, and a bath temperature of 80 °C. The pressure was decreased in 50 bar intervals from atmospheric pressure, until smooth continuous evaporation of the solvent was observed. Once the excess water had been removed, leaving a paste, the sample was then dried in an oven at 110 °C overnight. Upon removal from the oven the sample was then calcined in free air, heated at a ramp rate of 10 °C/min, up to 500 °C, where it was held for 3 hours, before cooling to room temperature. The sample was then ground into a powder, before being pelletized, with pellet size of 0.47-0.85 mm (corresponding to the use of 20 and 40 mesh sieves).

Example calculation for nickel loading:

Hence to obtain roughly 10 % loading of nickel in a 10 g sample of catalyst, 4.96 g of the nickel nitrate salt were dissolved in the minimal quantity of water, along with 9 g of the CeO_2-ZrO_2 support.

For convenience, this catalyst will often be referred to by the abbreviated name “Ni10CZ”. Where the 10 refers to the 10 % loading of nickel, and CZ to CeO_2-ZrO_2.

Based on the discussion in the Introduction chapter, nickel was chosen as a suitable base metal catalyst due to its high selectivity towards hydrogen production during reforming applications. The impregnation method of preparation was deemed appropriate due to the high loadings of nickel required, along with

the techniques simplicity for preliminary stage testing. Furthermore, as discussed in Chapter 1, though the technique may not be as precise as other techniques, it has been shown to produce active and stable reforming catalysts.

The Rhodium Catalyst

In the final part of this work, a 1 % rhodium catalyst, supported on ceria zirconia, was also prepared. It will often be referred to in the abbreviated form as Rh1CZ. It too was prepared via the wet impregnation method described above, with some alterations. The alterations were that the appropriate quantities of rhodium (III) salt ($Rh(C_5H_7O_2)_3$, or $Rh(acac)_3$ – Alfa Aesar) were dissolved in toluene, rather than water. The resulting powder catalyst was also pelletized as above.

The reason for choosing to prepare this catalyst will be made clear later.

Johnson Matthey Commercial Reforming Catalyst

A benchmark industrial reforming catalyst was sourced from Johnson Matthey. This was in the form of a cordierite monolith substrate, with the catalytic components washcoated on the surface. The catalyst was a proprietary formulation, therefore its exact composition was unknown, however it was known to contain relatively high loadings (1-2 %) of platinum and rhodium, supported on ceria zirconia doped alumina. This formulation was used throughout the project as the benchmark for performance, against which any developed catalysts would be compared. The original monolith was cut into two differently sized pieces, a larger unit which was approximately 1/3 bigger than the smaller unit. It should be noted that neither of the units were fresh; rather they had been used for a number of projects previously.

The larger monolith was used for the bulk of this project and for convenience will be referred to as the PM catalyst in the rest of this work (for precious metal).

Catalyst Activation

The PM catalyst was used as supplied, without any pre-activation. Both dilute and pure hydrogen pre-reduction treatments were found to have no beneficial effect on the performance of the nickel catalyst. Therefore, no activation methods were throughout this work.

Catalyst Characterization

Several characterization methods were used in combination in order to help to explain the observed performance of each catalyst. Specialist techniques are required in order to probe the catalytically important surface properties, both physical (e.g. surface area, active metal dispersion) and chemical (e.g. species present and component interactions) of supported metal catalysts. Where relevant, these methods were carried out on fresh and/or used catalysts. A brief discussion of the theory and the information obtained from these methods is discussed here.

Brunauer-Emmett-Teller Surface Area (BET)

The BET method allows measurement of a sample's surface area through its ability to adsorb a measureable quantity of known gas [92-94]. Simply put, the more gas the sample adsorbs, the higher the surface area and vice versa.

Adsorption of molecules in the fluid phase, onto those in the solid phase is brought about by the interaction between those molecules. Two types of forces can give rise to this (1) Physisorption and (2) Chemisorption. The latter involves chemical bonding, and hence can involve some form of chemical reaction, and tends to occur at reactive parts of the solid surface. Physisorption on the other hand is a physical process, and therefore has low specificity. The lack of chemical bonding/reactivity involved means the physisorbed molecule keeps it identity, and can return to the fluid phase through desorption.

It is this physisorption of gas that is used to determine the surface area of solids. The key theoretical underpinnings of this technique were first provided by Irving Langmuir's description of monolayer formation during adsorption, which was then extended by Brunauer, Emmett and Teller (BET) in 1938. BET theory has since become an accepted standard procedure for the determination of surface are, even if it rests on some simplistic assumptions (such as the surface being homogenous and the adsorbed molecules not interacting with each other).

The use of BET theory to determine the surface area of substances is based on the observation that the adsorption isotherms (a plot of the amount of adsorbate taken up by the adsorbent, at a constant temperature, as the pressure/concentration of the adsorbate is increased) of a range of gases were often S-shaped (see Figure 2.1 below of a Type II Isotherm).

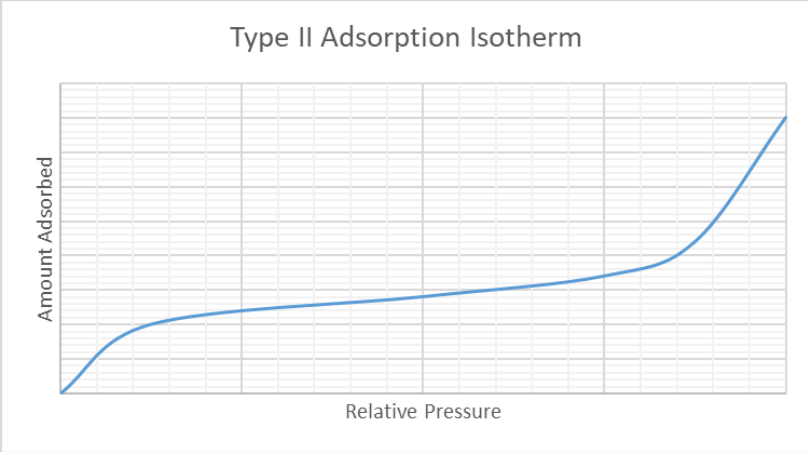

Figure 2.1: Type II adsorption isotherm

They proposed that the monolayer was fully formed at the first inflection point in such an isotherm, and that therefore if the quantity of adsorbate taken up until that point was determined then the monolayer capacity of the adsorbent could be calculated. This monolayer capacity could then be used to calculate the surface area of the adsorbent if the cross sectional area of the adsorbate (nitrogen) was known.

(2.1)

In this project a Quantachrome Quadrasorb surface area and pore size analyzer was used. A small quantity (approximately 0.2 g) of the sample to be analyzed was first degassed in order to remove any contaminants. This was done at 125 °C for 1 hour under vacuum.

The sample was then placed in the analyzer, evacuated and cooled to cryogenic temperatures by submersing the sample tube with liquid nitrogen. The sample was then exposed to the adsorbate gas, in this case nitrogen, initially at low pressure. The amount of gas adsorbed was then measured as the pressure of gas was further increased, until a monolayer was formed (as the pressure of gas is increased, so does the amount adsorbed to the surface). This was then plotted as a BET isotherm plot, to obtain a value for the monolayer capacity of the sample. This monolayer capacity, along with Avagadro's constant and the cross sectional area of the adsorbate can yield a value for the BET surface area (carried out automatically by the computer program, calculated as shown in Eqn. 2.1).

This method was used to analyze both fresh and used catalysts. Surface area is intimately linked to catalytic performance, in that the more exposed active sites there are, the higher the potential activity. It is therefore a key analytical technique to help explain catalytic performance [19].

Temperature Programmed Reduction (TPR)

TPR measures the reducibility of a solid sample as the temperature is changed. Most commonly this is performed using hydrogen gas as the reducing agent, which is flowed over the solid sample as the temperature is increased, at a pre-determined rate, to a pre-determined maximum [19, 95, 96].

The off-gases are analyzed to determine the quantity of hydrogen (usually via a Thermal Conductivity Detector or TCD), which will then show peaks, representing specific reduction events of species in the solid sample.

The occurrence of the peaks at certain temperatures, and nature of these reduction events (shape/size of peaks) can yield information on the chemical nature and environment of species present in the solid, such as its chemical identity and interaction between components.

Redox properties are crucial to catalytic activity, and exhaust gas reforming is no exception. As discussed in the Introduction, the active steam reforming species in a Ni/CeO_2 is the metallic phase of the active component (e.g Ni^0) [73].

Therefore, this is a useful technique to analyze at what temperature the catalyst is reduced, and to what extent. More detailed TPR analysis can give insight into the extent of metal-support interactions (since the metal oxide support may also be reduced) as discussed in the Introduction. The reducibility of a sample can also be influenced by other factors such as its surface area and particle size.

In this project a Thermo TPDRO1100 instrument was used. A small quantity of the sample in question (0.05 g) was first pre-treated to remove containments. This was done in flowing argon gas, at 110 °C

(heating ramp rate of 20 °C/min) for 45 minutes. Then 10 % hydrogen in argon was passed over the sample as the temperature was raised at 15 °C/min up to 800 °C. The off-gases were continuously measured by TCD, which can detect the presence, and quantify the levels of hydrogen gas. This was then be plotted as hydrogen consumption against temperature, to yield the reduction peaks which signify a reduction event (for example Ni^{2+} to Ni^{0}).

Thermogravimetric Analysis (TGA)

TGA is a technique whereby the sample is placed on a precision balance, and its mass is continuously, and precisely measured, in a known atmosphere, as the temperature is increased linearly. Any weight loss or weight gain events during the treatment will therefore be detected. Data can be presented as a thermogravimetric (TG) curve, which shows the percentage weight change against temperature [19, 97].

Used on fresh catalysts, this technique can give information on the thermal stability and purity (for example if the precursor salt used in preparation has completely dissociated). When compared to used catalysts it can reveal any changes that occurred during testing, yielding information on any potential poisons or species adsorbed to the surface. The removal of these species and impurities during the analysis will be observed as weight loss events. In addition, if carried out in an oxidizing atmosphere, then oxidation of the active catalytic components can also be observed as weight gain events.

In this project the thermogravimetric analysis was carried out using a PerkinElmer TGA 4000. Each run used approximately 20-30 mg of powdered sample, which were loaded into a ceramic crucible. The heating program was carried out in air (50 mL min^{-1}), from 30 °C to 800 °C, with a ramp rate of 5 °C/min.

Powder X-ray Diffraction (XRD)

XRD is a technique used to identify any bulk phases present in a sample by comparison to pure reference samples – this is known as fingerprinting. Quantitative information on the crystal lattice structure can be obtained from the Bragg Equation, as well as estimates of the particle size via the Scherrer equation (see later) [19, 95, 98-100].

Crystalline solid state materials consist of regular arrays of atoms, with the distances (lattice spacing) between these atoms determined by their identity. If radiation with wavelength closely matching the spacing between atom layers is passed through such a solid sample, then a diffraction pattern, which is characteristic of the phases present will be obtained. This is the basis for XRD, since x-rays meet this criteria for wavelength.

The x-rays are produced by cathode ray tube. This is done by heating a filament under voltage which produces electrons which are then accelerated towards a metal target.

The electrons have sufficient energy to knock out other electrons from the core shells of the metal target. Electrons from the outer orbitals then drop down to fill these vacancies, releasing energy as they do so

in the form of photons. In the case of the metal target used in cathode ray tubes, the energy of the photons corresponds to wavelengths in the x-ray region of the spectrum.

These waves are directed at the sample to be analyzed, the interaction of the waves with the solid crystal lattice of the sample causes a scattering of the waves in a diffraction pattern which is characteristic of the phases present in the sample. The diffraction pattern is obtained by scanning over a range of incident x-ray angles.

If Bragg's Law is satisfied (see equation below) then interaction between the incident rays with the sample produces constructive interference and hence peaks in the resulting spectra. Bragg's Law relates the x-ray wavelength to the diffraction angle and lattice spacing of the crystal, where λ is the wavelength of the x-rays, n is an integer, θ is the angle of incidence of the x-rays, and d is the spacing between atom layers.

(2.2)

The diffracted rays are analyzed by a detector, and the data presented as 2θ against the intensity of the detected rays, producing a range of peaks of varying intensity at certain angles. These peaks have characteristic position and intensity relating to the phase the wave interacted with, and can therefore allow the phase to be identified by comparison to a pure reference sample.

Quantitative information such as the crystal unit cell constants and crystal spacing can be obtained from d in Eqn. 2.2. Further quantitative information can be obtained from the line widths (β) of the peaks, using the Scherrer Equation, which relates the crystallite size to the inverse of β, so the smaller the crystal size the broader the peak. This is because the smaller the crystallite size of a sample in an XRD experiment is analogous to decreasing the slit size in a simple single slit diffraction test – the result is a less well-defined (broader) diffraction pattern. The Scherrer can be seen in Equation 2.3 below:

(2.3)

As before in the Bragg Equation, λ is the wavelength of the radiation used and θ is the Bragg Angle. K is a constant which depends on the shape of the crystallite.

The line width, β is normally given using the Full-Width-at-Half-Maximum (FWHM) in radians of the diffraction line ($\beta_{1/2}$). This method therefore allows estimation of the particle size of a sample.

The basic set up for powder x-ray diffraction is shown below [101].

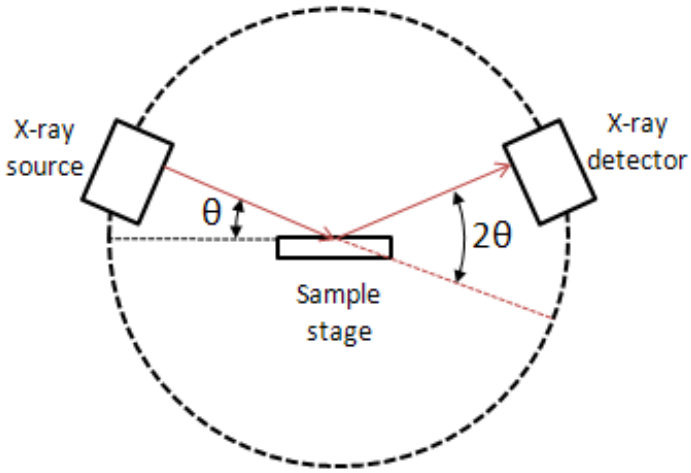

Figure 2.2: A basic powder X-ray diffraction set up [101]

In this project, XRD data was taken using a PANalytical X'PertPRO X-ray diffractometer. The x-ray source was CuKα, which produced radiation of wavelength 1.5418 Å (from 40 kV and 40 mA), with a nickel filter. The data was collected over the range of 5 ° to 80 °, with steps of 0.0167 °, and a rate of 150 seconds per step. The data was then analyzed within the software to identify the phases by comparison to reference data, as well as for estimates of crystallite size using the Scherrer equation.

Catalyst Performance Testing

Initial Reactor Set Up

The initial test rig, prior to the adaptations described later, was suitable for testing the exhaust gas reforming of gaseous hydrocarbon fuels. The gases for the synthetic exhaust gas (N_2, O_2, CO_2 and CO) were provided from cylinder supplies, along with the surrogate fuel (C_3H_8). Each individual gas flow rate (and therefore the composition of the synthetic exhaust gas) into the reactor was controlled by Bronkhorst Mass Flow Controllers (MFC's). HPLC grade water (VWR) was pumped directly into a furnace from a medical syringe pump, upon which it was vaporized and mixed with the gas flow. This synthetic exhaust gas and fuel mixture was then passed through a reactor inside a vertical tube-furnace, which consisted of three separate heating zones, of which each section could be heated independently to, and held at, a desired temperature. The reactor was positioned so that the catalyst bed was situated in the final section of the furnace. The temperature in the catalyst bed was monitored by K-type thermocouple, which was situated as close to the bottom of the catalyst bed as possible. The product gases then exited the reactor, and any remaining water vapor was crashed out in a water trap. The gas and liquid lines were made with stainless steel tubing and Swagelok fittings.

The product gases were then analyzed by gas chromatography (GC), which will be discussed in the next section.

A diagram of the setup is shown below in Figure 2.3:

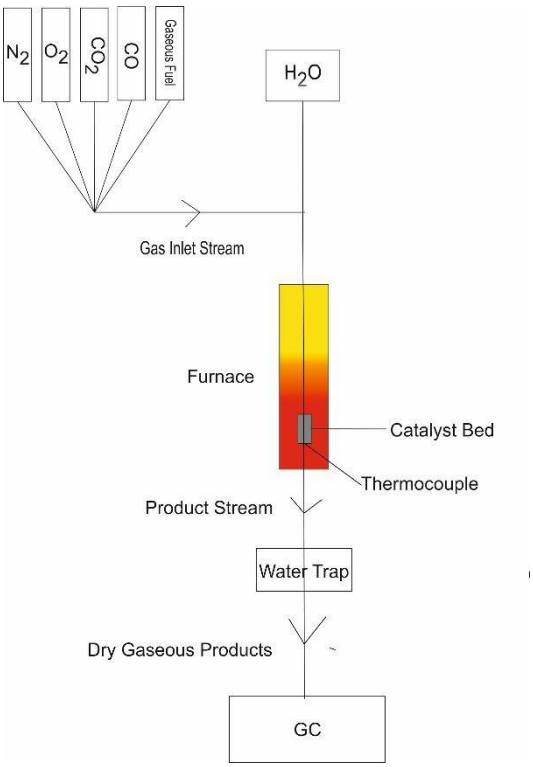

Figure 2.3: The initial reactor set up

Gas Chromatography

The GC used in this project was a Bruker 450 Gas Chromatograph. Gas chromatography is a widely used technique to identify and quantify levels of individual gases in a gaseous mixture.

The gas mixture that is to be analyzed (the mobile phase) is carried by a carrier gas through a narrow column or columns, that are packed with a stationary phase. The different components of the gas mixture are then separated as they travel through the column based on their individual affinity for the particular stationary phase in use. The time it takes the individual components to travel through the column is called the retention time. The higher the affinity of a component for the stationary phase, then the greater the retention time and vice versa.

Depending on the components of the gas to be analyzed, different detectors are then used to identify and quantify the mixture. The detectors respond in predictable ways to the presence of the compounds, which allows identification and quantification. Quantification is enabled since the intensity of response is proportional to the quantity of the individual compounds. Identification is enabled based on the retention time. The chromatogram is reported as detector response against retention time, with responses showing as individual peaks. The detector response is reported as a peak area, which is proportional to the amount of that specific analyte present in the sample. Hence gases can be identified, and quantified, in terms of a volume percentage (on a dry basis since any liquids are removed prior to the GC), through calibration, based on their retention times and peak area.

The system used in this project was set up to allow continuous (online) analysis of complex gas mixtures. A schematic for the system is shown in Figure 2.4. It consisted of three analysis “channels”. The first

channel detected hydrogen, the second permanent gases (N_2, O_2, CO_2 and CO), and the final channel gaseous organic components. The set up shown below made possible the separation, detection, identification and quantification of multiple components through the use of a series of valves, loops, columns and detectors. Prior to sample injection, the gases continuously flow through the system from the reactor, and exit to vent, while simultaneously filling up the sample loops of each channel. Then the measurement processes is initiated with injection of the sample from the loops into the columns, and on to the detectors. The valves then return to position to allow the filling of the sample loops, and exit of gases to vent, and this cycle repeated for each measurement.

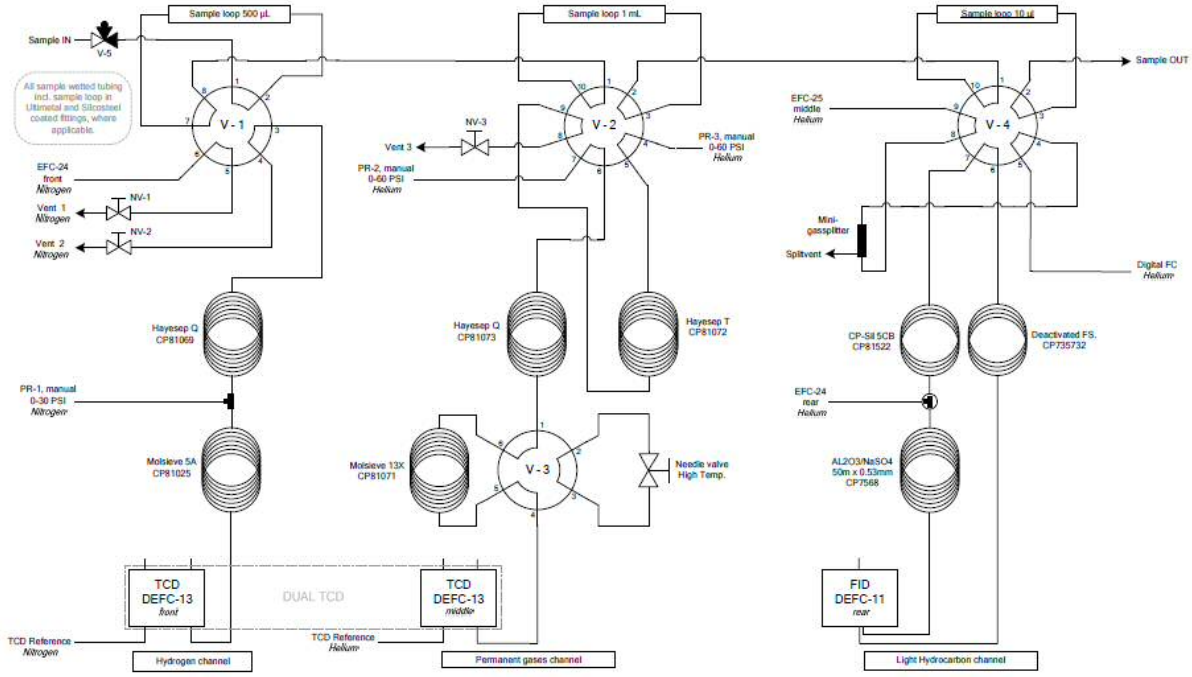

Figure 2.4: Schematic of the Bruker 450-GC system

The components in the first two channels were detected by Thermal Conductivity Detectors (TCDs). TCDs consist of two filament wires in a temperature-controlled cell, which heats up when a current passes through them. A TCD registers the presence of an analyte gas through the difference between the high thermal conductivity of the carrier gas, and the lower thermal conductivity of the analyte. When the analyte gas passes through the column, the thermal conductivity of the cell as a whole is reduced, resulting in the filament heating up and the corresponding change in resistance is measured. Hence, the presence of the gas is detected at a particular time, and the size of the response is proportional to the quantity of any analyte present in the cell.

The final channel, for the detection of organic compounds, uses a Flame Ionisation Detector (FID). This uses a hydrogen-air flame, which burns the sample molecules as they pass through, producing a spike in the level of ions reaching the detector. A high potential difference is set up across the detector so as to attract the ions to a plate. These ions produce a detectable current. This current is proportional to the

concentration of the molecule being burnt, and can be identified by the time the signal is registered at the detector.

Calibration and Data Collection

The identity and quantification of the gases was enabled by calibration. This was done by analyzing mixtures of gases in known proportions. The calibration mixtures were created using the lab supplies and mass flow controllers. The mixtures by-passed the reactor, so as to enter directly into the inlet of the GC, to avoid contamination.

Initially, single component gas flows (of H_2, N_2, O_2, CO_2, CO and C_3H_8) were analyzed, so that the retention time of each component could be recorded, and therefore peaks in later chromatograms could be identifies based on these retention times.

Then various known mixtures of the above gases were used so that each gas was analyzed at three different quantities, in terms of volume percentage of the calibration mixture. The peak areas for each component detected were recorded. A calibration plot was then produced with peak area response on the y-axis and the known % value by volume of that gas in the calibration mixture on the x-axis. The resulting plots yielded a straight line graph.

During catalyst performance testing, the peak areas of the main components of the product gas (H_2, N_2, O_2, CO_2, CO and C_3H_8) were recorded. Then through comparison with the calibration data, this enabled the quantification of the product gas composition. The calibration plot was in the form:

(2.3)

(2.4)

Re-arranging, and using the gradient and intercept of the line of best fit from the calibration plot for each individual gas, allowed the input of a peak area obtained during performance testing to be converted to an output of the % by volume of that gas in the product gas sample being analyzed (carried out in Microsoft Excel).

(2.5)

During the initial calibration work it was discovered that the detector response was slightly dependent on the flow rate of the gases entering the GC, in that as the flow rate increased so did the detector responses. The size of this dependence varied for each of the gases. This was unexpected, and attempts to fix this were unsuccessful. Hence it was decided that the most suitable option, given the time constraints, was to work around this dependence by carrying out the calibrations at each total gas flow rate value that was to be used in performance testing, the specifics of which will be given later.

Reactor Modification for Liquid Fuel Testing

The work for Chapter 4 was carried out prior to the modifications. Though the above set up was suitable for testing with gaseous fuels, it required significant modification to supplement it with the capability to test liquid fuels. At issue was how best to deliver, vaporize and mix the liquid fuel with the synthetic exhaust gas. The aim was to create a system that could function with both single component liquid fuels, but also cope with multicomponent fuels such as gasoline and diesel. Fuel delivery needed to be continuous and as smooth as possible (i.e. avoid pulsing). It was therefore decided that the best way to deliver the fuel was through a spray nozzle directly into the hot synthetic exhaust gas mixture.

Liquid Fuel Delivery via Spray Nozzle

A spray nozzle was chosen as the best method to provide smooth and continuous fuel deliver and mixing with the exhaust gas stream. Due to the low liquid flow rates used on this laboratory scale set up, simple shaping nozzles were not suitable.

Therefore an ultrasonic spray nozzle system was purchased from Sono-Tek Corporation. Fuel was pumped by syringe pump into a specially designed Microflow Ultrasonic Atomizing Nozzle. The ultrasound vibrations within the nozzle were created by an Echo Ultrasonic Generator, which atomized the liquid passing through the nozzle. This allowed for the production of a controlled, fine mist spray of the liquid. The level of dispersion was controlled by simply adjusting the frequency with the ultrasonic generator.

The upper section of the nozzle body consisted of an inlet for the liquid and connections for the echo ultrasonic generator. The mechanism for the generation of the vibrations were contained in the nozzle housing, which involved the use of piezoelectric crystals. The nozzle connected and sealed to the furnace inlet via flange and stainless steel fittings. K-type thermocouples monitored the temperature of the electronics in the nozzle housing, and air cooling ports allowed that temperature to be kept at around 30 °C during operation [102].

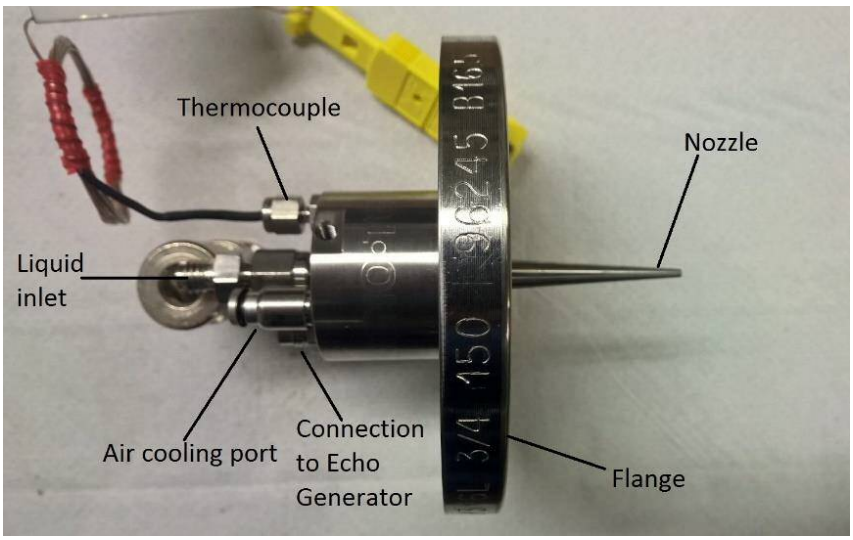

Figure 2.5: Sono-Tek Microflow Ultrasonic Atomising Nozzle

Preliminary Spray Nozzle Testing

In order to optimize the use of the spray nozzle, some preliminary tests were carried out. Replicas of potential furnace inlet set ups were made with equivalent transparent plastic tubing and fittings. The spray nozzle, along with an inlet for a gas flow, were attached to the tubing via different junctions. The nozzle was operated with a water and fluorescent dye mixture. This allowed the spray mist to be easily observed. The effect of echo generator frequency/power load, gas flow rate and orientation of the nozzle relative to the gas flow was tested.

The optimum frequency and power setting for the flow rate range likely to be used during testing was found to be 48 kHz and 3 W. The optimum set up arrangement was one where the spray nozzle was situated directly above, and as close to the furnace inlet as possible, with the gas inlet entering through a T-junction perpendicular to the spray nozzle.

Modifications to the Reactor

Modifications were made to the reactor set up shown in Figure 2.3 for the purposes of incorporating the spray nozzle, enabling testing at higher temperatures and to further assist in the testing of liquid fuels.

The furnace inlet was altered so as to allow the optimum arrangement for liquid fuel delivery described in the previous section. This required the shifting of the water inlet further upstream in the gas inlet lines, and the incorporation of a T-junction as close to the top of the furnace as possible. This was in order to achieve vaporization and mixing of the water with the hot gas stream prior to the spray nozzle. The gas lines were wrapped in heating tape and insulated. The water inlet was orientated at 90 ° to the gas stream to facilitate mixing. The heating chord was also incorporated around the T-junction where liquid fuel spray and gas stream mixed before entering the furnace.

Modifications were also made to the furnace to allow much higher reaction temperatures to be tested. Thermocouples were incorporated at various points in the system, so as to allow the monitoring of temperature to ensure that any liquid components were being vaporized. A condenser and waste pot were included post-furnace, and positioned directly below it, so as to ensure that any unconsumed water and liquid hydrocarbon fractions were crashed out prior to the GC.

This set up still allowed testing with gaseous fuels such as propane, simply by removal of the spray nozzle, and the use of a stopper to seal the spray inlet.

A diagram of the modified set up is shown below in Figure 2.6:

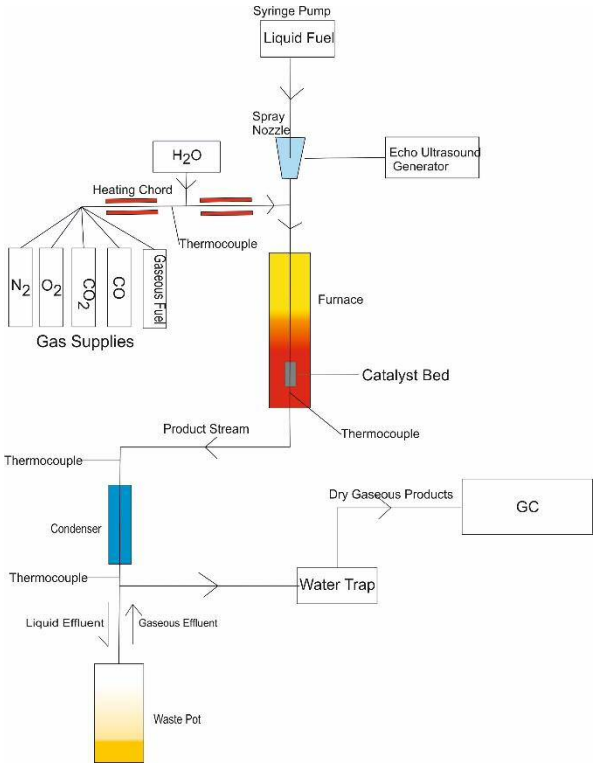

Figure 2.6: The modified reactor set up

The Standard Performance Testing Regime

Some of aspects of the testing conditions (GHSV, λ-value etc.) were discussed in the Introduction chapter in general terms, however the specific standard testing conditions used in this work will be described here.

Fuels and Synthetic Exhaust Gas Composition

Propane and iso-octane were used as surrogate fuels for gasoline in this work. They were both tested with the nickel, PM and rhodium catalysts. As discussed in the Introduction, propane and iso-octane have previously been used as surrogates for gasoline.

Some key properties of both these fuels are shown below in Table 2.1, along with that of gasoline for comparison [38, 51, 52, 103-105].

	Fuels		
	Gasoline	**Propane**	**Iso-octane**
Information	C5-C12 paraffinic, olefin and aromatic fractions of crude oil, with contaminants such as sulfur compounds.	Single component gaseous fuel.	Single component liquid fuel. Important fraction in gasoline – standard against which octane rating is measured.
Chemical Formula	$C_nH_{1.92n}$	C_3H_8	C_8H_{18}
Molecular Mass /g mol^{-1}	~100	44	114
Boiling Point /°C	<200	-42	99

Table 2.1: Information & properties of gasoline and the surrogate fuels used in this project

The synthetic exhaust gas mixture was modelled on the output of a gasoline fueled spark ignition engine under low, medium and high load, corresponding to λ-values of 1, 1.5 and 2.12 respectively (used by Peucheret et al. [43]).

For testing with propane as the surrogate for gasoline the reactant feed compositions (by % volume) at these conditions are given below in Table 2.2, where the quantity of propane added to the synthetic exhaust gas is chosen to consume all the oxygen and steam present in the exhaust gas. In the case of iso-octane, at least initially, the compositions were identical.

% by volume	**λ=1**	**λ=1.5**	**λ=2.12**
O_2	0.4	6.8	10.7
CO_2	12.9	9.3	5.9
CO	0.3	0.14	0.14
H_2O	12.5	8.3	5.6
N_2	71.9	70.46	69.66
C_3H_8/C_8H_{18}	2	5	8

Table 2.2: Synthetic exhaust gas and fuel mixtures

Note: These proportions are of the total reactant flow, rather than the dry reactant flow, which would be detected by the GC after the vapor fractions have been condensed in the waste pot and water trap.

Later experiments, which varied these experimental conditions, will be described in the relevant sections. The resulting O_2/Fuel, O_2/C, H_2O/Fuel and H_2O/C ratios, for each condition and each fuel are shown below in Table 2.3 and 2.4.

C_3H_8	H_2O/C_3H_8	H_2O/C	O_2/C_3H_8	O_2/C
λ=1	6.25	2.08	0.20	0.07
λ=1.5	1.66	0.55	1.36	0.45
λ=2.12	0.70	0.23	1.34	0.46

Table 2.3: Key reactant ratios with propane as the surrogate fuel

C_8H_{18}	H_2O/C_8H_{18}	H_2O/C	O_2/C_8H_{18}	O_2/C
λ=1	6.25	0.78	0.20	0.03
λ=1.5	1.66	0.21	1.36	0.17
λ=2.12	0.70	0.09	1.34	0.16

Table 2.4: Key reactant ratios with iso-octane as the surrogate fuel

As mentioned previously, the balance of gases in the mixture was controlled by mass flow controllers. However, in the case of both water and iso-octane, they were controlled by syringe pump, which operates in liquid flow rates. The % by volume values above relate to gas volumes, therefore an estimate of the expansion of these liquids upon vaporization was used to calculate an approximation for the liquid flow rate required to obtain the desired gas flow rate (the conversion factor). The method for water was as follows:

Given the density of water = 1g/mL [106], the liquid volume of 1 mole is:

Assuming it is an ideal gas, the gaseous volume of 1 mole is:

Therefore, the expansion associated with vaporization from water to steam is:

So,

And,

The equivalent approximation for iso-octane would take into account the fact it's density is 0.69 g/mL [103], instead of 1 g/mL, therefore:

Given the density of iso-octane, the liquid volume of 1 mole is:

Again assuming ideal gas applies, the gaseous volume of 1 mole is:

Therefore, the expansion from liquid to vapor is given by:

So,

And,

So for example, if 5 mL/min of steam and iso-octane vapor each was required, this would correspond to 0.0004 mL/min and 0.035 mL/min liquid water and liquid iso-octane provided by the syringe pumps.

The Gas Hourly Space Velocity

In order for the comparison between catalysts to be fair, all samples were tested at the same GHSV. The equation for GHSV is given below:

(2.6)

Due to experimental limitations on the maximum gas flow rate possible, this value was chosen to be as high as was possible for the large PM catalyst (since the precious metal reforming monolith has a set volume, whereas the quantity powdered/pelletized samples could be varied to obtain desired GHSV values). Given the volume of the PM catalyst, and the maximum gas flow rate obtainable, this resulted

in a GHSV of approximately 8,500 h^{-1} with the large monolith, at 175 mL min^{-1} total gas flow rate. This is lower than found in real exhaust systems (see Introduction chapter), but was as high as possible with the experimental set up available (due to the maximum flow rates of the mass flow controllers).

In order to match this GHSV, and to avoid higher back pressure in the system associated with packed bed catalysts, the powdered/pelletized samples were tested at a total gas flow rate of 50 mL min^{-1}. Hence, the volume of catalyst required to obtain a GHSV of 8,500 h^{-1} was 0.35 mL. The density of the catalysts were obtained by a simple experiment of placing a certain mass of catalyst in a volumetric cylinder, and recording the volume. This allowed the calculation (through Density = Mass/Volume) of the mass of catalyst required to obtain the desired volume, and hence the desired GHSV.

The density of the catalysts, when powdered was found to be around 1 g/mL, and when pelletized was found to be roughly 1.3 g/mL. This meant that for the pelletized samples, around 0.46 g of sample was required for each test to obtain a GHSV of 8,500 h^{-1} at 50 mL min^{-1} total gas flow rate.

As discussed previously, this therefore meant that calibration of the GC was carried out at 175 mL/min and 50 mL/min total gas flow rates.

Temperature Range

Prior to the reactor modifications, the catalysts were tested in the range of 150 °C to 400 °C (Chapter 4), and after the modifications the tests were carried out in the range of 150 °C to 600 °C (Chapter 5 & Chapter 6), as measured by the thermocouple situated immediately below the catalyst bed.

Testing Regime for Gaseous Fuels

For gaseous fuels, the following testing procedure was used. The catalyst was loaded into the reactor tube between quartz wool layers, positioned so that the thermocouple would sit as close as possible to the bottom of the catalyst bed. The synthetic exhaust gas flow, minus steam, was then initiated using the mass flow controllers. The heating tape and furnace were then heated to 120 °C, upon which the water was then injected into the hot gas flow via syringe pump, so as to ensure vaporization. The furnace temperature was then raised further until the bed temperature was 150 °C, upon which the first measurement of the effluent gas was taken, by GC. The temperature was then raised further until light off was observed – indicated by a rise in bed temperature not resulting from an increase in the furnace temperature (which is caused by the exothermicity of the initial oxidation reactions). GC measurements were then carried out immediately post light off. Further GC measurements were then carried out as the temperature was raised further, typically at 100 °C intervals, with three measurements taken at each measurements.

The method of shut down was an initial area of focus, and will be described in Chapter 4. In general, though, the furnace heating was first turned off and the reactants drained from the system while the catalyst cooled back down to room temperature.

Testing Regime for Liquid Fuels

The testing regime for liquid fuels was as above for gaseous fuels, except that fuel and water injection were delayed until the inlet line and catalyst bed temperatures were approximately 50 °C above the boiling point of the liquid fuel (in the case of multi-component fuels, the equivalent should be the highest boiling point fraction found in the mixture), due to the presence of some cold spots in the inlet when the spray nozzle was attached to the set up. So in the case of iso-octane, fuel and water injection were delayed until the system temperature had reached around 150 °C and above.

Data Collection, Analysis, Errors and Presentation

As briefly mentioned, the GC data was collected pre-light off, post-light off and at regular temperature intervals thereafter. This generally corresponded to data being collected at 150 °C, 200 °C, 300 °C, 400 °C, 500 °C and 600 °C. Other temperatures were also sometimes analyzed, depending on the specific experiment. Three GC measurements were carried out at each temperature. Each catalyst was usually tested for a minimum of three consecutive full day tests (corresponding to three instances of 8 hours on stream), with corresponding start up and shutdown cycles.

The data was collected and analyzed in Microsoft Excel. The raw results were in the form of vol.% of the dry product gas as measured by GC. The data was averaged over three consecutive measurements at each temperature point.

This raw data was used to calculate other valuable metrics of catalyst performance such as the hydrogen yield, propane conversion (iso-octane conversion was not possible due to experimental limitations in detecting unconverted iso-octane and other hydrocarbon fractions), oxygen conversion and carbon balance. The flow rate into the GC after the reactor was not measured; therefore, it was calculated using the nitrogen balance, and could then be used alongside the dry vol. % results from the GC to calculate molar flows of each of the key products measured.

The calculations for these items are shown in equations 2.7 to 2.10 below respectively:

(2.7)

(2.8)

(2.9)

(2.10)

An understanding of the limitations of the data obtained, through the discussion of errors, is important to establish the reliability of any results. In this work, there were a number of potential sources of error in the catalyst performance data, such as those arising from:

- GC detector sensitivity
- Inconsistencies of water and/or liquid fuel delivery.
- Variations in thermocouple position (which were thought to have significant effects on temperature readings)
- Inconsistencies arising from the dependence of the GC on the total gas flow rate
- Other general equipment/experimental error

The above is not an exhaustive list, therefore each of these errors mentioned, and any others present, were difficult to quantify. Hence in order to determine the reliability of the results between experiments presented in this work, data from five separate but equivalent experiments (using a fresh nickel catalyst, tested under the same exhaust gas reforming conditions with propane at 400 °C) were analyzed to obtain the standard deviation of the GC measurements (often used to quantify variability [107]):

(2.11)

In the above, x is the individual data point, is the mean, and N is the number of data points.

The results yielded a combined average standard deviation, across each of the gases, of ± 0.58 % in terms of volume %. The standard deviation for the other catalytic metrics used in this study were ± 0.008 % for propane conversion, and ± 0.066 mol H_2 out/mol C_3H_8 in for hydrogen yield (oxygen was fully consumed during these tests, therefore there were no data points available to assess the standard deviation). These values will therefore be used as an estimation of the error in each measurement, so as to help with comparison between experiments and give confidence in the reliability of any conclusions drawn. They will be represented in the form of error bars in the relevant figures.

The results data will be presented in the form of a "progression plot", which will display how the catalyst performance, in terms of the dry vol. % of the product gas for each of the measured gases, varies over the temperature range and over the course of the consecutive tests. An example of this can be seen below in Figure 2.7, where the gas in question will be denoted in the top corner and the individual tests by the line type.

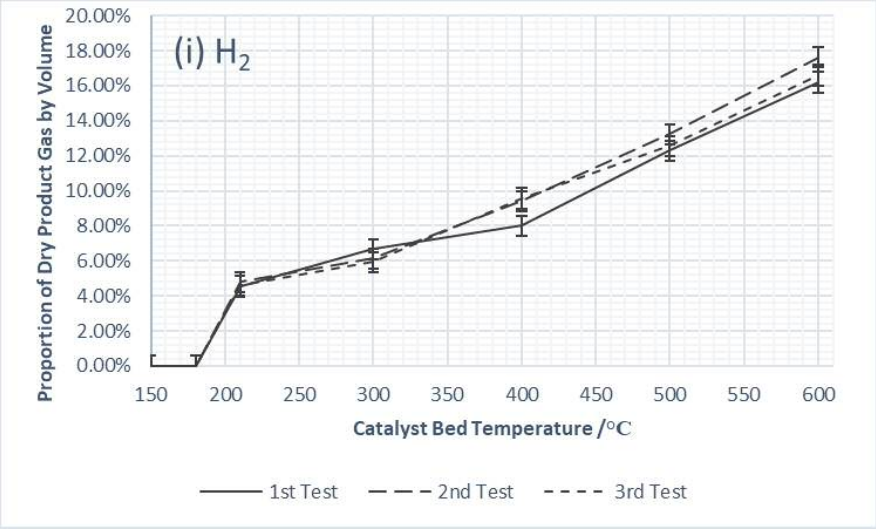

Figure 2.7: An illustrative plot of how the catalytic testing data from the GC will be presented in this work

When comparing across experiments/conditions, or when comparing multiple gases in one plot, the differentiation between the series will be made through a combination of line color and/or type, such as in the example below:

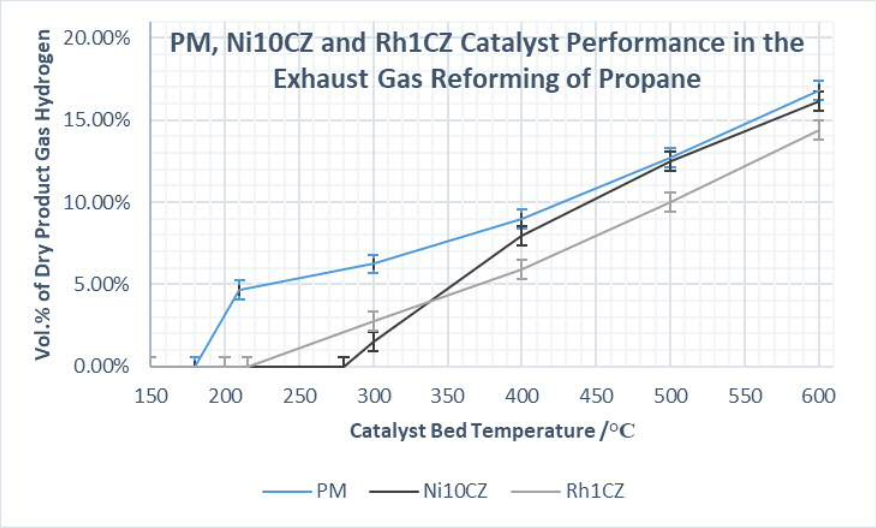

Figure 2.8: Another illustrative example of how the data in this work will be presented, showing the comparison of three different catalysts in terms of hydrogen content of the dried product gas

These are illustrative examples, it will be made clear for each figure what data is being represented.

Hydrogen yield, in terms of moles hydrogen produced per mole of fuel in the reactant stream, is a common choice for assessing the activity of reforming catalysts [31, 48], since it allows a fair comparison across varied experimental conditions. The data from the GC could have been presented in mol min $^{-1}$ of X in the product stream, as a function of catalyst bed temperature, where X is the specific product gas being measured. However, when used within experiment "groups", such as testing the same catalyst, under the same conditions, this is directly proportional to the concentration of the gas in question – i.e. a doubling of concentration, as measure by the GC means a doubling of the molar output of the catalyst. This is why presenting results in the form of Vol. % of a dried product gas is common in the exhaust

gas reforming literature [29, 35, 43, 49]. Furthermore, reformate gas containing 5-20 % hydrogen is a one of the goals of exhaust gas reforming [41, 43], so presenting the results in this way allows the catalyst performance to be considered against this target.

This relationship between concentration and molar rate can clearly be seen in the below plot, which shows the vol. % hydrogen detected by the GC for one of the catalysts tested in this work on the primary (left) vertical axis, and mol min^{-1} of hydrogen in the product stream on the secondary (right) vertical axis, as a function of bed temperature.

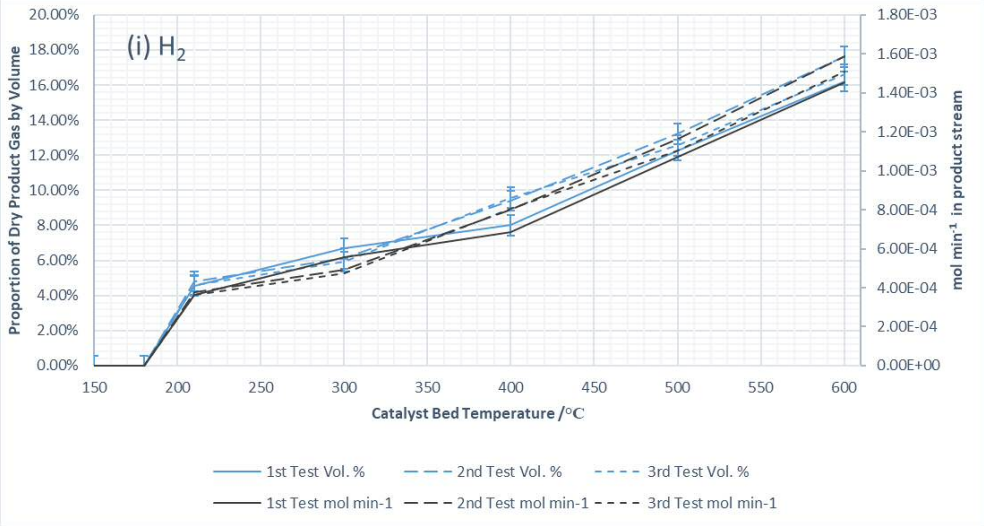

Figure 2.9: Illustrative example of the direct relationship between concentration of hydrogen in the product gas and molar rate of hydrogen production

Furthermore, the precious metal catalyst monolith and the powder/pelletised catalysts evaluated in this work were tested under differing reaction conditions so as to achieve an equal GHSV within the back pressure and flow rate limits of the experimental set up (as detailed in this chapter). This meant that the PM catalyst was tested at a gas flow rate of 175 ml min^{-1}, whereas the powder/pelletized catalysts were tested at 50 ml min^{-1} gas flow, but both at a GHSV = 8,500 h^{-1}. This also means the molar flow rate into the reactor was significantly different for the two catalysts, and hence a comparison of molar flow rates in the product gas between these catalysts would be misleading. The PM catalyst had a higher molar input and would there yield a higher molar output than would be achievable for the powder/pelletized catalyst.

It is for these reasons hydrogen yield was chosen to compliment Vol. % as suitable catalytic metrics for the assessment of the hydrogen production of each catalyst under the various reaction conditions.

With regards to error in characterization measurements, a similar standard deviation analysis was performed for BET surface area measurements, since each sample was tested three times. The quoted surface areas therefore will be given as the average of the three results, ± the standard deviation for that sample. For TGA data, each sample was tested three times and the data presented as the average TG curve from the three tests.

The details for how the data from the other characterization methods are presented has already been discussed in the relevant sections, but any further relevant details will be given where necessary in the relevant chapters.

The next chapters will present the results obtained during the experiments in the order they were performed. The first of which covers the characterization of the fresh catalysts prepared as described earlier in this chapter.

Chapter 3 - Characterization of the Fresh Catalysts

Introduction

The results for the characterization of the fresh catalysts prepared for this project are presented here, which were the Ni10CZ and Rh1CZ catalysts, prepared by impregnation. Both the preparation and characterization techniques were described in the Experimental chapter.

Results and Discussion

BET Surface Area

BET surface area measurements were taken three times for each sample. Average values for the BET surface area are shown in Table 3.1 for all the fresh catalysts prepared in this project. The values for the fresh and calcined supports are also included. As mentioned in the experimental chapter, the ± value represents the standard deviation from the three measurements.

Sample	**Surface Area /m^2g^{-1}**
CZ-support	79.3 ± 0.6
Calcined CZ-support	76.6 ± 0.8
Ni10CZ	62.7 ± 1.3
Rh1CZ	71.1 ± 0.8

Table 3.1: Average surface area values for the support, calcined support and fresh catalysts

The results show that there was a slight decrease in surface area of the support material after being exposed to the calcination program described in the experimental section. This is often the case with high temperature treatments such as calcination [67], which as described in the Introduction is possible as the temperature is raised towards the melting point of the compounds present, specifically at around the Huttig and Tammann temperatures [65, 108] . The calcination program used for these catalysts reached a maximum of 500 °C. This would therefore have been in the region of these temperatures for NiO, Ni(0), Rh(0) and Rh_2O_3, species likely to be present (and in the case of NiO, known to be present as shown in the XRD data shown below), hence some sintering would be expected to occur to some extent during calcination [69].

A further drop in surface area, on top of that expected from the calcination of the support alone, was observed resulting from the impregnation of the active metal onto the support. In the case of the Ni10CZ catalyst, this was a roughly 21 % decrease from the fresh support, and an 18 % decrease relative to the calcined support. A decrease was also observed for the rhodium catalyst, though to a lesser degree than

the nickel catalyst. The decrease was roughly 10% from the fresh support, and roughly 7 % relative to the calcined support.

A drop in surface area resulting from the deposition of the active species has been reported previously [80, 109]. Given the difference between the high loading in the nickel catalyst (10 %) compared to the low loading (1 %) in the rhodium catalyst, it is clear that the higher the loading of metal impregnated onto the support the larger the decrease in surface area, possibly suggesting agglomeration of the active species on the surface.

Temperature Programmed Reduction

Note: For ease of comparison between samples, the data has been displayed as temperature against hydrogen consumption, where the latter is in arbitrary units (a.u). The data for the fresh support (blue), Rh1CZ (orange) and Ni10CZ (grey) are presented below in Figure 3.1:

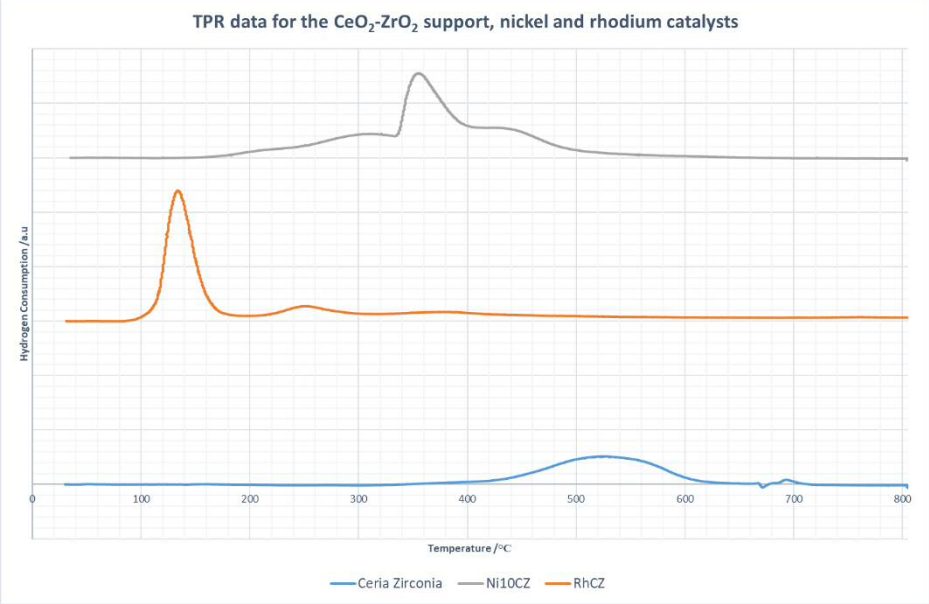

Figure 3.1: TPR data for the ceria zirconia support, Rh1CZ catalyst and Ni10CZ catalyst

The support showed a small reduction peak beginning at around 400 °C, reaching a maximum around 520-530 °C, and ending just above 600 °C. Zirconia is not reducible in this temperature range (it does not easily reduce at temperatures lower than 1000 °C [110]), and hence was not observed here. Ceria on the other hand is known to reduce in two stages [111]. The first or low temperature reduction event is the reduction of surface Ce^{4+} species, followed by Ce^{4+} bulk species. The surface species is often a surface capping oxygen anion attached to the Ce^{4+} ion in octahedral coordination, whereas the bulk species is often an oxygen anion bonded to two Ce^{4+} ions. The temperature at which these stages occur can depend on the particle size of the support – smaller particle sizes lead to lower reduction temperatures [112]. In addition, the incorporation of zirconia into the ceria lattice can also decrease the reduction temperature of the ceria [113].

The reduction event observed in the data in Figure 3.1 was therefore associated with the first reduction, that of the surface Ce^{4+} species. This event was observed at the lower end of the temperature range reported in the literature for the reduction of surface Ce species, which was most likely due to the presence of high surface area and small particle size, along with the incorporation of zirconia in the support material provided by Solvay Rhodia. The second reduction event, that of the bulk ceria species, was not observed because it occurs outside the temperature range of the treatment used here.

The addition of active metals to supports such as ceria is known to enhance the reductive properties of the support (through hydrogen spillover from the more reducible metal to the support), as well as displaying reduction events associated with the reduction of the active metal itself [111, 114].

In the case of the Rh1CZ catalyst, the first reduction peak, began at just over 100 °C, and reached a maximum hydrogen uptake at just below 140 °C. This event is therefore in the region of well dispersed surface Rh^{3+}, becoming reduced to Rh^{0}, as reported in the literature [44, 80, 115]. The presence of two smaller peaks around 250 °C, and just below 400 °C can be assigned to less well dispersed, or bulk Rh species, and surface ceria reduction. As mentioned already, the presence of the noble metal lowers the reduction temperature of the surface ceria species through spill over processes.

The Ni10CZ catalyst displayed a shoulder beginning at just over 200 °C, peaking around 300 °C. This was followed by the main reduction peak at around 350 °C, with another shoulder between 400 °C and 500°C.

These temperatures were again lower than the CZ support alone, showing spillover from the nickel to the ceria and therefore promoting the reduction of the surface ceria species. The low temperature shoulder and main reduction peak can be assigned to the reduction of the nickel species. The first reduction event is likely to be the reduction of non-stoichiometric Ni^{3+} species or “free” NiO species, followed by well dispersed NiO, and moving into bulk NiO species interacting with the support [110, 116].

In summary, the addition of the active metals enhanced the reducibility of the ceria-zircnoia support, and rhodium was more easily reduced than nickel, which consistent with the literature.

X-ray Diffraction

The ceria-zirconia support, along with the Ni10CZ and Rh1CZ catalysts were also analyzed using XRD. The diffraction patterns are shown below in Figure 3.2. Again, for ease of comparison, the intensity of the detected peaks is presented in arbitrary units (a.u).

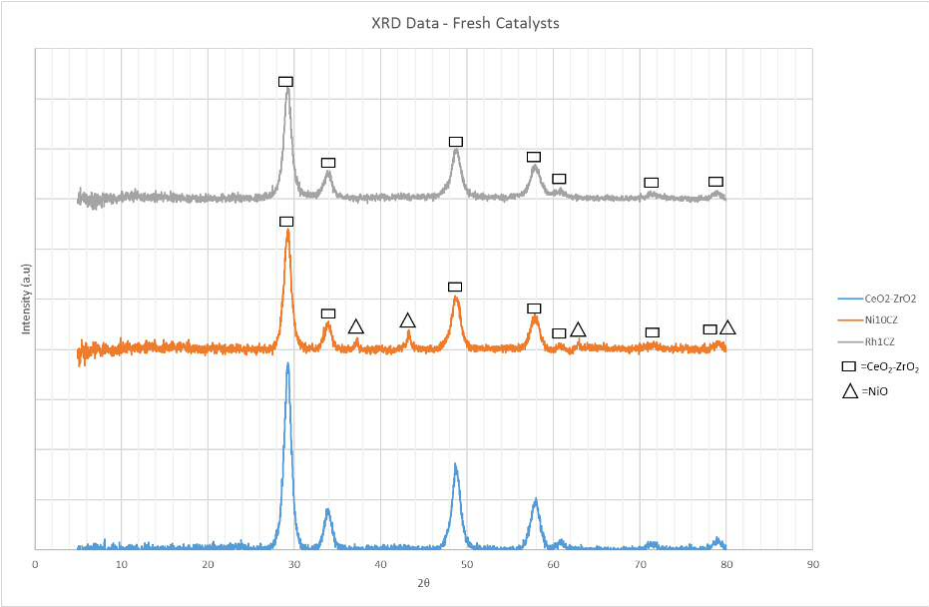

Figure 3.2: XRD data for the ceriz zirconia support, Ni10CZ catalyst, and Rh1CZ catalyst

The phases were identified by comparison to reference data within the X'PertPro software associated with the PANalytical X'PertPro x-ray diffractometer used in this work. The reference data can be found in Appendices 1, 2 and 3.

No phases associated with rhodium were able to be detected in the Rh1CZ catalyst. This is most likely due to the relatively low loading of rhodium relative to ceria-zirconia [44, 80]. Regardless, the successful impregnation of the rhodium onto the support had already been observed in the TPR measurements, so was not of concern.

The reference sample which gave the highest match to the ceria-zirconia support was a tetragonal system, with the main peaks at around 29 ° (intensity 100 %), 34 °, 49 °, 58 ° assigned to the 101, 110, 200, 211 planes respectively.

The pattern for the Ni10CZ catalyst showed the same peaks listed above for ceria-zirconia (matching the same reference sample planes), but with notable additional peaks present – indicating the presence of nickel species. The best match for the peaks was for a cubic nickel oxide system, with characteristic peaks at 37.3 ° and 43.3 °, corresponding to the 111 and 200 planes, as has previously been reported in the literature for nickel supported on ceria-zirconia [117].

Scherrer calculations performed in the X'PertPro software yielded estimates of the crystallite size, shown below in Table 3.2. The estimates were calculated using the most intense peaks for the species in question.

Sample	Species	Estimated Crystallite Size /Å
CZ	CeO_2-ZrO_2	79
Ni10CZ	CeO_2-ZrO_2	78
	NiO	115
Rh1CZ	CeO_2-ZrO_2	79
	RhO	-

Table 3.2: Scherrer calculation estimates of crystallite sizes for the ceria zirconia support, Ni10CZ catalyst, and Rh1CZ catalyst

The particle size of the support does not change significantly from the fresh support when the active components are included in the Ni10CZ and Rh1CZ catalysts. This could suggest little interaction between the metal and the support.

This is further supported, due to the observed NiO particle size estimates being significantly larger than the support particle size. This is likely due to sintering of the NiO, as well as the bulk deposition of the NiO in large clusters on the support surface, rather than its incorporation into the support. A similar relationship between smaller support particle sizes and larger active metal particle sizes was reported by Ambroise et al. [44, 80] in the case of their cobalt oxide on ceria-zirconia catalyst. Furthermore, this large nickel particle size, and possible agglomeration on the surface might have been expected given the method of preparation was a simple, non-optimized impregnation method, with relatively high nickel loading. High metal loadings are known to result in higher particle sizes [118], and the impregnation method has no morphology or size controlling agents inherent in the process [119].

Conclusions

The data presented in this chapter serves to characterize the two fresh catalysts prepared and tested under exhaust gas reforming conditions in this project, in order to determine some basic properties such as surface area and the likely chemical species present, as well as to confirm that the preparation process had successfully resulted in a catalyst with the desired composition. The results show, that though the preparation methods were not necessarily optimized, that a Ni/CeO_2-ZrO_2 and Rh/CeO_2-ZrO_2 catalyst were successfully prepared. They also show that the reducibility of the support was enhanced by the addition of these metals, and that rhodium oxide was more reducible than the nickel oxide. In the case of the Ni10CZ catalyst, particles size estimates, through the Scherrer calculation, suggested that the nickel oxide was deposited largely on the support surface, in large clusters.

Chapter 4 - Investigation of Post-Reactivity Testing, Atmosphere Induced, Catalyst Deactivation

Introduction

During preliminary testing for this work, occasional deactivation of the nickel catalyst was observed. However, the precise cause and nature of this deactivation was not discovered.

The starting point for the investigation was the observation of a temperature spike in the catalyst bed during the shutdown phase, where the gases in the system were bled off after testing.

The symptoms of the deactivation, were observed in the first test of the used catalyst (i.e immediately after the fresh catalyst test). These symptoms were a reduced/non-existent exotherm at around the light off temperature, as well as an absence of hydrogen in the product gas until higher temperatures

This deactivation was only observed with the Ni10CZ catalyst, not with the PM catalyst (whose performance had remained fairly consistent after several years of use under various conditions). This, as discussed in the Introduction, was unsurprising as one of the main problems with base metal reforming catalysts is that they are not as stable as their precious metal counterparts. However, the deactivation experienced here was not gradual deactivation over long time periods, rather the deactivation observed was sporadic, and often severe.

The focus in this section was to discover the cause and nature of the deactivation, and therefore to establish what, if anything, could be done to avoid or overcome it.

Additional Experimental Details and Observations

The testing conditions used were $\lambda = 2.12$, and a GHSV of 8,500 h^{-1}, with propane as the model fuel. As described in pages 17-18 in Chapter 1, the λ-value is the ratio of the air/fuel ratio the engine is operating under to the stoichiometric fuel ratio for the fuel in question. A $\lambda = 1$ would therefore signify stoichiometric conditions in the engine, $\lambda > 1$ would represent air-rich conditions, and $\lambda < 1$ would be a engine intake mixture lean in air. Therefore, a $\lambda = 2.12$ would refer to the expected exhaust gas composition of an engine operating in air rich conditions. The temperature range was up to 400 °C due to limitations with the heating at this stage. However, this was sufficient to cover light off as well as the region where the deactivation was most noticeable.

The initial shutdown procedure, during which the aforementioned temperature spike was observed, involved a period where the hot catalyst was exposed to a mixture containing high levels of oxygen (1:1 flow rate ratio with nitrogen), during the bleeding of individual gases.

If the catalyst bed temperature was high enough at around the time the oxygen rich mixture was passed over the catalyst bed, then a temperature spike of between 80-150 °C was observed.

This original shutdown method was hence called the "oxygen cool-down". In order to check whether this phenomenon was the cause of the deactivation, a new shutdown method was devised. After the water flow to the reactor and furnace had been turned off, then all of the gases, except nitrogen, were turned off at both the supplies and with the MFCs. The catalyst was then allowed to cool completely under nitrogen before turning off the nitrogen flow. This was therefore called the "nitrogen cool-down". A simulated "air cool-down" was also tested – where a mixture of 21 % O_2 and 79 % N_2 was flowed over the hot catalyst during cool-down. In addition, the reversibility of the deactivation was tested.

As already mentioned in the Experimental chapter, two activation methods were tested during this phase of the project (pre-reductions in dilute and pure hydrogen), however neither had any effect on catalyst performance. Therefore the data is not presented here, but these experiments are referenced at points in the discussion.

Characterization (BET, TGA and XRD) was carried out on all used samples and compared to the results already shown for the fresh samples (see Chapter 3).

Results

The Effect of Atmosphere During the Cool-Down Phase of Reactivity Testing

Nickel Catalyst Performance after Cooling in an Oxygen Rich Atmosphere (the "Oxygen Cool-Down")

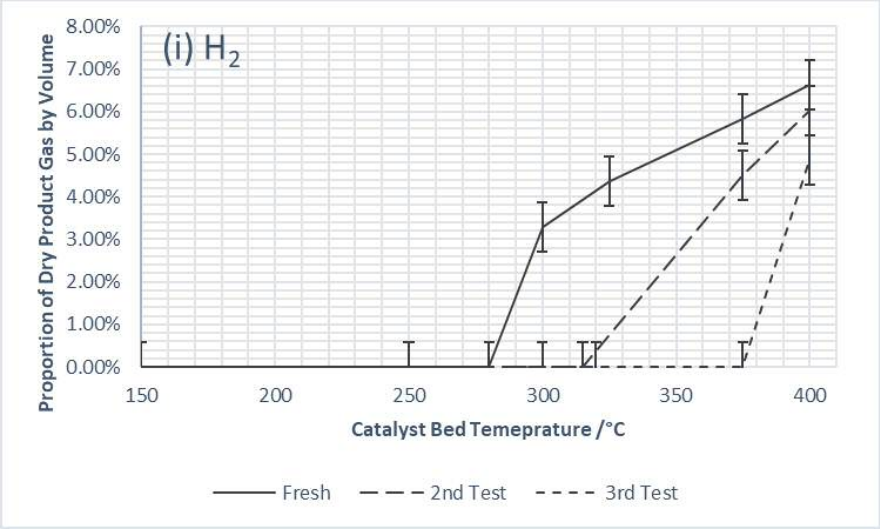

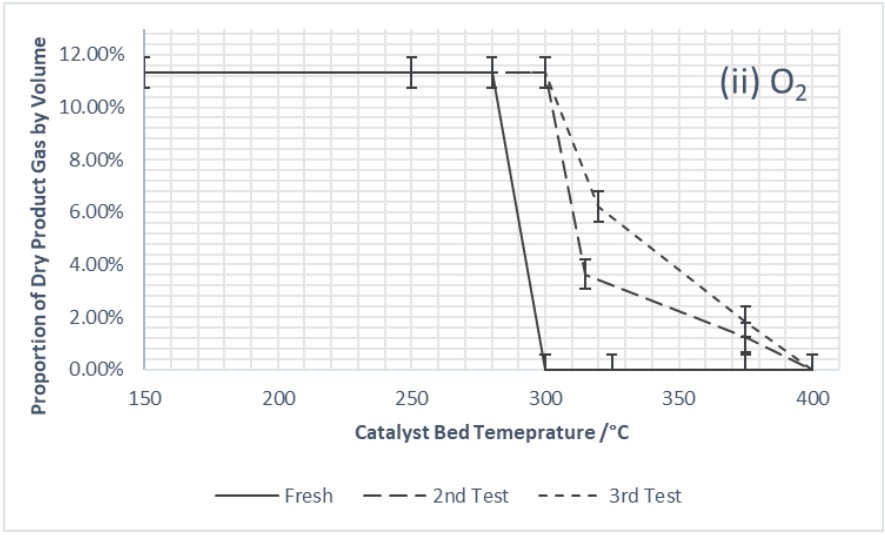
(ii) O_2
Proportion of Dry Product Gas by Volume
12.00%
10.00%
8.00%
6.00%
4.00%
2.00%
0.00%
150
200
250
300
350
400
Catalyst Bed Temeprature /°C
Fresh
2nd Test
3rd Test

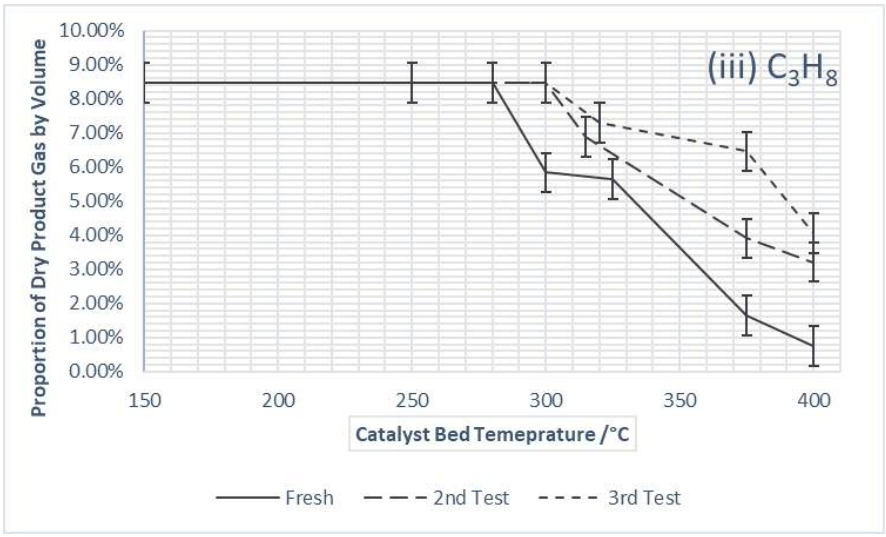
(iii) C_3H_8
Proportion of Dry Product Gas by Volume
10.00%
9.00%
8.00%
7.00%
6.00%
5.00%
4.00%
3.00%
2.00%
1.00%
0.00%
150
200
250
300
350
400
Catalyst Bed Temeprature /°C
Fresh
2nd Test
3rd Test

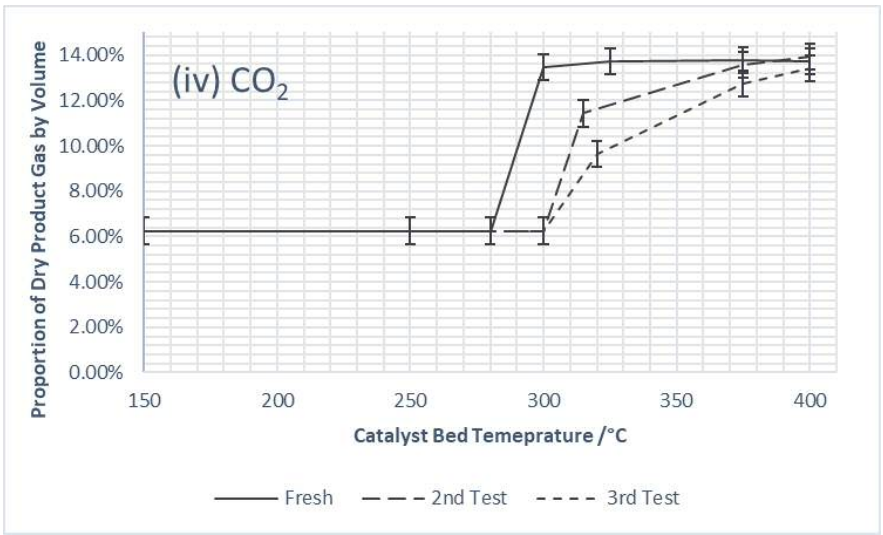
(iv) CO_2
Proportion of Dry Product Gas by Volume
14.00%
12.00%
10.00%
8.00%
6.00%
4.00%
2.00%
0.00%
150
200
250
300
350
400
Catalyst Bed Temeprature /°C
Fresh
2nd Test
3rd Test

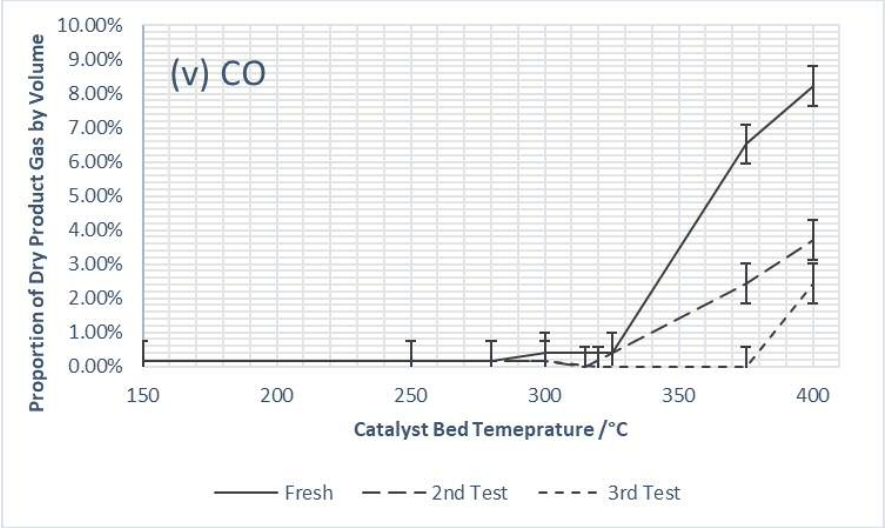

Figure 4.1: Nickel catalyst performance during exhaust gas reforming of propane at λ = 2.12, cooled under an oxygen rich atmosphere in-between tests. The concentrations of major components of the dried product gas are shown

These results show a rapid deactivation of the catalyst. Figure 4.1(i) shows the proportion of the product gas constituting hydrogen falling dramatically with each test – both in terms of volume of hydrogen produced at each temperature, as well as in terms of the increase in minimum temperature at which hydrogen started to be produced.

Light off for the fresh catalyst was at 280 °C, with the exotherm taking the temperature to 300 °C, upon which hydrogen production begins. After one oxygen cool-down, light off was delayed until 300 °C, with the exotherm being roughly 5 °C less. Furthermore, hydrogen production did not occur until temperatures higher than 320 °C. After an additional oxygen cool-down, hydrogen production was delayed until temperatures higher than 375 °C.

Figure 4.1(ii) shows the oxygen consumption began at 280 °C with the fresh catalyst, and once the bed temperature had settled at 300 °C after the exotherm, that all of the oxygen had been consumed (i.e light off was complete). After one oxygen cool-down the results show that the onset of oxygen consumption was delayed until 300 °C and full consumption was not complete until 400 °C. After an additional oxygen cool-down, oxygen consumption again began at 300 °C, but there was a higher proportion of oxygen left in the product gas at each temperature, with full consumption delayed until 400 °C.

Figure 4.1(iii) shows the progression of propane consumption. The results were as expected given the above results for hydrogen and oxygen - the delayed onset of consumption, and lower consumption of the fuel at each temperature (shown by increased concentration of propane in the product gas mixture (see Chapter 2 for explanation). The fresh catalyst displayed almost complete propane consumption at 400 °C, while after two testing/oxygen cool-down cycles, approximately 50 % of the propane was consumed based on the volume % in the product gas relative to the dry reactant stream.

Similarly, Figure 4.1(iv) and 4.1(v) show an accompanying decrease in the proportion of the dry product gas constituting carbon dioxide and carbon monoxide as the catalyst degraded with consecutive tests.

Nickel Catalyst Performance after Cooling in a Nitrogen Atmosphere (the "Nitrogen Cool-Down")

Note: The plot for oxygen consumption is not included since it was completely consumed at light off for each test.

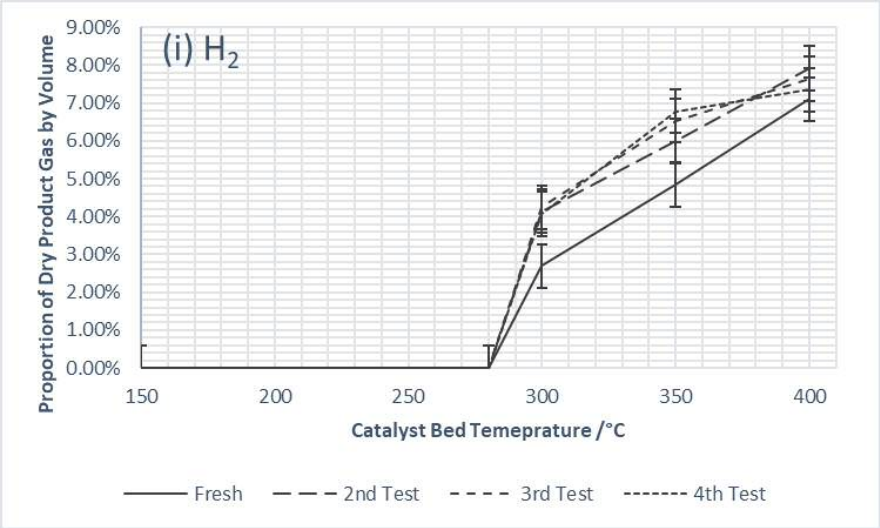

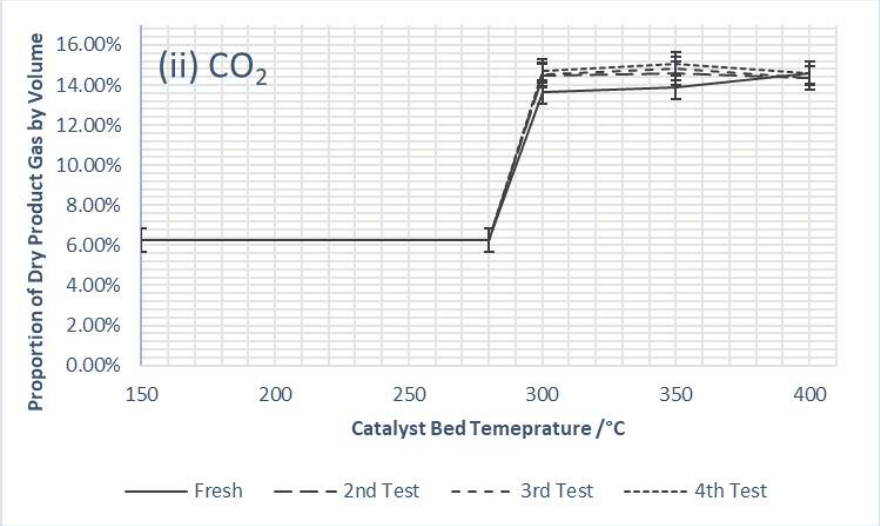

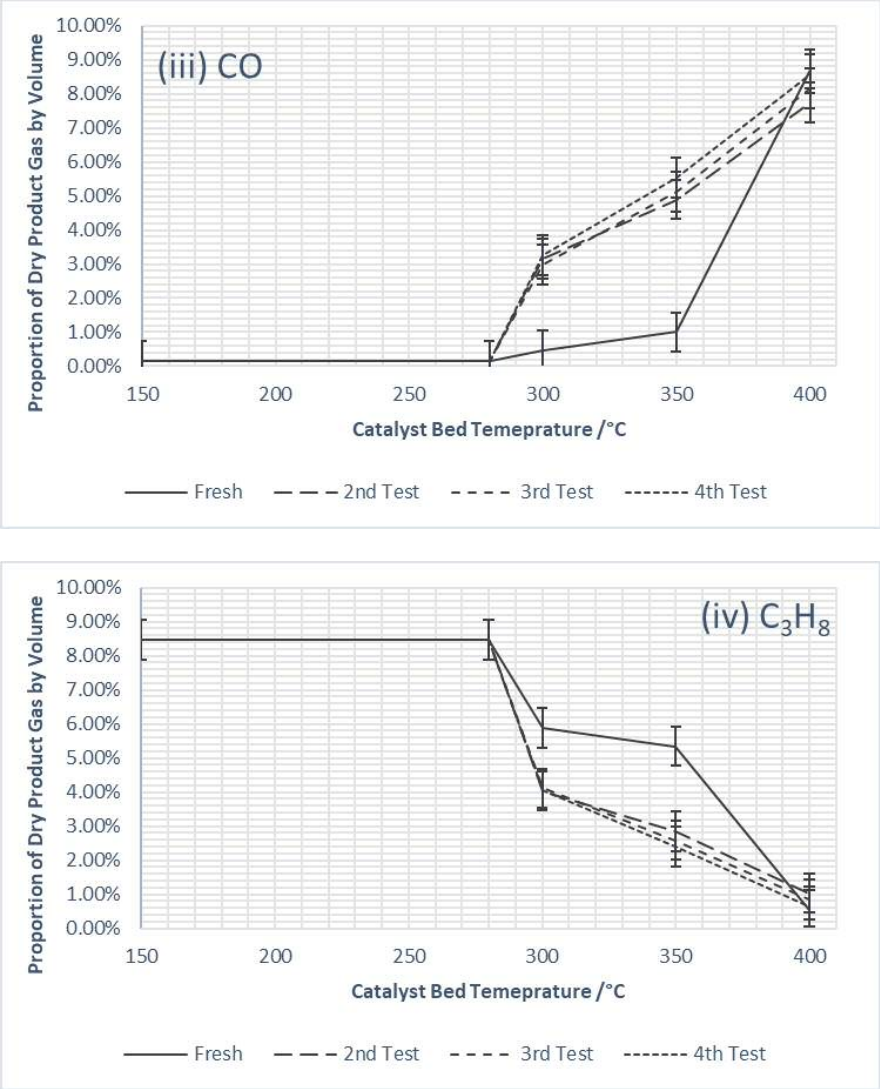

Figure 4.2: Nickel catalyst performance during exhaust gas reforming of propane at λ = 2.12, cooled under a nitrogen atmosphere between tests. The concentrations of major components of the dried product gas are shown

As opposed to the oxygen cool-down results, which showed deactivation of the catalyst, the results from using three consecutive testing/nitrogen cool-down cycles instead show catalyst activation.

Figure 4.2(i) shows that hydrogen production for the fresh catalyst again started at 300 °C, with light off at 280 °C. After the first nitrogen cool down, the results show an increase in the hydrogen content of the dry product gas at all temperatures relative to the fresh catalyst. This was followed by another, but smaller, increase after the second nitrogen shutdown. Improvements in hydrogen production then leveled off, with no significant change between the third and fourth tests.

Figure 4.2(ii) shows a small increase in carbon dioxide content of the dry product gas between fresh and used samples.

Figure 4.2(iii), for carbon monoxide production, shows a similar trend to hydrogen production in the form of an increase in the proportion product gas constituting carbon monoxide after the first nitrogen cool-down, before levelling off with further testing/nitrogen cool-down cycles.

Figure 4.2(iv) shows the associated increase in propane consumption after the first nitrogen cool-down that was to be expected given the increase in production of hydrogen, carbon dioxide and carbon monoxide. Again, the largest increase is between the fresh catalyst and the second test. Consumption then leveled out with additional tests and nitrogen cool-down cycles.

Nickel Catalyst Performance after Cooling in a Simulated Air Atmosphere (the "Air Cool-Down")

The final cool-down method tested was a simulated air cool-down. After testing the catalyst was exposed to a mixture of 21 mL/min O_2 and 79 mL/min N_2 during cooling. The catalyst was tested for four consecutive test, with the air cool-down method used after each test. The results are shown below.

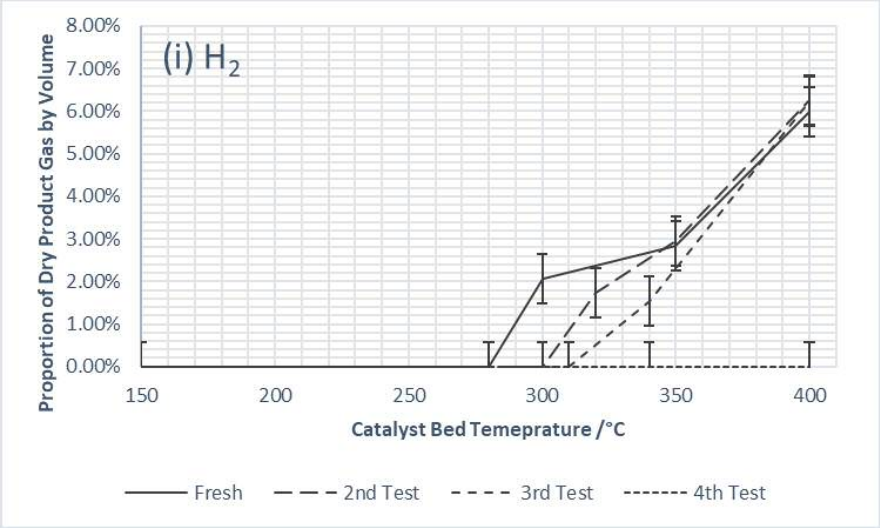

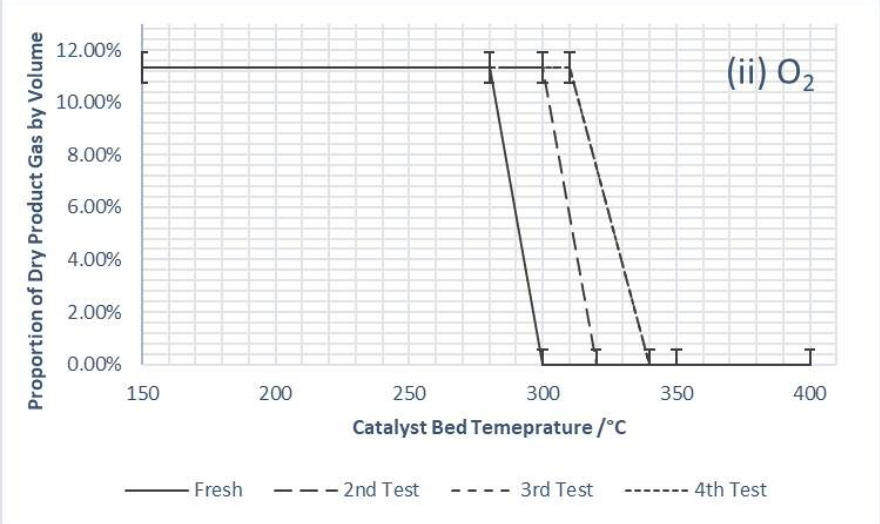

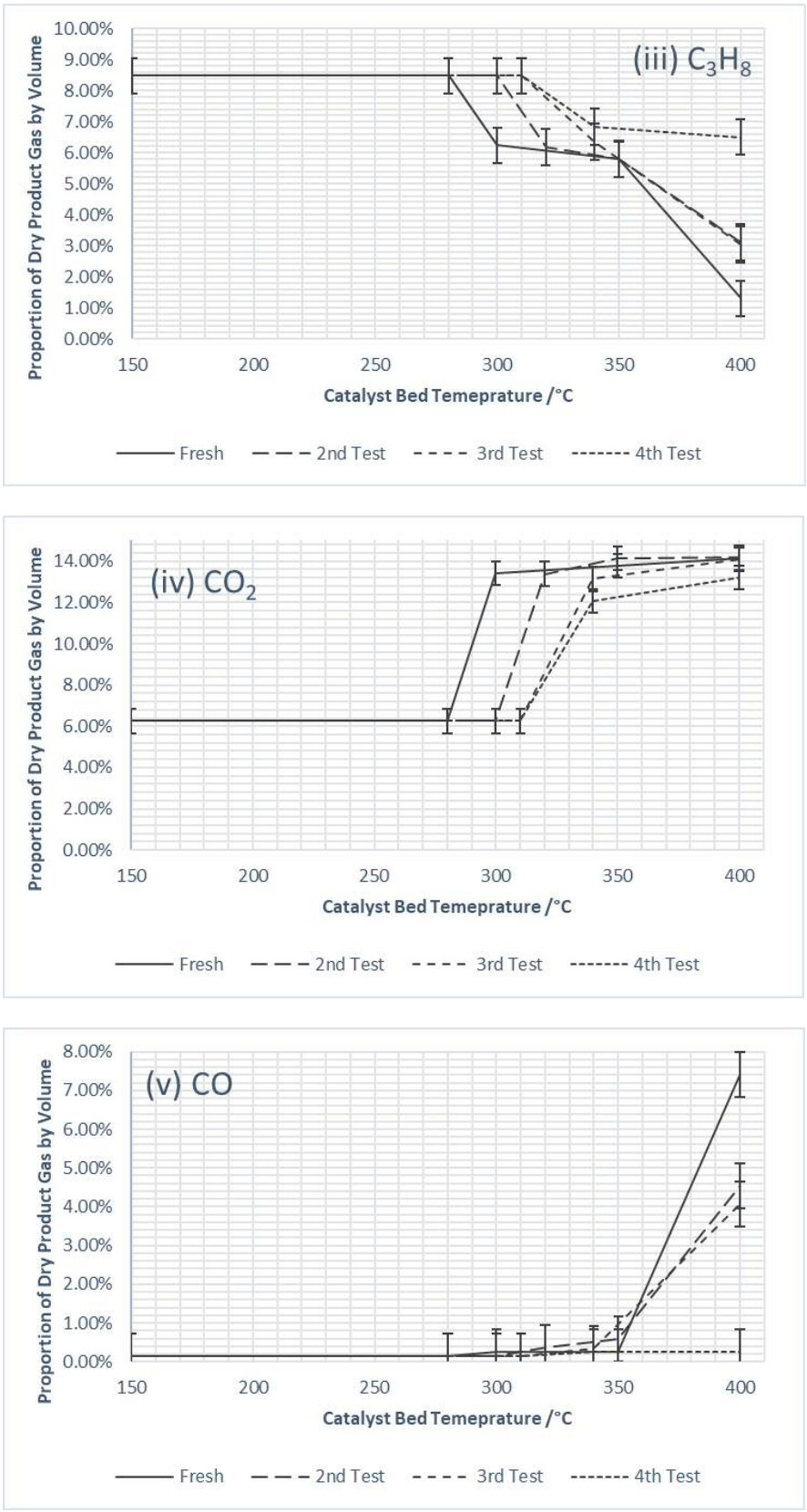

Figure 4.3: Nickel catalyst performance during exhaust gas reforming of propane at λ = 2.12, cooled in an "air" atmosphere between tests. The concentrations of major components of the dried product gas are shown

As with the oxygen cool down – the results show a decrease in rate of hydrogen, carbon dioxide and carbon monoxide production (Figure 4.3(i), 4.3(iv) and 4.3(v)) with consecutive testing and air cool down cycles (as per Chapter 2, rate and concentration were found to be directly proportional).

There was also a delay in the temperature at which the oxygen was consumed (Figure 4.3(ii)).

Hence, there was the expected decrease in propane consumption with each test (Figure 4.3(iii)).

So again, as with the oxygen cool down, exposing the catalyst to air during the cool down phase had the effect of deactivating the catalyst over consecutive tests.

Testing the Reversibility of the Observed Deactivation

In order to test the reversibility of the deactivation observed from exposing the hot catalyst to an oxidizing atmosphere during the cool down phase of reactivity testing, an experiment was performed where two testing/oxygen cool down cycles were followed by five testing/nitrogen cooling cycles. The former was found above to be deactivating, whereas the latter was found to be activating.

For the purpose of clarity the data progression of the hydrogen production is first presented for the testing/oxygen-cool down cycle phase of the experiment (the "deactivation phase"), then during the subsequent testing/nitrogen cool-down cycles (the "regeneration phase").

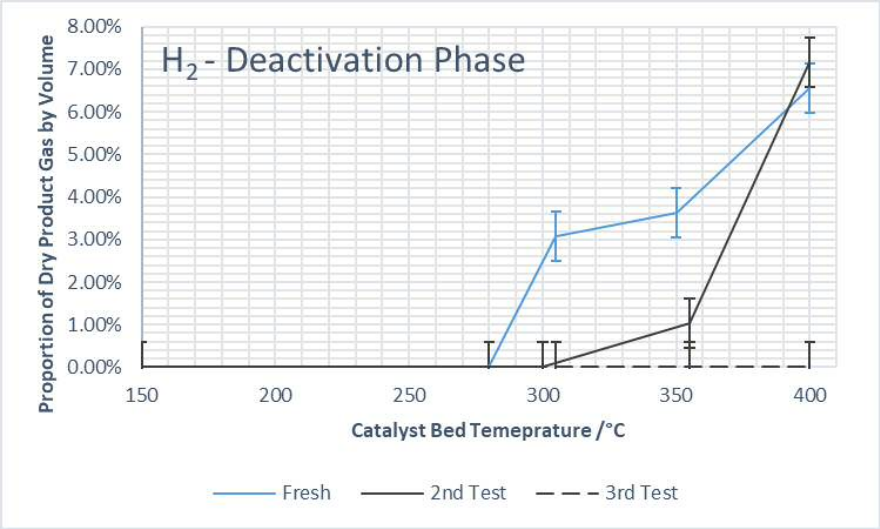

Figure 4.4: Nickel catalyst performance in terms of hydrogen production in the exhaust gas reforming of propane at λ = 2.12, during the "deactivation phase" (cooling under an oxygen rich atmosphere between tests)

Deactivation was again observed after the two testing/oxygen cool-down cycles, shown above in Figure 4.4 by the rapid decrease in the proportion of the product gas constituting hydrogen over the temperature range, as well as the delay in the onset of hydrogen production.

The deactivation was severe enough that the catalyst showed complete deactivation throughout the temperature range in the third test.

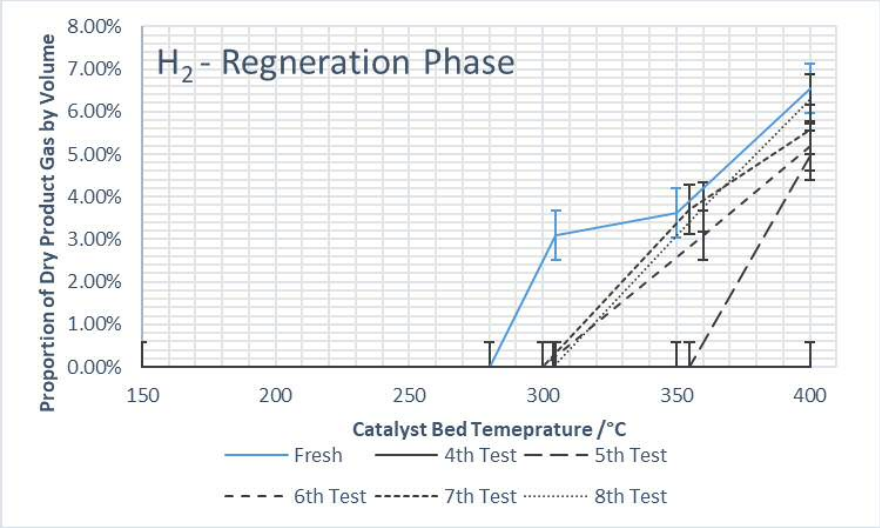

Figure 4.5: Nickel catalyst performance in terms of hydrogen production in the exhaust gas reforming of propane at λ = 2.12, during the "regeneration phase" (cooling in a nitrogen atmosphere between tests)

However, it is clear that the deactivation was partially reversible, as shown in Figure 4.5 above, where after two testing/nitrogen cool-down cycles, some hydrogen production returned at 400 °C. Additional reforming activity returned with subsequence cycles before levelling off to just below the levels of the fresh catalyst.

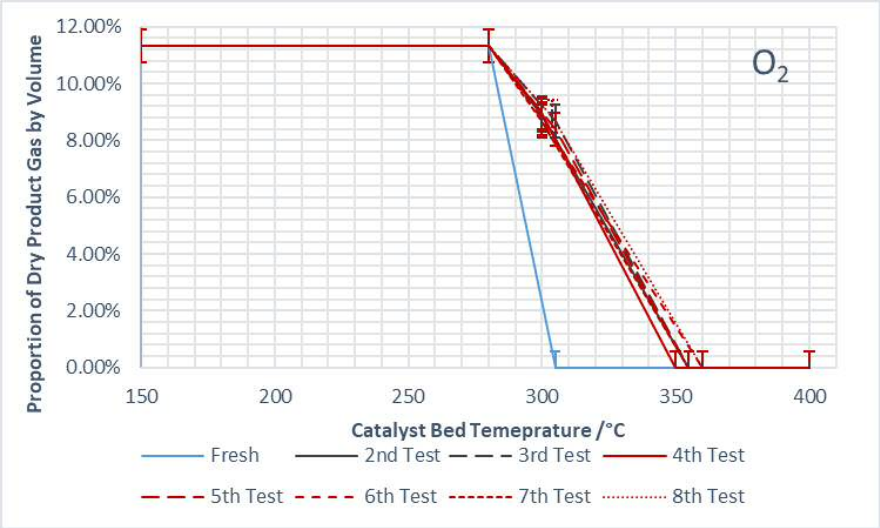

Figure 4.6: Nickel catalyst performance in the exhaust gas reforming of propane at λ = 2.12, in terms of oxygen consumption during the deactivation and regeneration phases

Figure 4.6 above shows that oxygen was consumed at 280 °C for the fresh catalyst, and had been completely consumed when the temperature levelled out at 300 °C. The results then show the previously observed delay in onset of oxygen consumption, and decrease in consumption up to 350 °C, after two testing/oxygen cool-down cycles.

The results then show a stabilization/small increase in oxygen consumption at all temperatures as the catalyzed was exposed to five consecutive tests and accompanying testing/nitrogen cool down cycles.

Although not shown here, the data for carbon dioxide and carbon monoxide also showed decreased content levels in the product gas during the deactivation phase of the experiment, before recovering during the subsequent testing/nitrogen cool-down cycles.

As would be expected, the propane consumption showed a resulting decrease during deactivation, followed by an increase as the catalyst activity returned.

Catalyst Characterization

Characterization experiments were carried out on all the used samples, to compare to the fresh samples (see Chapter 3). The techniques used were BET, XRD and TGA.

BET

The BET results are shown in Table 4.1 below:

Sample	**Details**	**Surface Area / m^2g^{-1}**
Ceria Zirconia	Fresh	79.3 ± 0.6
Ceria Zirconia	Calcined	76.6 ± 0.8
Ni10CZ	Fresh	62.7 ± 1.3
	Oxygen Cool-Down	41.6 ± 0.8
	Nitrogen Cool-Down	91.5 ± 2.3
	Air Cool-Down	48.2 ± 0.4
	Regenerated	63.3 ± 1.9

Table 4.1: BET surface area data for the ceria zirconia support, and the nickel catalyst samples tested in this chapter

The results for the fresh samples and supports have been discussed in Chapter 3. In addition to these results, Table 4.1 shows the effect of the experiments carried out in this section of work. Specifically they show a large decrease, of ~34%, in surface area from the fresh catalyst to the oxygen deactivated sample. The air deactivated sample also showed a decrease in surface area relative to the fresh sample, though to a lesser degree of ~23 %.

The sample which was exposed to the cycles of testing/nitrogen cool-down showed a ~45 % increase in surface area relative to the fresh sample. In fact, the surface area of this sample was higher than the fresh support.

However, the sample that was exposed to testing/oxygen cool-down cycles, followed by testing/nitrogen cool-down cycles (i.e the regenerated sample) showed almost identical surface area to the fresh sample. Assuming that during the oxygen cool down phase there had been a decrease in surface area (as seen with oxygen and air cooled samples), then this results suggests that the loss had been recovered in some manner with consecutive test/nitrogen cool-down cycles.

XRD

Figure 4.7 below shows the XRD results for some of the samples tested in this section of work. The reference data for the fresh samples are shown in Appendices 1, 2 and 3, while the nitrogen-cooled samples are included in Appendix 4.

The results for the fresh Ni10CZ sample shows some additional peaks relative to the fresh support, which as in Chapter 3 were assigned to nickel oxides. This data was almost identical to that for the oxygen cooled and air cooled samples.

The data for the nitrogen cooled sample show a similar set of peaks, with the exception of the disappearance/significant reduction of the peak at 37 ° (a nickel oxide peak), and the appearance of a new peak at 44 °. This was also seen in the regenerated sample. This new peak was assigned to metallic nickel in the 111 plane.

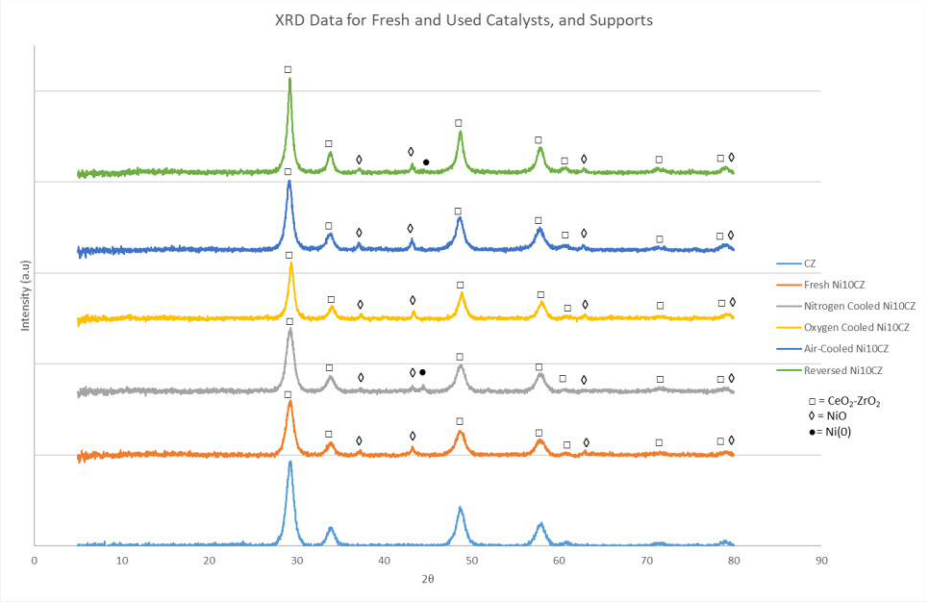

Figure 4.7: XRD data for the support and nickel catalyst samples tested in this chapter

From the XRD data, estimates for NiO crystal size were obtained using the Scherrer Calculator in the X'PertPro software. The NiO peak at 43 ° was used for the calculation. The results are tabulated below.

Sample	NiO Crystal Size / Å
Ni10CZ - Fresh	115
Ni10CZ - Oxygen Cooled	290
Ni10CZ - Air Cooled	270
Ni10CZ - Nitrogen Cooled	125
Ni10CZ - Regenerated	300

Table 4.2: Scherrer calculated estimates of NiO crystallite size

The results showed large increases in crystal size for the samples exposed to testing/oxygen or air cool-down cycles (including the regenerated sample). The nitrogen cooled sample on the other hand only showed a small increase.

TGA

Thermogravimetric analysis, in air, was carried out with the method as described in the experimental chapter. The analysis was carried out for the fresh Ni10CZ, oxygen cooled, air cooled, nitrogen cooled and regenerated catalysts.

The results are shown below in Figure 4.8:

Figure 4.8: Thermogravimetric analysis data for the nickel catalyst samples tested in this chapter

It can be seen that the fresh, oxygen cooled and air cooled catalysts experienced very minor and gradual weight loss in the temperature range, each having lost around 4 % of the initial weight at 800 °C. Most of the weight loss for the fresh sample had occurred by around about 200 °C. The oxygen and air cooled samples lost some initial weight in the region of 30-200 °C, and then show another small weight loss around 450 °C. On the other hand the nitrogen cooled and regenerated catalysts show much more drastic weight loss, beginning at 400 °C, before leveling off at around 550 °C-600 °C, and both with total weight loss of just under 20 %.

Additional Observations

Color Changes

During this section of work it was noticed that the appearance and color of the catalysts post-testing changed depending on which cool down method was used.

The fresh catalyst started off as a dark grey powder. The oxygen and air cooled samples, when taken out of the reactor were a little lighter colored.

The nitrogen cooled and regenerated samples on the other hand were seen to be completely black when removed from the reactor.

See Appendix 5 for photos.

Oxygen Treated Fresh Catalyst

An additional experiment was performed, in which a fresh batch of Ni10CZ was loaded into the reactor, and exposed to an oxidizing atmosphere (50 % oxygen and 50 % nitrogen) and the temperature in the catalyst bed was taken gradually up to 500 °C, upon which it was held for 2 hours. This was done in order to see if there would be any temperature spike, similar to that observed during testing/oxygen and air cool-down cycles.

This was not observed, making it clear the combination of testing under reaction conditions prior to cooling under an oxidative atmosphere was required for the temperature spike to occur.

Discussion

The results, presented in this chapter show the sensitivity of the nickel catalyst towards the changes in atmosphere to which it was exposed. This is important with respect to the potential application. In practice, requiring extra care in cooling the catalyst would add to the complexity and therefore cost of implementation in a real vehicle since engineering solutions would need to be found and incorporated in order to protect the catalyst during shut down.

Furthermore, though not shown here, neither of the activation methods (pure and dilute hydrogen) showed any real benefit to performance when compared to the fresh catalyst. This was unexpected, as some form of pre-reduction is common (and found to be beneficial) for supported base metal catalysts, especially for applications such as reforming [19, 31, 120, 121]. In fact, simply using the catalyst in consecutive tests, coupled with a nitrogen cool down was found to function as a beneficial activation treatment instead. It is possible that the activation methods tested here could be altered so as to achieve improved performance relative to the fresh catalyst. This could include increasing the time under reductive atmosphere, changing the T_{MAX}, or changing the ramp rate so as to be less or more aggressive during the heating phase. Alternative reductive atmospheres could also be tested in any future studies.

The aim in this chapter was to further investigate and understand the cause of occasionally observed deactivation of the nickel catalyst. The results shed some light on this observation. The observed temperature spike during the old (oxygen) cool down method was indeed found to be relevant. Two additional cool down methods were tried. The temperature spike was also observed in the simulated air cool down (21 % oxygen and 79 % nitrogen), however it was not observed when a nitrogen cool down was used. In addition, this temperature spike was not observed during a separate experiment in which a fresh batch of catalyst was exposed to an oxidative atmosphere at high temperatures. This suggests that both using the catalyst under reaction conditions and then exposing it to an oxidative atmosphere is required for the exotherm to be observed. Hence, it is therefore likely that the cause of the exotherm was any carbon, deposited during the reaction testing, being burnt off in the oxidative atmosphere, along with some re-oxidation of metallic nickel formed during testing. Since this caused the monitored bed temperature (recorded by thermocouple sitting just below the catalyst bed) to rise by 80-150 °C, it is likely that the temperature increase on the catalyst surface was by a much greater amount. This is because the thermocouple was positioned below the catalyst bed, but was not in contact with it. Both experience and results from the literature suggest that the temperature can fall rapidly over short distances [50].

The result for both the oxygen and air cool down methods, if done over several consecutive tests, was the deactivation, sometimes total, of the catalyst. This was most obviously seen in both the decrease in proportion of hydrogen in the product gas, and the delay in the onset of hydrogen production.

However, under an inert cooling atmosphere, in this case nitrogen, no temperature spike was observed, and the subsequent catalyst deactivation did not occur. In fact, quite the opposite was observed, this cycle was found to act as a kind of activation treatment – with the catalyst performance improving slightly relative to the fresh catalyst. – producing a product gas with just over 4 % hydrogen by volume immediately after light off compared to around 2.5 % with the fresh catalyst (Figure 4.9 below).

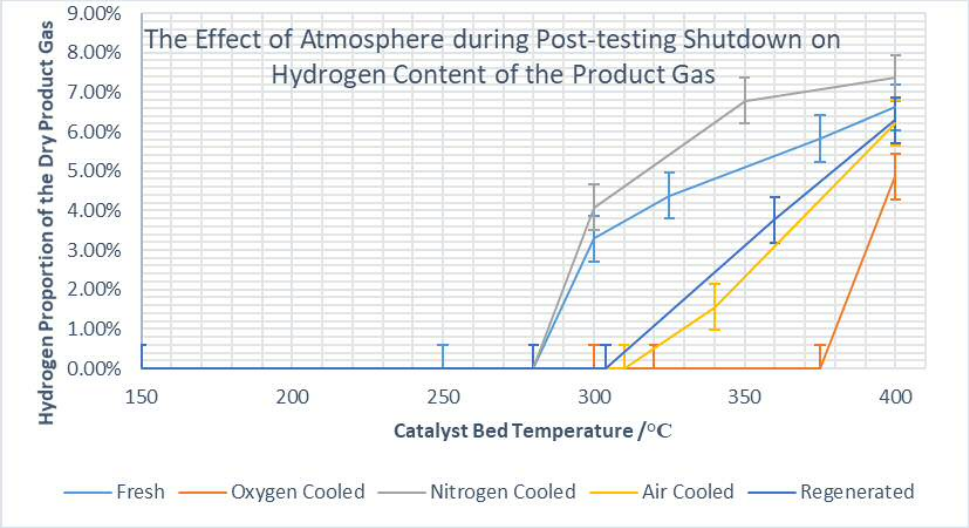

Figure 4.9: Nickel catalyst performance during the exhaust gas reforming of propane at λ = 2.12, and the effect of post-operation atmosphere control on the proportion of hydrogen in the product gas mixture

Note: So as to ensure a useful comparison, the data for the oxygen and air-cooled samples were chosen as the data for the 3rd test. The data for the nitrogen cooled and regenerated sample was chosen as the final run for each.

The equivalent plot of hydrogen yield (mol min^{-1} H_2 produced per mol min^{-1} propane in the reactant feed) as a function of catalyst bed temperature, shown in Figure 4.10 below, and shows the same trends.

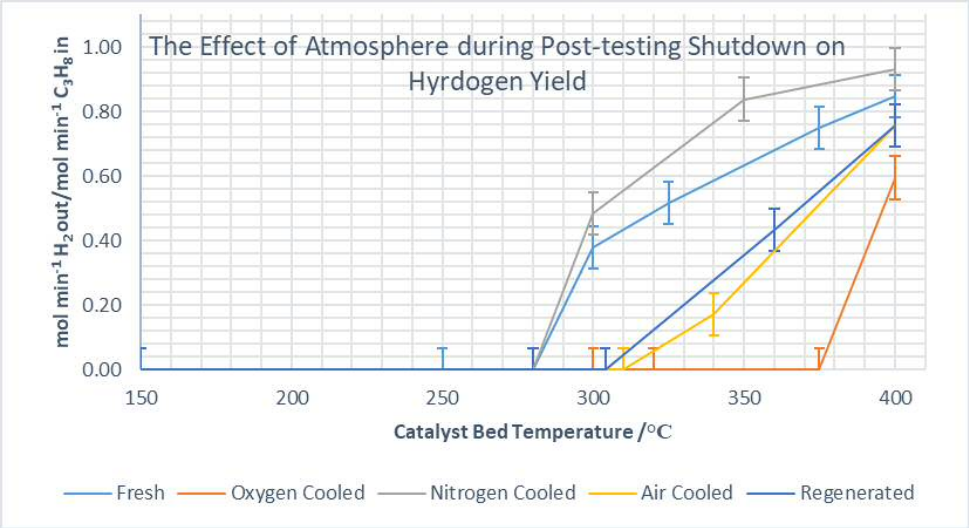

Figure 4.10: Nickel catalyst performance during exhaust gas reforming of propane at λ = 2.12, and the effect of post-operation atmosphere control on mol min^{-1} hydrogen produced per mol min^{-1} propane in the reactant feed

This dependence on the post-operation atmosphere control is also reflected in the equivalent propane conversion for each sample presented above, shown below in Figure 4.11.

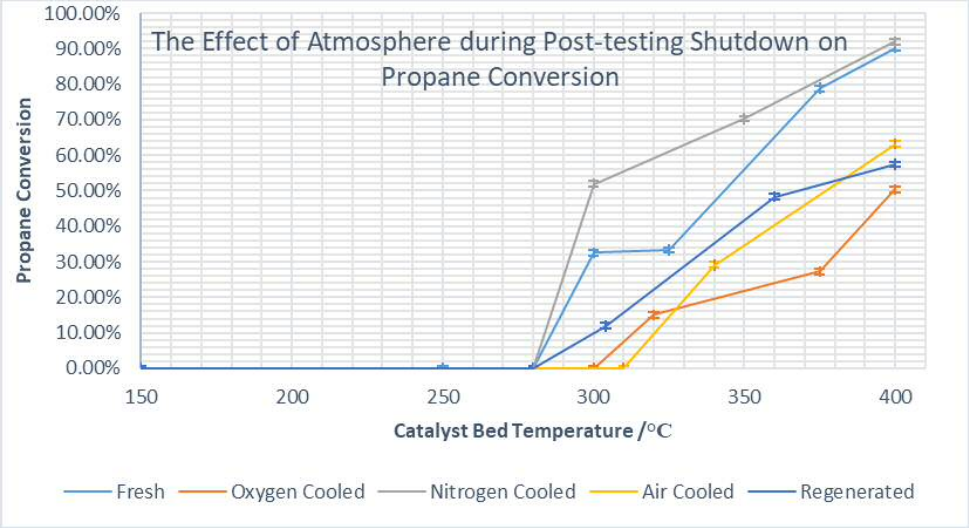

Figure 4.11: Nickel catalyst performance during exhaust gas reforming of propane at λ = 2.12, and the effect of post-operation atmosphere control on propane conversion

So these results do indeed suggest that the cause of the sporadic catalyst deactivation (in terms of hydrogen production and propane conversion) was exposing the used catalyst to an oxidative atmosphere after testing (likely through oxidation of deposited carbon and accompanying temperature spike on the catalyst surface).

The deactivation was found to be somewhat reversible, with hydrogen production falling to nothing at 400 °C after two testing/oxygen cool-down cycles, before recovering to just over 6 % by volume of the product gas after five consecutive test/nitrogen cool down cycles. However, the performance at lower temperature did not recover as well, with the catalyst failing to recover hydrogen production at 300 °C. It is possible that with further test/nitrogen cool down cycles that further catalyst activity would have been recovered – but for now all that can be said is that the deactivation was somewhat reversible.

Characterisation techniques were used to further shed light on this phenomenon. Deactivated samples were found to have significantly lower surface areas than the fresh catalyst. This suggests that there was at least some physical change occurring on the surface, during the deactivation process. The nitrogen-cooled sample was found to have significantly increased surface areas relative to the fresh catalyst. It is possible that such a large increase as this was an increase in the surface area of the active components.

However, it is proposed that this result was mostly caused by the presence of other high surface area species (such as high surface area carbon nanofibers) that were deposited on the surface of the catalyst during testing – hence giving the impression of an increased catalyst surface area. A similar phenomenon has been reported [122], whereby the deposition of carbon nanofibers has affected the measured pore size distribution of a Ni-Alumina aerogel catalyst for dry reforming of methane. The aforementioned activation treatments had no effect on surface area, relative to the fresh catalyst, suggesting that mere reduction of NiO is not responsible for the increase in surface area.

The sample that had been initially deactivated using the oxygen cool-down method, then reactivated using the nitrogen cool-down method, had the same surface area as the fresh catalyst (if not slightly higher). If it is assumed that this sample also experienced a decrease in surface area during the oxygen cool down phase of the experiment, this result suggests that that loss was then regained with consecutive test/nitrogen cool down cycles. However, it is not clear again whether this gain in surface area was of the catalyst itself, or from deposition of some higher surface area species onto the catalyst surface. If the latter was the case, then it could in part explain why the catalyst activity did not fully recover to the level of the fresh catalyst, since the surface area of the catalyst itself may not have actually been recovered.

The XRD (Figure 4.7) results suggest that the composition of the deactivated samples were similar to that of the fresh catalyst – containing mostly NiO supported on ceria zirconia. In contrast, the used sample exposed to test/nitrogen cool down cycles, shows a loss of NiO and gain of Ni(0) in the XRD peaks. This has been reported elsewhere, as a result of the catalyst becoming reduced in steam reforming reaction conditions [117]. The regenerated sample also showed this, if to a lesser degree. Estimations of crystal particle size for NiO showed that there was an increase in particle size for the deactivated samples, and the regenerated sample, in the range of 155-185 Å relative to the fresh catalyst. There was a small increase in particle size for the nitrogen cooled sample of approximately 10 Å.

These results therefore suggest that the nature of the deactivation at least had a physical transformation component to it – both BET and XRD data suggest some loss of surface area or increase in particle size of the NiO.

The TGA results for the fresh sample showed that its weight loss occurred at the low temperature end of the analysis – suggesting this was most likely loss of water, and other weakly bound contaminants. The air-cooled and oxygen cooled samples showed this initial weight loss, followed by another small weight loss around 450 °C. The nitrogen cooled and regenerated samples also showed a small weight loss associated with water, but then showed much larger losses around 400 °C. This second weight loss can be assigned to oxidation of coke deposited on the surface during the reforming reactions (ranging from amorphous carbon at lower temperatures to more graphitic carbon at higher temperatures [123, 124]). This suggests that both the nitrogen and regenerated samples have a much greater degree of carbon left on the surface compared to the oxygen and air cooled samples. One would expect to see some weight gain during TGA in oxidising conditions (flowing air), as any Ni(0) was oxidised to NiO. In fact this weight gain can often disguise any weight loss from coke/carbon oxidation [124]. However this seems to not be the case for these samples, rather weight loss through oxidation of carbon species outweighed any weight gain from oxidation of nickel metal. So these results do indeed suggest that the exotherm observed during the oxygen/air cool down methods was the oxidation of the carbon on the surface, and that this carbon was left on the surface when the sample was cooled in a nitrogen atmosphere.

The observed colour changes also support this. The deactivated sample seemed to be similar in colour to the fresh sample (if a little lighter/sandier coloured) while the used samples appeared black – hinting at the presence of carbon.

So the evidence certainly suggests that there is a physical component to the deactivation (BET and XRD), brought about by high surface temperatures during the oxidation of deposited carbon. However there may also be some form of chemical transformation occurring at the same time (reversibility of the deactivation, XRD and BET). This is assuming the following:

- That the recovered surface area of the regenerated sample resulted from deposition of species onto the catalyst surface rather than an actual physical recovery of catalyst surface area (as suggested by BET and XRD). Hence the recovery in activity in the regenerated sample was down to chemical transformations that occurred to return reforming activity.
- That the catalyst activity would not have fully recovered had it been treated further, since part of the deactivation was due to unrecoverable loss of surface area during the deactivation phase.

Catalyst deactivation, discussed at length in a review by Argyle and Bartholomew [69], broadly falls into three categories:

- Chemical: e.g poisoning, vapor formation, vapor/gas-solid reactions and solid-solid reactions.
- Thermal: Thermal degradation and sintering
- Mechanical: attrition/crushing and fouling

As mentioned, there was clearly some thermal degradation/sintering occurring. This is the thermally induced loss of surface area – either of the support or the catalytic active material, or both. This process can often be complex, involving many different types of migration of different species. This process requires high temperatures, since it requires enough lattice vibration for atoms/crystallites to become mobile enough to migrate. Less strongly bound species can become mobile around the Huttig temperature (defined as 0.3 T_{MP}), followed by bulk species becoming mobile at the higher Tamman temperature (0.5 T_{MP}). The process is usually impossible to reverse, but can sometimes be possible but with great difficulty [65, 108].

The Scherrer calculated NiO particle sizes (Table 4.2) suggest that the sintering was not reversed, despite measured BET surface area recovery. Indeed it seems unlikely that simply using the catalyst under reaction conditions and then cooling under nitrogen could reverse any sintering that occurred during deactivation. Therefore the additional potential deactivation types need to also be considered to explain the reversibility of the observed deactivation.

Mechanical attrition/crushing is the forced loss of catalyst due to abrasion and crushing of catalyst particles. This generally applies to pellet or monolith form catalysts, hence this can be ruled out for this

section of work since the catalyst was tested in powder form (pelletized Ni10CZ was used in the following chapters).

Fouling is a mechanical process whereby species are physically deposited onto the catalyst surface and into the catalyst pores. Though this would be expected to, and did occur on all samples (in the form of carbon deposition) during testing, this cannot be the principal cause of the deactivation. This is because, as the TGA data shows the nitrogen cooled sample had a significant amount of carbon deposited on the surface, yet produced the mixture richest in hydrogen content. So although carbon deposition would likely have ended up being deactivating, it was not found to be significantly so over this time scale. Additionally carbon deposition would not cause the drop in surface area observed in the BET data of the deactivated samples. Fouling, in extreme cases can also lead to loss of active metal through fracturing of the catalyst. Though the fact there was no real change in the intensity of the NiO peaks in the XRD data suggests this is not the case (since the intensity of the peak is related to the concentration of the species producing it). Furthermore, the loss of active metal would fail to explain the measured loss of BET surface area and increase in particle size.

Chemical deactivation pathways would likely not explain the data, such as the loss of BET surface area, as well as the fact that the XRD spectrum is almost identical for the deactivated samples as the spectrum for the fresh catalyst.

So only thermal degradation seems to explain the data adequately, yet the reversibility of the deactivation suggests it must be a slightly more complicated picture than just simple sintering.

The Huttig/Tamman temperature of Ni(0) and NiO are 245 °C/590 °C and 395 °C/841 °C [69]. So both temperatures are higher for NiO than for Ni(0). This suggests that metallic nickel will begin to migrate/sinter sooner than nickel oxide. For example the results in Figures 4.4 and 4.6 shows that even when the catalyst was fully deactivated (not producing hydrogen) that oxygen was still being consumed, and NiO is the species involved for the oxidative first step in the exhaust gas reforming process – the oxidation of the hydrocarbon source. The metallic nickel is then responsible for the reforming reactions, via activating the hydrocarbon, and therefore production of hydrogen [82, 117].

Therefore it is proposed that, during the deactivating cool-down methods (oxygen and air atmospheres) that the carbon is being burnt off (TGA and colour changes), along with some metallic nickel oxidation (XRD), resulting in an exotherm and therefore spike in catalyst surface temperature. This is sufficient to surpass the Huttig temperature of both Ni(0) and NiO species on the surface, as well as the Tamman temperature of Ni(0), but not the Tamman temperature of NiO. Hence the overwhelming effect is the sintering of nickel metal, and conversion of the remaining nickel metal to nickel oxide, and the migration of this surface nickel oxide to loosely form larger particles as well as some sintering (BET and XRD). This results in both a loss of active species for reforming, as well as a decrease in surface area – hence catalytic activity is lost, both in terms of a delay in light off and loss of reforming activity.

In the case of reforming with nickel catalysts, their activity is strongly determined by the reducibility, surface area and metal dispersion of the catalyst. Hence losses in these areas will result in a loss of activity [83].

During the reversal process, the active surface area is not recovered (assuming the measured increase in surface area is from carbon species deposited on the surface, as in the nitrogen-cooled sample) however after testing under reaction conditions some of the NiO is converted back to Ni(0), and eventually some catalytic activity is restored. Not all of the initial activity is recovered since the sintering (and resulting loss of active species – both Ni(0) and NiO) is irreversible, as well as the contribution to deactivation from the build-up of carbon on the surface after consecutive nitrogen cooling cycles.

Hence the deactivation was a largely thermal driven process, but with an additional component involving which chemical species were present on the surface after the thermal degradation. This therefore means that the reversal of the deactivation was purely a chemical transformation in the form of reappearance of Ni(0) from the remaining exposed NiO, from testing under reaction conditions combined with cooling under nitrogen.

The oxidation of the carbon species during cooling under oxidative atmospheres, in effect, acts like oxidation methods used to regenerate catalysts fouled by carbon formation in industry. These methods are indeed effective at quickly removing coke, however their highly exothermic nature can be a problem. This regeneration process is sometimes called coke burn-off. Therefore in order to avoid damagingly high temperatures (and the resulting thermal degradation), the reaction conditions are always optimised to be operated at the lowest possible temperature [19, 108].

Though not precisely the same effects as is proposed to be occurring here, the importance of controlling the conditions a catalyst is exposed to during repeated start-up/shut-down cycles has also been reported in applications for fuel cells, both for reforming, and water gas shift catalysts in such systems [125-128]. In the work by Li et al. [125] on the use of nickel catalysts for methane steam reforming for fuel cells, they note that such systems require the reformer to be purged by steam post-operation to enhance safety. However, like oxygen, steam can be oxidising in those conditions – and that this can cause catalyst deactivation during shut-down, in part through severe sintering. In their work, the authors report that the nickel in their catalyst can be self-regenerated, with the help of ruthenium as a doping agent in the catalyst formulation. They later report that doping the nickel catalyst with platinum yields improved regenerative ability [126].

Conclusions

The work in this chapter investigated the deactivation of the nickel catalyst during repeated exhaust gas reforming testing. The cause was found to be exposing the hot catalyst to an oxidative atmosphere during post-testing cool down. This deactivation was found to be severe if somewhat reversible.

It was proposed that the cause of the deactivation was the oxidation of carbon species left on the catalyst surface during testing, which caused a spike in surface temperature sufficient to cause sintering and a combination of permanent and temporary loss of a quantity of the key active component for reforming – Ni(0).

In the remainder of this project, the testing/nitrogen cool-down regime was used as standard operating conditions. This was so as to avoid any deactivation resulting from catalyst cool down conditions, and therefore allow easier performance comparison, as well as the post-testing characterisation of the catalysts, since the inert cooling atmosphere would preserve any changes to the catalyst that had occurred under reaction conditions (such as carbon species). Though this situation would not be representative of what would happen in the real application, it was deemed suitable this early stage of testing.

Further work into the deactivation reported here should involve additional characterisation techniques on fresh/activated/used/deactivated samples so as to more fully understand any physical and chemical transformations resulting from these different treatments. Techniques such as microscopy (SEM or TEM, with elemental analysis) could be of use in identifying species present at the surface in each of the samples. Chemisorption techniques to analyse the amount of nickel present could also be used.

It is clear from the work in this chapter that this catalyst formulation, of nickel impregnated ceria zirconia is very sensitive to both activation and cool down phases of its use. In fact, catalyst stability (whether to start-up/shut-down cycles as reported here, as well as general stability under reaction conditions) was a recurring issue throughout this work.

Chapter 5 - Establishing the Baseline Exhaust Gas Reforming Performance of the Precious and Base Metal Catalysts with Gaseous and Liquid Fuels

Introduction

The aim of this section of work was to carry out testing of both the PM and nickel catalyst at three exhaust gas reforming conditions (λ = 1, 1.5 and 2.12), with both propane and iso-octane as surrogates for gasoline. The lambda value is the ratio of the air/fuel ratio of the mixture present in the engine intake to the stoichiometric air/fuel ratio for combustion of the fuel in question. A value of 1 would therefore signify stoichiometric conditions, and values > 1 would imply air rich mixtures. These different engine-operating conditions would produce differing exhaust gas compositions – as detailed in Chapter 1 in general terms, and in Chapter 2 for the specific conditions tested here.

The goal was to establish some baselines for their performance with both fuels under the differing conditions so as to gain an understanding of the processes occurring.

Additional Experimental Details

The procedures used here for the liquid and gaseous fuels were described in the Experimental chapter. Based on the work detailed in Chapter 4, which highlighted the importance of the atmosphere during the cool down phase of testing, it was also decided that for each experiment the catalyst would be exposed to the inert nitrogen atmosphere during the cool down phase.

This was in order to remove complications associated with catalyst deactivation that were found in the previous chapter, as well as to preserve any species deposited on the catalyst during testing so as to allow more information to be obtained from post-testing characterization, particularly with respect to the rates of carbon deposition.

Each test was designed to be carried out over three consecutive days, with a nitrogen cool down phase at the end of each day. This equated to roughly 24 hours under reaction conditions.

Catalysts were testing in the range of 150°C to 600°C. The catalysts were then removed from the reactor after the tests were completed, inspected, weighed, and in the case of the nickel catalyst characterized by TGA.

Results

Note: As per Chapter 2, the concentration of the gases in the dried product stream were found to be directly proportional to the rate of production/consumption (mol min^{-1}).

Precious Metal Catalyst Performance for Exhaust Gas Reforming of Propane

At the λ = 1 Condition

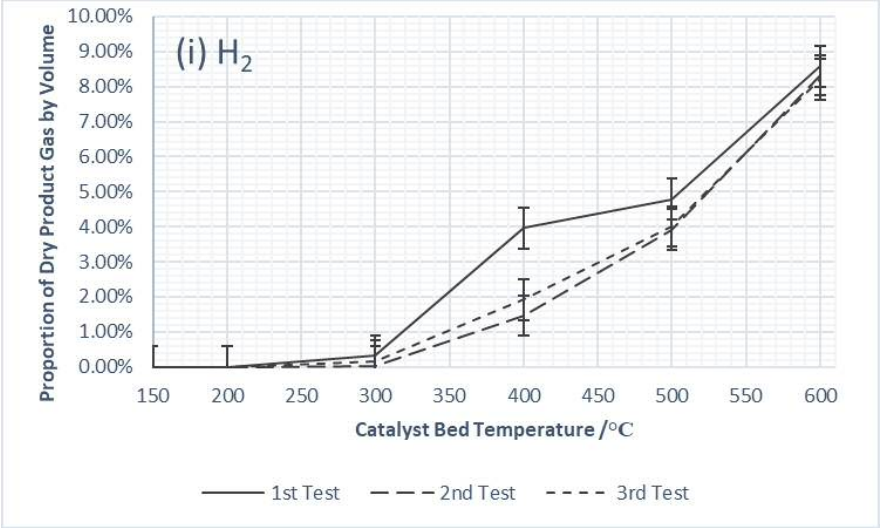

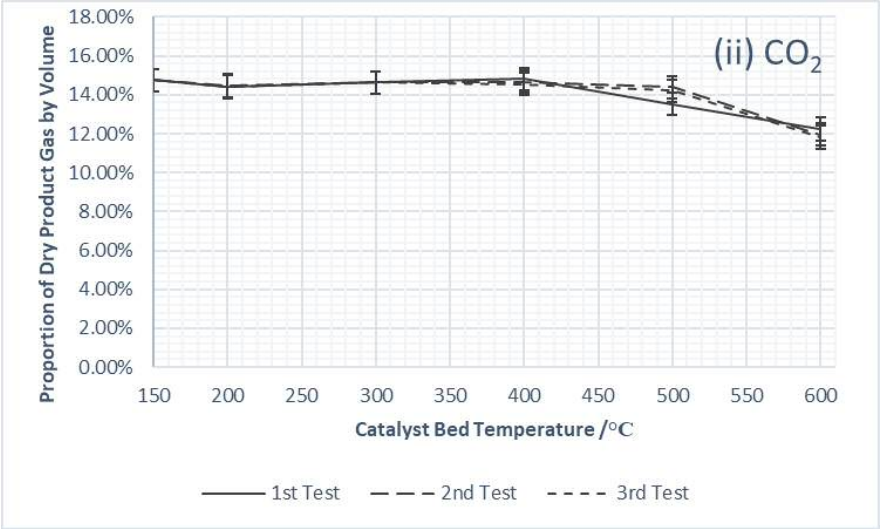

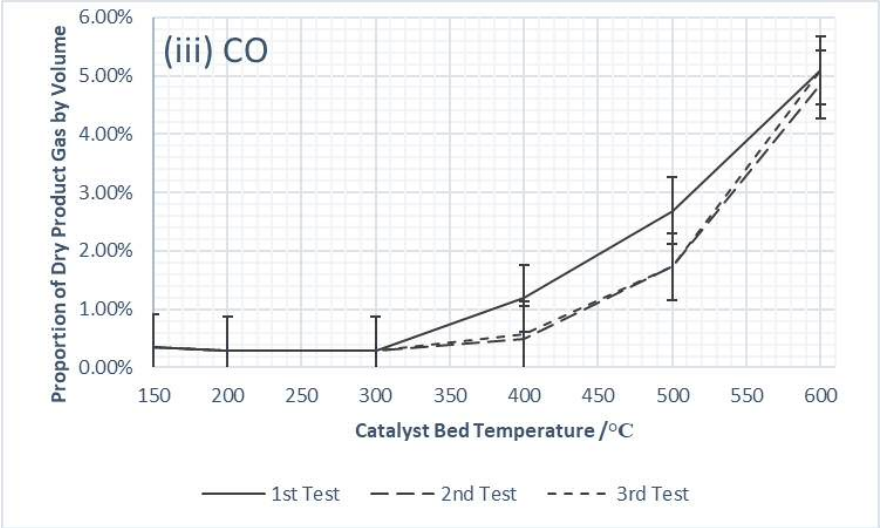

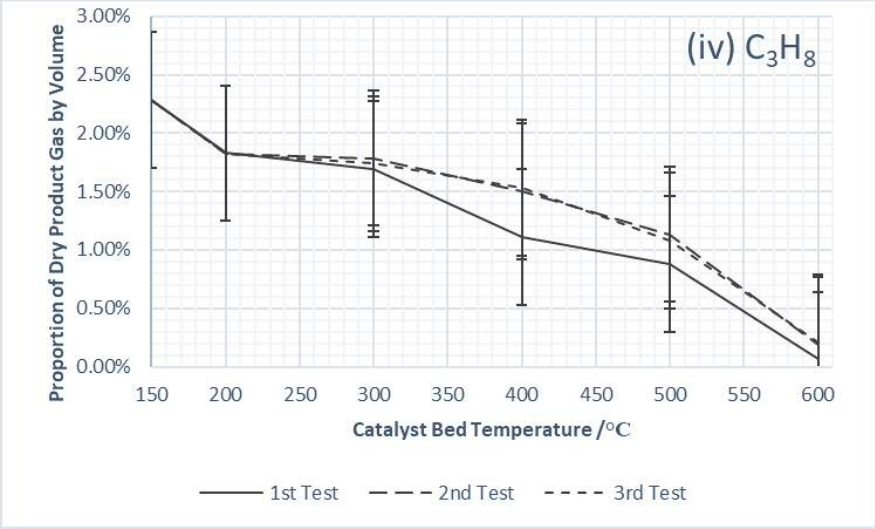

Figure 5.1: PM catalyst performance in the exhaust gas reforming of propane at λ = 1, in terms of the composition of the dried product gas as a function of bed temperature

The results above in Figures 5.1(i) to 5.1(iv) show how the PM catalyst performed over three consecutive exhaust gas reforming tests, with nitrogen cool down cycles in between each test, at λ = 1 and 2 % (of the total reactant feed) propane as the model fuel. There is no equivalent data for oxygen since the reactant stream contained only 0.4 % oxygen, which is below the GC's sensitivity, even before any of it was consumed in reactions.

Indeed, it can be seen in Figure 5.1(iv) that there was some propane consumption around 180 °C, suggesting that the 0.4 % oxygen in the reactant stream was most likely also consumed. The consumption of propane then increased with temperature, to almost full consumption at 600 °C.The second and third tests displayed slightly lower propane consumption at each temperature interval.

The carbon dioxide content of the dry product gas, shown in Figure 5.1(ii), stayed roughly flat relative to the dry reactant stream at low temperature, before decreasing at high temperature due to either dilution, consumption or lower selectivity (more on this in the Discussion section).

As shown in Figure 5.1(i), production of hydrogen, to levels around 0.2 % by volume of the product gas at 300 °C, was slightly offset relative to carbon dioxide. It then increased throughout the temperature range, reaching a maximum of 8.5 % by volume of the product gas at 600 °C. The second and third tests displayed similar hydrogen levels to the first tests at 300, 500 and 600 °C. However, there was a significant difference in the amount of hydrogen produced at 400 °C in the first test, compared to the second and third. This was reflected in the greater difference in propane consumption seen at 400 °C between the first test compared to the second and third tests.

The proportion of the dry product gas constituting carbon monoxide is shown in Figure 5.1(iii), and also showed a gradual increase throughout the temperature range, with a maximum value of just over 5 % by volume of the product gas at 600 °C. Again, these levels decreased in the second and third tests,

relative to the first test. This combined with the slightly lower proportion of hydrogen mentioned above likely explains the lower propane consumption in these tests.

At the λ = 1.5 Condition

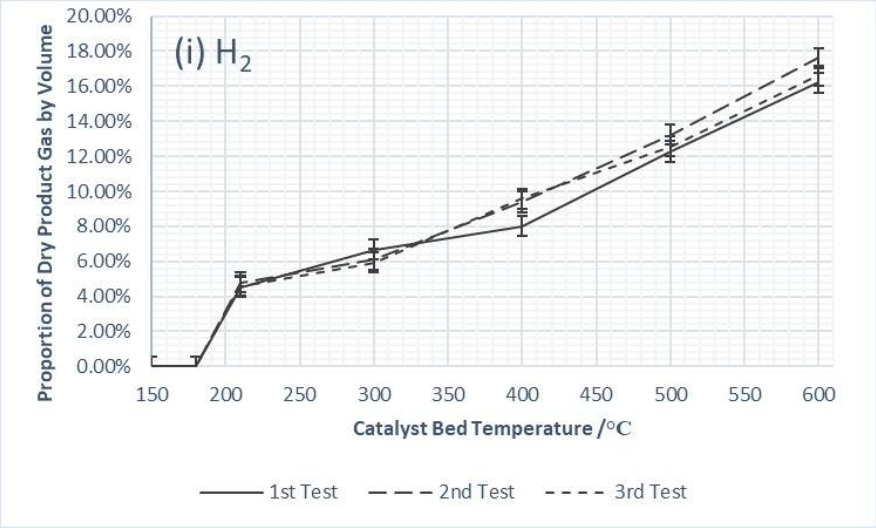

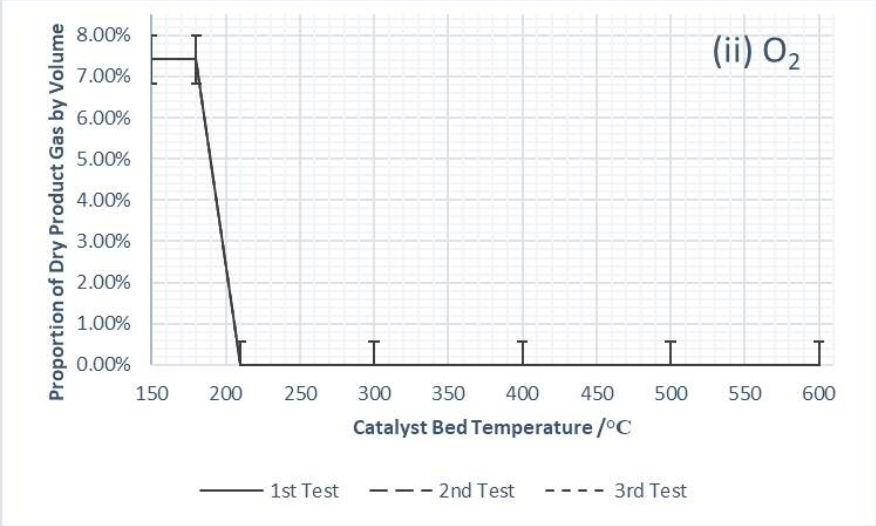

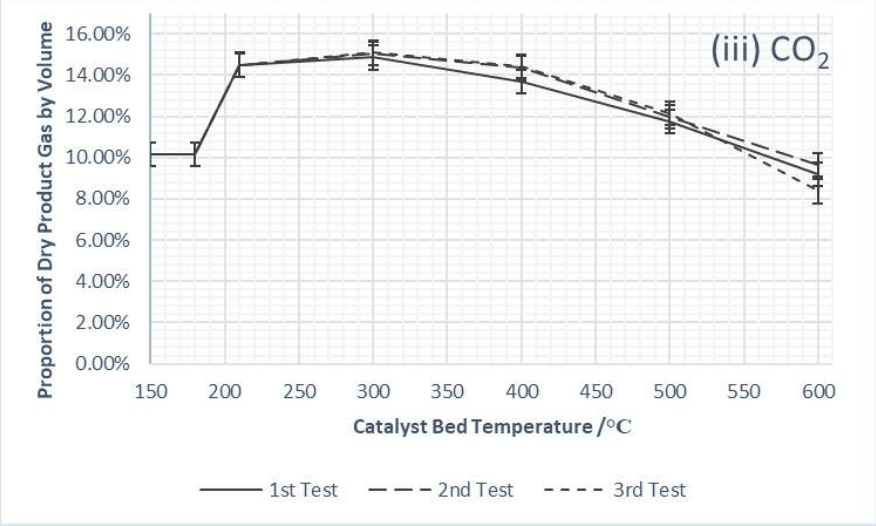

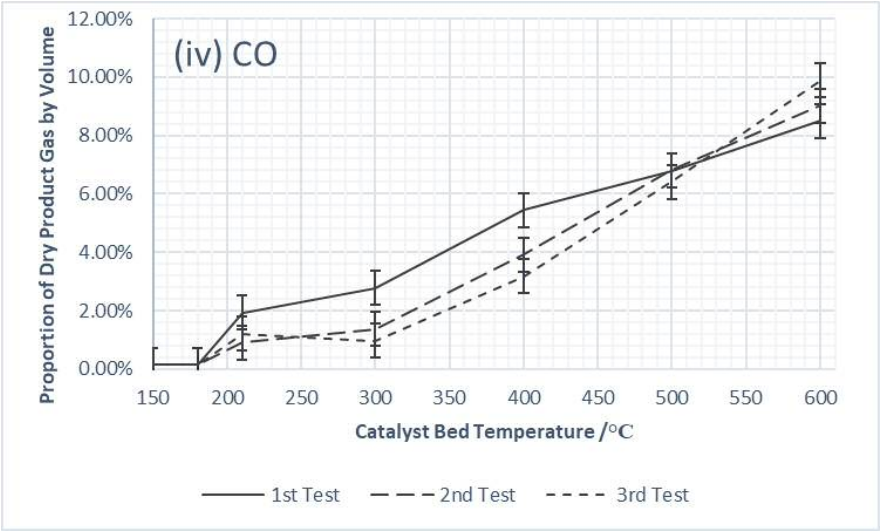

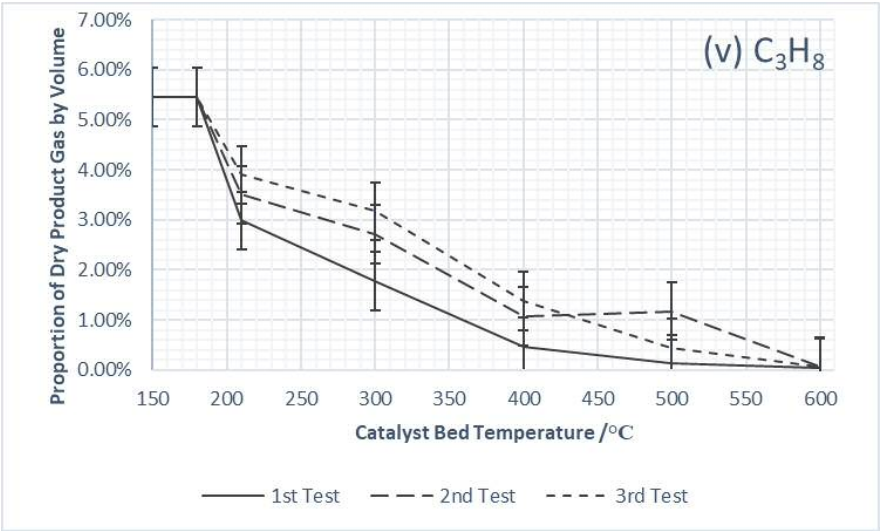

Figure 5.2: PM catalyst performance in the exhaust gas reforming of propane at λ = 1.5, in terms of the composition of the dried product gas as a function of bed temperature

The results above show that at λ = 1.5, with 5 % (of the total reactant feed) propane, that consumption of propane (Figure 5.2(v)) and oxygen (Figure 5.2(ii)) in the oxidation reactions happened simultaneously with significant hydrogen production (Figure 5.2(i)), promoted by the exotherm generated by these oxidation reactions.

The oxygen consumption was completed in the light off process, once the temperature had settled at just over 200 °C. Just under 5 % by volume of the product gas was hydrogen at this stage. The hydrogen content of the product gas continued to increase as the temperature was raised, reaching a maximum of just under 18 % by volume at 600 °C, and remained consistent between runs.

Propane consumption, shown in Figure 5.2(v), during light off decreased between tests. The consumption of propane, shown by the lower proportion detected in the dried product stream, was also observed to decrease between tests across the rest of the temperature range, except for 600°C, where total consumption was measured. This fall in the consumption of propane was not accompanied by a decrease in oxygen consumption or a decrease in hydrogen production.

The results in Figure 5.2(iv) show that this was likely to be due to a decrease in carbon monoxide production between runs.

The amount of carbon dioxide in the stream (Figure 5.2(iii)) increased during the light off process, likely from the oxidation of the propane, before levelling off and then decreasing as the temperature was increased. Again this could be down to it being consumed and/or diluted.

At the λ = 2.12 Condition

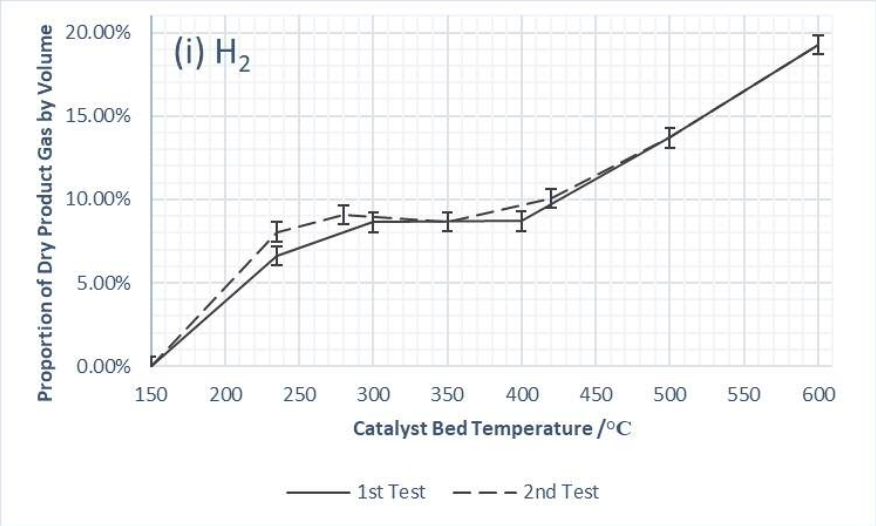

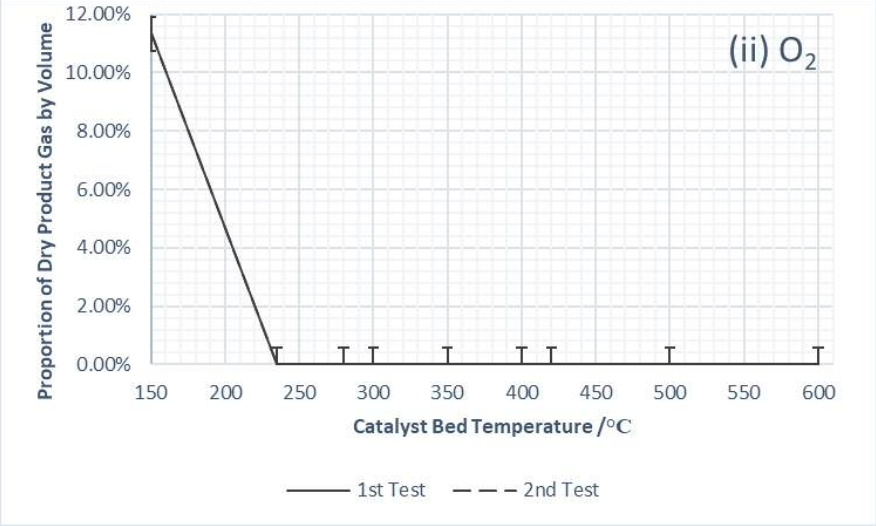

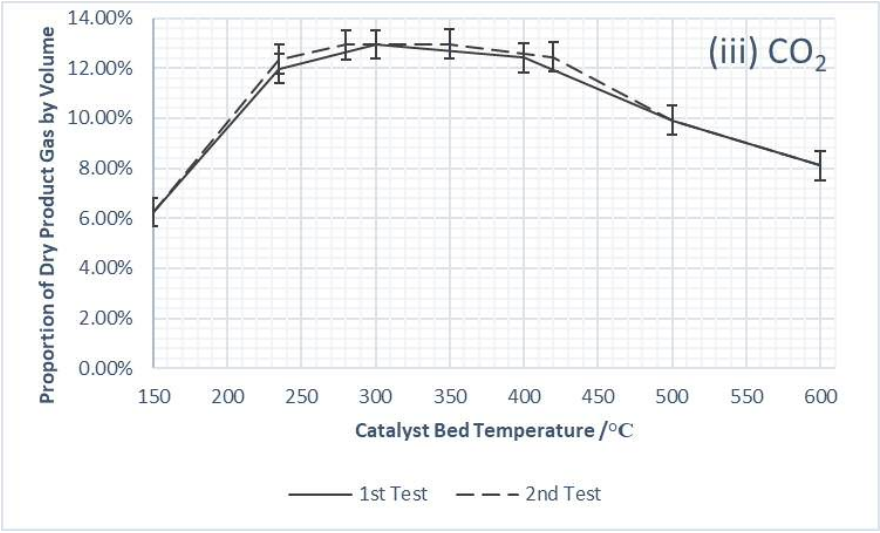

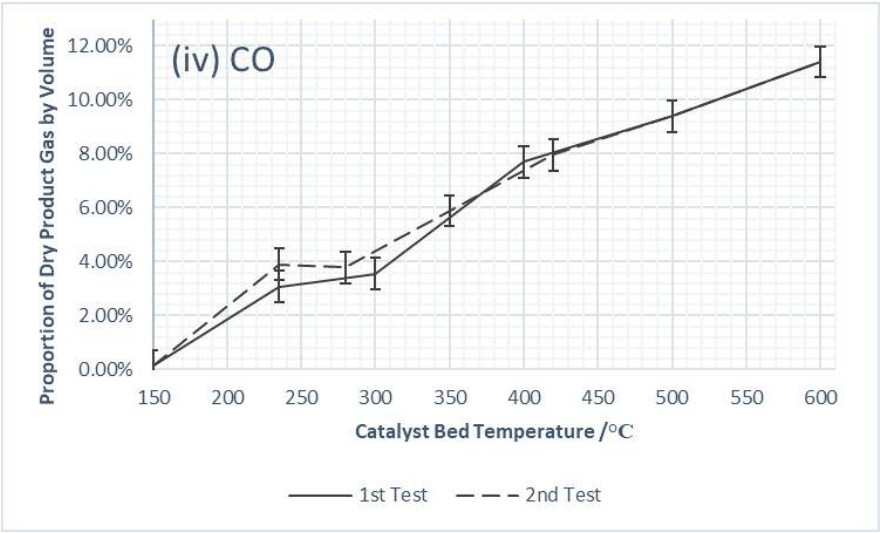

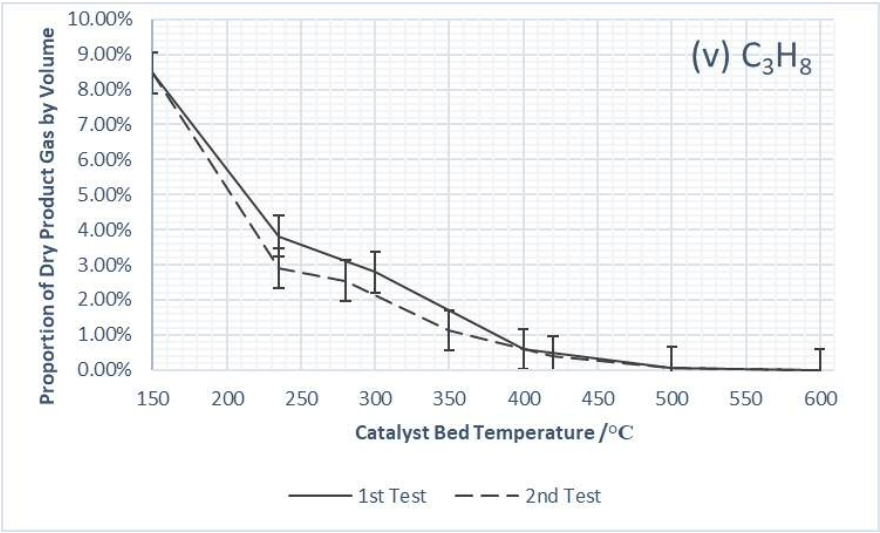

Figure 5.3: PM catalyst performance in the exhaust gas reforming of propane at λ = 2.12, in terms of the composition of the dried product gas as a function of bed temperature

When the PM catalyst was tested at λ = 2.12, with 8 % (of the total feed) propane, it can be seen that the first step again involved the complete consumption of oxygen (Figure 5.3(ii)), which consumed around

half of the propane (Figure 5.3(v)), at 235 °C. The propane consumption was nearly complete at 500 °C, and was at 600 °C.

Accompanying these oxidation reactions was production of hydrogen (Figure 5.3(i)) of around 7-8 % of the product gas by volume, and carbon monoxide production in the region of 3-4 % (Figure 5.3(iv)). The quantity of hydrogen and carbon monoxide then rose to a maximum of just under 20 % and 11 % by volume of the product gas respectively at 600 °C.

The results between the two runs were also relatively consistent, with a slight increase in hydrogen and carbon monoxide in the second test, and accompanying increase in propane consumption.

Nickel Catalyst Performance for Exhaust Gas Reforming of Propane

At the λ = 1 Condition

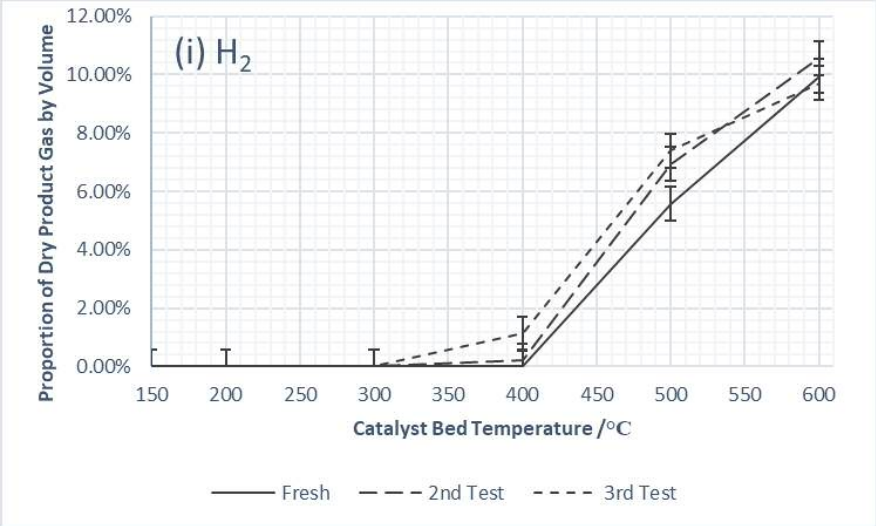

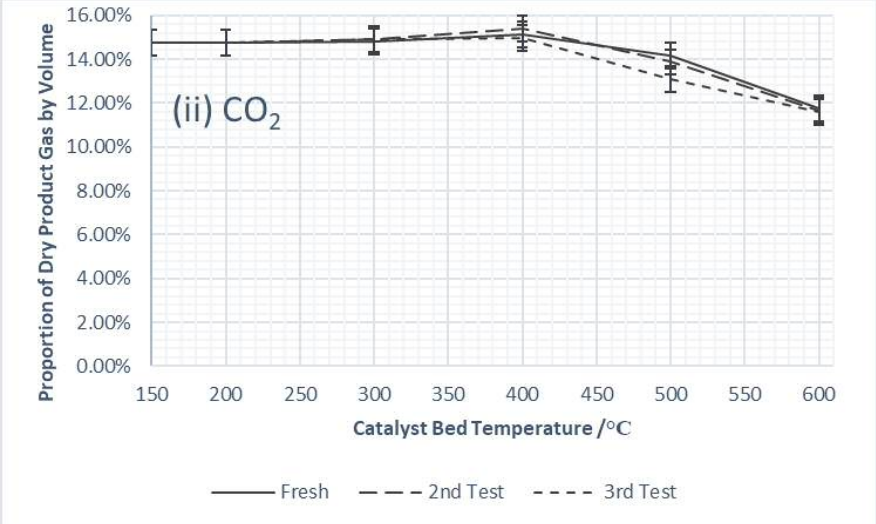

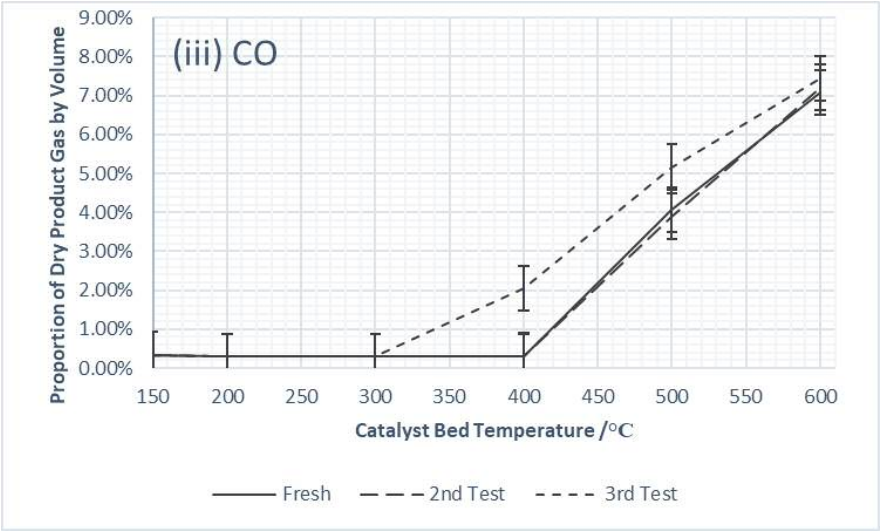

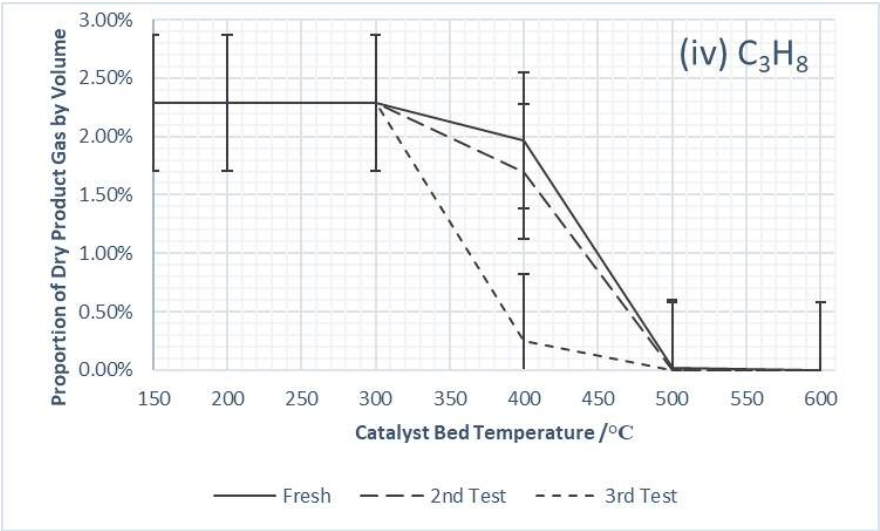

Figure 5.4: Nickel catalyst performance in the exhaust gas reforming of propane at λ = 1, in terms of the composition of the dried product gas as a function of bed temperature

The results above show the progression of the product gas composition, for the 10 % nickel on ceria zirconia catalyst, at λ = 1 with 2 % (of total reactant feed) propane, over three consecutive testing/nitrogen cooling cycles. The data for oxygen is again not shown at the λ = 1 condition for the reasons discussed previously.

Figure 5.4(ii) shows there was small increase in the quantity of carbon dioxide in the product gas at 300 °C, suggesting some oxidation of the fuel had occurred, and the small amount of oxygen in the stream had been consumed.

However, this was a small increase in the quantity of carbon dioxide, and as can be seen in Figure 5.4(iv), there was very little propane consumed at 300 °C. Nor in fact was there much propane consumed at 400 °C in the test with the fresh catalyst, however the amount consumed at this temperature had increased significantly by the third test.

The hydrogen content of the product gas increased throughout the temperature range (Figure 5.4(i)) as well as slightly between tests. This result is similar to that seen in Chapter 4, when the testing/nitrogen cool down cycles seemed to activate the catalyst.

The quantity of hydrogen increased throughout the range in each test, reaching a maximum of around 10 % of the product gas by volume at 600 °C.

There was no carbon monoxide produced in the first two tests until 500 °C, and product gas levels reached a maximum of around 7 % of the product gas at 600 °C (Figure 5.4(iii)).

However, in the final test, there was around 2 % by volume carbon monoxide in the product gas at 400 °C, and this increase, along with the increase in hydrogen production at 400 °C between tests, likely explains the large increase in propane consumption in the final test relative to the first two tests.

At the λ = 1.5 Condition

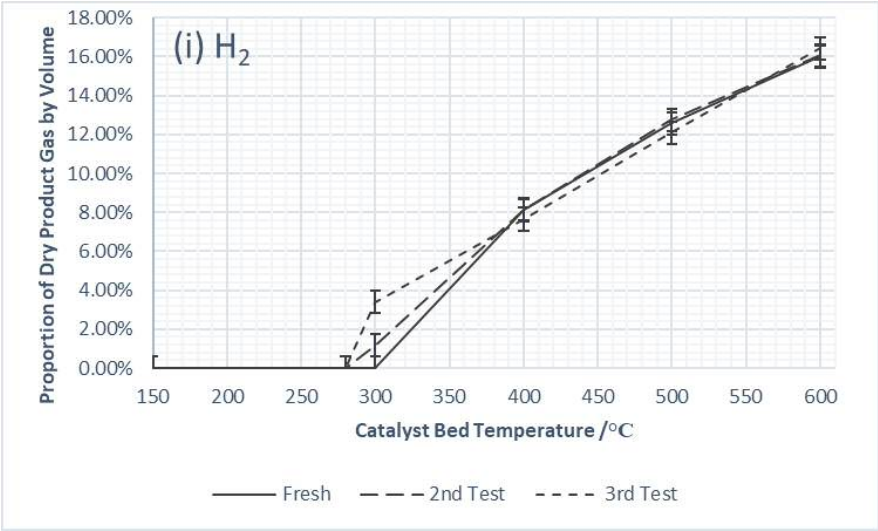

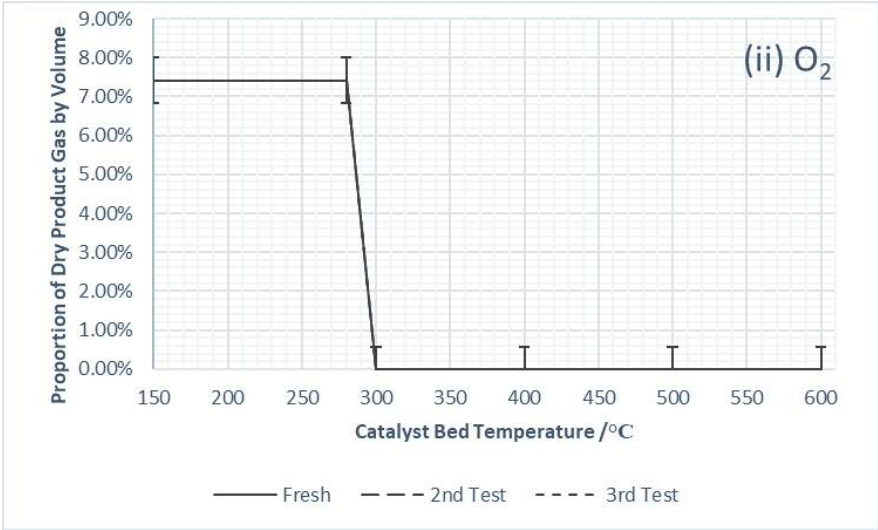

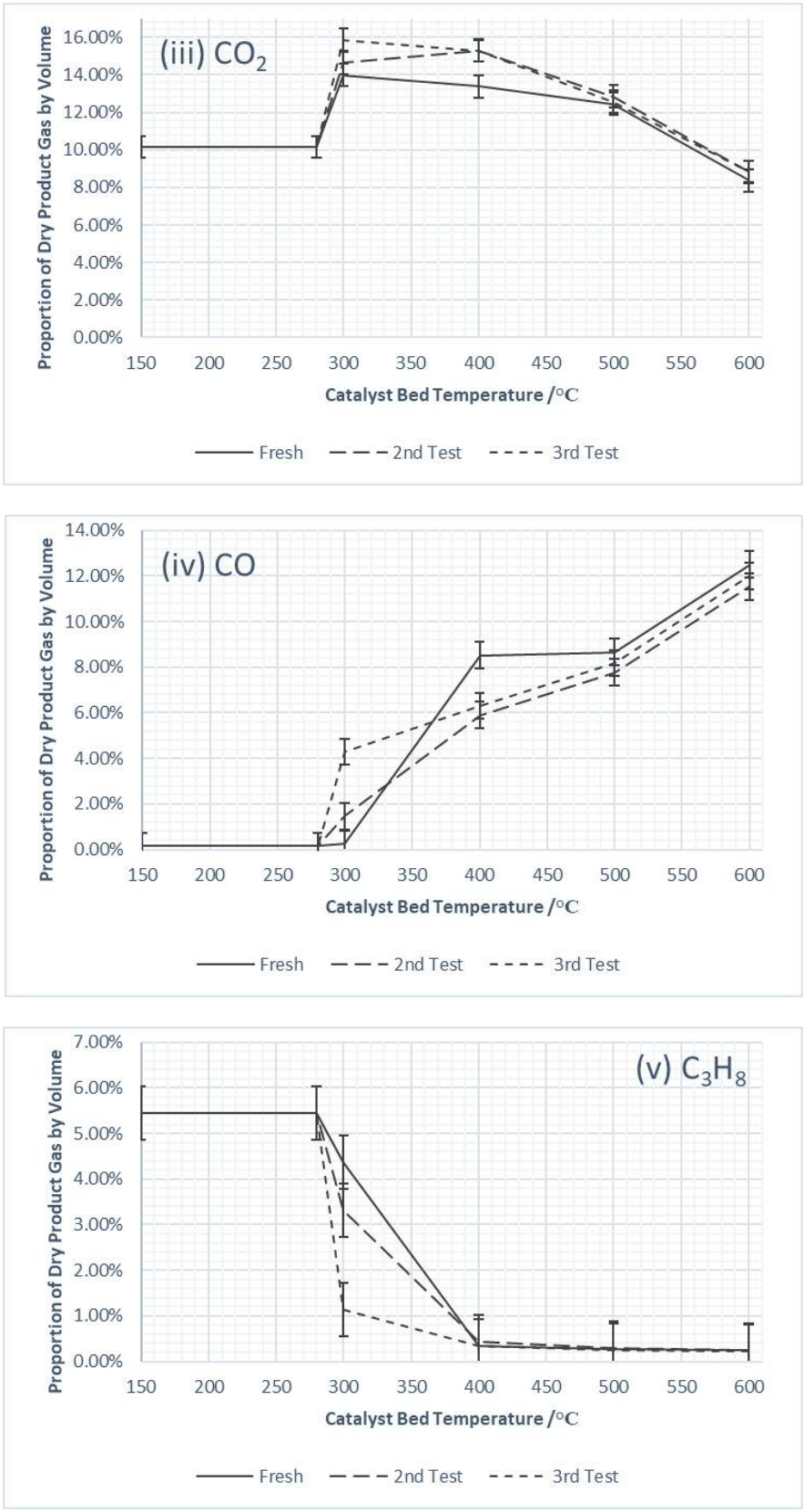

Figure 5.5: Nickel catalyst performance in the exhaust gas reforming of propane at λ = 1.5, in terms of the composition of the dried product gas as a function of bed temperature

It can be seen in Figure 5.5(ii) above that for the Ni10CZ catalyst under the λ = 1.5 condition, with 5 % (of total reactant feed) propane, that light off and associated total oxygen consumption occurred at around 280°C, and the exotherm took the bed temperature to 300 °C. There was also the associated

consumption of propane (Figure 5.5(v)), and increase in carbon dioxide content (Figure 5.5(iii)), as a portion of the fuel was oxidized.

The consumption of propane at 300 °C increased significantly between tests, and is likely associated with the increase in hydrogen and carbon monoxide production, shown by increasing concentrations in the dry product gas, at that temperature between the fresh catalyst and the final test (Figure 5.5(i) and 5.5(iv) respectively).

The proportions of the product gas containing hydrogen, carbon monoxide and the consumption of propane all further increased through the temperature range. Hydrogen and carbon monoxide content reached a maximum of around 16 % and 12 % by volume of the product gas respectively at 600 °C, and propane was completely consumed.

So again, a slight activation of the catalyst was observed, particularly at low temperature, by the use of the testing/nitrogen cool down cycles.

At the λ = 2.12 Condition

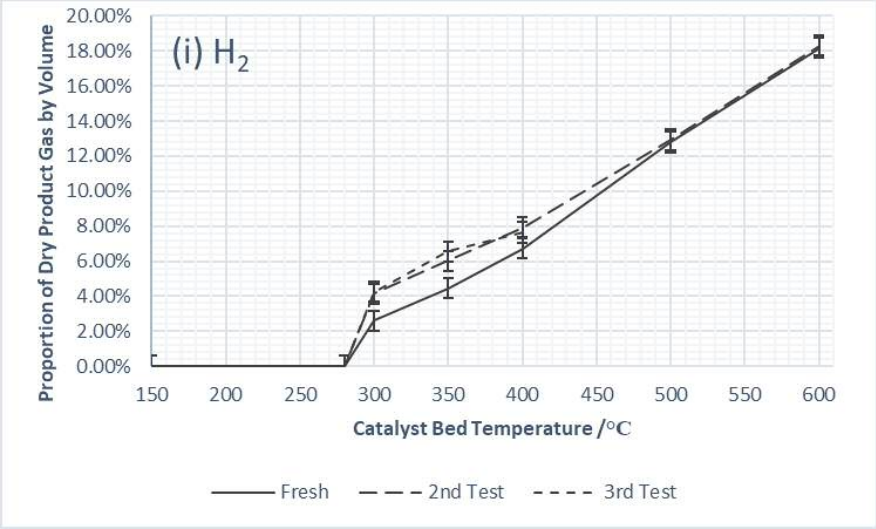

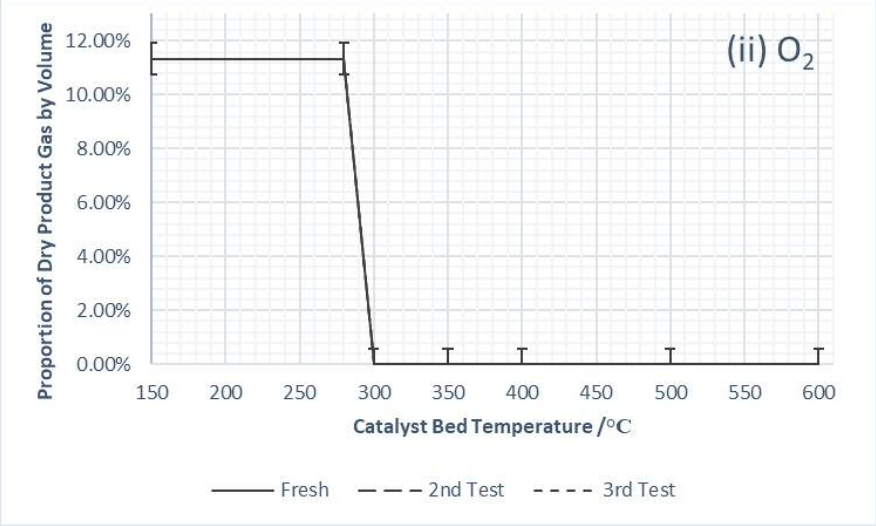

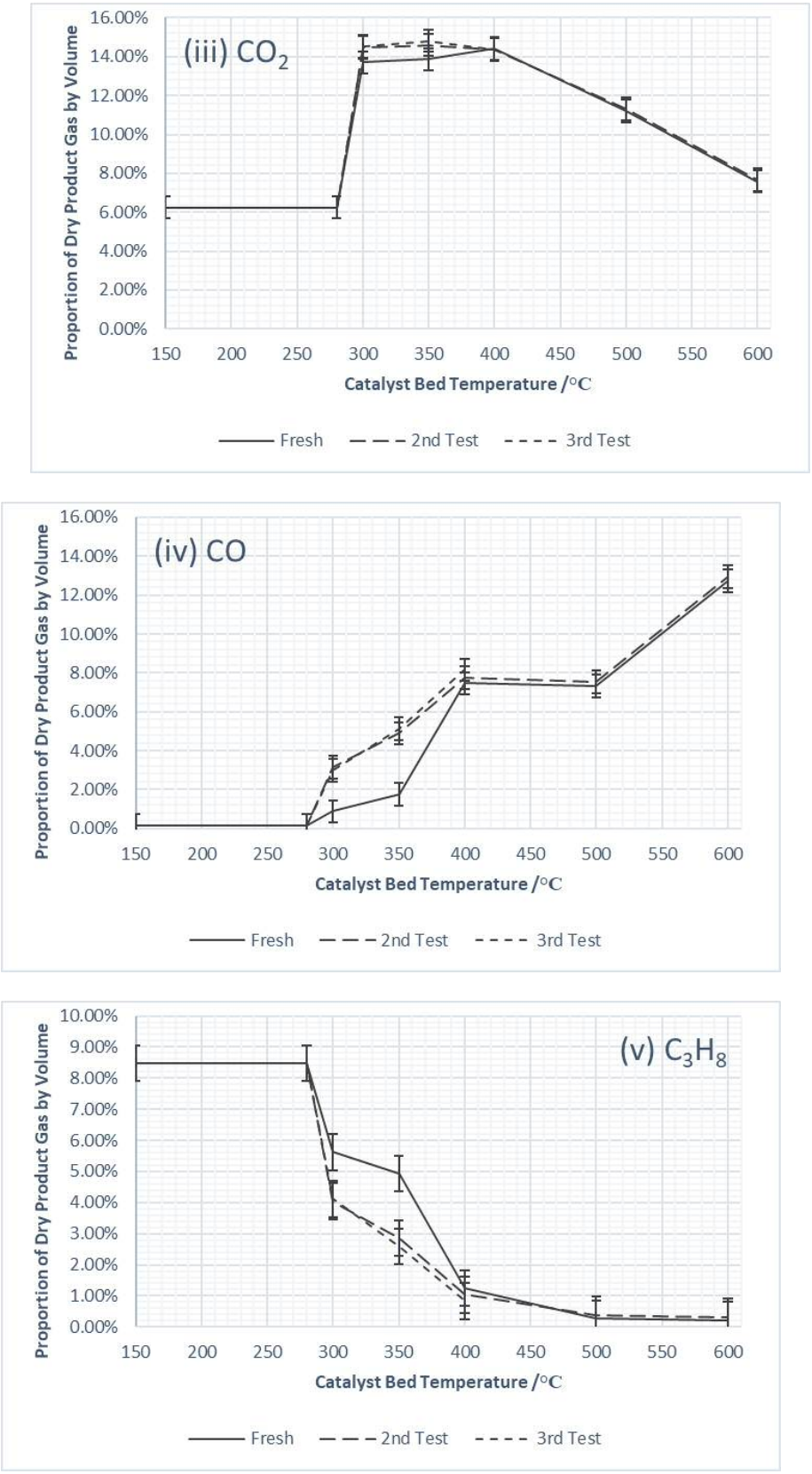

Figure 5.6: Nickel catalyst performance in the exhaust gas reforming of propane at λ = 2.12, in terms of the composition of the dried product gas as a function of bed temperature

The results above for the Ni10CZ at the λ = 2.12 condition, with 8 % (of total reactant feed) fuel showed light off and complete oxygen consumption (Figure 5.6(ii)) starting at 280 °C, and raising the bed temperature to 300 °C. The corresponding consumption of propane was also observed (Figure 5.6(v))

along with the increase in the carbon dioxide content of the product gas from the oxidation of the fuel (Figure 5.6(iii)).

Hydrogen production also began at 300 °C (Figure 5.6(i)), as did carbon monoxide production (Figure 5.6(iv)). Both then increased throughout the temperature range to maximums of around 17 % and 12 % by volume of the product gas respectively at 600 °C.

There was again an increase in hydrogen and carbon monoxide production, along with the accompanying increase in propane consumption between 300 °C and 400 °C, for the used catalysts relative to the fresh catalyst.

Precious Metal Catalyst Performance for Exhaust Gas Reforming of Iso-octane

At the λ = 1 Condition

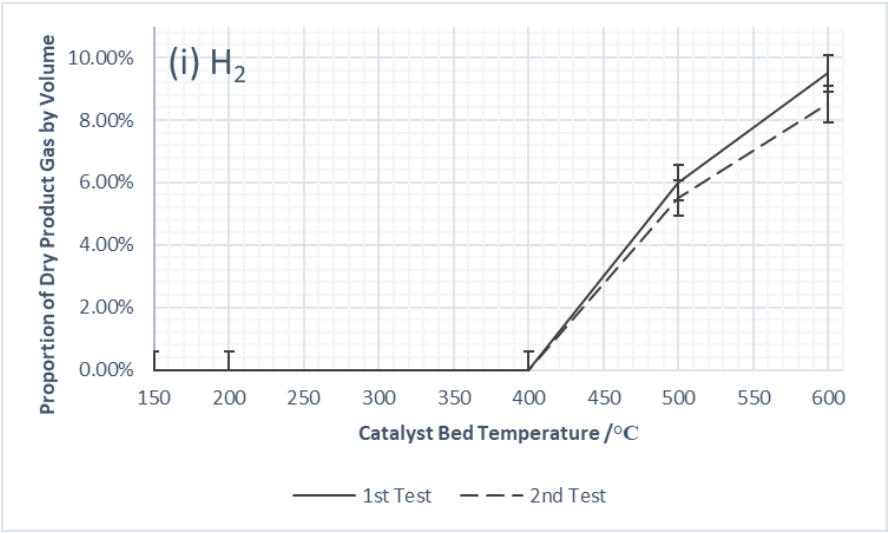

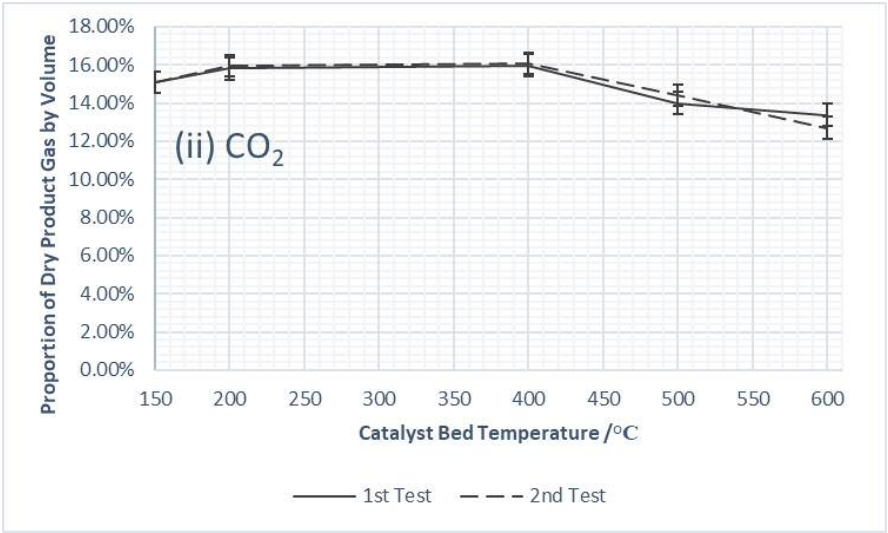

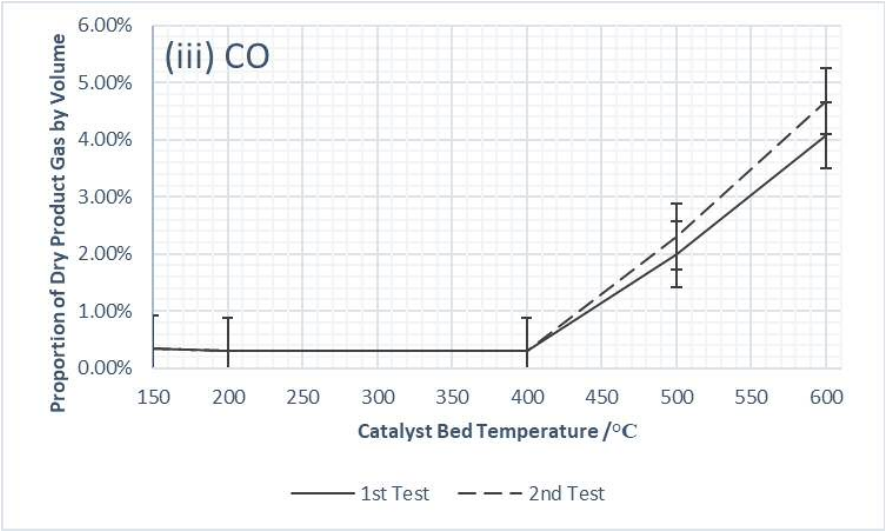

Figure 5.7: PM catalyst performance in the exhaust gas reforming of iso-octane at λ = 1, in terms of the dried product gas composition as a function of bed temperature

The results above show that the performance of the PM catalyst over two consecutive runs, at λ = 1 with 2 % iso-octane fuel, was fairly consistent.

There was potentially a very small exotherm observed in the region of 170 °C, suggesting light off occurred at a slightly lower temperature than with propane, though the exotherm was not as strong.

It can be seen in Figure 5.7(i) that there was no measureable hydrogen production at 200 °C, 300 °C or 400 °C. Then around 6 % and 9 % by volume of the product gas was measured as hydrogen at 500 °C and 600 °C respectively.

Figure 5.7(ii) shows the data for carbon dioxide, and it can be seen that there was an increase in the amount of carbon dioxide at 200 °C relative to the reactant level, suggesting that there likely has been some oxidation of the fuel, consuming the 0.4 % oxygen in the reactant stream and some of the fuel. The carbon dioxide levels are then flat between 200 °C and 400 °C, before either being consumed and/or diluted at 500 °C and 600 °C.

Figure 5.7(iii) shows that as with hydrogen, there was no carbon monoxide observed until 500 °C and 600 °C, reaching a maximum of around 4.5 % by volume of the product gas at 600 °C.

At the λ = 1.5 Condition

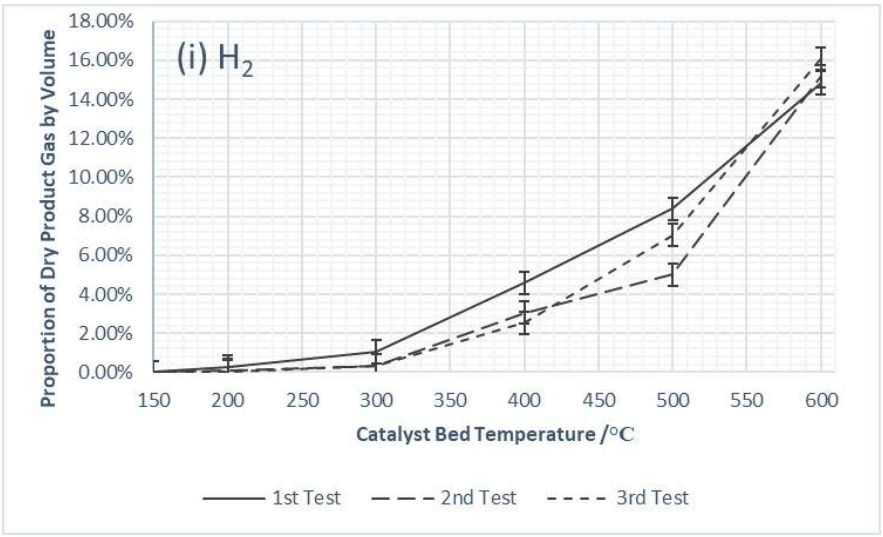

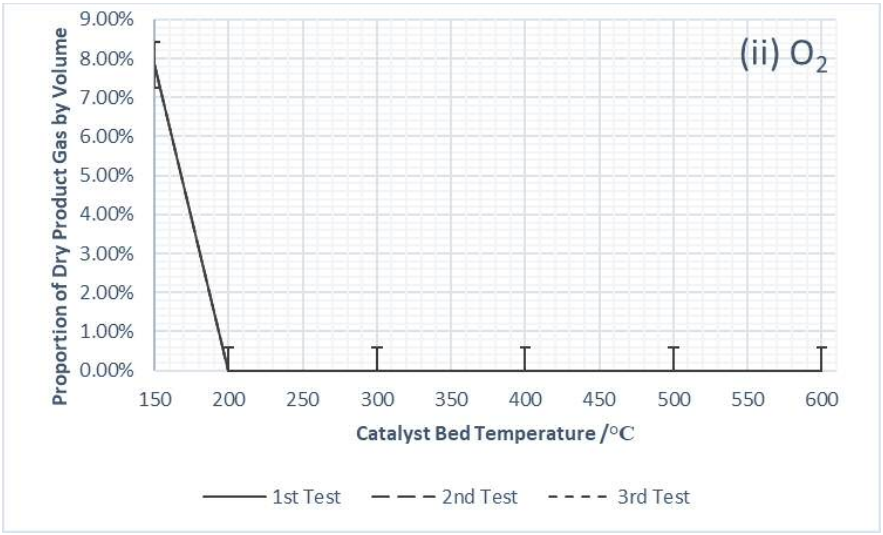

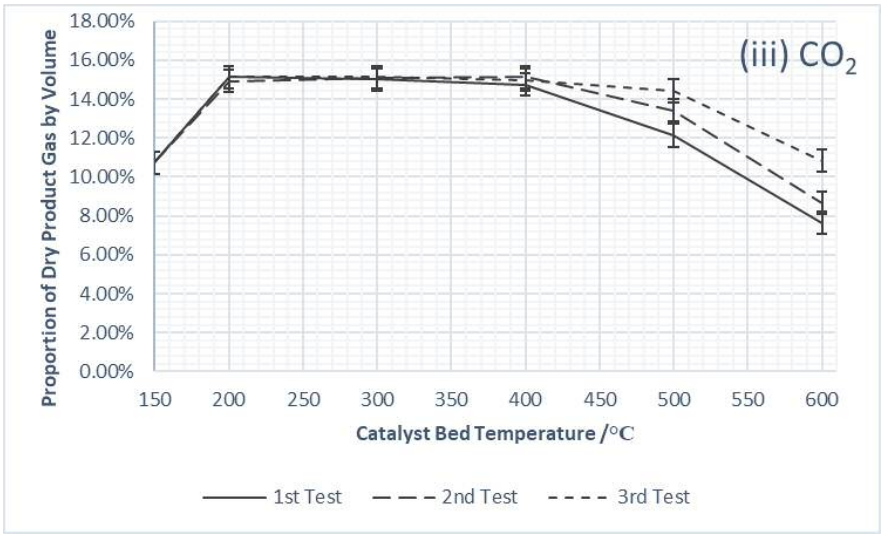

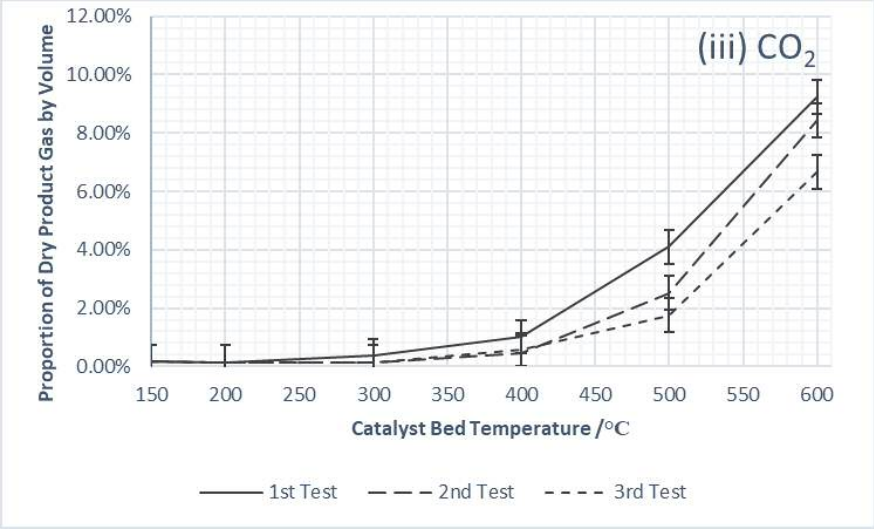

Figure 5.8: PM catalyst performance in the exhaust gas reforming of iso-octane at λ = 1.5, in terms of the composition of the dried product gas as a function of bed temperature

The results above, for the PM catalyst with 5 % iso-octane fuel at λ = 1.5, show that once light off was complete, there was total oxygen consumption at 200 °C (Figure 5.8(ii)). The exotherm was observed to be in the region of 170 °C. The corresponding increase in carbon dioxide content, from the oxidation of the fuel, was also observed (Figure 5.8(iii)).

However, there was very little hydrogen production after light off (Figure 5.8(i)), nor at 300 °C. There was then a noticeable increase in the proportion of the product gas containing hydrogen through 400 °C, 500 °C and 600 °C, reaching a maximum of around 16 % by volume of the product gas at 600 °C. The first test showed slightly higher hydrogen levels in the product gas than the subsequent tests.

Carbon monoxide was also seen to be low at 200 °C and 300 °C, with a slight increase at 400 °C, before larger increases to 500 °C and 600 °C (Figure 5.8(iv)).

At the λ = 2.12 Condition

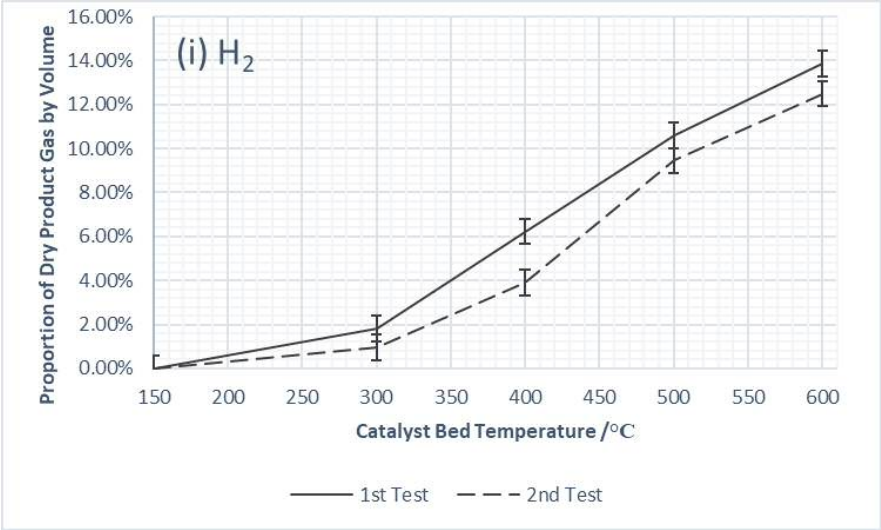

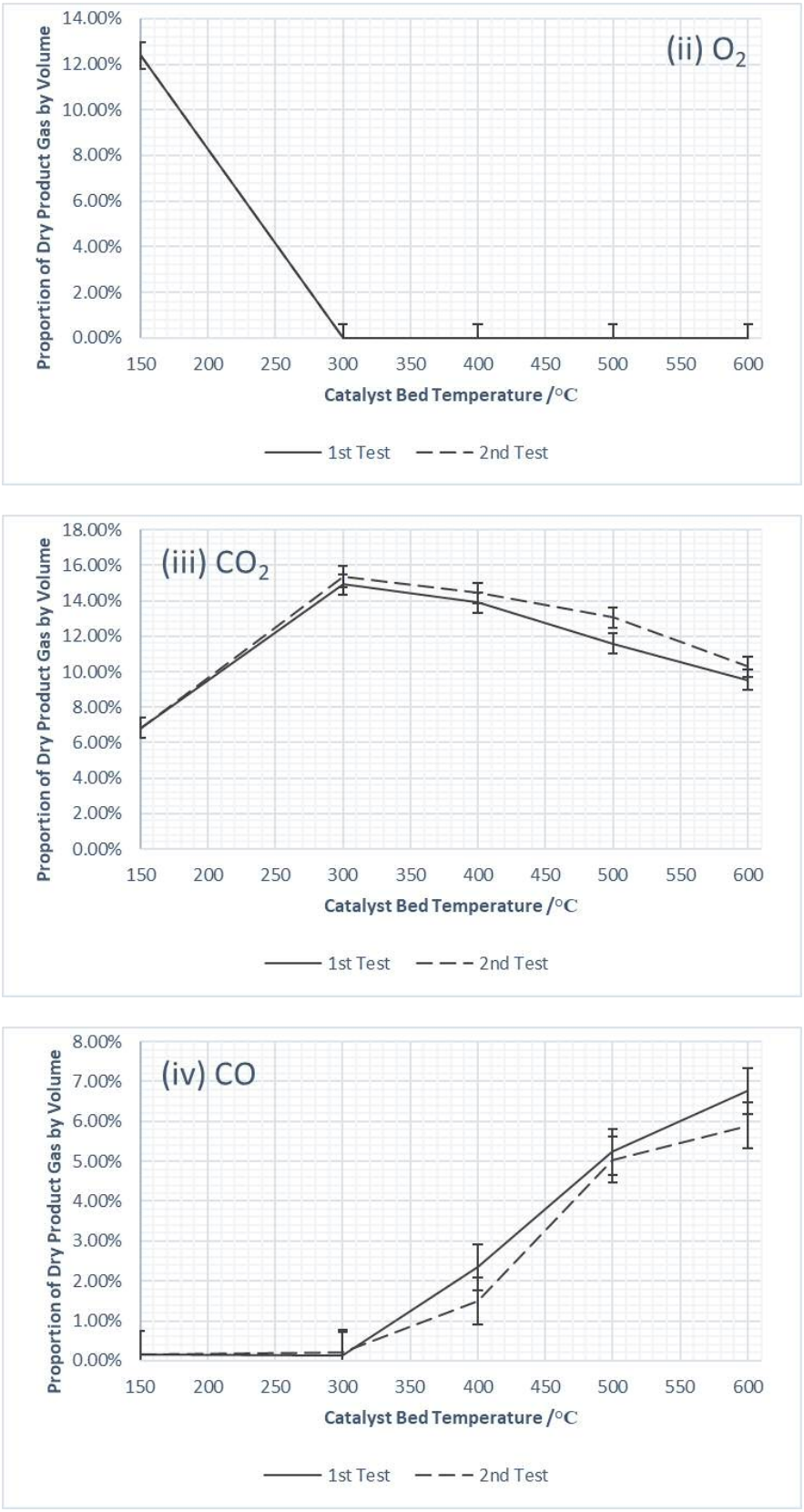

Figure 5.9: PM catalyst performance in the exhaust gas reforming of iso-octane at λ = 2.12, in terms of the composition of the dried product gas as a function of bed temperature

The results above show that when tested at λ = 2.12, with 8 % iso-octane, that there was a significant exotherm associated with the oxidation of the fuel. The bed temperature rose from 170 °C and settled at 270 °C, before being raised by the furnace to 300 °C. Oxygen consumption was complete in the light

off process (Figure 5.9(ii)), with carbon dioxide content in the product gas rising from the oxidation reactions (Figure 5.9(iii)).

Low levels of hydrogen and carbon monoxide were detected in the product gas after light off at 300 °C (Figures 5.9(i) and 5.9(iv) respectively). The proportion of both gases in the product stream then rose throughout the rest of the temperature range, reaching maximum amounts of around 13 % and 6.5 % by volume of the product gas respectively at 600 °C.

In terms of hydrogen and carbon monoxide production, a drop in levels were observed through decreased concentrations in the product gas for the second test relative to the first test with the fresh catalyst.

Nickel Catalyst Performance for Exhaust Gas Reforming of Iso-octane

At the λ = 1 Condition

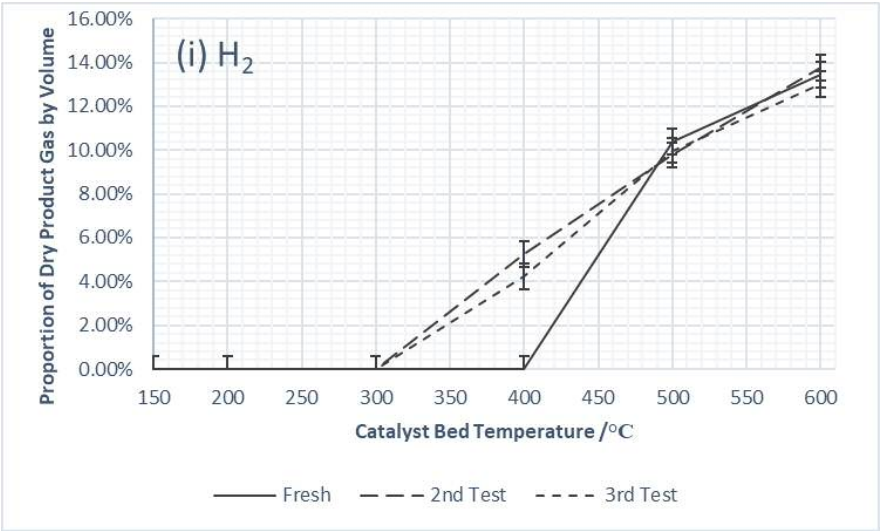

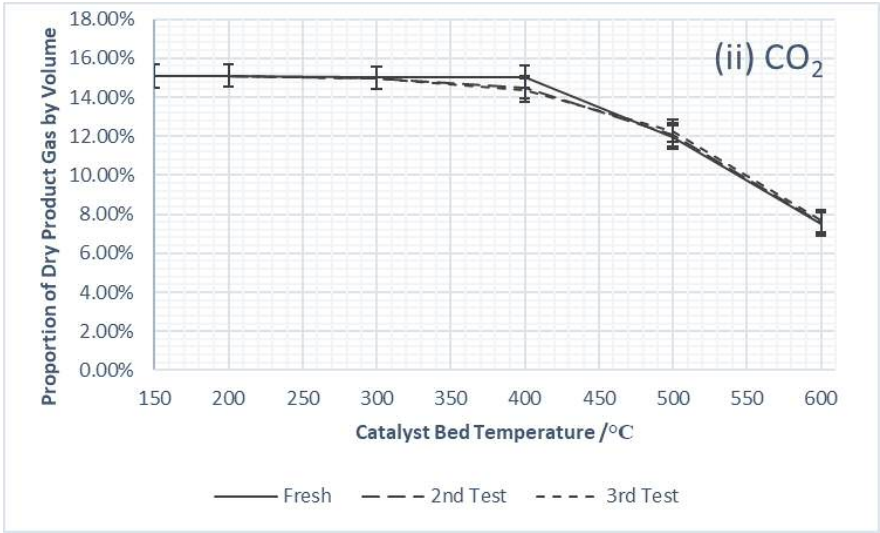

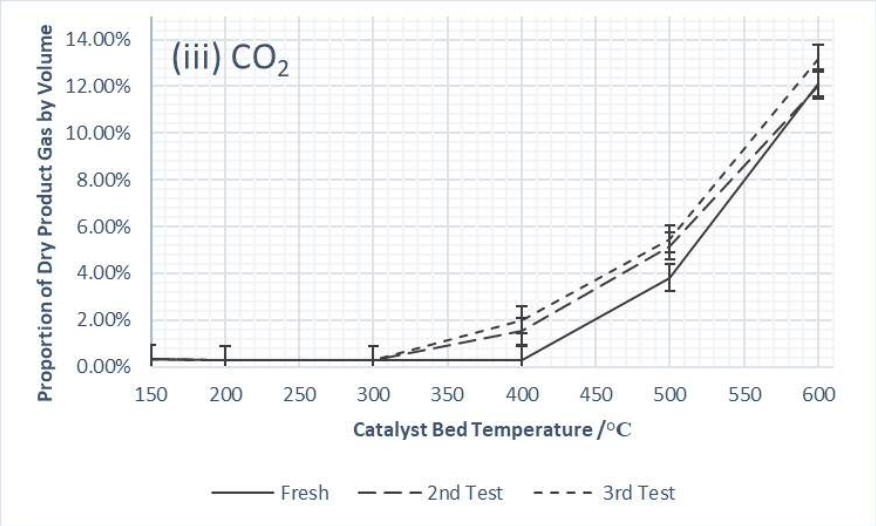

Figure 5.10: Nickel catalyst performance in the exhaust gas reforming of iso-octane at λ = 1, in terms of the composition of the dried product gas a function of bed temperature

Under the λ = 1 condition, with 2 % iso-octane, the nickel catalyst showed a small exotherm at around 180 °C, and the bed temperature was raised to 200 °C.

Hydrogen was not detected in the product gas until the temperature was at 500 °C in the test of the fresh catalyst (Figure 5.10(i)). However, in the second and third test there was 4-5 % hydrogen recorded at 400 °C, suggesting an activation of the fresh catalyst during the first test as seen with propane. The hydrogen production reached a maximum of around 13% by volume of the product gas composition at 600 °C.

Carbon monoxide production, shown in Figure 5.10(iii), shows similar behavior to hydrogen with regard to the differences between the fresh catalyst and the second and third tests. The proportion of the product gas constituting carbon monoxide reached a maximum of around 12 % by volume of the product gas at 600 °C.

At the λ = 1.5 Condition

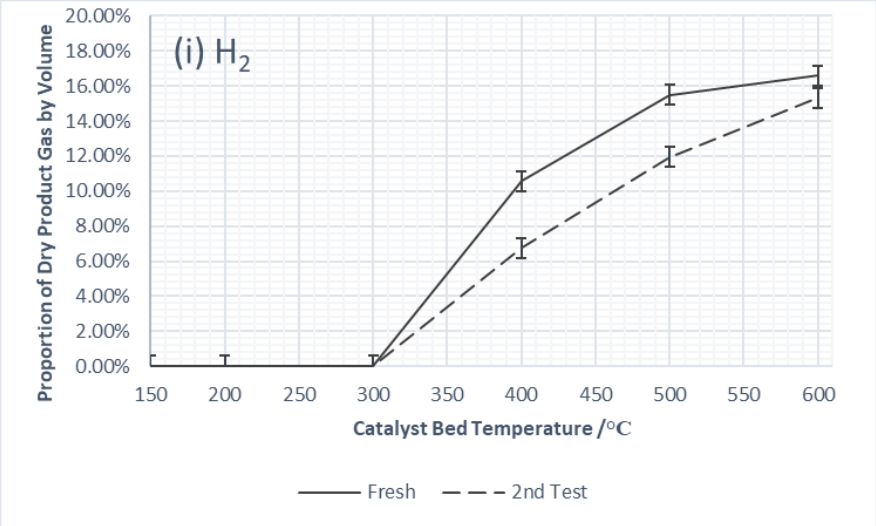

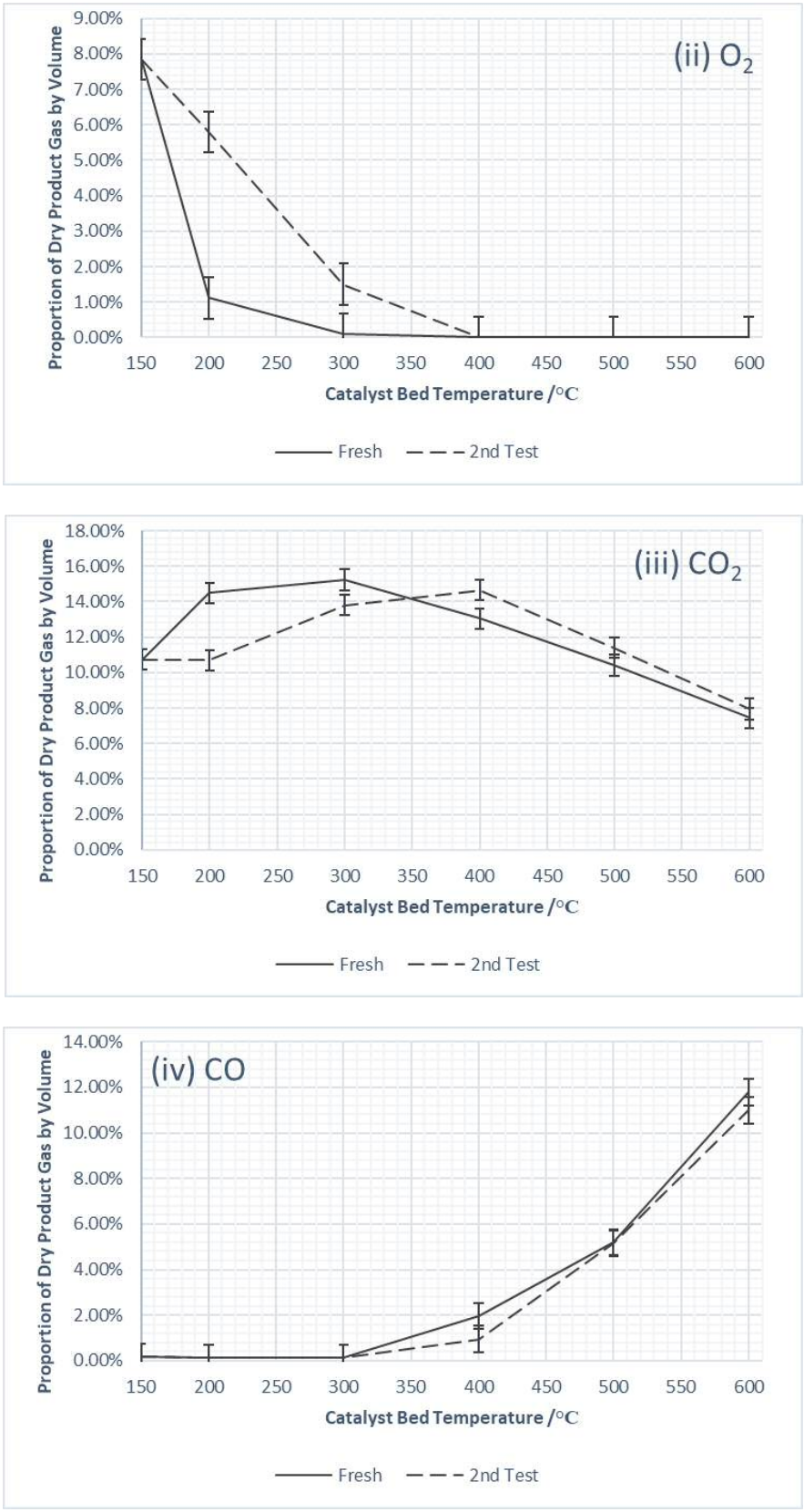

Figure 5.11: Nickel catalyst performance in the exhaust gas reforming of iso-octane at λ = 1.5, in terms of the composition of the dried product gas as a function of temperature

When the nickel catalyst was tested under the λ = 1.5 condition, with 5 % iso-octane, an exotherm was observed at around 170 °C, and the bed temperature was raised to just under 200 °C. It can be seen from Figure 5.11(ii) that oxygen consumption was almost complete during light off with the fresh catalyst,

however there was a significant reduction in consumption during light off in the second test, suggesting a deactivation had occurred. In either test, total oxygen consumption occurred by 400 °C.

This deactivation during light off was also reflected in the proportion of the product gas constituting carbon dioxide, shown in Figure 5.11(iii), where approximately 4 % by volume less carbon dioxide was detected in the product gas for the used catalyst relative to the fresh catalyst after light off.

Hydrogen production (Figure 5.11i)) again did not occur until all of the oxygen had been consumed, which meant no hydrogen was detected until 400 °C. Hydrogen levels in the product gas reached a maximum of around 16% by volume of the product gas at 600 °C. The deactivation of the catalyst can also be seen in the difference in hydrogen content of the product stream at 400 °C and 500 °C between the fresh catalyst and the used catalyst.

The proportion of the product gas constituting carbon monoxide (Figure 5.11(iv)) remained fairly consistent between tests. As with hydrogen, no carbon monoxide was detected until 400 °C, and reached a maximum of around 11.5 % by volume of the product gas at 600 °C.

The testing was stopped after the second test because the reactor tube had begun to become blocked (detected by a pressure build up during the final measurements). When the catalyst was removed it was clear that a significant amount of carbon had built up in the catalyst bed. The drop in performance between tests was therefore likely down to this carbon deposition and the resulting blockage.

At the λ = 2.12 Condition

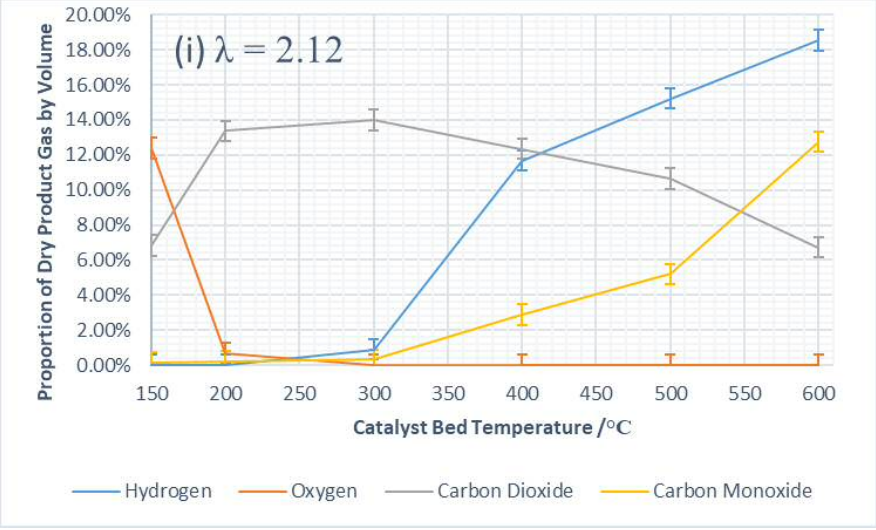

Figure 5.12: Nickel catalyst performance in the exhaust gas reforming of iso-octane at λ = 2.12, in terms of the composition of the dried product gas composition as a function of temperature

The results above in Figure 5.12 show the data for the test of the fresh nickel catalyst at the λ = 2.12 condition with 8 % iso-octane. The pressure in the reactor had begun to build up at the end of the run, so only the fresh catalyst test was possible. As before, a significant amount of carbon had built up in the catalyst bed.

It can be seen that light off again occurred in the region of 170 °C, with almost complete oxygen consumption detected once the bed temperature had settled at 200 °C. Carbon dioxide content again increased in the light off process, and was later consumed/diluted at 500 °C and 600 °C. A small amount of hydrogen and carbon monoxide was recorded at 300 °C, with both continuing to rise throughout the temperature range, reaching a maximum at 600 °C of around 18 % and 13 % by volume of the product gas respectively.

Catalyst Characterization

TGA

Thermogravimetric analysis was carried out in flowing air as described in the Experimental chapter. The results below in Figure 5.13 show the TGA data for all the nickel catalyst samples tested in this chapter.

There were significant differences between the weight loss events for those samples tested with propane and those tested with iso-octane.

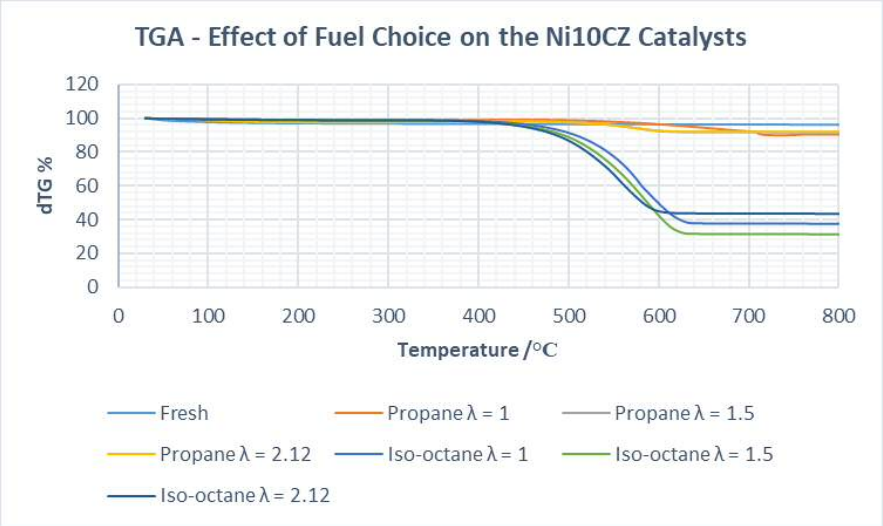

Figure 5.13: Thermogravimetric data for the nickel catalyst samples tested in this chapter

The samples tested with propane showed just under 10 % weight loss when exposed to the TGA treatment. In comparison, the samples tested with iso-octane showed weight loss in the region of 60-70 %. The significant weight loss for the iso-octane tested samples occurred in the 450 °C to 600-630 °C.

Additional Observations

Weight Gain and Changes in Sample Appearance

Sample	Conditions	Fuel	Approx. Time on Stream /hrs	Weight Change /%	Observations
Fresh Ni10CZ	-	-	-	-	Dark grey pellets
Ni10CZ	λ = 1	Propane	24	+2	Dark grey/black pellets
Ni10CZ	λ = 1.5	Propane	24	+4	Black pellets
Ni10CZ	λ = 2.12	Propane	24	+5	Black pellets
Ni10CZ	λ = 1	Iso-octane	24	+120	Large black clumps
Ni10CZ	λ = 1.5	Iso-octane	16	+190	Large black clumps
Ni10CZ	λ = 2.12	Iso-octane	6	+70	Large black clumps

Table 5.1: Recorded post-testing weight gain, and observed appearance of the nickel catalyst samples tested in this chapter

The results in Table 5.1 show that the iso-octane tested samples showed very significant weight gains compared to the propane tested samples. The propane samples showed single figure percentage increases in weight, and had visibly less black carbon amongst the catalyst pellets. In comparison the iso-octane tested samples showed minimum of 70 % gained weight, up to 190 %, and the catalyst pellets were no longer visible, but were covered in large black clumps. When taking into account the amount of time on stream for the iso-octane tested samples (three tests for λ = 1, two for λ = 1.5, and one for λ = 2.12) it suggests that as the λ-value increases so did the rate of carbon deposition.

Discussion

The work in this chapter aimed to establish the baseline performance of both the PM catalyst, as well as the Ni10CZ catalyst, with the gaseous and liquid hydrocarbon fuels (propane and iso-octane). The results presented above will now be discussed in more detail.

Precious Metal Catalyst Performance for Exhaust Gas Reforming of Propane

This section will discuss the results presented in Figures 5.1(i) through 5.3(v). The PM catalyst was tested with propane as the model fuel at the three λ-values. The first step under each condition was the oxidation of the fuel, shown by a complete consumption of the oxygen available in the reactant stream, partial consumption of the propane fuel, and an increase in the quantity of carbon dioxide, as has been shown previously [41].

This light off produced an exotherm which was observed to raise the bed temperature by increasing amounts as the λ-value increased. In all cases, the exotherm was initiated at around 180 °C. At λ = 1 the

bed temperature was raised to just under 200 °C, at λ = 1.5 to around 210 °C, and at λ = 2.12, the bed temperature was raised to around 235 °C. The strength of the exotherm therefore was correlated to the amount of fuel and oxygen available in the reactant stream, i.e the higher the λ-value/the more air and fuel rich the mixture of the simulated exhaust gas.

In all cases, as the temperature was raised the hydrogen and carbon monoxide content in the product gas increased. The was accompanied by the decrease of propane content, from consumption, in the product gas relative to the reactant feed (to roughly total consumption at 600 °C). The proportion of the product gas consisting of carbon dioxide increased after light off, however it then levelled out before then falling below reactant levels at high temperature.

The proportion of the dried product gas constituting nitrogen detected by the GC also decreased from reactant levels as the temperature was raised. Since nitrogen does not react under these conditions, this is a result of dilution. This dilution occurs because the quantity of gas exiting the reactor (and entering the GC) is greater than that in the inlet stream, while the molar flow of nitrogen in the stream remains the same.

The gain in the quantity of gas reaching the GC relative to the inlet stream is due to water, which would otherwise condense out in the waste pot and not contribute to the flow into the GC, being converted in the reforming reactions to produce additional dry gaseous products which do then reach the GC (this same effect would also apply to liquid fuels).

The levelling off and reduction of carbon dioxide in the product gas stream relative to those at low temperatures after light off is most likely affected a little by this dilution affect, but is primarily driven by a reduction CO_2 yield. This effect is shown below in Figure 5.14. This behavior was observed under the other conditions tested in this work.

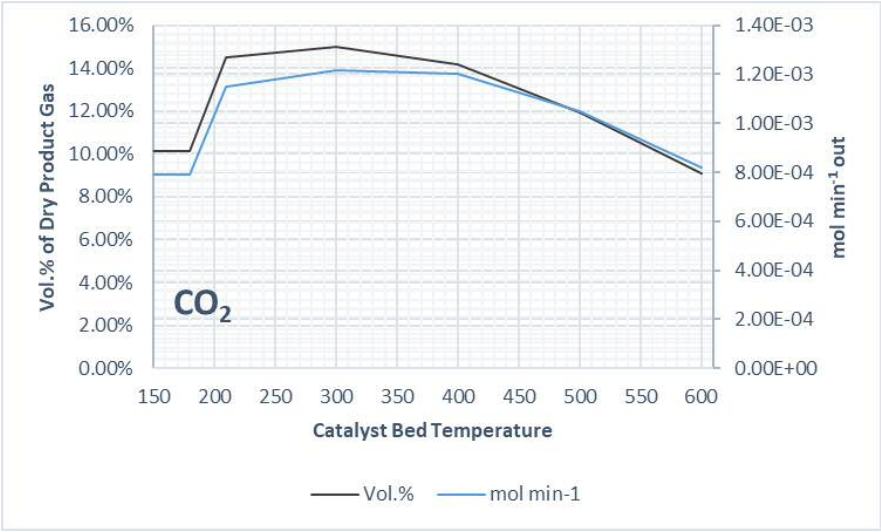

Figure 5.14: Showing both the proportion of the dried product gas constituting carbon dioxide (vol. %), and the molar flow rate of carbon dioxide (mol min-1) as a function of catalyst bed temperature at λ = 1.5 in the exhaust gas reforming of propane

Figure 5.15 below shows the average hydrogen content of the dried product gas as a function of catalyst bed temperature for each of the λ-values.

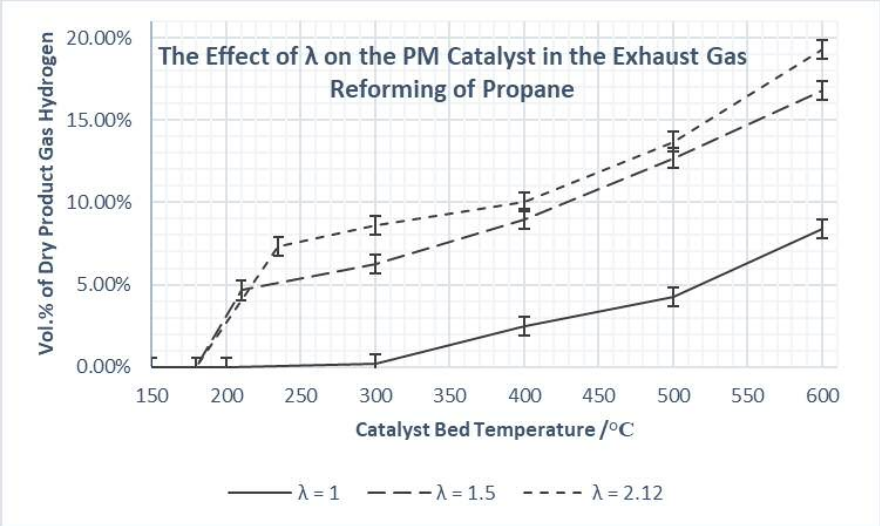

Figure 5.15: PM catalyst performance in the exhaust gas reforming of propane, in terms of hydrogen content of the dry product stream, as a function of λ and bed temperature

The average H_2 yield (mol min^{-1} H_2 produced per mol min^{-1} C_3H_8 in the reactant feed), as a function of temperature and λ-value is shown below in Figure 5.16 for the PM catalyst.

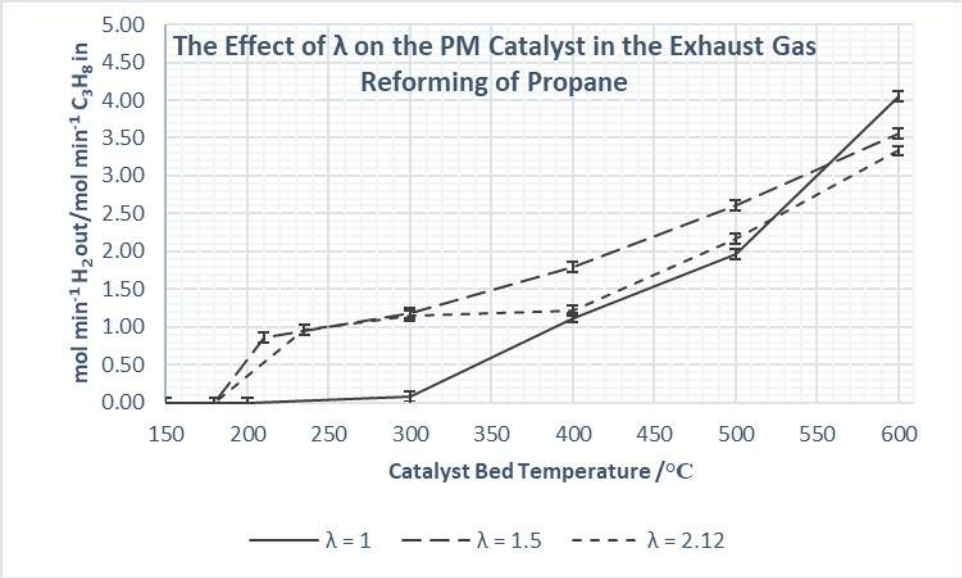

Figure 5.16: PM catalyst performance in the exhaust gas reforming of propane, in terms of hydrogen yield as a function of λ and bed temperature

Figure 5.17 below shows the average propane conversion of the PM catalyst, as a function of bed temperature and λ.

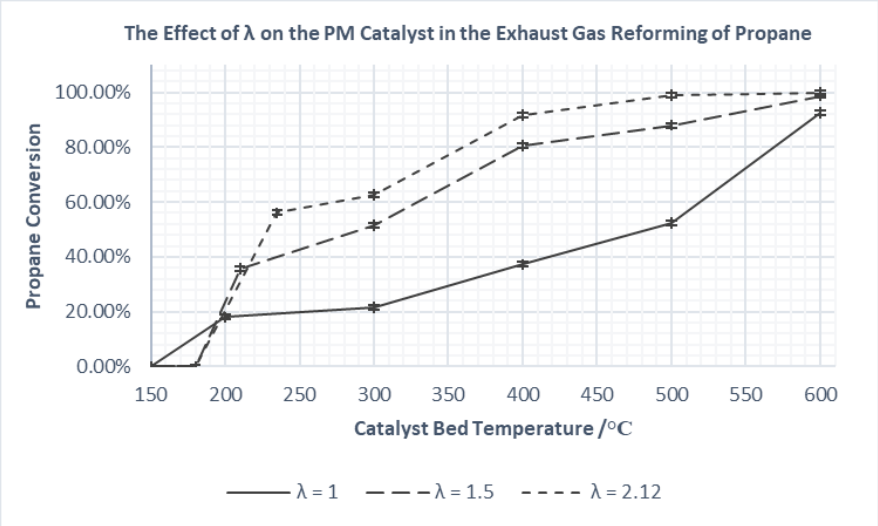

Figure 5.17: Propane conversion as a function of bed temperature and -value for the PM catalyst in the exhaust gas reforming of propane

From Figure 5.15, it is clear that the product gas was richer in hydrogen at all temperatures as the the λ-value increases. The maximum hydrogen proportions of the product gas were 8.37%, 16.8% and 19.27% at λ = 1, 1.5 and 2.12 respectively. Furthermore, the λ = 1.5 and 2.12 conditions showed much earlier onset of hydrogen production than the λ = 1 condition. At λ = 1, hydrogen was first detected at volume at 400 °C, whereas it was detected below 250 °C for the other conditions.

However, as shown in Figure 5.16, when considering hydrogen yield, rather than hydrogen content of the product gas, though the λ = 1 condition was still the lowest performance condition at low temperature, it can be seen that at 600 °C, this condition was the highest yielding in terms of hydrogen.

Additionally, the λ = 2.12 condition, though as seen in Figure 5.15 to produce the product gas richest in hydrogen at all temperatures, was not the highest yielding in terms of hydrogen, as shown in Figure 5.16.

Propane conversion (Figure 5.17) is either total, or near total for all the λ-conditions at 600 °C. However, the λ = 1.5 and 2.12 conditions consume significantly more of the fuel at lower temperatures than the λ = 1 condition, which given the higher hydrogen yields at lower temperature would be expected.

Hydrogen production occurred in parallel with carbon monoxide production under each condition. Tables 5.2 below shows how the average H_2/CO ratio varies with λ-value.

Condition	**Average H_2/CO**
λ = 1	2.28
λ = 1.5	2.61
λ = 2.12	1.79

Table 5.2: H_2/C ratios for the PM catalyst in the exhaust gas reforming of propane at λ = 1, λ = 1.5 and λ = 2.12

As discussed in the Introduction chapter, hydrogen and carbon monoxide are the major products of reforming reactions. However, the ratio of hydrogen to carbon monoxide (and other products) depends on the reaction balance.

The expected hydrogen to carbon monoxide ratios for the main reactions with propane as the fuel are shown below in Table 5.3.

Reaction	Equation	H_2/CO
Steam Reforming 1 (SR1)		2.33.
Steam Reforming 2 (SR2)		N/A
Dry Reforming (DR)		0.66.
Partial Oxidation (POx)		1.33.

Table 5.3: Theoretical H_2O/C ratios for the main reactions in the exhaust gas reforming of propane

Though SR1 is normally the dominant reaction, ratios lower than its characteristic $H_2/CO = 2.3$ can suggest increased contributions from DR/POX. The higher H_2/CO ratios, above that of SR1, could suggest the prevalence of SR2/increased hydrogen production from WGS reactivity.

The average H_2/CO ratio was in the order of $\lambda = 2.12 < \lambda = 1 < \lambda = 1.5$. The $\lambda = 1.5$ condition showed an average H_2/CO ratio greater than that expected for SR1, whereas the $\lambda = 1$ condition showed almost exactly the ratio expected for SR1.

These results are best interpreted with reference to the composition of the synthetic exhaust gas mixture – simulating the expected output of a gasoline engine at different operating conditions.

As the λ-value increases, the oxygen content increases and steam content decreases. As discussed in the Introduction chapter, this balance is known to be important [42, 49, 58] in terms of reaction and heat balance. The oxygen is required so that the resulting exotherm from the oxidation reactions can promote reforming, and the steam is required for SR1/SR2, which are the most productive reforming reactions (in terms of hydrogen yields), and also in terms of recovering waste heat in the exhaust since these reactions are endothermic.

At $\lambda = 1$, there is negligible oxygen present, therefore the contribution from POx towards hydrogen production was also likely negligible – and hence the ratio is almost exactly what would be expected for SR1.

The lack of oxygen in the exhaust gas at $\lambda = 1$ most likely also explains the high hydrogen yield at 600°C. Since there is negligible oxygen present, the propane fuel would be expected to be converted via steam reforming reactions, and as shown in Table 5.3, steam reforming is the highest yielding in terms of hydrogen produced per mole of fuel.

However, this performance was not achieved until the bed temperature had been raised using the furnace to 600 °C (in a real vehicle this heat could be provided by the waste heat in the exhaust). This is because steam reforming is endothermic, and without the heat contribution of exothermic oxidation reactions, an external heat source was required to achieve these high yields.

By the same reasoning, the superior hydrogen yield, propane conversion and hydrogen richness of the product gas at lower temperature under the higher lambda conditions is explained by the higher oxygen content of the simulated exhaust gas feed. This enables increased contribution from oxidation reactions such as POx, which produces hydrogen directly, but also help promote steam reforming by raising the catalyst bed temperature through these exothermic reactions.

However, reliance on oxidation reactivity is not necessarily the best route, since POx is lower yielding in terms of hydrogen per mole fuel consumed (Table 5.3). The average H_2/CO product ratio at $\lambda = 2.12$, along with the lower hydrogen yield per mole of fuel, suggest that under this condition the PM catalyst was producing hydrogen primarily via POx.

Though this condition produced the product gas richest in hydrogen, as discussed in the Introduction the goal of exhaust gas reforming is not just the recirculation to the engine of a reformate containing 5-20 % hydrogen by volume, but that the production of the hydrogen was primarily via steam reforming in order to achieve thermochemical recuperation of the waste heat from internal combustion engine [35, 41, 43].

The data therefore suggests that, unless the exhaust gas temperature is expected to be sustained at 600 °C during operating, that the optimum conditions for the favoring of high hydrogen yield through steam reforming are those where some oxygen is present, but also with significant steam – such as those at $\lambda = 1.5$. This condition produced an exhaust gas mixture of sufficient hydrogen richness at all temperatures tested, and showed the best balance of performance in terms of hydrogen yield across the whole temperature range.

These experimental results for the PM are a close match to that seen in the literature, when using a precious metal catalyst with propane fuel, under exhaust gas reforming conditions at these λ-values [43].

In terms of catalyst stability over the consecutive tests, the results suggest that the oxidation reactions in the light off process remained consistent between runs. This can be seen in that the oxygen consumption and carbon dioxide levels were consistent between tests for each condition, as measured immediately after light off. Hydrogen production also remained consistent between tests.

Nickel Catalyst Performance for Exhaust Gas Reforming of Propane

This section will discuss the results presented in Figures 5.4(i) through 5.6(v). It can be seen from the results that light off occurred at around 280°C under each λ-value condition, for each of the fresh nickel catalysts tested. The bed temperature was raised from the resulting exotherm to just under 300 °C for the $\lambda = 1.5$ condition, and just over 300 °C for the $\lambda = 2.12$ condition, and less for the $\lambda = 1$ condition to

approximately 290 °C. Oxygen consumption for all conditions was complete during this light off process in oxidation reactions, and therefore all showed the corresponding rise in carbon dioxide content of the product gas, resulting from oxidation of the hydrocarbon fuel. Shown below in Figure 5.18 is a comparison of the average hydrogen content of the dry product gas at the three λ-values.

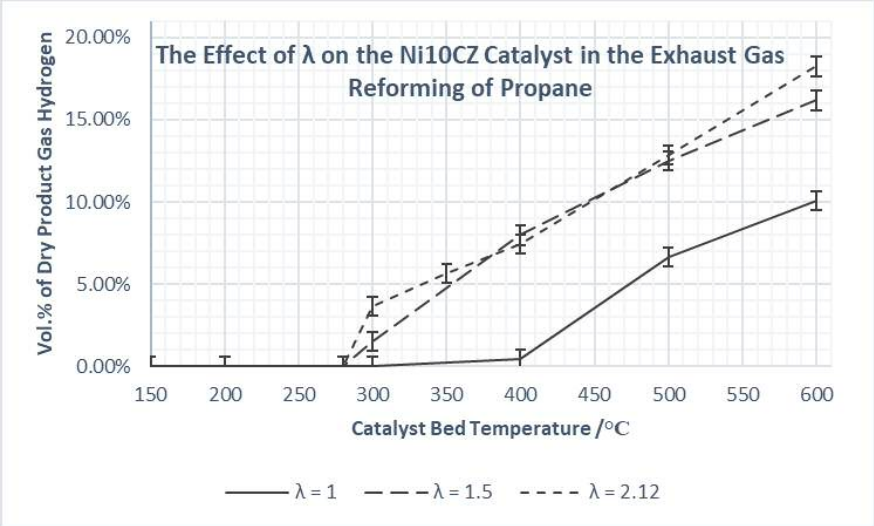

Figure 5.18: Nickel catalyst performance in the exhaust gas reforming of propane, in terms of hydrogen content of the dry product stream, as a function of λ and catalyst bed temperature

The proportion of the product gas constituting hydrogen increased as the temperature was raised for all three lambda conditions. The λ = 1 condition also showed delayed onset in hydrogen production relative to the two higher lambda conditions. It can be seen that, as with the PM catalyst (Figure 5.15), the higher the lambda value the richer the product gas stream in terms of hydrogen content.

Figure 5.19 below shows the hydrogen yield under each condition, as a function of bed temperature.

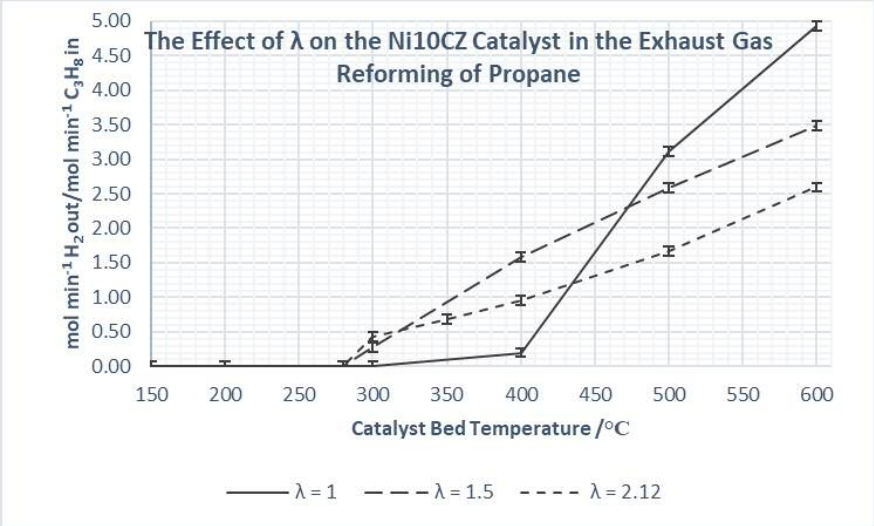

Figure 5.19: Nickel catalyst performance in the exhaust gas reforming of propane in terms of hydrogen yield as a function of λ and catalyst bed temperature

Similar to the results seen in Figure 5.16 for the PM catalyst, the higher lambda conditions show superior hydrogen yield at low temperature, but then the λ = 1 condition shows superior hydrogen yields at 500

°C and 600 °C. The λ = 2.12 condition again shows the lowest hydrogen yield of the three conditions at higher temperatures.

Figure 5.20 below then shows the propane conversion under the three lambda conditions of the nickel catalyst as a function of catalyst bed temperature.

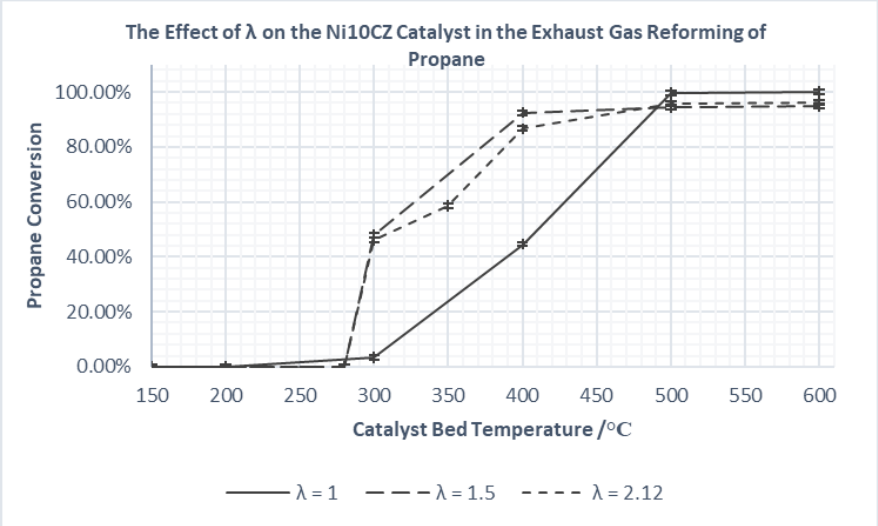

Figure 5.20: Propane conversion as a function of bed temperature and -value for the nickel catalyst in the exhaust gas reforming of propane

As with the PM catalyst (Figure 5.17), propane conversion at low temperature is higher at higher lambda, with all conditions reaching 100%, or close to 100% conversion at high temperature.

The average H_2/CO values for each condition are shown in Table 5.4 below.

Condition	Average H_2/CO
λ = 1	1.14
λ = 1.5	1.20
λ = 2.12	1.49

Table 5.4: H_2/C ratios for the nickel catalyst in the exhaust gas reforming of propane at λ = 1, λ = 1.5 and λ = 2.12

The data in Table 5.3 and 5.4 shows that the H_2/CO ratio for the nickel catalyst remained consistently below that expected for SR1. This could be from significant contributions from other reforming reactions such as POX or DR, or the lack of WGS consuming CO and producing hydrogen among others. The values were also similar across lambda values. This was not the case with the PM catalyst.

The explanation for these trends is therefore most likely the same as provided to explain the PM catalysts results in the previous section. The comparison between the two catalysts will be discussed further in the next section.

More significant differences were observed in terms of the progression between tests of the quantity of hydrogen, carbon monoxide and propane consumption, for the nickel catalyst under each of the conditions. In all cases, the testing/nitrogen cooling method combination seemed to activate the catalyst, as seen previously in Chapter 4. Hydrogen and carbon monoxide production, especially at onset of the reforming reactions after light off, increased between the fresh and used catalysts. There was also the corresponding increase in propane consumption between fresh and used catalysts. The fresh sample tested under the $\lambda = 1$ condition showed no hydrogen production until above 400 °C, and the fresh sample tested at $\lambda = 1.5$ did not produce hydrogen until above 300 °C. However after being exposed to the testing/nitrogen cool down cycles, the used catalysts displayed improved hydrogen production at these low temperatures.

The results in Table 5.1 and Figure 5.13 suggest that there was also a small amount of carbon deposition on the nickel catalyst after testing both in the color change and total weight gain of the sample, and the weight loss observed in the TGA. The total weight gain results suggest that as the λ-value is increased, so was the total weight gain from carbon deposition. This was likely to be explained by the decreasing steam to carbon ratio (H_2O/C) as the λ-value increases [77, 129]. The weight loss observed in the TGA occurs in the region of 550-700 °C, resulting from the loss of carbon species [123, 124], likely ranging from amorphous carbon at lower temperatures to more graphitic carbon at higher temperatures.

Comparing the Performance of the Precious Metal and Nickel Catalysts for Exhaust Gas Reforming of Propane

Following on from the discussion above, it is clear that the precious metal catalyst promotes light off at a lower temperature than the nickel catalyst (180 °C compared to 280 °C). This is shown below in Figure 5.21 by the lower temperature consumption of oxygen. Both catalysts show complete oxygen consumption during light off, and both show the same trend of increased strength of the exotherm associated with light off as the reactant stream becomes richer in fuel and oxygen (i.e. increased λ-value).

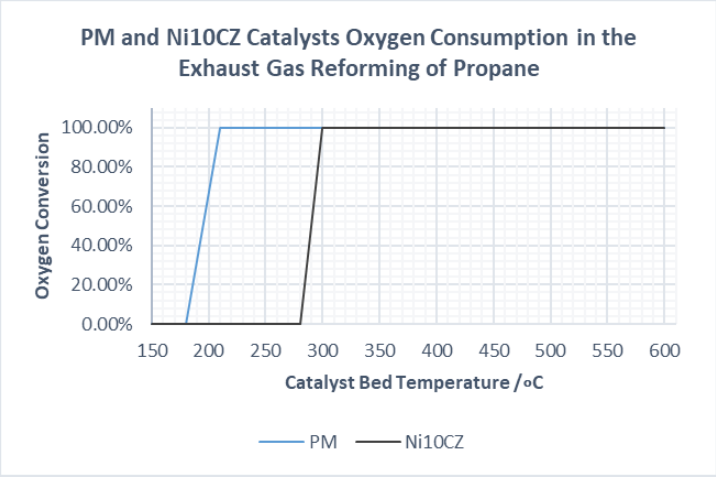

Figure 5.21: Comparing the exhaust gas reforming of propane performance of the PM and nickel catalysts, in terms of oxygen consumption as a function of bed temperature at λ = 1.5

The results below in Figure 5.22 give a side by side comparison of the average hydrogen content in the dry product gas produced by both catalysts at each λ-value.

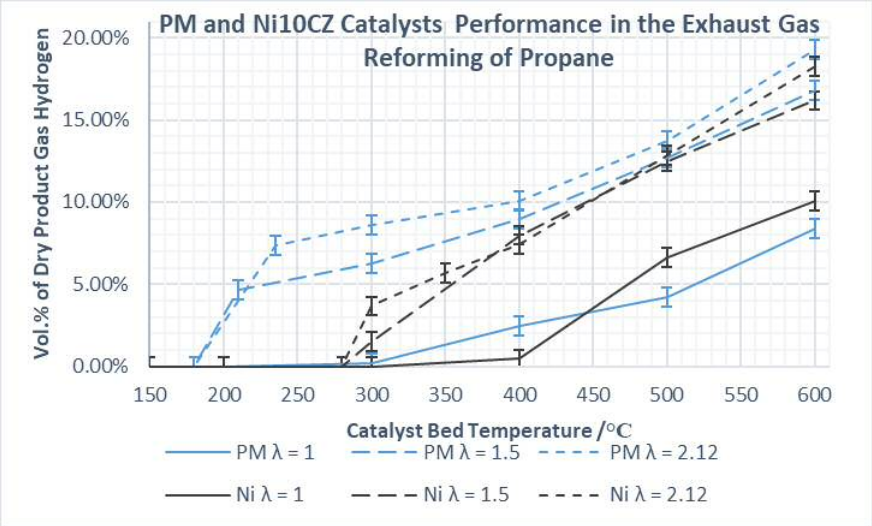

Figure 5.22: Comparing the performance of the PM and nickel catalysts in the exhaust gas reforming of propane, in terms of hydrogen content of the product ga,s as a function of λ and bed temperature.

It can be seen that not only light off occurred at lower temperatures for the PM catalyst, but so did the onset of the reforming reactions, and resulting hydrogen production. Furthermore, even after onset of the reforming reactions, the PM catalyst produced a product gas richer in hydrogen at temperatures of 400 °C and under. However, at 500 °C and 600 °C the performance of the nickel catalyst (in terms of the hydrogen content of the product gas) was comparable, if slightly lower, to that of the PM. In addition, both catalysts show the same behavior with respect to the effect of the λ-value. For both catalysts the lean reactant mixture with low oxygen and fuel (λ = 1) produced a leaner product mixture in terms of hydrogen content. The lower activity of the Ni10CZ catalyst at low temperature can also be seen when considering hydrogen yields, as shown in Figure 5.23 below.

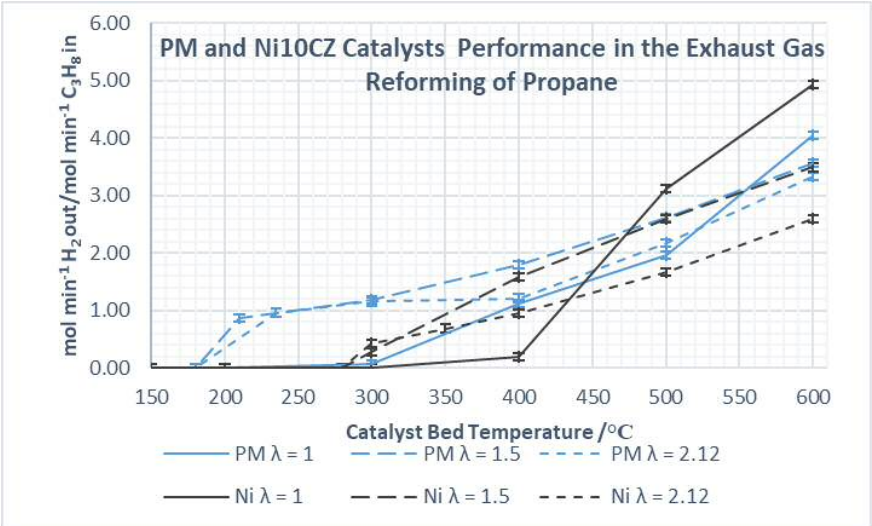

Figure 5.23: Comparing the performance of the PM and nickel catalysts in the exhaust gas reforming of propane in terms of hydrogen yield, as a function of bed temperature and λ.

Additionally, the λ = 1 condition was the best performing in terms of hydrogen yield for both catalysts at higher temperatures, despite being the lowest performing condition when considering the hydrogen richness of the product gas. Under this condition, the nickel catalyst also outperformed the PM catalyst.

The propane conversion of the catalysts, as a function of bed temperature and λ-value is shown below in Figure 5.24.

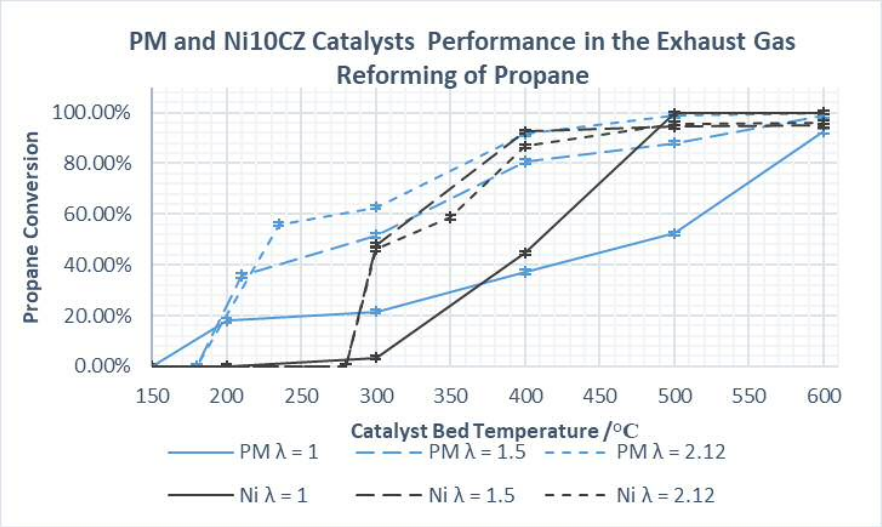

Figure 5.24: Comparing the performance of the PM and nickel catalysts in the exhaust gas reforming of propane, in terms of propane conversion as a function of bed temperature and λ.

The propane conversion is mostly a reflection of the reforming/hydrogen producing activity of the catalysts. The higher λ conditions produce more hydrogen at low temperature (both in terms of hydrogen content of the resulting product gas and hydrogen yield), and hence propane conversion is higher. Additionally, the propane conversion of the PM catalyst is higher than the nickel catalyst at low temperature. All catalysts and conditions reach approximately 100% conversion by 600°C.

The H_2/CO ratios (Tables 5.2, 5.3 and 5.4) for the two catalysts also displayed differences. The PM catalyst showed higher average H_2/CO ratios, more indicative of SR1 for the production of hydrogen.

Following on from the separate discussions of the PM and Ni10CZ catalyst performance in the sections above, these results are most likely explained with reference to the likely reaction balances determined by the catalyst and reactant compositions in question.

For both PM and Ni10CZ catalysts, operating at higher lambda conditions resulted in a product gas richer in hydrogen, and at lower temperature higher yielding in terms of hydrogen. This again is most likely due to the higher proportion of oxygen in the reactant stream – enabling stronger contribution from POx, which due to its exothermicity does not require heat input as do the endothermic reforming reactions. This exothermicity can also help raise the surface temperature of the catalyst, and therefore better promote the endothermic reforming reactions. As discussed in the previous sections, given that both yield and hydrogen content of the product gas are important in exhaust gas reforming, this suggests that for both catalysts, operating the system at a condition where both reasonable quantities of steam and oxygen are present in the exhaust gas would be best.

However, at higher simulated exhaust temperatures, when sufficient heat is provided by the exhaust gas to promote steam reforming, this reliance on oxidation activity results in lower hydrogen yields compared to the λ = 1 condition, where negligible oxygen is present in the reactant stream and hence propane conversion will be primarily through SR. This is because as shown in Table 5.3 POx is lower yielding per mole of propane than steam reforming.

Similar rationale can be used to explain the differences between the two catalysts. At lower temperatures the PM catalyst was found to be more active than the nickel catalyst, both in terms of hydrogen content of the product gas and hydrogen yield. This is most likely due to the superior oxidation activity (shown by the lower temperature oxygen consumption in Figure 5.21) of the PM catalyst, yielding hydrogen through stronger POx activity, and the exotherm from this activity better promoting SR.

Though the H_2/CO ratios of the PM catalyst do however suggest a healthy contribution from steam reforming, likely promoted by better POx activity of the catalyst, these product ratios could also be explained by the fact that the PM is most likely to be a superior WGS catalyst than the Ni10CZ. The PM catalyst is thought to contain Pt and Rh, and whereas Ni and Rh are relatively inactive towards WGS, platinum is known as an effective WGS catalyst [62]. Increased contribution from WGS, which consumes CO and produces H_2 would raise the H_2/CO product ratio.

If the hydrogen producing capability of the PM was dependent on its ability as a POx/WGS catalyst however, then as Chang et al. [54, 55] showed, despite the superior hydrogen content of the product gas produced by the PM catalyst, this is not the most beneficial way to operate an exhaust gas reforming catalyst, since the catalyst is not performing as a TCR device.

Another significant difference between the catalysts is the activation of the nickel catalyst under testing/nitrogen cooling cycles, which was not observed with the PM catalyst, whose results did not show a clear trend between consecutive tests, regardless of the condition. This is not unexpected since base metal catalyst are known to more often require activation than their precious metal equivalents [19, 120, 121]. This trend has already been explored in more detail in Chapter 4.

There was some carbon deposition on the nickel catalyst after testing (see Table 5.1 and Figure 5.13). Though it is not possible to perform the TGA experiment on the PM catalyst, visually there was no blackening of the monolith, suggesting there was more carbon deposition on the nickel catalyst under these conditions, which despite propane's short chain length is not unheard of with a nickel catalyst [91].

Importantly, neither catalyst showed any deactivation during the testing period, even despite the small quantity of carbon deposited on the nickel catalyst.

Precious Metal Catalyst Performance for Exhaust Gas Reforming of Iso-octane

This section will discuss the results shown in Figures 5.7(i) through 5.9(iv). The PM catalyst was tested at each of the three λ-values with the liquid hydrocarbon, iso-octane, as the model fuel. In each of the three conditions there was an exotherm observed shortly after injection of the fuel when the bed

temperature was around 170 °C. The size of this exotherm increased with increasing λ-value. At λ = 1 the exotherm was barely noticeable, at λ=1.5 the exotherm raised the bed temperature to 200 °C, whereas at λ = 2.12 the exotherm raised the bed temperature to around 270 °C. In all cases, these oxidation reactions increased the carbon dioxide content in the product gas through oxidation of the fuel. In all cases the oxygen was fully consumed in the light off process.

The average H_2/CO ratio for each lambda value is given below in Tables 5.5.

Condition	Average H_2/CO
λ=1	2.37
λ=1.5	2.60
λ=2.12	2.26

Table 5.5: H_2/C ratios for the PM catalyst in the exhaust gas reforming of iso-octane at λ = 1, λ = 1.5, and λ = 2.12

Below is the expected H_2/CO ratios for SR1, DR and POX of iso-octane.

Reaction	Equation	H_2/CO
Steam Reforming 1 (SR1)		2.13
Steam Reforming 2 (SR2)		N/A
Dry Reforming (DR)		0.56
Partial Oxidation (POx)		1.13

Table 5.6: Theoretical H_2/C ratios for the main reactions in the exhaust gas reforming of iso-octane

Again, the λ = 1 condition showed a ratio close to that expected for SR1, which again, given the lack of oxygen in the exhaust gas was expected. The H_2/CO ratio then increases again at λ = 1.5, before dropping again at λ = 2.12. This was the same order as with the PM catalyst and propane, and so likely reflects the heat and reaction balance discussed previously.

In terms of quantities of hydrogen, the results below in Figure 5.25 show a comparison of the average hydrogen content of the product gas at the different λ-values.

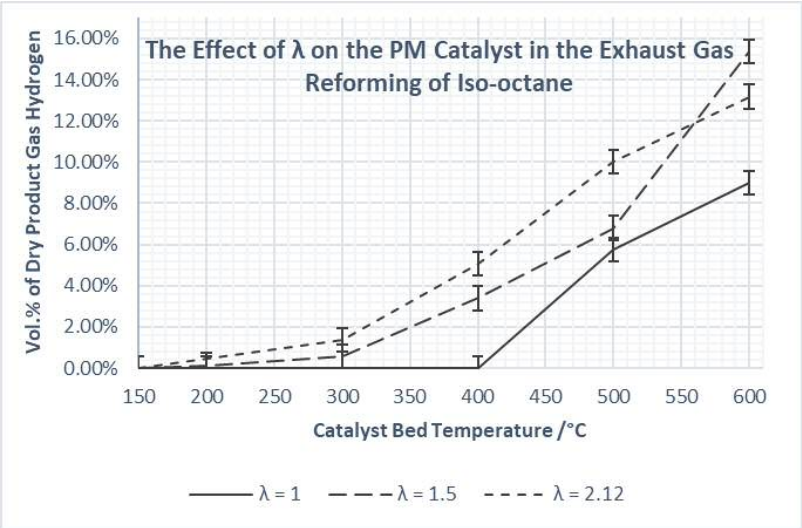

Figure 5.25: PM catalyst performance in the exhaust gas reforming of iso-octane, in terms of hydrogen content of the product gas as a function of λ and bed temperature

The average hydrogen yield under the same conditions is shown below in Figure 5.26.

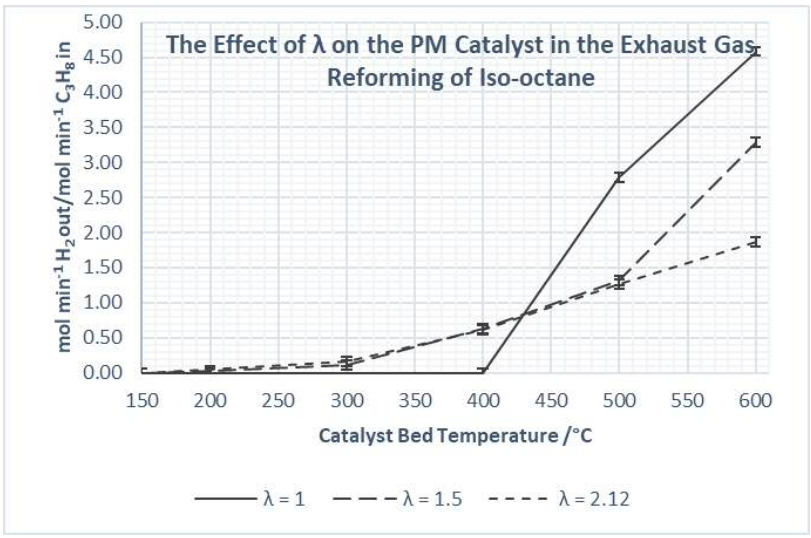

Figure 5.26: PM catalyst performance in the exhaust gas reforming of iso-octane, in terms of hydrogen yield as a function of catalyst bed temperature and λ.

It can be seen from the results above that under the λ = 1 condition the onset of the reforming reactions is delayed (not measured until 500 °C compared to 300 °C), and the proportion of hydrogen in the product gas is lower than at the other two λ-values. However, when hydrogen yield is considered, as when propane was the surrogate fuel, the λ = 1 condition was the highest yielding at high temperatures. The explanations for these trends are therefore most likely the same as discussed in the previous sections when considering the results with propane.

It was observed that after testing, the PM monolith had turned from a dark grey colour to black. This suggests that some carbon had been deposited on the monolith. This observation could help explain the fact that the hydrogen production seemed to decrease slightly with consecutive tests, particularly at

lower temperatures (as did carbon monoxide production). Therefore, it seems that when the heavier iso-octane fuel is used that carbon deposition becomes an issue for the PM catalyst also.

Comparing the Precious Metal Catalyst Performance for the Exhaust Gas Reforming of Propane and Iso-octane

Light off temperatures were very similar for the PM catalyst with either fuel, if slightly lower temperature for iso-octane, oxygen consumption was complete in the light off process for both fuels, and the size of the exotherm was proportional to the increase in λ-value for both fuels. The lower light off with iso-octane is in line with the lower ignition temperatures for higher hydrocarbons [89].

Though H_2/CO ratios were slightly different for the two fuels, with those for iso-octane being more indicative of SR1. The trend between lambda values and the H_2/CO was the same for both fuels. The fact the H_2/CO ratio was more characteristic of SR1 for iso-octane than with propane could be related to the fact that the heavier the hydrocarbon the lower the activation energy for steam reforming [70].

In terms of quantities of hydrogen, the results below in Figure 5.27 compare the performance of the PM catalyst with propane and iso-octane.

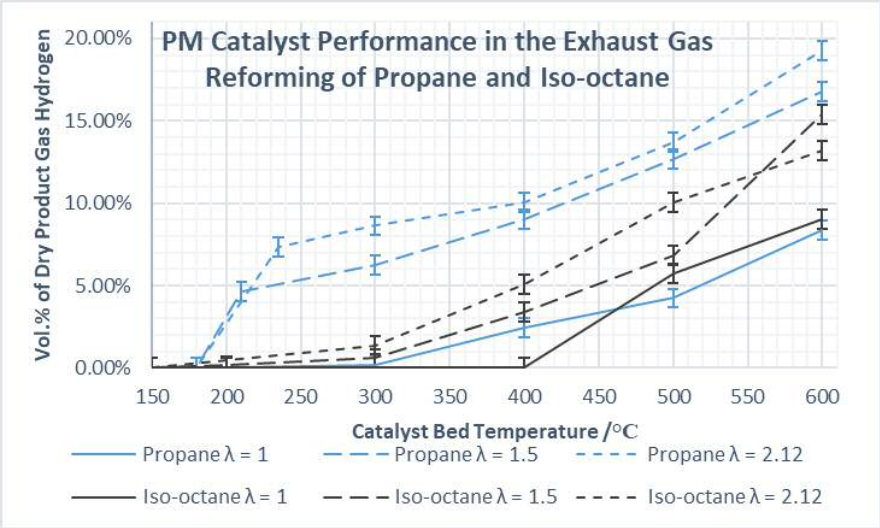

Figure 5.27: Comparing the exhaust gas reforming performance of the PM catalyst with propane and iso-octane, in terms of hydrogen content of the product gas as a function of λ and bed temperature

The average hydrogen yield under the same conditions is shown below in Figure 5.28.

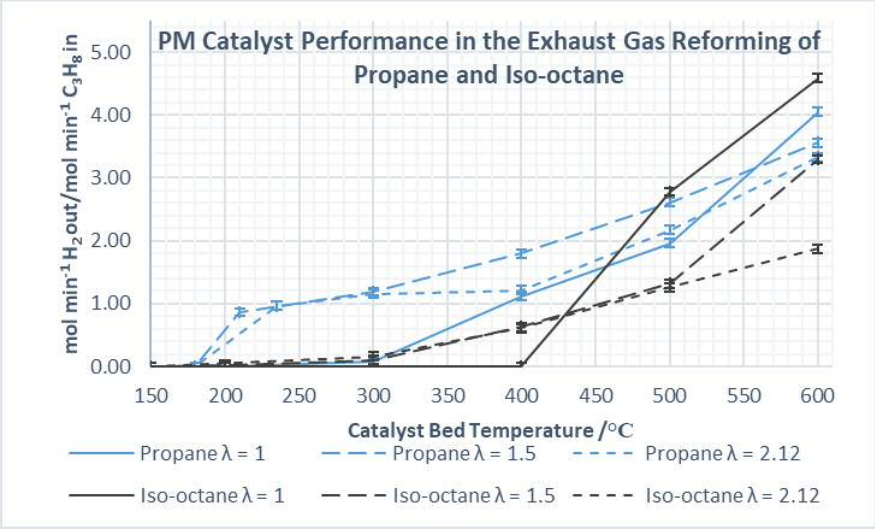

Figure 5.28: Comparing the exhaust gas reforming performance of the PM catalyst with propane and iso-octane, in terms of hydrogen yield as a function of λ and bed temperature

It is clear from the results above, with the exception of the high yielding λ = 1 condition at high temperatures when iso-octane was used, that the performance of the PM catalyst was significantly poorer with iso-octane on the whole than with propane, particularly at lower temperatures. Despite the light off occurring at a similar temperature for both fuels, the onset of hydrogen production was also delayed with iso-octane relative to propane.

The cause of this lower performance was unclear at this stage, and was an important issue throughout the project, and therefore will be discussed in more detail in the following sections and chapters.

Nickel Catalyst Performance for Exhaust Gas Reforming of Iso-octane

This section will discuss the results shown in Figures 5.10(i) through 5.12(iv). When the nickel catalyst was tested with iso-octane as the fuel, the exotherm was observed in the region of 170 °C to 180 °C. The size of the exotherm was again in proportion to the λ-value. Oxygen consumption was not complete during this initial light off process. This is shown clearly by the data in Figures 5.11(ii) and 5.12(ii), for λ = 1.5 and λ = 2.12, however the same is hinted at under the λ = 1 condition by the fact that the carbon dioxide levels did not reach a maximum until 400 °C.

Condition	Average H_2/CO
λ = 1	1.90
λ = 1.5	3.33
λ = 2.12	2.83

Table 5.7: H_2/C ratios for nickel catalyst in the exhaust gas reforming of iso-octane at λ = 1, λ = 1.5, and λ =2.12

The results above show the average H_2/CO ratios for the nickel catalyst with iso-octane at each lambda condition. Again the ratio at λ=1 was close to the characteristic ratio for SR1, then increases at λ = 1.5,

before decreasing to λ = 2.12. The two higher lambda conditions had H_2/CO ratios higher than SR1, suggesting increased contributions from SR2 and/or WGS.

In terms of hydrogen production, the data also shows that the onset of reforming was delayed until the completion of oxygen consumption in the oxidation reactions. The performance of the nickel catalyst in the exhaust gas reforming of iso-octane, in terms of hydrogen content of the product gas and hydrogen yield are shown below in Figure 5.29 and 5.30 respectively.

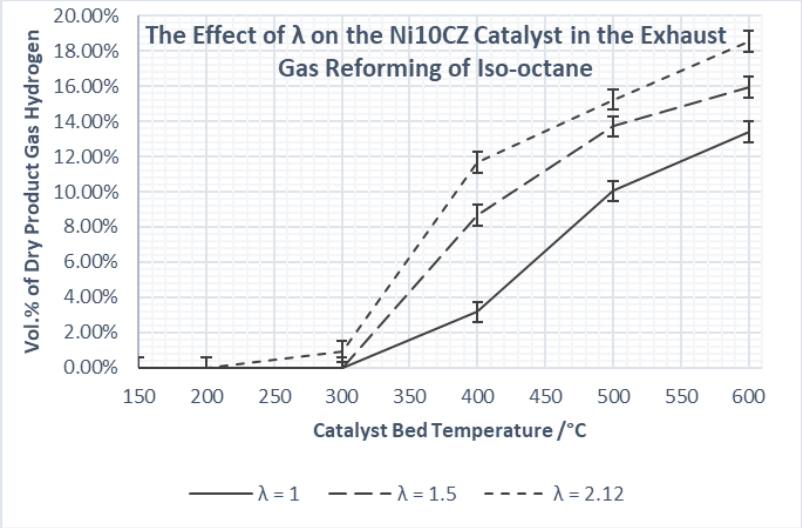

Figure 5.29: Nickel catalyst performance in the exhaust gas reforming of iso-octane, in terms of hydrogen content of the product gas as a function of λ and bed temperature

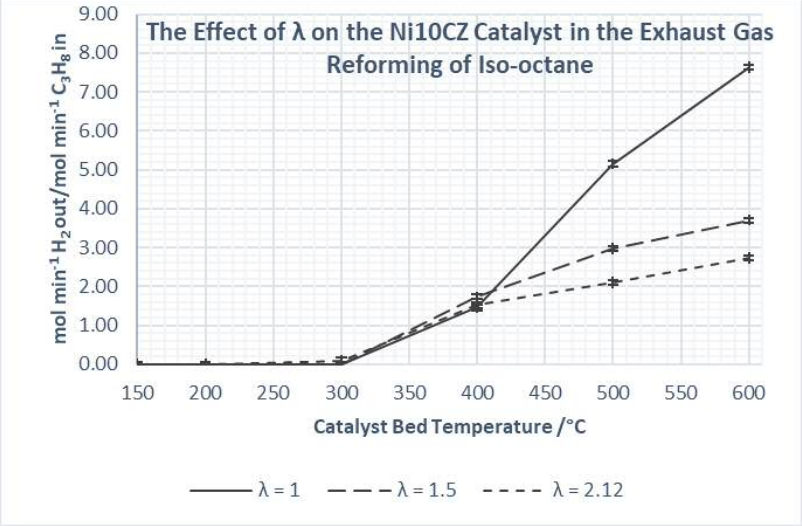

Figure 5.30: Nickel catalyst performance in the exhaust gas reforming of iso-octane, in terms of hydrogen production as a function of λ and bed temperature

It can be seen that the proportion of the product gas constituting hydrogen tended to increase with increasing λ-value, but that the trend was largely reversed in terms of hydrogen yield, where the λ = 1 condition yielded significantly more hydrogen per mole of iso-octane in the reactant feed. The explanations, in terms of reaction balance at the different conditions, for these observations are therefore proposed to be the same as those previously discussed for propane.

There were some differences in terms of the progression of hydrogen production under the different λ-conditions, between fresh and used catalysts. At λ = 1, the fresh catalyst did not produce any hydrogen at 400 °C, however the used sample did. Therefore it seemed to have been activated by the testing/nitrogen cool down cycle. However, this certainly was not the case at the λ = 1.5, where, especially at 400 °C and 500 °C, there was a decrease in hydrogen production measured between the fresh and used catalysts.

For the λ = 1.5 condition, this effect was also seen in the oxidation function of the catalyst. This test showed a significant drop in the oxygen consumption during the light off process between the fresh and used catalyst (Figures 5.11(i) and 5.11(ii)).

The likely explanation for this was carbon deposition. As already mentioned, the reactor tube had begun to become blocked and pressure built up towards the end of the λ = 1.5 test, hence a third test was not carried out. This was also the case, if earlier, for the fresh sample tested at λ = 2.12.

This is supported by the TGA data (Figure 5.13) and the observations recorded in Table 5.1. All samples showed significant total weight gain, as well as blackening and the change from pellets as fresh catalyst to black clumps after testing. The TGA data showed significant weight loss in the region off 450 °C to 600-630 °C, from carbon deposition [123, 124]. When the time on stream is taken into account, it suggests that as the λ-value increases, so did the rate of carbon deposition.

This again is most likely down to the decrease in the steam to carbon ratio with increasing λ. However, given the weight gain of the sample tested at λ = 1, it was most likely only a matter of time before the reactor also became blocked under those conditions also.

Therefore carbon deposition was a significant problem for the nickel catalyst with the heavier iso-octane fuel, not just in terms of catalyst performance, but also in terms of experimental considerations. Between the TGA and weight gain results, it is unclear whether the bulk of this carbon deposition is throughout the catalyst bed and located on the catalyst itself, or whether it is concentrated in a certain part of the bed. Given the reactor blocked after a lower amount of total carbon was deposited under the λ = 2.12 condition, it is possible that rather than total amount of carbon being of importance, it was the nature of the carbon deposition that caused the blockage.

It could also be the case that the drop in performance is in part due to the blockage of the reactor tube, and the resulting hindrance to reactant flow, combined with the deactivation of the catalyst due to carbon deposition on the catalyst surface.

Comparing the Nickel Catalyst Performance for the Exhaust Gas Reforming of Propane and Iso-octane

There was significant difference in light off characteristics between the two fuels for the Ni10CZ catalyst. In the case of propane, light off was observed around 280 °C, whereas for iso-octane it was observed approximately 100 °C lower, at around 170-180 °C. Secondly, with propane the consumption of oxygen in the reactant stream was complete during the light off, whereas with iso-octane it was not.

This behavior is shown below in Figure 5.31 below, which shows the oxygen consumption data for the fresh nickel catalyst with both propane and iso-octane at λ = 1.5. Oxygen consumption with propane did not change between runs, however this was not the case with iso-octane where the used catalyst showed decreased oxygen consumption during light off. This was most likely due to the deactivation associated with the buildup of carbon.

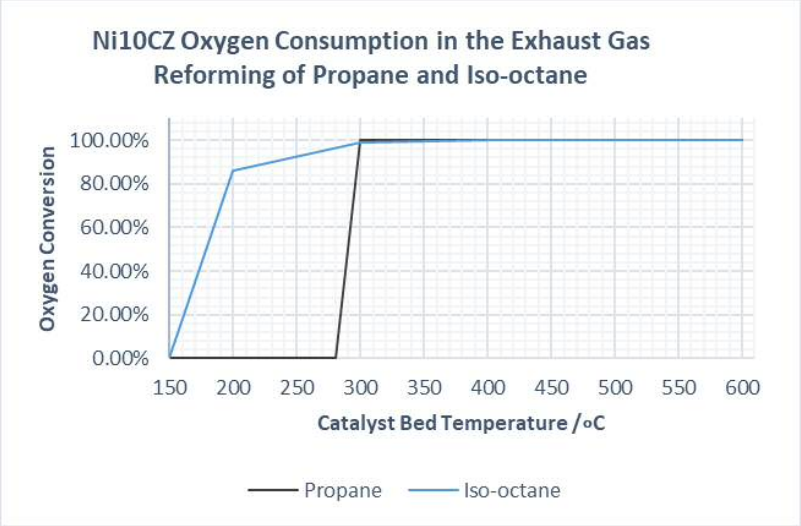

Figure 5.31: Nickel catalyst performance in the exhaust gas reforming of propane and iso-octane, in terms of oxygen consumption as a function of bed temperature at λ = 1.5

It can be seen that though consumption begins at lower temperature when iso-octane was the fuel source, consumption was actually complete for both fuels at around 300 °C. So it was just the onset and therefore duration of the consumption process that differed.

This can be explained by the fact that, as mentioned in the Introduction chapter, the oxidation of iso-octane has been found to occur in the gas phase, rather than solely on the catalyst surface [31, 48], combined with the lower auto ignition for heavier hydrocarbons [89].

Light off with both fuels showed an exotherm which increased in size with increasing λ-value. The H_2/CO product ratios for iso-octane were much higher, and more indicative of steam reforming, than those found with propane. Again this could be due to the lower activation energy for steam reforming of heavier hydrocarbons [70]. In terms of proportion of hydrogen in the product gas, the results below in Figure 5.32 directly compare the performance of the nickel catalyst with both fuels.

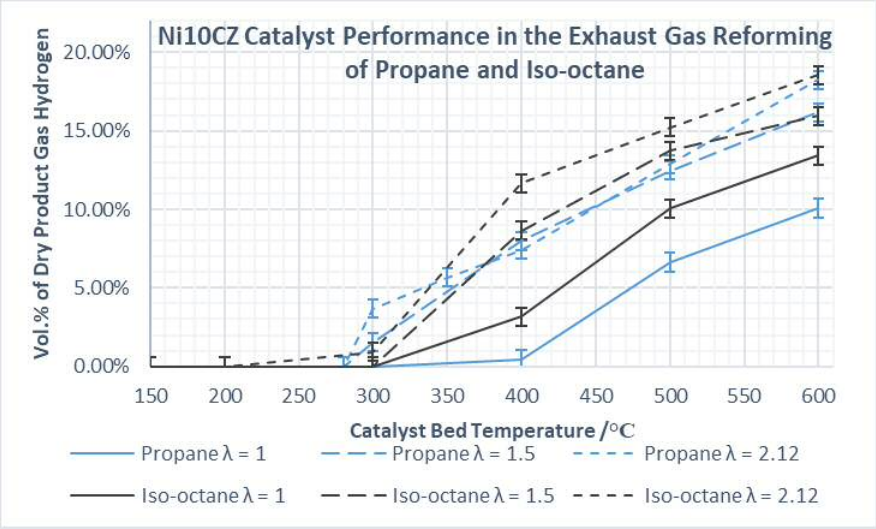

Figure 5.32: Comparing the exhaust gas reforming performance of the nickel catalyst with propane and iso-octane, in terms of the hydrogen content of the product gas as a function of λ and bed temperature

The average hydrogen yields of the Ni10CZ catalyst with both fuels at each λ condition are shown below in Figure 5.33.

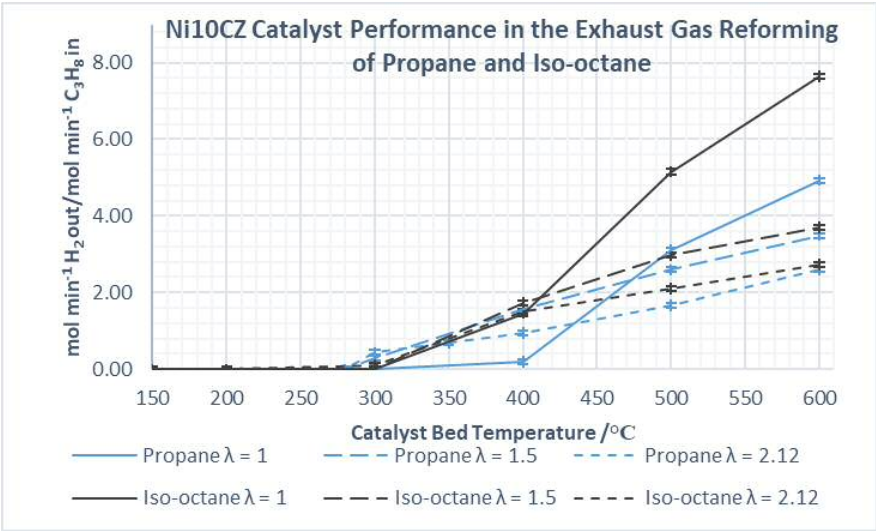

Figure 5.33: Comparing the exhaust gas reforming performance of the nickel catalyst with propane and iso-octane, in terms of hydrogen yield as a function of λ and bed temperature

The results show that for both fuels, as the λ-value increased, so did the hydrogen richness of the product gas, but that the λ = 1 condition was the highest yielding in terms of moles of hydrogen produced per mole of fuel in the reactant feed. The most likely explanation, focusing on reaction balances, has been discussed previously when analyzing the results for propane.

The performance of the nickel catalyst was largely comparable across the two fuels, with the exception of the λ = 1 condition, where testing with iso-octane yielded more hydrogen and a product gas richer in hydrogen relative to testing with propane. As mentioned above, the activation energy towards steam reforming is lower for the heavier hydrocarbon, therefore given that the λ = 1 condition favors steam

reforming due to the negligible oxygen content in the feed, this could explain the difference between the two fuels.

However, over the course of consecutive tests, from fresh to used catalyst, there were significant differences. For example the catalyst appeared to be activated by consecutive testing/nitrogen cooling cycles when propane was used as the fuel, under all λ-conditions. This effect was also observed under the λ = 1 condition and iso-octane fuel, but only at 400 °C. Outside of that, as clearly shown by the results in Figure 5.11(i) for the test with iso-octane at λ = 1.5, the catalyst showed a deactivation between consecutive tests. Not only was there a drop in hydrogen production, but also in oxygen consumption between fresh and used catalyst when iso-octane was used, which was not the case with propane.

As shown by the TGA (Figure 5.13) and observations in Table 5.1, carbon deposition was much greater for the samples tested with iso-octane. This is proposed to be the cause of the decrease in performance with consecutive tests with iso-octane as the fuel. Not only was the performance with propane improved with consecutive tests, but there was no issue with pressure build ups/reactor blockages. With iso-octane however, this occurred towards the end of the second test at λ = 1.5, and towards the end of the fresh test at λ = 2.12. A higher rate of carbon deposition was to be expected with the heavier hydrocarbon both because longer, and branched chain hydrocarbons are more prone to carbon deposition , but also because in these experiments the same % of fuel was used for both propane and iso-octane, which meant that the H_2O/C ratio in the iso-octane experiments was lower than with propane, and lower H_2O/C ratios can also increase the rate of carbon deposition [76]. However, the severity of the deposition observed with iso-octane in these experiments was unexpected.

So though the fresh and average performance was largely comparable between the two catalysts with both the gaseous and liquid fuels, there were drastic differences in terms of carbon deposition, and these had manifested themselves to varying degrees over the timescales of the tests. This will be part of the focus of the next chapter.

Comparing the Precious Metal and Nickel Catalyst Performance for Exhaust Gas Reforming of Iso-octane

Light off initiated around the same temperature (170-180 °C) for both catalysts when iso-octane was the fuel, however oxygen consumption was complete during the light off process for the PM catalyst, but not for the nickel catalyst. The exotherm (shown by the rise in bed temperature) was also greater, especially under the λ = 2.12 condition, with the PM catalyst compared to the nickel catalyst. The oxygen consumption did not change with consecutive tests for the PM catalyst, whereas it decreased between the fresh and used tests for the nickel catalyst, likely due to the buildup of carbon, and resulting deactivation of the catalyst. This suggests that the oxidation characteristics of the PM were stronger with iso-octane than those of the nickel catalyst. This difference in light off performance is shown clearly in Figure 5.34 below by the differences in oxygen consumption.

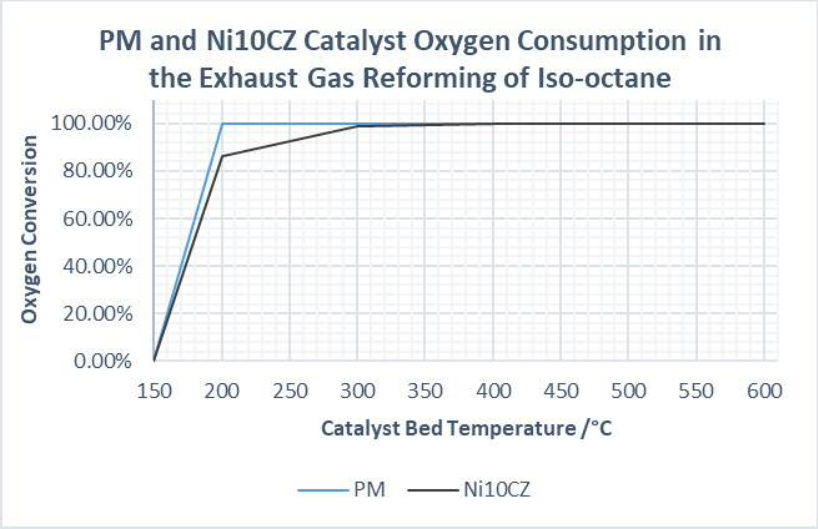

Figure 5.34: Comparing the exhaust gas reforming performance of iso-octane of the PM and nickel catalysts, in terms of oxygen consumption as a function of bed temperature at λ = 1.5

It should also be noted that the data above is for the fresh nickel catalyst, and that the consumption decreased for the used catalyst as the catalyst deactivated due to the buildup of carbon. The superior oxidation properties of the PM were to be expected given the assumed precious metal composition of the PM (Pt and Rh), compared to the base metal nickel catalyst, since precious metals are known to generally outperform base metals in this regard [130], in part due to their enhanced reducibility [131] (which was seen and discussed in the TPR results in Figure 3.1 in Chapter 3). In particular the ability of platinum to promote oxidation reactions is known [132], and has also been reported in exhaust gas reforming conditions [43].

In terms of reforming performance, the two catalysts are compared below, in terms of average hydrogen content of the product gas, and average hydrogen yield in Figures 5.35 and 5.36 respectively.

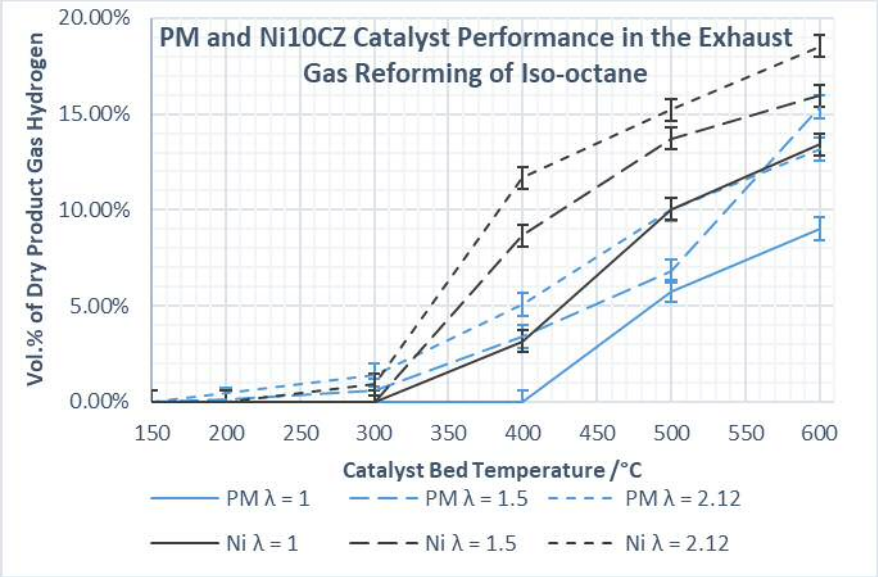

Figure 5.35: Comparing the exhaust gas reforming of iso-octane performance of the PM and nickel catalysts, in terms of hydrogen content of the product gas as a function of λ and bed temperature

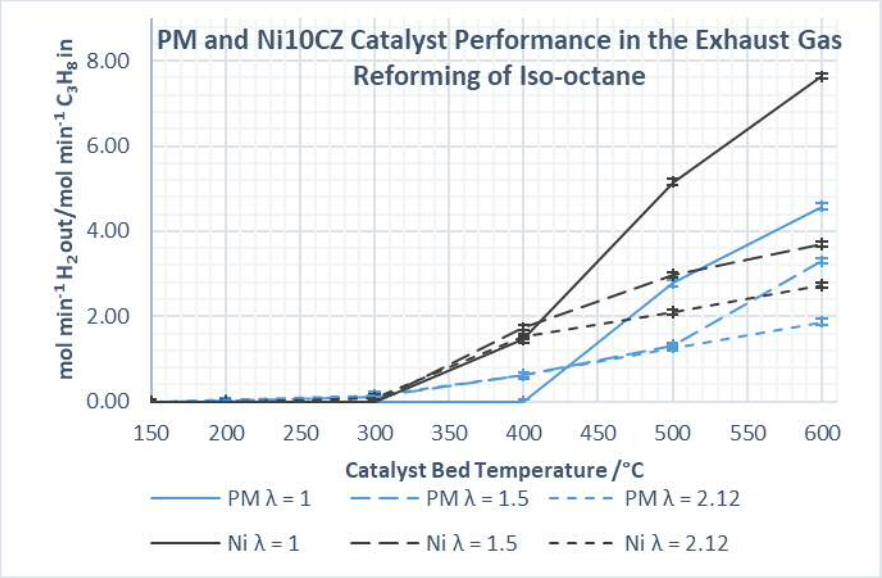

Figure 5.36: Comparing the exhaust gas reforming of iso-octane of the PM and nickel catalysts, in terms of hydrogen yield as a function of λ and bed temperature

It can be seen that the nickel catalyst outperformed the PM catalyst in this regard at all λ-values. Again it was unclear at this stage as to the cause of this lower performance of the PM catalyst with iso-octane, given it's strong performance with propane.

The H_2/CO ratios for both catalysts were indicative of steam reforming, both being in the region of SR1 or SR2.

In terms of progression between tests, both catalysts showed a decrease in hydrogen production (except the nickel catalyst at λ = 1 and at 400 °C) over consecutive testing/nitrogen cooling cycles. This was most likely down to the previously described carbon deposition, which was found to be significantly worse on the nickel catalyst, but was present on the PM also.

Comparing Propane and Iso-octane as Surrogate Fuels for Gasoline in Exhaust Gas Reforming

Crucially, it should be noted that the relative performance of the two catalysts with iso-octane had reversed from what was observed when propane was used as the surrogate fuel. When propane was used, the PM catalyst was superior, both in terms of earlier onset and quantity of hydrogen production. Whereas when iso-octane, the catalysts were similar in performance at low temperatures (below 300 °C), but then, for equivalent λ-values the nickel catalyst was superior at the higher temperatures.

As previously discussed, the choice of fuel had no great effect on the fresh nickel catalysts performance in terms of hydrogen production (Figures 5.32 and 5.33). However, the PM underperforms with iso-octane relative to its performance with propane (Figures 5.27 and 5.28). Therefore the above suggests that either the nickel catalyst could have been "over performing" with iso-octane if it was a lower performing fuel for exhaust gas reforming relative to propane, or more likely that the PM was "underperforming" with iso-octane.

This reversal in catalyst performance was unexpected, since as discussed in the Introduction, precious metal catalysts are generally superior reforming catalysts, regardless of fuel choice. It is unclear at this stage what the cause of this was, whether it was simply down to the catalysts themselves or experimental in nature.

The literature on exhaust gas reforming using iso-octane as a model fuel, are consistent with the experimental results shown here, specifically the experimental data and thermodynamic predictions from the work of Gomes et al. [31, 48] and Ambroise et al. [44, 80], who performed their experiments under conditions almost identical to $\lambda = 1$. This suggests that, at $\lambda = 1$ at least, the results here are reliable.

Furthermore, in terms of hydrogen yield for the nickel catalyst, the results presented here are in line with those predicted in the above works for thermodynamic equilibrium compositions – suggesting that it was operating at close to equilibrium. The PM on the other was operating at below equilibrium yields of hydrogen. As mentioned, this lack of performance was a continued focus of this work and will be covered further in the later chapters.

It was therefore unclear at this stage as to the origin of the observed reversal in performance in terms of hydrogen production between catalysts when iso-octane was used relative to when propane was the model fuel. Furthermore, detailed studies of exhaust gas reforming with heavier fuels are not common in the literature. Therefore this required further investigation and hence was part of the remaining work in this project, the details of which will be covered in more detail in the next chapter.

Another significant difference between fuels was the aforementioned rate of carbon deposition. This was found to be somewhat non-existent for the PM (based on visual observation, since characterization was not possible), and negligible for the nickel catalyst (based on total weight gain and TGA) when propane was used as the fuel. However when iso-octane was used, the rate of deposition was found to be significantly higher on both catalysts (through visual blackening of the PM monolith, and the considerable total weight gain of the nickel samples, and the significant weight loss events observed in the TGA experiments).

As previously mentioned part of the explanation was most likely the lower H_2O/C ratios used during the iso-octane tests, relative to the propane testing conditions, but also from the fact the heavier, branched hydrocarbon is known to be more prone to coking [76]. This greater rate of coking likely contributed to the degradation in catalyst performance with consecutive testing/nitrogen cooling cycles, and was certainly the cause of the reactor blockages in the nickel catalyst tests. This again stood in contrast to the tests with propane which did not result in reactor blockages, as well as showing that testing/nitrogen cooling cycles were found to be activating. It is proposed that the nitrogen cool down, as discussed in Chapter 4, preserves any species deposited during testing, which given the much lower rate of deposition of propane means that this did not result in significant enough build up to cause problems. However, this was not the case with the much higher rate of deposition with iso-octane, where the preservation of the vast amount of carbon became an issue.

This was the other key result from in this chapter, and hence the other area of focus in the remainder of this project was to determine to what extent this rate of deposition could be controlled when iso-octane was used as the surrogate fuel.

Conclusions & Further Work

The key conclusions from the work presented in this chapter were therefore:

- The reactions sequence during exhaust gas reforming, as expected, was initiated by the oxidation of a portion of the fuel, which raised the bed temperature, promoting reforming reactions as the temperature was raised.
    - When propane was used the PM had ~100 °C lower light off than the nickel catalyst.
    - However, when iso-octane was used the light off occurred at around 170 °C for both catalysts. This was probably due to the oxidation of a quantity of the isooctane taking place in the gas phase.
    - The exotherm from the oxidation of the fuel, as measured by the thermocouple just below the catalyst bed, was found increase with increasing lambda value, likely due to the increased presence of oxygen and fuel (richer feed).
    - The hydrogen richness of the product gas was found to increase with increasing lambda – assigned to greater POx reactivity due to the higher oxygen content of the feed, and better promotion the endothermic reforming reactions through the exothermicity of these POx reactions.
    - However, in terms of hydrogen yield, as would be expected, the $\lambda = 1$ condition was consistently found to be the best performing at high temperatures due to the negligible oxygen content of the feed leaving the fuel to be consumed in higher yielding steam reforming reactions.
    - It is there suggested that the ideal exhaust gas reforming conditions, to obtain a product gas sufficiently rich in hydrogen, where the hydrogen was produced via high yielding and thermochemical recuperating steam reforming reactions, were intermediate conditions where the exhaust feed contained sufficient quantities of both oxygen and steam.
- The PM catalyst was superior when propane was used as the surrogate fuel, both in terms of lower light off, lower temperature onset of hydrogen production and quantity of hydrogen produced.
- However, the nickel did display reasonable performance, particularly at the higher temperatures.
- This relationship was reversed when iso-octane was used as the surrogate fuel where the nickel catalyst displayed stronger reforming performance.
- The nickel catalyst showed comparable performance between fuels, whereas the PM showed lower performance with iso-octane compared to propane.

- Carbon deposition was negligible for either catalyst with propane as the surrogate fuel.
- Carbon deposition was significant when iso-octane was used as the fuel.
- This was particularly the case for the nickel catalyst which showed significant buildup of carbon, resulting in blocking of the reactor, and decreasing performance with consecutive tests.
- The higher rate of carbon deposition was assigned to the lower H_2O/C ratios present during iso-octane testing, as well as the proclivity of the heavier branched fuel towards carbon deposition.
- The nitrogen cooling method used during these tests contributed to the issues since it preserved the greater quantities of carbon resulting from testing with iso-octane.

Based on the above, it was decided that for the remainder of this project the focus should be on:

1. Determining to what extent the carbon deposition on the nickel catalyst could be controlled through changes in experimental conditions.
2. Investigating the origin of the lack of performance from the PM catalyst with iso-octane.

The details of these investigations will be discussed in the next chapter.

Chapter 6 - Further Investigations into the use of Iso-octane as a Surrogate for Gasoline, and the Performance of the Precious Metal Catalyst

Introduction

The aim in this chapter was to carry out a range of experiments to further investigate the two main issues resulting from the work in the previous chapter. These issues were:

1. The reversal in performance between the PM and nickel catalyst and,
2. The significantly higher rate of carbon deposition, when iso-octane was used instead of propane as the surrogate fuel for gasoline.

Additional Experimental Details

Investigating the Effect of Reaction Conditions on the Rate of Carbon Deposition

The first set of experiments carried out were designed to determine to what extent the rate of carbon deposition during iso-octane testing could be controlled by experimental conditions. Specifically, these experiments involved the following:

- Raising the H_2O/C by decreasing the quantity of iso-octane in the reactant stream from 5 % to 3 % at $\lambda = 1.5$. This had the effect of raising the H_2O/C from 0.21 to 0.35.
- Lowering the H_2O/C by increasing the quantity of iso-octane in the reactant stream from 5 % to 7.5 % at $\lambda = 1.5$. This had the effect of lowering the H_2O/C from 0.21 to 0.14.
- Combining the lower fuel condition described above with the air-cool down method described in Chapter 4.
- The H_2O/C ratio was raised further by arbitrarily increasing the steam content of the synthetic exhaust gas. Due to limitations with how low the fuel flow rate could be lowered this meant that in order to dramatically raise the H_2O/C ratio the quantity of steam in the exhaust gas had to be artificially raised – in this case by a factor of 10. This therefore raised the steam to carbon ratio from 0.21 in standard conditions at $\lambda = 1.5$ to 2.1.

It was expect that increasing the H_2O/C and using the air cool down method would both decrease the quantity of carbon left on the catalyst surface after testing.

Investigating the Poor Performance of the Precious Metal Catalyst in the Exhaust Gas Reforming of Iso-octane

The next set of experiments were designed to determine at what temperature the onset of coking occurred when iso-octane was the fuel. Furthermore, these experiments would highlight if the rate of deposition

was dependent on temperature. Finally, the below experiments were also performed to see if there was any differences between the nickel and PM catalysts in this regard – which could hint at differing reaction mechanisms between the catalysts and hence help explain the difference in performance.

- Both catalysts were held at 200 °C and 300 °C for 2 hours under the standard λ = 1.5 exhaust gas reforming of iso-octane conditions.
- The nickel catalyst was also tested by being held at 400 °C and 600 °C for 2 hours under the same conditions.

Further experiments were designed to test whether simple experimental causes were the origin of the lack of performance from the PM with iso-octane. In particular potential issues around the hindrance/inconsistency of fuel flow at the higher flow rates and pressures associated with testing the PM at the same GHSV as the nickel catalyst (see Experimental chapter) were investigated.

- The PM was tested under λ = 1.5 conditions, with 5 % iso-octane, but at a range of lower total gas flow rates (50, 100 and 125 mL/min compared to the standard 175 mL/min used to achieve the desired GHSV of 8,500 h^{-1}). It was thought the higher flow rates used could have been disturbing the fine mist of liquid fuel delivered by the spray nozzle.
- Through modifications to the reactor, the pressure in the system was lowered by using a bypass to vent. It was thought that the higher pressure arising from testing at the aforementioned higher total gas flow rates could have been hindering fuel flow.

Another test was carried out in order to determine if the age of the PM catalyst was the cause of its poor performance with iso-octane:

- The smaller PM monolith from Johnson Matthey, described in Chapter 2, was tested at λ = 1.5 with 5 % iso-octane. This monolith was also not fresh; it had been used previously.

The final two experiments were designed to see if the precious metal nature of the PM could explain the lack of performance. Since the PM catalyst was thought to contain rhodium, a 1 % rhodium on ceria-zirconia catalyst was synthesized (see Experimental chapter). It was then tested as follows:

- With 5 % propane at λ = 1.5, for three consecutive tests, before characterization by TGA was performed.
- As above but with iso-octane as the surrogate fuel.

The above two tests would also examine whether the rhodium catalyst was more or less resistant (predicted to be more resistant, see Introduction chapter) than the nickel catalyst to coking.

The λ = 1.5 condition was chosen for these tests since it is the intermediate condition.

The results of these experiments will now be presented in the next section.

Results

Note: As per Chapter 2, the concentration of the gases in the dried product stream were found to be directly proportional to the rate of production/consumption (mol min^{-1}).

Nickel Catalyst Performance in the Exhaust Gas Reforming of 3 % Iso-octane at λ = 1.5

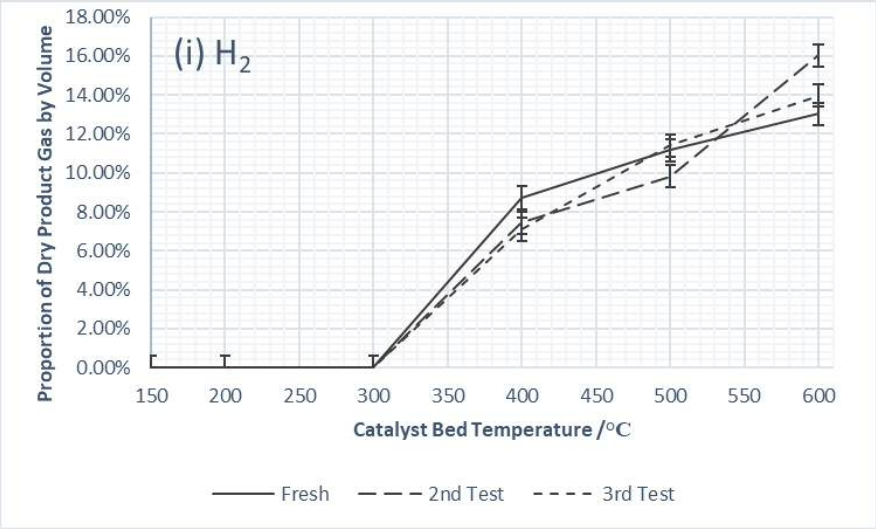

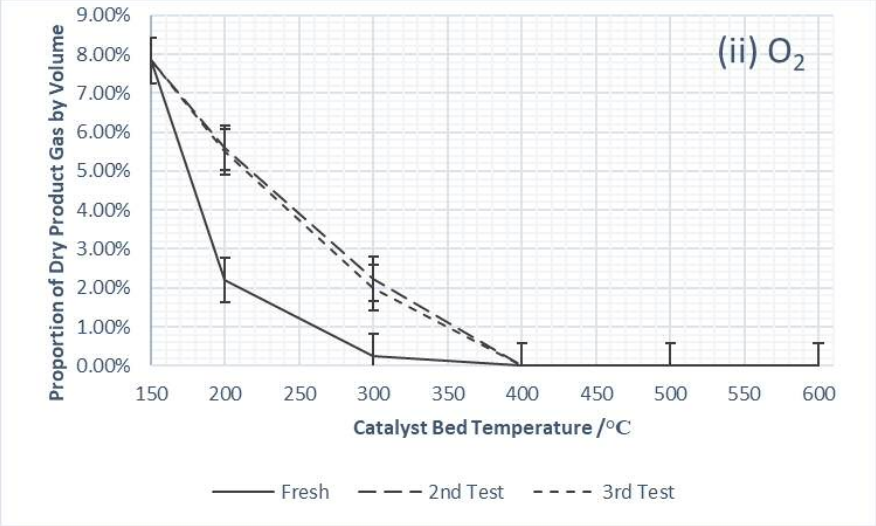

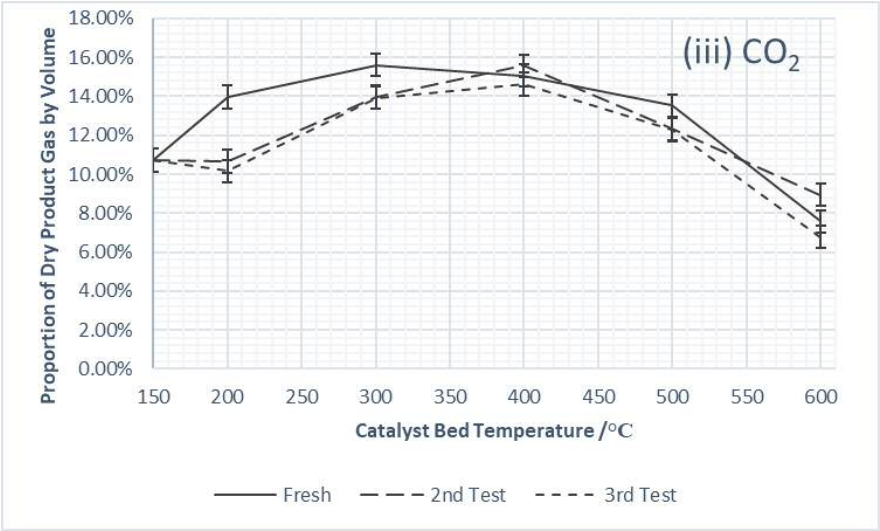

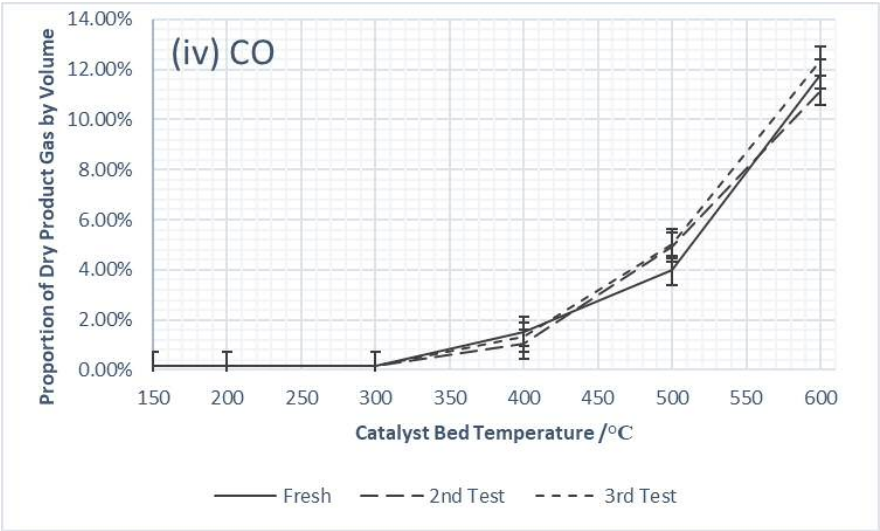

Figure 6.1: Nickel catalyst performance in the exhaust gas reforming of 3 % iso-octane at λ = 1.5, in terms of the composition of the dried product gas as a function of temperature

The data above show the results for when the quantity of iso-octane was lowered to 3 % at the λ = 1.5 condition with the nickel catalyst.

Three full consecutive tests were possible without pressure build up or blockage in the reactor.

Light off again occurred at around 170 °C and oxygen consumption was not complete until 400 °C (Figure 6.1(ii)). It was again observed that oxygen consumption was lower for the used catalyst at 200 °C and 300 °C when compared to the fresh catalyst.

Carbon dioxide levels in the product gas increased during light off (to a lesser extent in the second and third test), shown in Figure 6.1(iii).

Hydrogen production again did not start until all the oxygen had been consumed (Figure 6.1(i)). The fresh catalyst showed slightly higher hydrogen levels in the product gas at 400 °C and 500 °C, suggesting a very slight deactivation with consecutive tests. All tests reached a maximum of around 15-16 % by volume of the product gas at 600 °C.

Carbon monoxide production (Figure 6.1(iv)) was consistent between tests, starting at 400 °C and reaching a maximum of around 12 % of the product gas by volume at 600 °C.

Nickel Catalyst Performance in the Exhaust Gas Reforming of 7.5 % Iso-octane at λ = 1.5

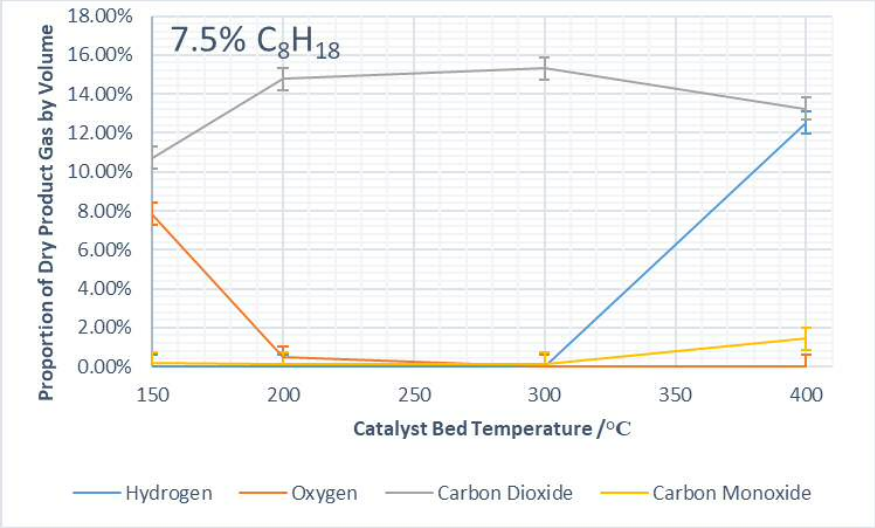

Figure 6.2: Nickel catalyst performance in the exhaust gas reforming of 7.5 % iso-octane at λ = 1.5, in terms of the composition of the dried product gas as a function of bed temperature

The data above show the results for when the quantity of iso-octane was raised to 7.5 % at the λ = 1.5 condition with the nickel catalyst. The pressure in the reactor had begun to build up before the measurements at 500 °C and 600 °C could be taken, meaning a full test cycle was not possible.

However, it can be seen that oxygen consumption was almost complete after the bed temperature had settled at around 200 °C from the resulting exotherm. Oxygen consumption was complete at 300 °C, however hydrogen production did not begin until 400 °C. A significant amount of hydrogen was produced at this temperature, equating to around 12 % of the product gas by volume. A small amount of carbon monoxide was also present at 400 °C.

Nickel Catalyst Performance in the Exhaust Gas Reforming of 3 % Iso-octane at λ = 1.5, after Cooling in a Simulated Air Atmosphere

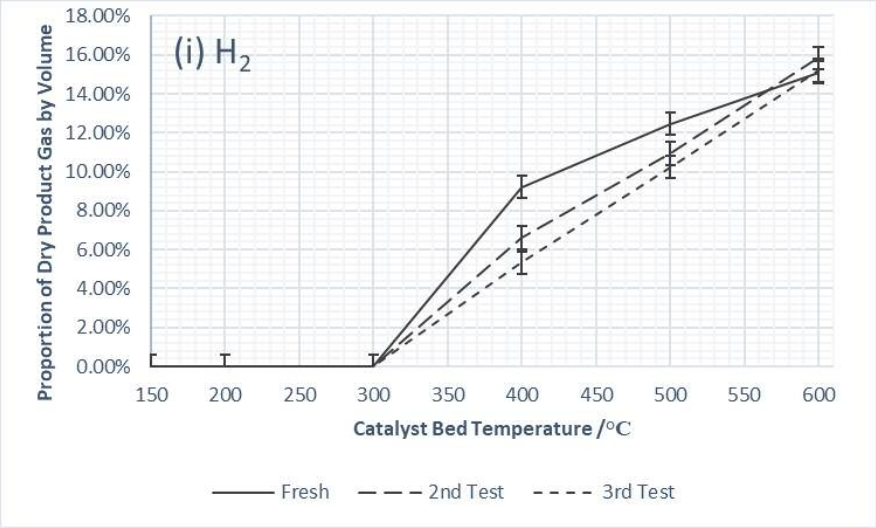

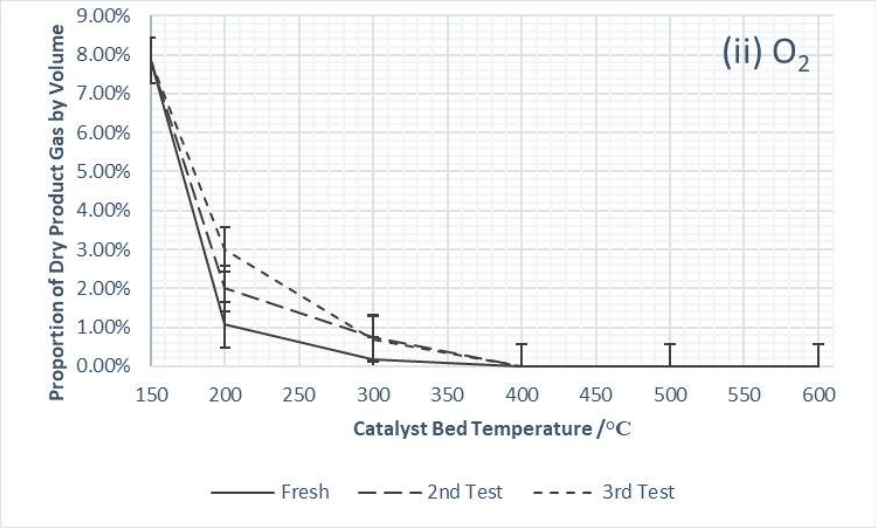

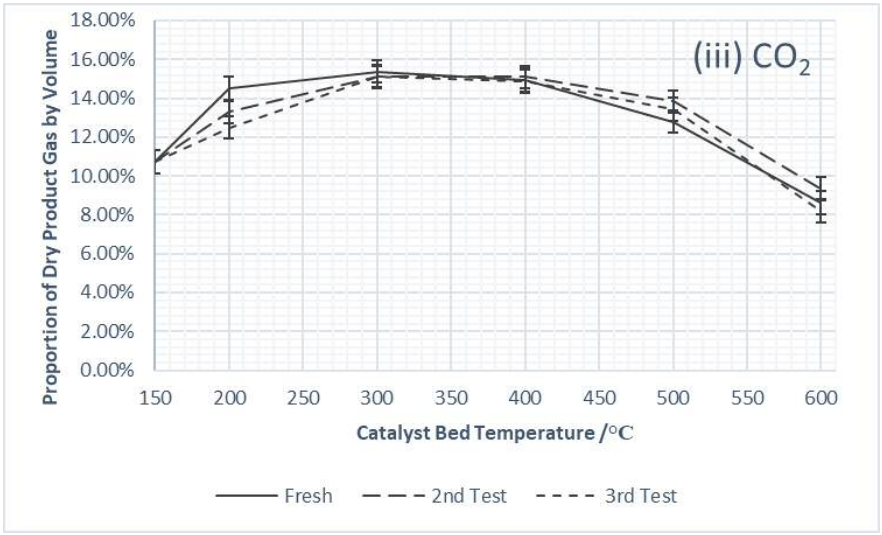

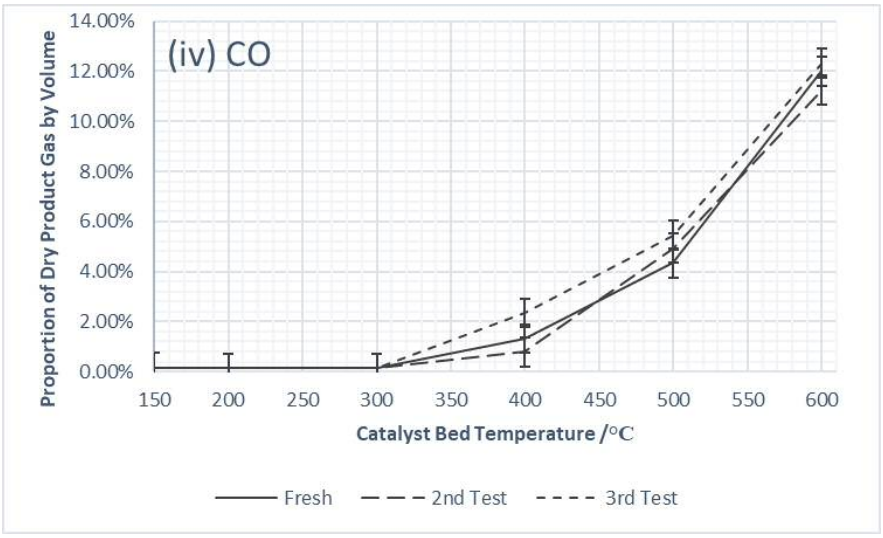

Figure 6.3: Nickel catalyst performance in the exhaust gas reforming of 3 % iso-octane at λ = 1.5, and the effect of exposing the catalyst to air during the cooling phase, in terms of the composition of the dried product gas as a function of bed temperature

The data above is for the experiment where the iso-octane content in the reactant stream was again lowered to 3 %, at the λ = 1.5 condition with the nickel catalyst. However, in between tests, the catalyst was exposed to the air cooling method, instead of the nitrogen cooling method. Three consecutive tests were possible without pressure build up.

Light off again started at around 170 °C, with almost complete oxygen consumption by the time the bed temperature had settled at 200 °C (Figure 6.3(ii)).

There was a more gradual decrease in oxygen consumption at 200 °C and 300 °C between the fresh catalyst and the second and third tests. All the oxygen had been consumed at 400 °C.

Hydrogen production (Figure 6.3(i)) again coincided with complete oxygen consumption, and rose to a maximum, shown by the concentration of hydrogen in the product gas, of around 15-16 % by volume of the product gas at 600 °C. Again a slight deactivation was observed between runs at the lower temperatures of 400 °C and 500 °C between the fresh and used catalyst.

Carbon dioxide (Figure 6.3(iii)) content in the product gas increased during light off, before levelling out and then decreasing as it was either consumed or diluted in the stream.

Carbon monoxide (Figure 6.3(iv)) was not recorded until 400 °C, and reached a maximum of around 12 % at 600 °C.

Nickel Catalyst Performance in the Exhaust Gas Reforming of Iso-octane at a H_2O/C of 2.1 under the λ = 1.5 Condition

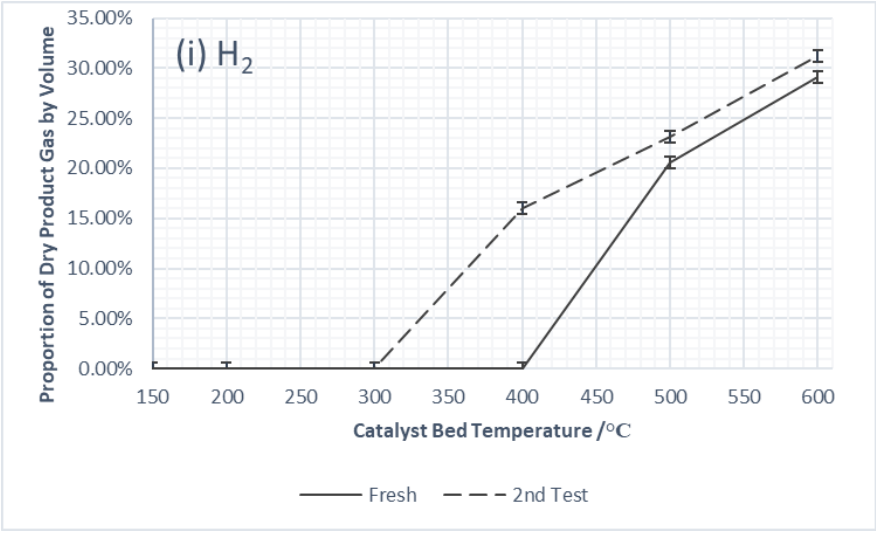

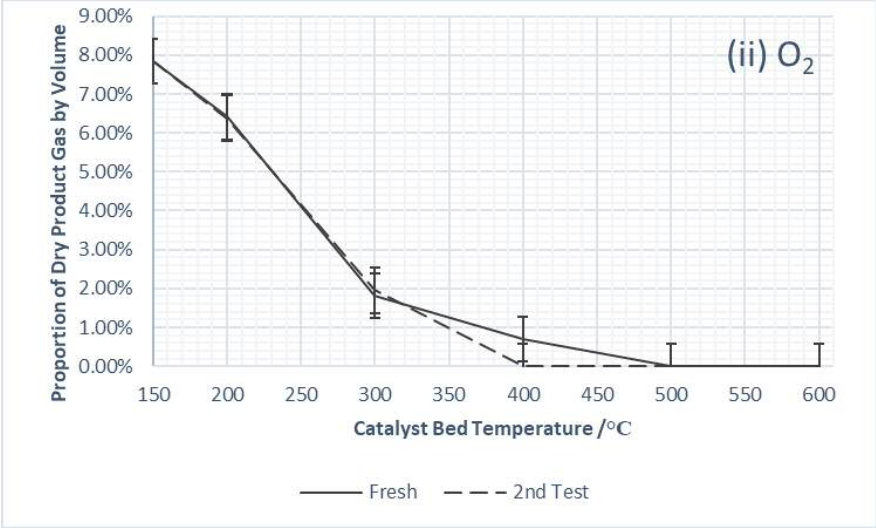

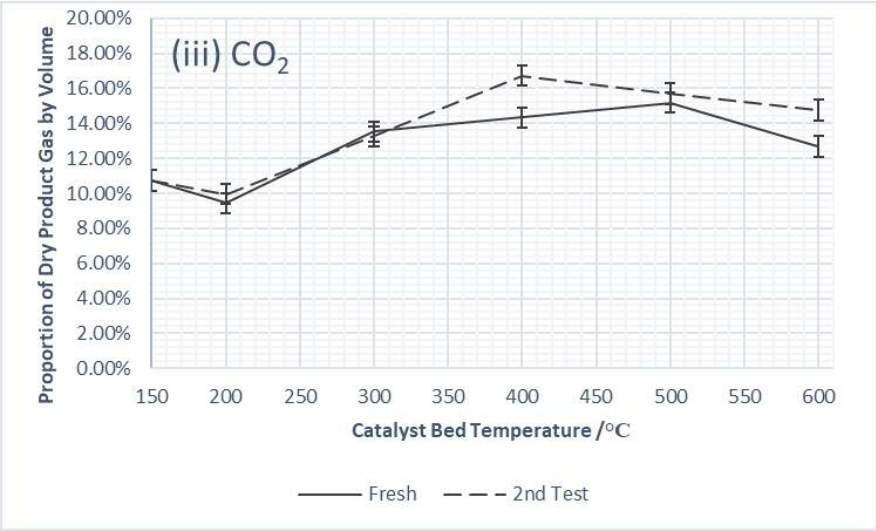

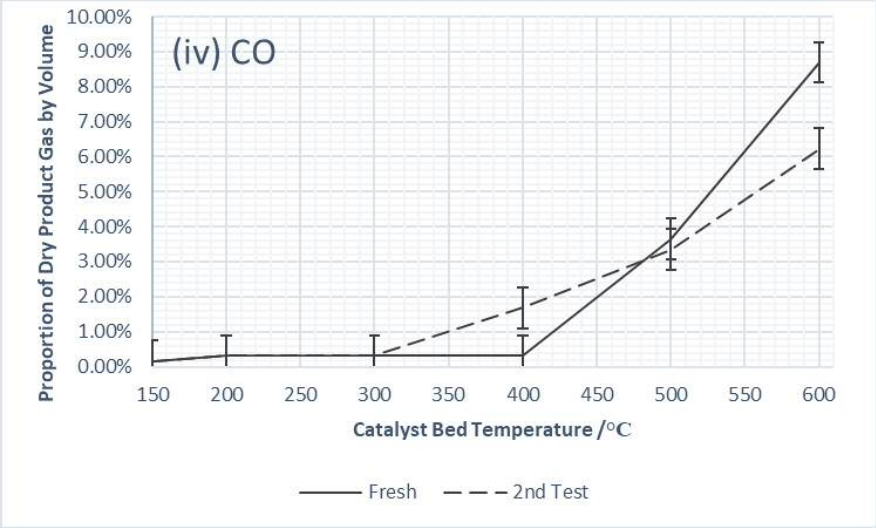

Figure 6.4: Nickel catalyst performance in the exhaust gas reforming of iso-octane at λ = 1.5, with a H_2O/C = 2.1, in terms of the composition of the dried product gas as a function of temperature

The data above is for the experiment where the steam to carbon ratio (H_2O/C) was raised significantly (x10), from around 0.21 in the standard λ = 1.5 condition, to 2.1. It can be seen from Figure 6.4(ii) that this increase in the steam content significantly depressed the light off.

Furthermore, there was still a significant amount of oxygen left at 300 °C, and in the fresh catalyst test, there was still just under 1 % by volume of the product gas left at 400 °C.

The data for carbon dioxide (Figure 6.4(iii)) reflects this depressed oxidation activity, with only a small increase at 200 °C, and rising further until reaching a maximum at 500 °C in the fresh catalyst test, and 400 °C in the used catalyst.

Hydrogen production (Figure 6.4(i)) again coincided with complete oxygen consumption, first recorded at 500 °C with the fresh catalyst, and 400 °C with the used catalyst. Once initiated however, a much larger quantity of hydrogen was produced, shown by the increased concentration of hydrogen in the product gas, than previously seen, reaching a maximum of around 30 % by volume of the product gas at 600 °C.

Carbon monoxide (Figure 6.4(iv)) however did not show the same gains as hydrogen did, reaching a maximum of around 9 % at 600 °C with the fresh catalyst.

The fact that oxygen consumption was complete at 400 °C for the used catalyst, and that hydrogen production was first recorded at the same temperature suggests that the catalyst was activated by the first use under reaction conditions.

Only two consecutive tests were carried out in order to match the amount of time on stream as the test under standard λ = 1.5 and 5 % iso-octane conditions. No pressure build-up was observed in this time frame.

Rhodium Catalyst Performance in the Exhaust Gas Reforming of Propane

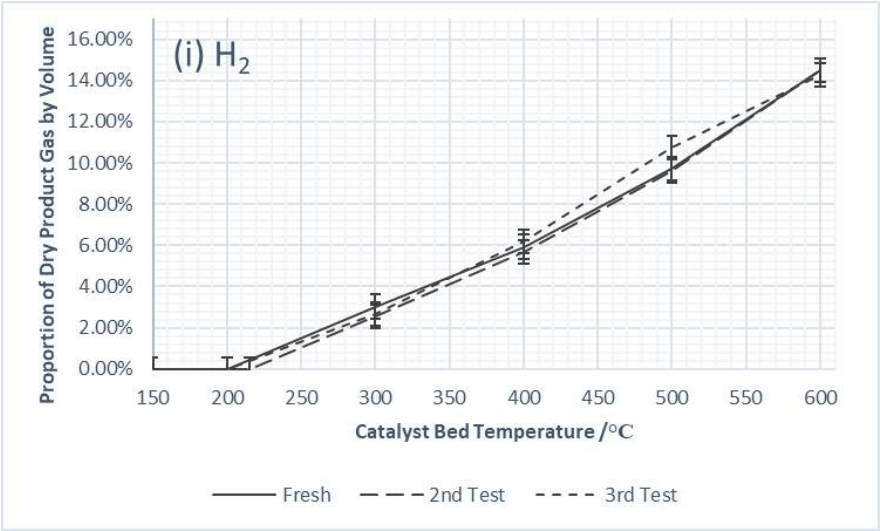

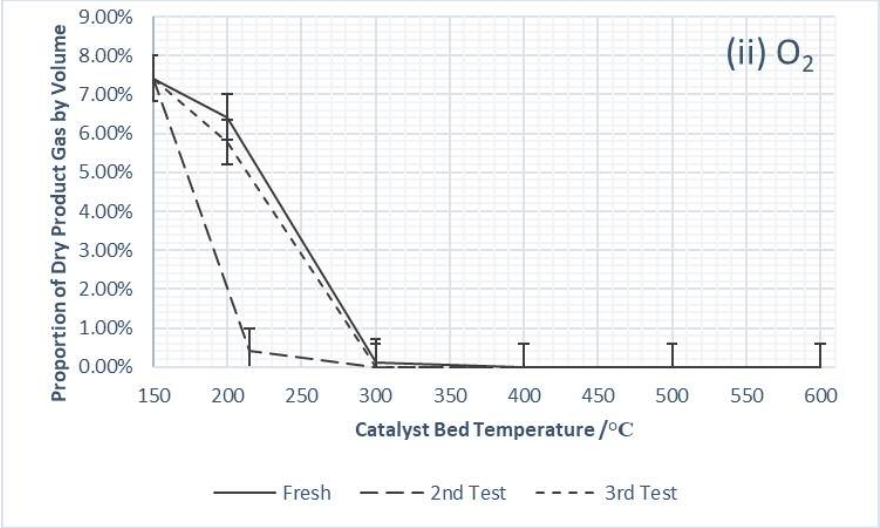

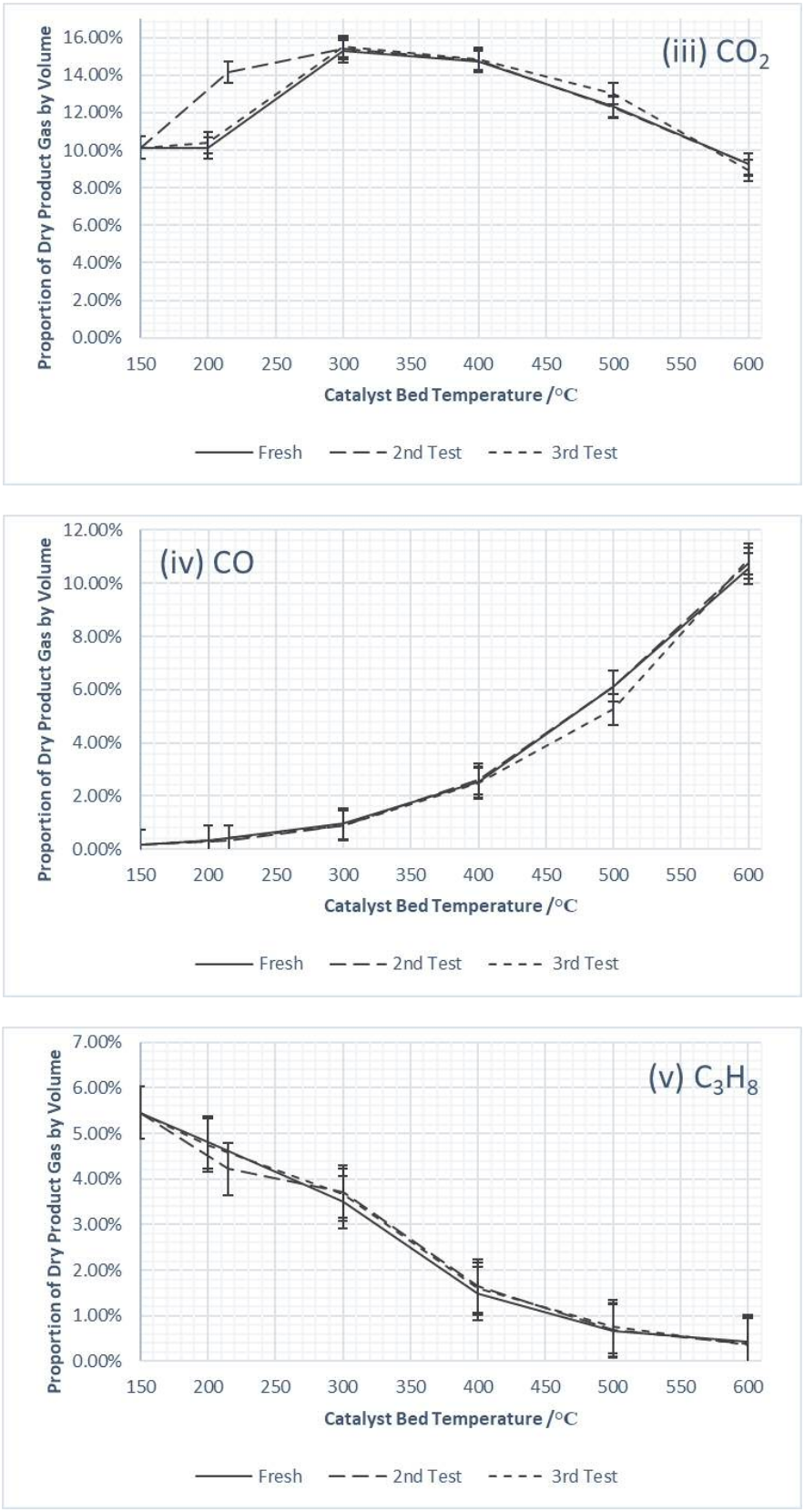

Figure 6.5: Rhodium catalyst performance in the exhaust gas reforming of propane at λ = 1.5, in terms of the composition of the dried product gas as a function of bed temperature

Light off for the rhodium catalyst and propane at the λ=1.5 condition seemed to occur at approximately 200 °C. As such it was possible to record a GC measurement pre-light off at 200 °C, but for the fresh catalyst and the third test the heating overshot the light off point.

This can be seen by the oxygen consumption data in Figure 6.5(ii). Oxygen consumption was complete at 300 °C in all tests, and carbon dioxide content correspondingly peaked at the same temperature as a result of the oxidation of the fuel (Figure 6.5(iii)).

Hydrogen and carbon monoxide production both were recorded at 300 °C, and their content in the product gas rose smoothly throughout the temperature range (Figures 6.5(i) and 6.5(iv) respectively). They reached maximums of just above 14 % and 10 % by volume of the product gas respectively at 600 °C. The performance of the catalyst between runs was very consistent.

After light off, propane consumption (Figure 6.5(v)) increased smoothly, with around 0.5 %, by volume of the product gas, of propane remaining unconsumed at 600 °C. The consumption was very similar between runs (once light off has been accounted for).

Rhodium Catalyst Performance in the Exhaust Gas Reforming of Iso-octane

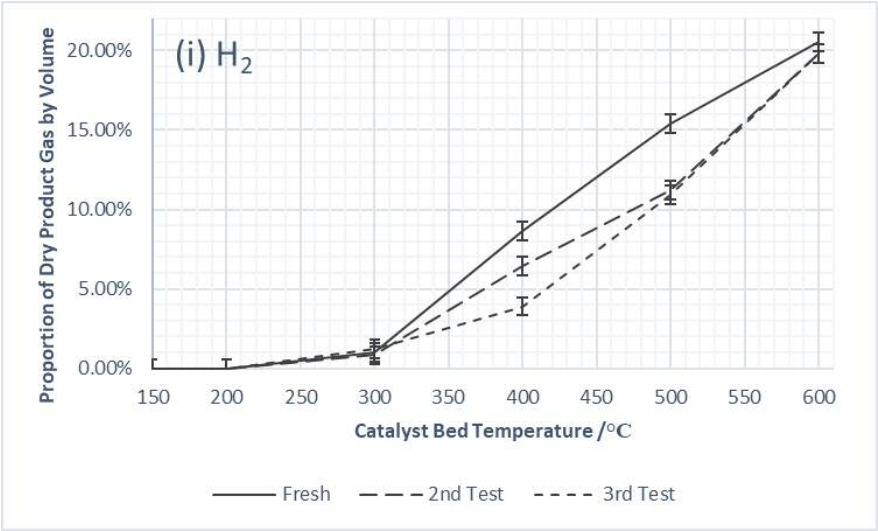

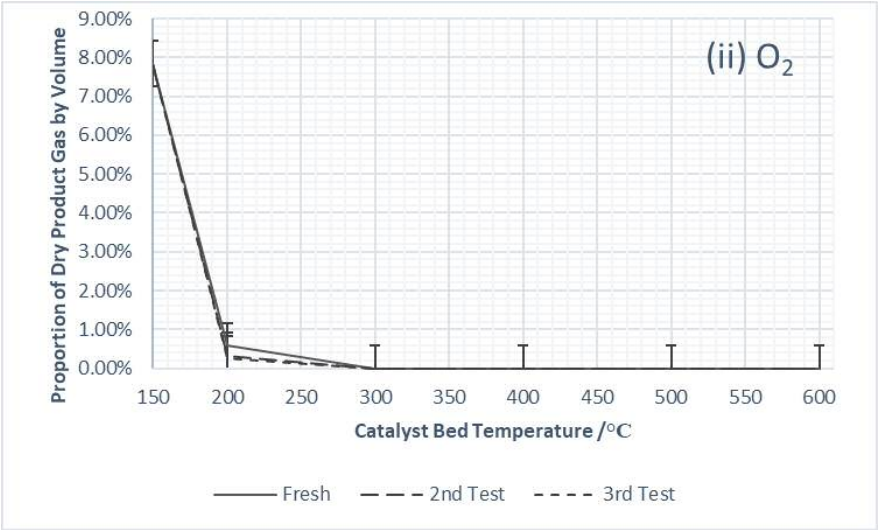

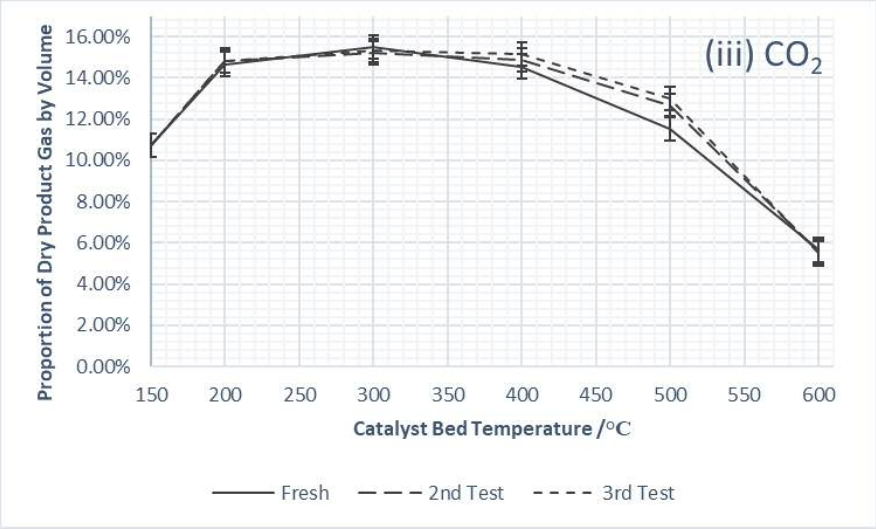

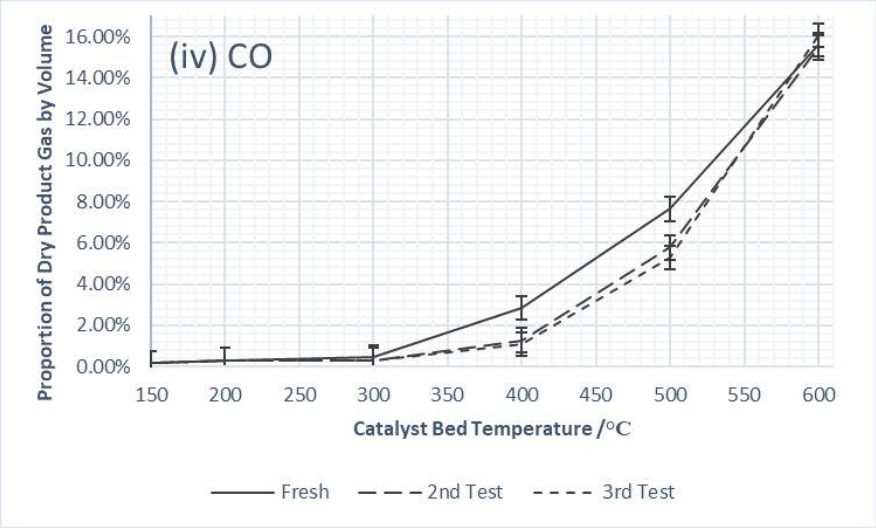

Figure 6.6: Rhodium catalyst performance in the exhaust gas reforming of iso-octane at λ = 1.5, in terms of the composition of the dried product gas as a function of bed temperature

The results above show how the rhodium catalyst performed with 5% iso-octane as the fuel, at the λ=1.5 condition, over three consecutive testing/nitrogen cooling cycles.

Light off started at around 170 °C, with the exotherm taking the bed temperature to just under 200 °C. It can be seen from Figure 6.6(ii), that oxygen consumption was almost complete during light off, and was complete by 300 °C. The oxygen consumption was very consistent between runs. The proportion of the product gas constituting carbon dioxide (Figure 6.6(iii)) increased during light off, and again was either consumed/diluted at 500 °C and 600 °C.

A small quantity of hydrogen was detected at 300 °C, rising to a peak of just under 20 % by volume of the product gas at 600 °C (Figure 6.6(i)). There was a slight decrease in performance at 400 °C and 500 °C of the used catalyst compared to the fresh.

Carbon monoxide (Figure 6.6(iv)) was detected at 400 °C, rising in concentration throughout the temperature range to just under 16 % by volume of the product gas at 600 °C.

Catalyst Characterization

Note: For clarity sake, the TGA data below do not always show the data for the fresh catalysts.

Both the nickel and rhodium fresh catalysts showed approximately 3-4 % weight loss in the TGA experiments most of which occurred around 100 °C, suggesting the loss of moisture and other loosely bound contaminants (for example any un-dissociated precursor salt from the preparation of the catalyst).

TGA: The Effect of Iso-octane Content in the Exhaust Gas Reforming Mixture

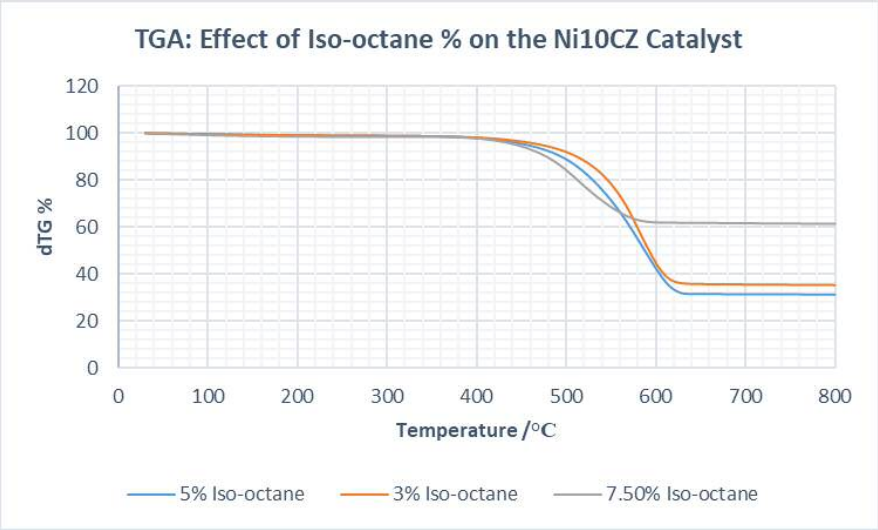

Figure 6.7: Thermogravimetric data for the nickel catalyst samples tested at λ = 1.5, with varying iso-octane content of the exhaust gas reforming feed

The results above in Figure 6.7 show the TGA results for the samples tested at λ = 1.5 with varying quantities of iso-octane in the reactant stream.

The sample tested with 3 % iso-octane showed a total weight loss of around 65 %, occurring in the region of 450-630 °C. The sample tested with 5 % iso-octane showed a total weight loss of almost 70 %, occurring in the same temperature region. The sample tested with 7.5 % iso-octane showed a weight loss of just under 40 %, occurring between 450 °C and 600 °C.

The sample tested with 3 % iso-octane was exposed to three consecutive tests (approx. 24 hrs on stream), the sample tested with 5 % iso-octane was exposed to two consecutive tests (approx. 16 hrs on stream), and the sample tested with 7.5 % iso-octane was exposed to less than one full test (approx. 6 hrs on stream).

Given the above exposure to reaction conditions, it is clear that as the fuel percentage in the reactant stream was increased, the weight loss observed in the TGA also increased.

TGA: The Effect of Cool Down Method when Iso-octane is the Surrogate for Gasoline

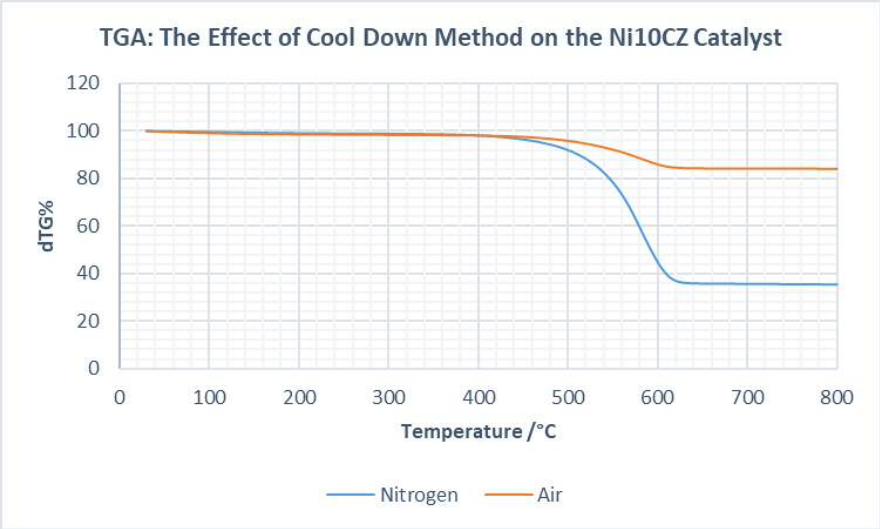

Figure 6.8: Thermogravimetric data for the nickel catalyst samples exposed to the nitrogen and air cool down methods, after the exhaust gas reforming of iso-octane

The results above in Figure 6.8 show the TGA results for the samples tested at λ = 1.5 with 3 % iso-octane, having either been exposed to the nitrogen cooling method in between tests, or the air cooling method. Both samples were exposed to three consecutive tests (approx. 24 hrs on stream).

Both samples showed a weight loss event beginning at around 450 °C and continuing until around 630 °C. However, the sample exposed to the nitrogen cool down method showed significantly greater weight loss in this region than the one exposed to the air cool down method. The nitrogen cooled sample showed a total weight loss of around 65 %, whereas the air cooled sample showed a weight loss of just over 15 %.

TGA: The Effect of Increased Steam Content in the Exhaust Gas Reforming Mixture

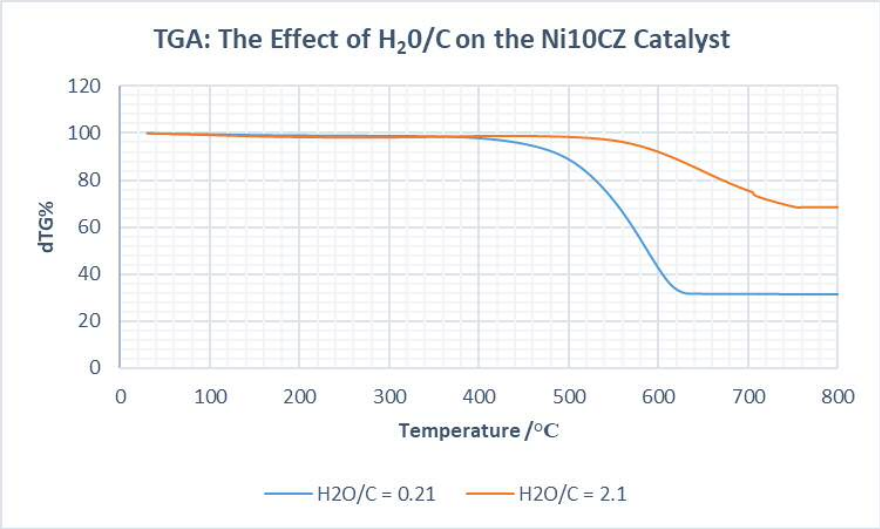

Figure 6.9: Thermogravimetric data for the nickel catalyst samples tested at different H_2O/C ratios during the exhaust gas reforming of iso-octane

The results above in Figure 6.9 show the effect of steam to carbon ratio on the nickel catalyst tested at λ = 1.5 with 5 % iso-octane. Both catalysts were exposed to two consecutive tests, or approx. 16 hrs on stream.

The sample tested at under the 'standard' λ = 1.5 conditions and H_2O/C ratio showed a weight loss event in the region of 450-600 °C, and showed a total weight loss of just under 70 %. Whereas the sample tested at the arbitrarily increased H_2O/C showed a significantly reduced weight loss of just over 30 %, occurring at between 500 °C and 750 °C.

TGA: Nickel and Rhodium Catalysts used in the Exhaust Gas Reforming of Propane and Iso-octane

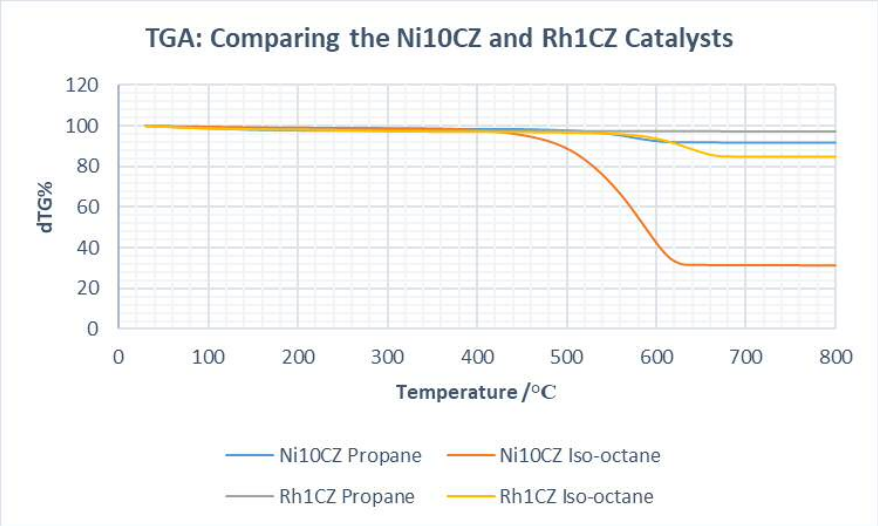

Figure 6.10: Thermogravimetric data for the nickel and rhodium catalyst samples tested in the exhaust gas reforming of propane and iso-octane at λ = 1.5

The results above in Figure 6.10 compare the TGA results for the nickel and rhodium catalysts with both iso-octane and propane fuel, tested at the λ=1.5 condition.

All samples, except the nickel catalyst tested with iso-octane (which was exposed to two consecutive tests, or approx. 16 hrs on stream), were exposed to three consecutive tests (approx. 24 hrs on stream).

The nickel sample tested with iso-octane showed the greatest weight loss event between 450-600 °C, of just under 70 %. This was followed by the rhodium catalyst tested with iso-octane, occurring in the region of 550-660 °C, though this weight loss was significantly less, at around 15 %. The nickel catalyst tested with propane showed just under a 10 % weight loss, occurring at temperatures of above 500 °C. The rhodium catalyst tested with propane showed a 3 % weight loss (which is approximately the same as that observed with the fresh rhodium catalyst).

TGA: Nickel Catalyst Samples Tested in the Static Temperature Experiments

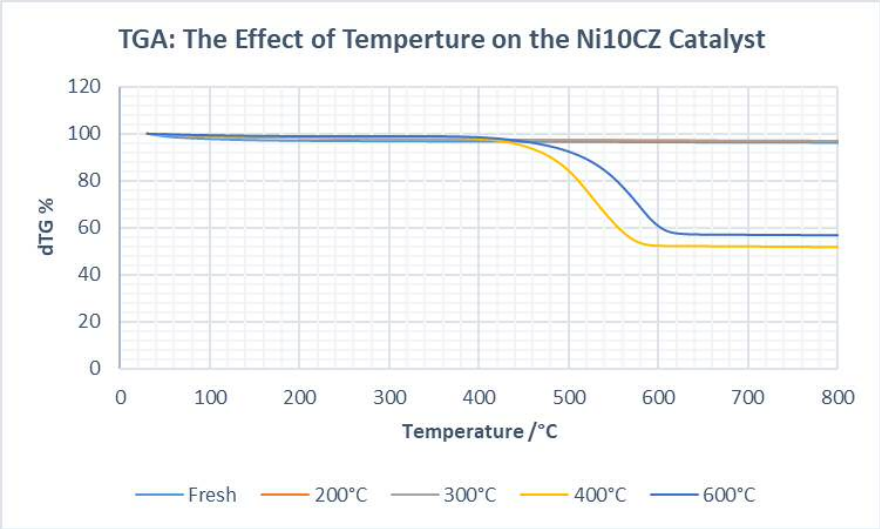

Figure 6.11: Thermogravimetric data for the nickel catalyst samples tested under exhaust gas reforming of iso-octane conditions at static temperature for two hours

The results above in Figure 6.11 show the TGA results for the nickel samples tested at static temperatures for a period of 2 hours under $\lambda = 1.5$ condition with iso-octane as the fuel. The fresh catalyst data is included for comparison.

The samples held at 200 °C and 300 °C were essentially identical to the fresh catalyst in the weight gain/loss events, ending at around a 3 % weight loss at the end of the analysis at 800 °C.

However, the samples tested at 400 °C and 600 °C showed significant weight loss events between 450 °C and 600 °C. The sample held at 400 °C showed a total weight loss of just under 50 %. The sample held at 600 °C showed just under 45 % weight loss.

Additional Observations

Weight Gain and Changes in Appearance

Sample	**Conditions**	**Fuel**	**Approx. Time on Stream /hrs**	**Weight Change /%**	**Observations**
Fresh Ni10CZ	-	-	-	-	Dark grey pellets
Ni10CZ	$\lambda = 1.5$	3 % Iso-octane	24	+130	Large black clumps
Ni10CZ	$\lambda = 1.5$ (Air Cool)	3 % Iso-octane	24	+20	Grey/black powder/pellets

Ni10CZ	λ = 1.5	7.5 % Iso-octane	6	+80	Large black clumps
Ni10CZ	λ = 1.5, H_2O/C = 2.1	5 % Iso-octane	16	+50	Some black clumps
Ni10CZ	λ = 1.5 200°C	5 % Iso-octane	2	<1	No change
Ni10CZ	λ = 1.5 300°C	5 % Iso-octane	2	<1	No Change
Ni10CZ	λ = 1.5 400°C	5 % Iso-octane	2	+75	Some black clumps
Ni10CZ	λ = 1.5 600°C	5 % Iso-octane	2	+80	Some black clumps
Fresh Rh1CZ	-	-	-	-	Brown/red pellets
Rh1CZ	λ = 1.5	5 % Propane	24	<1	Dark grey/silver pellets
Rh1CZ	λ = 1.5	5 % Iso-octane	24	+35	Black pellets, some small clumps

Table 6.1: Recorded weight gain and observations of appearance for the nickel and rhodium catalyst samples tested in this chapter under exhaust gas reforming conditions

The results above show the recorded weight changes for each sample tested, along with changes in appearance. Most of the nickel samples showed significant weight gain during testing, especially when time on stream is taken into account, for example the sample tested with 7.5 % iso-octane showed a 80 % increase in weight after only 6 hrs under reaction conditions. The nickel samples that showed minimal weight gain were those held at 200 °C and 300 °C for 2 hrs. This contrasts with the significant weight gain of 75 % and 80 % for the samples held at 400 °C and 600 °C respectively. They also showed the blackening associated with carbon deposition.

The air cooled sample showed lower weight gain, and also showed that the catalyst maintained some of its initial dark grey colour. Interestingly, the pellets in the fresh sample were also observed to have disintegrated during testing, and the sample was in a more powdered form.

The rhodium sample tested with propane changed color from brown/red to dark grey/silver during testing, and showed minimal weight change. The rhodium sample tested with iso-octane on the other hand showed 36 % weight gain, which though lower than most of the nickel samples, was much higher

than the rhodium sample tested with propane. It also showed the blackening associated with carbon deposition.

Additional tests with the Precious Metal Catalyst

In addition to the experiments already described, there were a number of experiments run with the PM catalyst and iso-octane, as detailed in the additional experimental section.

The first experiment was the same as was done with the nickel catalyst – the static temperature tests under reaction conditions. This was performed with a fresher monolith that had not been exposed to the exhaust gas reforming conditions with iso-octane as the fuel. When held at 200 °C and 300 °C for 2 hours, and then removed for inspection, the monolith showed no blackening in color. Therefore, carbon deposition was not found to occur at lower temperatures than the nickel catalyst.

The other experiments of testing the fresher monolith with iso-octane, varying the gas flow rates, and releasing the pressure in the system had no noticeable effect on catalyst performance.

Discussion

Nickel Catalyst Performance in the Exhaust Gas Reforming of Iso-octane: The Effect of Iso-octane Content

This section will discuss both the data in Figures 6.1(i)-(iv) (3 % iso-octane) and 6.2 (7.5 % iso-octane) in this chapter, along with Figures 5.11(i) through 5.11(iv) in Chapter 5 (5 % iso-octane).

The aim of these experiments was primarily to see if, by changing the quantity of fuel in the reactant stream, and hence changing the H_2O/C ratio (which is known to be an important factor controlling coking during reforming reactions [76]), whether the quantity of carbon deposited on the nickel catalyst could be significantly controlled, while maintaining performance.

As seen in the results from Figure 5.11 in Chapter 5 for the performance of the nickel catalyst in the exhaust gas reforming of 5 % iso-octane at $\lambda = 1.5$ condition, light off was initiated at around 170 °C, this was also the case when both 3 % and 7.5 % fuel was used.

As with the standard conditions the light off did not involve complete consumption of the oxygen in the reactant stream, but instead was a gradual consumption, shown below in Figure 6.12.

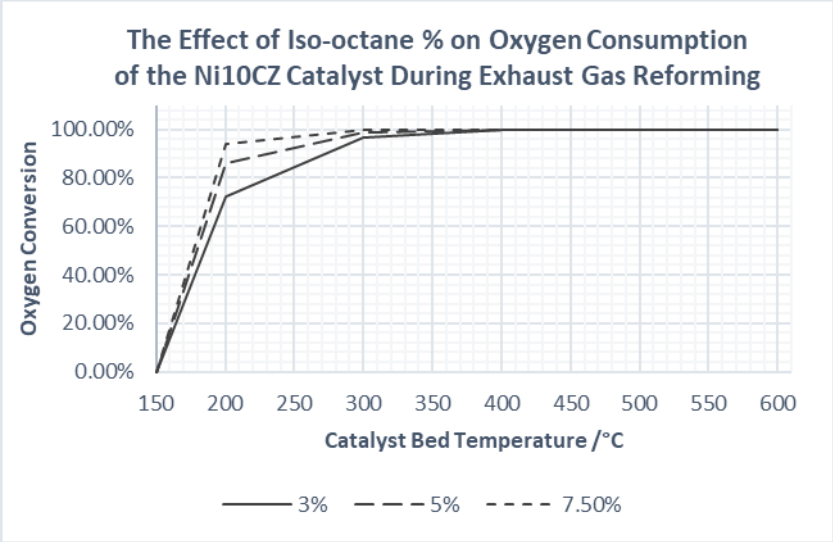

Figure 6.12: Nickel catalyst performance in the exhaust gas reforming of iso-octane at = 1.5, in terms of oxygen consumption as a function of % of iso-octane and bed temperature

Also clear from Figure 6.12 is that as the quantity of iso-octane in the reactant stream was increased, so was the amount of oxygen consumed in the initial light off stage. This should be expected, since the increased presence of fuel present would help promote oxidation reactions, therefore promoting the consumption of more oxygen.

Figures 6.13 and 6.14 below shows how hydrogen production for the fresh catalysts under each condition, in terms of hydrogen content of the product gas and hydrogen yield respectively.

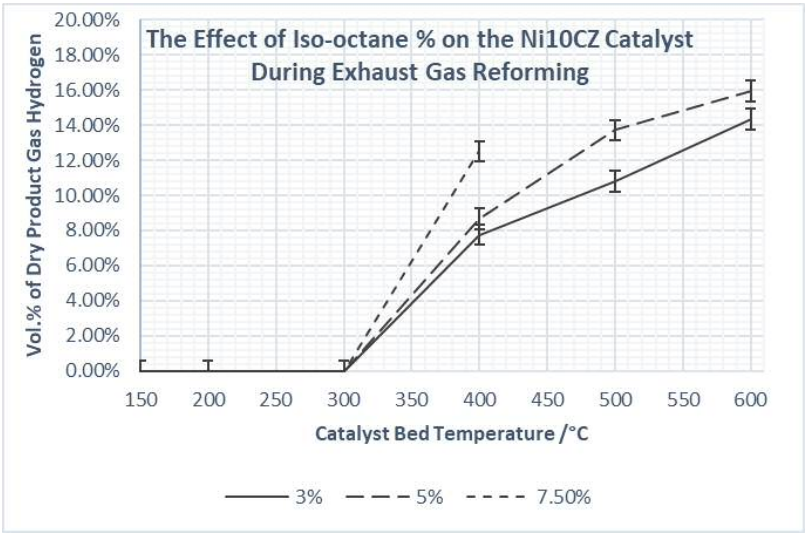

Figure 6.13: Nickel catalyst performance in the exhaust gas reforming of iso-octane at λ = 1.5, in terms of hydrogen content of the product gas as a function of iso-octane % and bed temperature

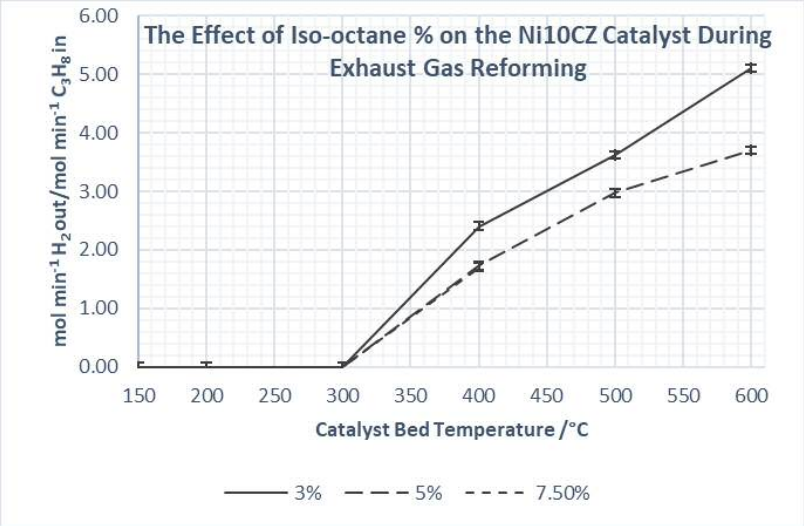

Figure 6.14: Nickel catalyst performance in the exhaust gas reforming of iso-octane at λ = 1.5, in terms of hydrogen yield as a function of iso-octane % and bed temperature

It can be seen that as the quantity of iso-octane in the feed was increased, so does the proportion of hydrogen in the product gas. However, the trend was reversed when considering hydrogen yield.

This was similar to the effect observed in previous experiemtns and the effect of the λ-value, that the highest yielding condition was not necessarily the condition that produced the most hydrogen rich product gas. Therefore, this is most likely explained by the fact, as shown in Figure 6.12, a higher proportion of fuel in the product stream promotes increased oxidation activity, such as POx. This would explain the higher hydrogen content of the product gas, and since POx is lower yielding than SR, a shift towards greater POx reactivity at the expense of SR would explain the lower hydrogen yield at higher iso-octane feed levels. Oxidation reactivity has been found to be kinetically limited in this way, and hence can be promoted by increased availability of reactants, through increased fuel and oxygen flow rates [49].

However, the results for the 3 % iso-octane condition and 5 % iso-octane condition, both in terms of oxygen consumption and hydrogen production, showed a decrease in performance from fresh to used catalyst, again particularly at low temperature. Furthermore, the 7.5 % condition was only tested for approx. 6 hrs due to pressure building up in the reactor.

Both these observations are again explained by the deposition of carbon on the catalyst/in the catalyst bed. The observations detailed in Table 6.1 and the TGA data in Figure 6.7 in this chapter support this.

All three samples (3 %, 5 % and 7.5 % iso-octane) showed significant total weight gain and significant weight loss events in the TGA in the region of 450 °C to 630 °C, again from the oxidation of carbon species deposited on the surface [123, 124]. The appearance of the samples post-testing as consisting of black clumps also points to this conclusion.

However, the quantity of iso-octane in the sample did seem to have an effect on the amount of carbon deposited. When time on stream is taken into account, as well how long it took the reactor to block, it is clear that the lower the quantity of iso-octane in the reactant feed, the lower the carbon deposition.

The explanation for this is likely down to the change in steam to carbon ratio associated with changing the fuel quantity. Steam to carbon ratio is known to have a large effect on the rate of coking [76]. Lowering the fuel percentage would increase the steam to carbon ratio, and therefore potentially depress the rate of carbon formation on the catalyst surface. The steam to carbon ratios for each condition at λ = 1.5 are shown below in Table 6.2.

% Iso-octane	H_2O/C
3	0.35
5	0.21
7.5	0.14

Table 6.2: H_2O/C raitio in the exhaust gas reforming of 3%, 5%, and 7.5% of iso-octane

However, the decrease in carbon on the catalyst from reducing the fuel quantity at the levels tested here was still not sufficient to solve the coking issue. The catalyst still more than doubled its initial weight, and still showed a 65 % weight loss event in the TGA. So coking was still a significant issue.

Hydrogen production was reasonable under the low fuel condition (if lower than with 5 % or 7.5 % iso-octane), when only 3 % iso-octane was used, therefore it seems that there may be scope for the quantity of iso-octane to be lowered further still, without critically harming the reforming performance of the catalyst and potentially lower the rate of carbon deposition further. However as already discussed, it was not possible to lower the fuel flow rate further given the limitations of the syringe pump, so the steam to carbon ratio was arbitrarily raised in order to see just how much of a reduction in carbon could be obtained. Regardless, even if the fuel rate could be further lowered, carbon deposition seems likely to remain a problem with this catalyst given that the H_2O/C ratio under the λ = 1.5 condition with propane as the fuel was only 0.55, which was not significantly higher than at the 3 % iso-octane condition. Therefore it seems likely that though there may be room to suppress carbon deposition a little further, that on this catalyst carbon deposition will remain a problem (again likely due to the heavier, branched chain nature of the fuel being more prone to carbon deposition [76]).

Nickel Catalyst Performance in the Exhaust Gas Reforming of Iso-octane: The Effect of Cool-Down Method

It was seen in Chapter 4 that the choice of cool down method had a large effect on catalyst performance. Exposing the hot catalyst to an oxidizing atmosphere for the cool down phase had the effect of oxidizing the carbon deposited on the surface during testing, which in turn seemed to result in catalyst deactivation, assigned to the sintering of active nickel species. In contrast, exposing the hot catalyst to an inert atmosphere during the cool down phase had the effect of preserving the state of the catalyst, and any deposited species, and did not deactivate the catalyst.

As discussed in the Introduction to this chapter, it was therefore hoped that, since the quantity of carbon deposited on the catalyst when iso-octane was used as the fuel was so great, that in this case the choice of an oxidizing atmosphere during cool down would assist in the removal of the carbon built up during testing, and therefore help avoid reactor blockage and catalyst deactivation. Hence a sample of the nickel catalyst was tested under the standard $\lambda = 1.5$ conditions, with 3 % iso-octane as the surrogate fuel. After testing, the hot catalyst was exposed to an air cool down.

The TGA data and observations in Figure 6.8 and Table 6.1 do indeed suggest that the air cool down method removes a significant quantity, if not all, of carbon from the catalyst surface. The sample exposed to the air cool down method showed a significant decrease in total weight gain of the sample (20 % gained as opposed to 130 %), and a much smaller weight loss event in the TGA (15 % compared to 65 %).

Interestingly, the air cooled sample was also observed to have partially disintegrated from the pelletized form that was put into the reactor. The sample was in a more powdered form, with some pellets after testing. One common pathway of catalyst deactivation associated with coking is that the catalyst pores become clogged with carbon, and in extreme cases result in the stress fracturing of the support material, as described by Argyle and Bartholomew in their review on catalyst deactivation [69]. It could therefore be that the carbon had built up in the pores during the tests, and that then the air cool down method exposed the catalyst to significant stress, during the oxidation of these carbon structures inside of the pores, that it caused the breakup of the catalyst support, to an extent that it was visible in the transition from the initial pelletized form to a powdered form after testing. It was however possible that this fracturing of the catalyst had actually occurred with the samples tested with iso-octane previously, and cooled in a nitrogen atmosphere, but this could have been masked by the fact the buildup of carbon was so great that the samples consisted of large clumps of black carbon.

The results in Figures 6.3(i) through 6.3(iv) show the performance of the nickel catalyst when tested consecutively with 3 % iso-octane and exposed to the air cool down. These can be compared to those in Figures 6.1(i) through 6.1(iv) in this chapter for the equivalent test with the nitrogen cooling method.

In both cases, light off still occurred at 170 °C, and was gradual in terms of oxygen consumption. Both samples then showed a decrease in oxygen consumption during the initial light off stage between the fresh and used catalysts, regardless of cool down method. However, the sample exposed to the nitrogen cool down showed a larger decrease in oxygen consumption. For example, the amount of amount of oxygen consumed between the fresh and used catalyst when exposed to the nitrogen cool down decreased at 200 °C from there being 2 % by volume of oxygen left in the product gas with the fresh catalyst to 5.5 % left with the used catalyst at 200 °C. The equivalent figures for the air cooled sample were 1 % and 3 %. So in terms of oxidation performance it seems carbon on the catalyst (left in place during the nitrogen cool down) deactivates the catalyst to a greater degree than the air-cool down, when isooctane was used as the fuel.

In terms of hydrogen production, both samples showed similar fresh catalyst performance, and then a slight deactivation at lower temperatures with consecutive tests. However, the sample exposed to the nitrogen cool down method seemed to fluctuate rather than displaying significant deactivation between each run. Whereas the oxygen cooled sample did deactivate a little with each consecutive step. Overall though, they were very similar in terms of performance over the three tests.

These results were different to those seen in Chapter 4 when propane was used as the surrogate fuel. In those experiments, when the catalyst cooled under a nitrogen atmosphere the performance tended to improve in terms of hydrogen production, and with no change in terms of oxidation performance (determined by oxygen consumption). It was hypothesized that the fresh catalyst, containing predominantly nickel oxide, was getting reduced under reaction conditions and maintained during the cooling phase in the inert atmosphere, and that since the Ni(0) is the active species for the reforming reactions [82, 117], this resulted in an improvement in reforming performance.

However, as discussed previously, when iso-octane was the surrogate fuel, cooling under a nitrogen atmosphere was not found to be activating in the same way. This was most likely due to the significantly greater quantity of carbon deposited with iso-octane, and resulting combination of catalyst deactivation and blockage of the reactor.

When tested with propane and cooled under an oxidizing atmosphere (simulated air, or “oxygen” cool down), both the reforming and oxidation performance of the catalyst were deactivated. At low temperature, the reforming capability was severely deactivated in particular (though this deactivation was found to be somewhat reversible). In the fourth consecutive test the catalyst was found to produce no hydrogen at 400°C. Furthermore, the light off temperature was shifted to higher temperatures. It was hypothesized that when the hot catalyst was exposed to an oxidizing atmosphere that the small amount of carbon on the catalyst after testing with propane was oxidized, resulting in a noticeable exotherm in the catalyst bed. This spike in surface temperature was then thought to oxidize the Ni(0) to Ni-oxides, and then begin to sinter both species and this loss of metallic nickel, and loss of active surface area caused the observed deactivation.

However, the effect of cooling in a simulated air atmosphere when iso-octane was used was not found to be deactivating in the same way. Even though the catalyst tested with iso-octane and the air cooling method in this chapter was only exposed to three tests rather than four, it did not completely deactivate, and its performance was marginally lower than that of the fresh catalyst. In terms of oxidation capacity of the catalyst, both showed decreases in oxygen consumption, but only when propane was used as the fuel did the air cooling method show a shift to higher temperatures of the light off temperature.

It is proposed that this difference was most likely due to the vastly different quantities of carbon deposited on the catalyst surface during testing with propane, compared to when testing with iso-octane. As mentioned, the deactivation mechanism related to the cool down method proposed in Chapter 4, involved the oxidation of carbon on the hot catalyst surface in the oxidizing atmosphere, resulting in a

temperature spike causing the oxidation of metallic nickel, followed by sintering. It is proposed that, since a much greater quantity of carbon was deposited on the catalyst during testing with iso-octane, that when exposed to the oxidizing atmosphere only/predominantly the oxidation of that carbon occurs, and the process was not able to get as far as effecting the catalyst surface to the same extent. Whereas when propane was the fuel, since there was much less carbon on the catalyst surface, that the process was able to oxidize the carbon, and the resulting exotherm had the capacity to also then effect the catalyst surface.

Nickel Catalyst Performance in the Exhaust Gas Reforming of Iso-octane: The Effect of the H_2O/C

Since changing the percentage of iso-octane in the reactant stream (and hence changing H_2O/C) did not have a large an effect on the deposition of carbon, and that there was no room to lower the fuel flow rate further, the steam to carbon ratio was arbitrarily changed by greatly increasing the steam content of the reactant stream. The steam to carbon ratio was increased by ten times, from 0.21 at the 'standard' λ = 1.5 condition, to 2.1. The steam content of the reactant stream at each λ-value is determined by the predicted water content of the exhaust gas under those conditions, so increasing the water content by this amount represents an unrealistic quantity of water in the exhaust gas of a real vehicle. The steam to carbon ratio would be equivalent to reducing the percentage of iso-octane in the feed from 5 % to 0.05 %, which would be possible in a real application. However, this would be a significant reduction in the availability of fuel for reforming, and as already discussed is unclear how this could affect catalyst performance at this stage.

The results from these two experiments (H_2O/C = 0.21 and 2.1) are shown in Figures 5.11(i) through 5.11(iv) in Chapter 5, and Figures 6.4(i) through 6.4(iv) in this chapter. Both samples were tested over two consecutive tests, or approximately 16hrs on stream. The sample tested under this higher steam to carbon ratio showed depressed oxidation activity during light off, as shown in Figure 6.15 below by the comparison in oxygen consumption.

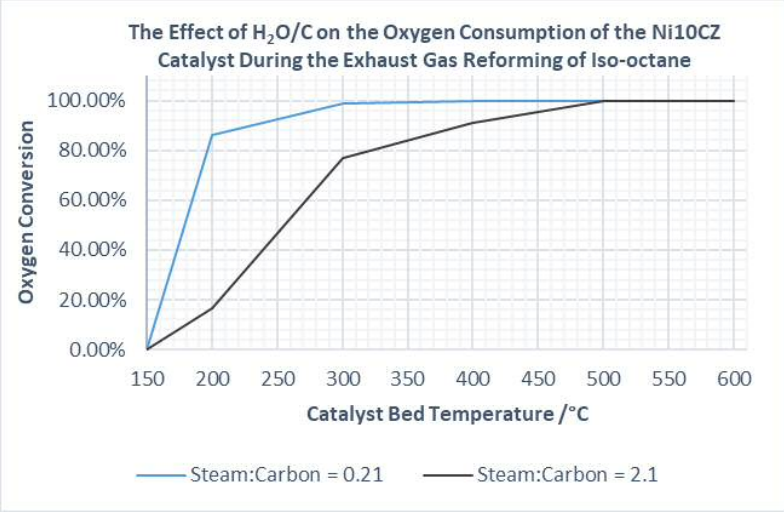

Figure 6.15: Nickel catalyst performance in the exhaust gas reforming of iso-octane, in terms of oxygen consumption as a function of H_2O/C of the feed and bed temperature

This was to be expected since the presence of steam is known to raise ignition temperatures [133].

In terms of reforming the fresh catalyst did not produce any hydrogen until 500 °C, however the used catalyst did produce hydrogen at 400 °C. This suggests that, as with the nickel catalyst tested with propane and cooled under nitrogen, that the catalyst had become activated during the testing cycle. This is also shown by the increased oxygen consumption in the used catalyst.

Oxygen consumption for the fresh catalyst was not complete until 500 °C, and reforming did not begin until 500 °C. However, the used catalyst showed complete oxygen consumption at 400 °C. By itself, this result suggests that potentially the carbon deposition that caused deactivation of the iso-octane samples tested previously had been significantly suppressed by the greatly increased steam to carbon ratio.

The used catalyst produced a similar quantity of hydrogen at 400 °C as under the standard steam to carbon ratio. However, at the higher temperature of 500 °C and 600 °C, the higher water content vastly increased the proportion of hydrogen present in the product gas, shown below in Figure 6.16.

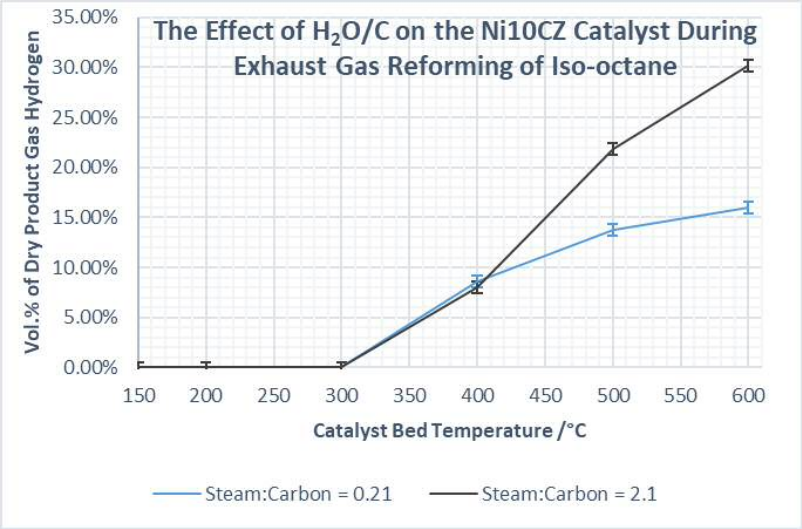

Figure 6.16: Nickel catalyst performance in the exhaust gas reforming of iso-octane, in terms of hydrogen content of the product gas as a function of H_2O/C of the feed and catalyst bed temperature

This is also shown in terms of hydrogen yield in Figure 6.17 below.

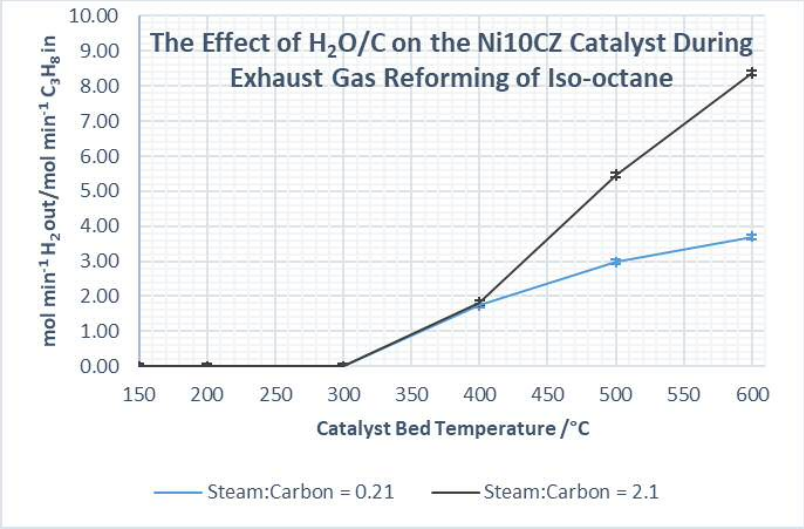

Figure 6.17: Nickel catalyst performance in the exhaust gas reforming of iso-octane, in terms of hydrogen yield as a function of H_2O/C of the feed and catalyst bed temperature

In fact, the higher water content promoted significant hydrogen production through the reforming reactions, to the point where the product gas consisted of around 30 % hydrogen at 600 °C. This was again expected since the increased presence of water would be expected to boost the potential for steam reforming reactions, and hence increase hydrogen production [24, 42].

Furthermore, this increased quantity of hydrogen was produced without a corresponding increase in the quantity of carbon monoxide produced. Instead, the carbon monoxide content of the product gas decreased, carbon dioxide increased. This suggests that the higher quantity of water promoted hydrogen production via increased water gas shift, or SR2, reactivity.

This result also suggests that, under the standard conditions tested previously, there could have been a significant quantity of iso-octane remaining unreacted, which will be discussed in the final chapter. As discussed in the Experimental chapter, analysis of the liquid waste products of the reaction was not carried out, so had not been determined previously.

Though this quantity of hydrogen would certainly be beneficial in exhaust gas reforming to be fed back into the engine, as already mentioned, the quantity of water used in this test was unrealistic for the composition of exhaust gas.

Given this, the performance of the catalyst was of less interest than studying the effect of the increased steam to carbon ratio on carbon deposition, and hence on catalyst stability over consecutive tests. As already mentioned, the used catalyst showed improved oxygen consumption and hydrogen production over the fresh catalyst. Though only tested for two consecutive tests, this was unlike the standard condition, where the used catalyst showed decreased oxygen consumption during light off, and decreased hydrogen production. Therefore, this does indeed suggest improved catalyst stability.

Furthermore, the data in Table 6.1 and TGA data in Figure 6.9 show decreased carbon deposition for the sample tested under this higher steam/carbon ratio. Under standard $\lambda = 1.5$ conditions with iso-octane as the surrogate fuel, the catalyst almost tripled its initial weight (see Chapter 5, Table 5.1). Under the

conditions tested here the catalyst increased its weight by roughly half, from its initial weight. This is supported further by the TGA data, where the sample tested at the standard steam to carbon ratio showed a weight loss event of just under 70 %, whereas the sample at the higher steam to carbon ratio showed a weight loss event of just over 30 %.

The temperature range of the weight loss events in the TGA potentially suggest a difference in the type of carbon deposited between the samples. The sample tested under $H_2O/C = 2.1$ showed a higher temperature onset of weight loss than the sample tested under the standard steam/carbon ratio (~550 °C compared to 400 °C). As discussed previously, the higher the temperature of carbon oxidation could be representative of more graphitic, rather than amorphous carbon species [123, 124]. However, it was later noticed that the TGA program for the $H_20/C = 2.1$ tested sample had been modified to use a slightly higher ramp rate (10 °C/min instead of 5 °C/min in all other tests). Since the weight loss levelled out in the trace for this sample, this error does therefore not affect the main conclusion regarding the total weight loss for this sample relative to the $H_2O/C = 0.21$ tested sample, however it does mean that the above conclusions regarding the differing nature of carbon species deposited between the two tests would need to be supported by other data before being confirmed.

Therefore, these results show that the higher steam to carbon ratio did indeed significantly depress carbon formation, and therefore stabilized the catalyst performance over consecutive tests. This was as hoped, since the higher steam to carbon ratios are known to suppress coke formation [76]. However, even though there were improvements, there was still a significant amount of carbon deposited in the relatively short testing period. Furthermore, as already mentioned, the water content of the feed in this experiment was unrealistic for a real system, and the equivalent decrease in fuel content of the feed needed to match this steam to carbon ratio could have a negative effect on catalyst performance. Therefore, it was clear that the carbon deposition remained an issue at this stage.

Nickel Catalyst Performance in the Exhaust Gas Reforming of Iso-octane: The Effect of Temperature on the Rate of Carbon Deposition

As described previously, some samples of the nickel catalyst were held at static temperatures, under reaction conditions of $\lambda = 1.5$ with 5 % iso-octane, for a period of two hours. This was done to test for the onset of carbon deposition.

The results in Table 6.1 and Figure 6.11 show that the samples held at 200 °C and 300 °C had no/very little carbon on them. Their total weight gain was <1 %, which given the error in the weighing balance, is negligible. The TGA data also shows no significant weight loss events, with curves almost identical to the fresh catalyst. The samples tested at 400 °C and 600 °C on the other hand showed both total weight gain, and weight loss events in the TGA.

The sample tested at 400 °C showed a total weight gain of 75 %, and a weight loss event in the TGA occurring in the region of 450-600 °C with a loss of 50 %. The sample tested at 600 °C showed a total

weight gain of 80 %, and a weight loss event in the TGA occurring in the region of 450-600 °C with a loss of 45 %.

This shows that the carbon deposition does not occur significantly until after 300 °C. As seen from the test data, this means the carbon deposition does not occur during the light off phase, but rather once the reforming reactions and hydrogen production begins, likely since the potential for coking is inherent in the process of steam reforming of hydrocarbons [76]. TGA data suggests the coking was more rapid at 400 °C, but the total weight gain result suggests that it is more rapid at 600 °C. However, the TGA data can be misleading due to the inconsistency of sample composition. Though the data displayed throughout this project is the average of three TGA runs, it is still possible that a disproportionate quantity of the carbon lumps can make it into a TGA sample therefore distorting the results. Furthermore, though the sample tested at 600 °C was also held for 2 hrs, there was the additional time under reaction conditions associated with getting the furnace up to the higher temperature. Therefore, given the above and the closeness of the TGA data and total weight gain data its seems reasonable to suggest that there is not a great difference in the rate of carbon deposition at 400 °C and 600 °C.

Given the large quantity of carbon deposited at 400 °C and 600 °C in only 2 hours of testing, which accounts for the majority of the carbon deposited in the longer consecutive runs used the previous performance tests. So it is clear that the carbon deposition is severe early on in the testing cycle, while additional testing only slightly adds to the deposited carbon. This could suggest that initial deposition was primarily located on the catalyst surface, whereas later deposition was more gradual and located on top of previous deposits.

Rhodium Catalyst Performance in the Exhaust Gas Reforming of Propane

A 1 % rhodium of ceria zirconia catalyst was synthesized in order to determine whether the lack of performance displaced by the PM with iso-octane was due to its precious metal composition, as well as whether the rhodium catalyst was more resistant to coking than the nickel catalyst. The catalyst was first tested with propane. The results in Figures 6.5(i) through 6.5(v) show the performance of the catalyst over three consecutive tests at the λ=1.5 condition.

The results show that the light off temperature for the rhodium catalyst was around 200 °C. This can be seen from the oxygen consumption data, and has been discussed previously. It was possible to measure the oxygen consumption at 200 °C, pre-light off, but if the furnace heating overshot by a couple of degrees then this would initiate light off. A light off temperature of 200 °C is slightly higher than the PM (180 °C), but still lower than the nickel catalyst (280 °C) with propane as the fuel. This was to be expected since the PM catalyst is believed to also contain a second precious metal such as platinum which, whereas discussed previously, would lower the light off temperature due to improved oxidation activity, and then rhodium is more active towards oxidation than nickel [43, 130-132]. It was also observed that in the second test, where heating the furnace to 200 °C was overshot, and the light off point was reached, that the oxygen consumption was not quite complete in the initial light off, with around 0.3 %

oxygen remaining in the product gas. This could be because, as mentioned, the measurements were being taken right on the cusp of light off, and therefore it is possible a couple of degrees more heating from the furnace would have seen complete oxygen consumption. The data for this test is compared to the oxygen consumption data for the PM and nickel catalyst under the same conditions in Figure 6.18 below to show the above differences.

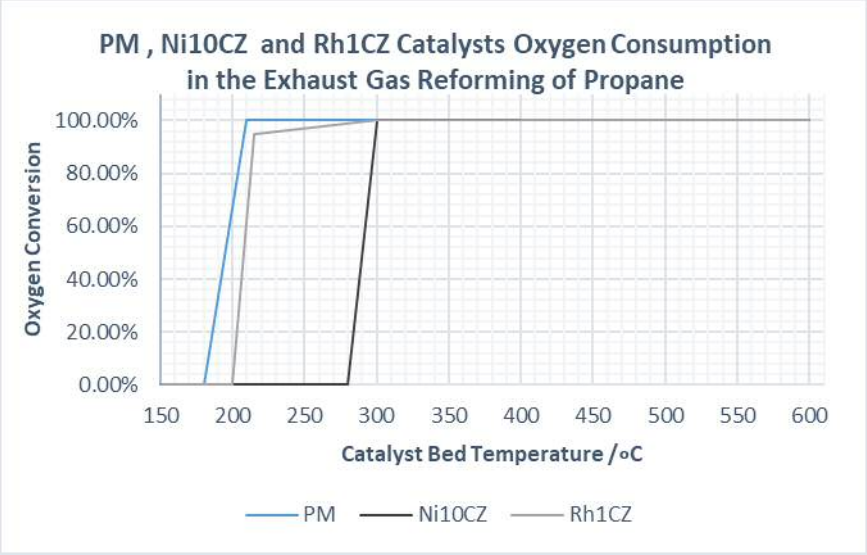

Figure 6.18: PM, nickel and rhodium catalyst performance in the exhaust gas reforming of propane at λ = 1.5, in terms of oxygen consumption as a function of bed temperature

Hydrogen production, carbon monoxide production, and propane consumption, all then increased smoothly throughout the temperature range. Furthermore, the rhodium catalyst showed very consistent performance between tests, showing no signs of activation under testing conditions, or deactivation as has been seen previously with the nickel catalyst under various conditions. Figure 6.19 below shows the average hydrogen content of the product gas for the rhodium catalyst compared to the PM and the nickel catalyst when tested with propane.

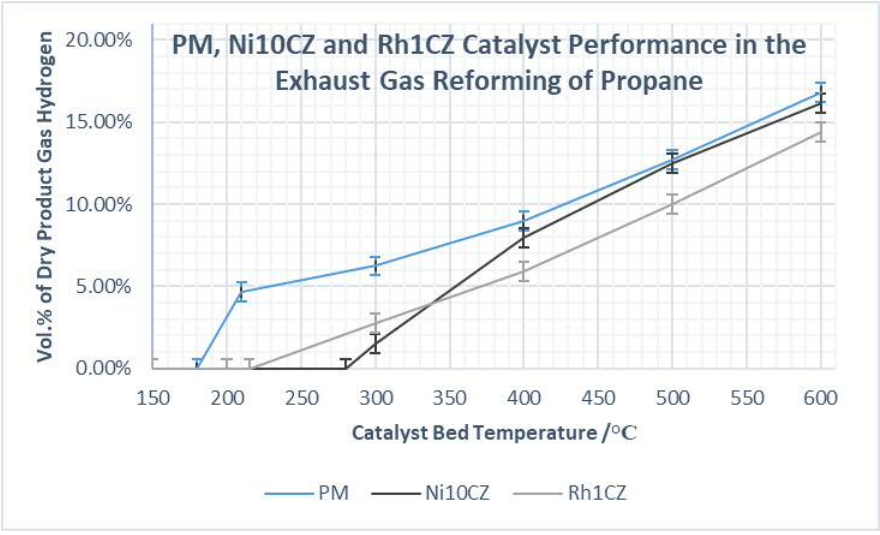

Figure 6.19: PM, nickel and rhodium catalyst performance in the exhaust gas reforming of propane at λ = 1.5, in terms of hydrogen content of the product gas as a function of bed temperature

The results are above are directly supported by the average hydrogen yields for each of the catalysts, shown below in Figure 6.20.

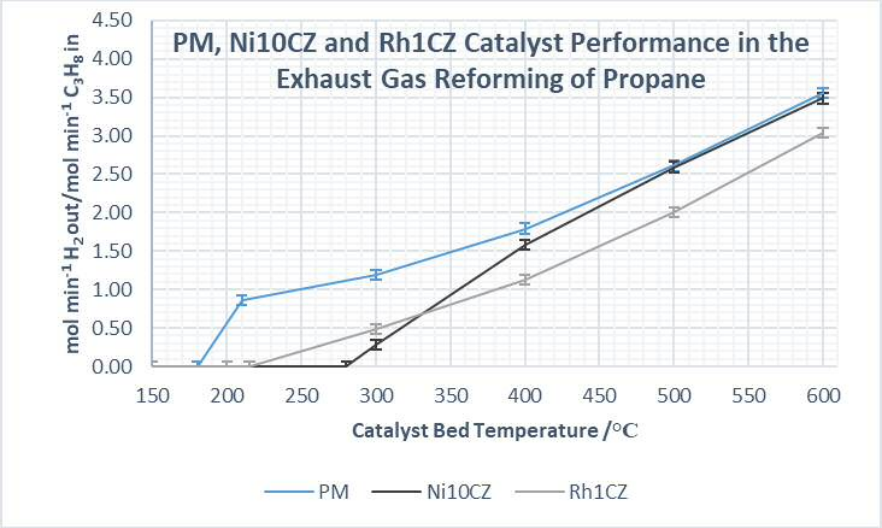

Figure 6.20: PM, nickel and rhodium catalyst performance in the exhaust gas reforming of propane at λ = 1.5, in terms of hydrogen yield as a function of bed temperature

It is clear that the PM was the superior catalyst with propane at the λ = 1.5 condition. The PM produced hydrogen at 200 °C, whereas the rhodium-only catalyst did not. This is likely due to the fact that the oxidation processes were not yet complete, as shown by the oxygen consumption data, with the rhodium catalyst. However, at 300 °C when the rhodium catalyst was first observed to produce hydrogen, the PM still produced more hydrogen in terms of yield and proportion of the product gas by volume.

However, the rhodium catalyst did outperform the nickel catalyst at this temperature. At higher temperatures however, the nickel catalyst and the PM were evenly matched, while the rhodium catalyst produced slightly less hydrogen. The gap between the PM and the rhodium catalyst is difficult to explain given that the true nature of the PM is unknown. However, assuming it contains rhodium then the difference could be explained by both the quantity of rhodium present and/or the likely bimetallic nature of the PM boosting its performance. The difference of around 1 % of hydrogen by volume of the product gas between the nickel and rhodium catalyst at low temperature is likely explained by rhodium's expected higher activity. However, the reversed performance at higher temperature could be explained by the large difference in metal loadings, 10% for the nickel catalyst and 1% for the rhodium catalyst.

Regardless, the rhodium-only catalyst performance with propane was somewhat comparable to the other two catalysts, therefore it was a reasonable sample to test with iso-octane to help explain the lack of PM performance with iso-octane, as well as observe any differences in carbon deposition to the nickel catalyst.

In terms of carbon deposition in this test with propane, Table 6.1 and the TGA data in Figure 6.10 show that the sample gained a negligible amount of total weight, and that there was no significant weight loss event in the TGA, and the data was almost identical to the fresh catalyst.

Therefore the results show that carbon deposition was negligible under these conditions, and less than that observed with the nickel catalyst under similar conditions (see Table 5.1 and Figure 6.10). This was also to be expected since, as discussed elsewhere in this report, rhodium is often found to be more resistant to coking than nickel under various reforming conditions [44, 62, 76].

Rhodium Catalyst Performance in the Exhaust Gas Reforming of Iso-octane

The rhodium-only catalyst was then tested with 5 % iso-octane as the fuel, at the $\lambda = 1.5$ condition, both to compare its performance to both the nickel and the PM catalyst (especially the latter), and to investigate its resistance to carbon deposition, which had been found to be a significant issue with the nickel catalyst in particular.

The rhodium catalyst was tested for three consecutive tests (approx. 24 hrs on stream), without any pressure build up, suggesting that a lower amount of carbon compared to the nickel catalyst, which under the same conditions was tested for 16 hrs on stream before the pressure begin to build up.

This lower amount of carbon on the rhodium catalyst is supported by the data in Figure 6.10 and Table 6.1. It can be seen that the rhodium sample after 24 hrs on stream showed a total weight gain of 36 % from its initial weight, whereas the nickel catalyst had increased its weight under the same conditions by 190 %, after only 16 hrs on stream. In addition, the TGA data showed a weight loss of around 15 % in the region of 550-660 °C for the rhodium catalyst, and around 70 % for the nickel catalyst in the region of 450-630 °C. In fact, the TGA data for the rhodium samples was closer to the nickel sample tested with propane as the fuel than it was to the nickel sample and iso-octane. So this again shows, as expected that the rhodium catalyst was more resistant to coking than nickel.

In terms of performance (see Figures 6.6(i) through 6.6(iv)), light off occurred again at around 170°C, as with the nickel and PM catalysts. The consumption of oxygen was mostly complete during the light off process, similar to the nickel catalyst with iso-octane, whereas the PM catalyst showed complete oxygen consumption during light off (again likely due to the presence of platinum or similar active oxidation metal).

There was negligible change in oxygen consumption between the fresh and used catalysts, unlike with the nickel catalyst, which displayed a large decrease in oxygen consumption between fresh and used catalyst. Given the above discussion, it is likely this was down to the higher resistance of the rhodium catalyst to coking.

Regarding hydrogen production, Figure 6.21 and Figure 6.22 below compares the data for the rhodium, nickel and PM catalysts under these conditions, in terms of the proportion of the product gas constituting hydrogen and hydrogen yield respectively.

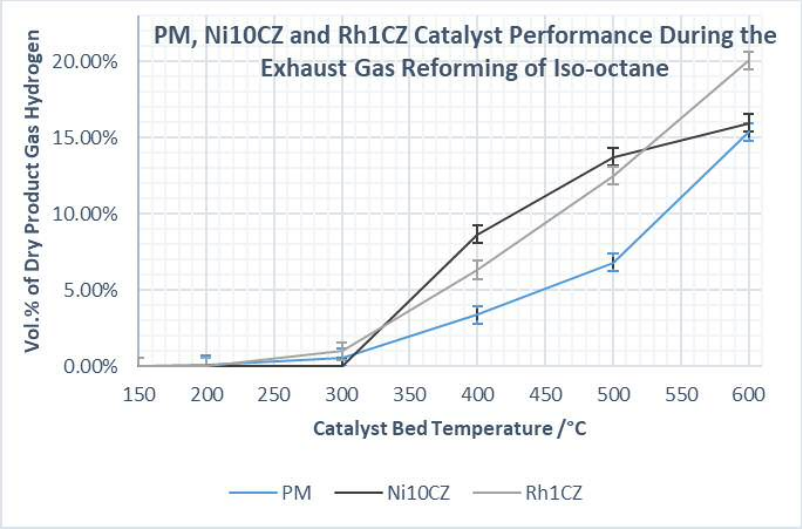

Figure 6.21: PM, nickel and rhodium catalyst performance in the exhaust gas reforming of iso-octane at λ = 1.5, in terms of hydrogen content of the product gas as a function of bed temperature

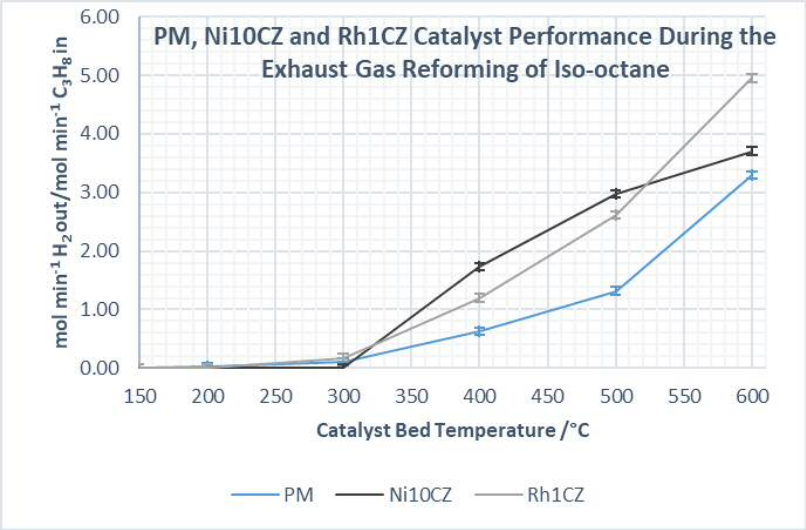

Figure 6.22: PM, nickel and rhodium catalyst performance in the exhaust gas reforming of iso-octane at λ = 1.5, in terms of hydrogen yield as a function of bed temperature

It can be seen that the rhodium catalyst performance was very comparable to that of the nickel catalyst, and was superior at 600 °C. It is also clear that the rhodium catalyst, like the nickel catalyst, outperformed the PM catalyst when iso-octane was used as the surrogate fuel, which again was the reverse of when propane was the model fuel.

In terms of progression from fresh to used catalyst, there was a slight decrease in performance in terms of hydrogen production, at 400 °C and 500 °C. This could suggest that the carbon deposition, though lower than the nickel catalyst, still had an effect on the reforming performance of the catalyst. The drop in hydrogen production was similar to that of the nickel catalyst, but again the nickel catalyst was only tested for 16 hrs, compared to 24 hrs for the rhodium catalyst.

So the results suggest that though carbon deposition was significantly lower for the rhodium catalyst than the nickel catalyst, it was still substantial enough under these conditions to cause some drop in

catalyst performance. They also suggest the potential presence of precious metals on the PM catalyst do not explain its lack of performance with iso-octane, since the rhodium catalyst outperformed both it and the nickel catalyst with iso-octane.

Rhodium Catalyst Performance in the Exhaust Gas Reforming: The Effect of Fuel Choice

In terms of the difference between fuels for the rhodium catalyst, the results in Table 6.1 and Figure 6.10 show that carbon deposition was negligible when propane was used as the fuel, where as it was an issue when iso-octane was used (<1 % total weight gain and 3 % weight loss in the TGA for the propane tested sample, and 35 % total weight gain and less than 20 % weight loss event in the TGA for the iso-octane tested sample).

In terms of performance (see Figures 6.5(i) through 6.5(v) and 6.6(i) through 6.6(iv)) light off and oxygen consumption, the light off was approximately 10 °C lower with iso-octane than with propane (similar to that seen with the PM), and most of the oxygen was consumed in the initial light off. Consistent oxygen consumption for both fuels was shown between fresh and used catalysts.

Regarding hydrogen production, Figure 6.23 and Figure 6.24 below compares the performance for the two fuels, in terms of hydrogen content of the product gas and hydrogen yield respectively.

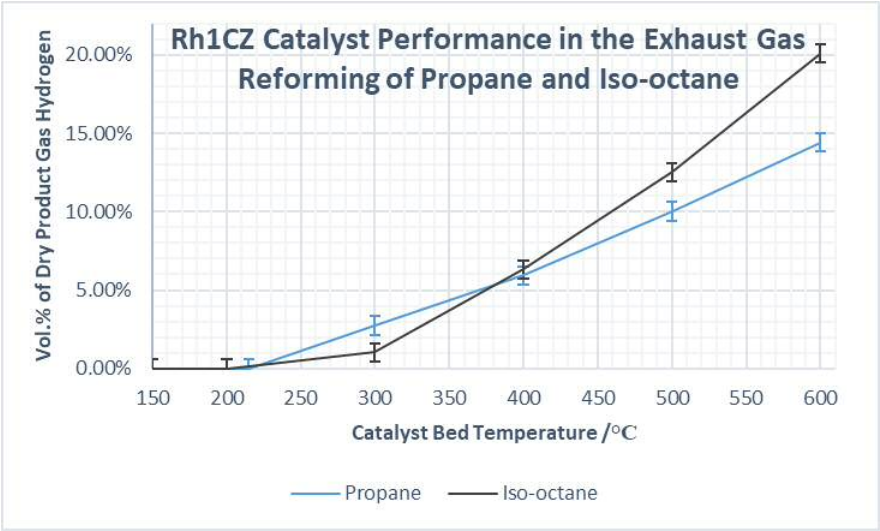

Figure 6.23: Rhodium catalyst performance in the exhaust gas reforming of propane and iso-octane, in terms of hydrogen content of the product gas as a function of bed temperature

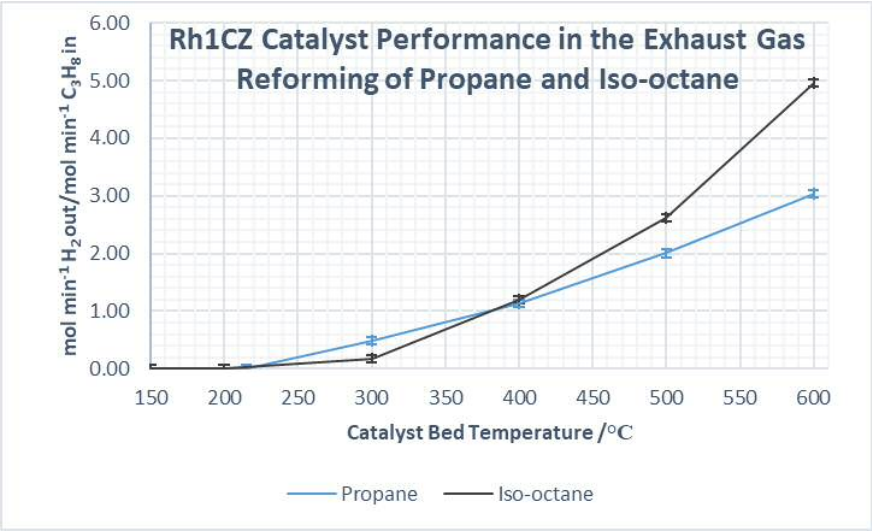

Figure 6.24: Rhodium catalyst performance in the exhaust gas refroming of propane and iso-octane, in terms of hydrogen yield as a function of bed temperature

It can be seen that more hydrogen was produced with propane at 300°C, but then more was produced with iso-octane at 500 °C and 600 °C. Hence, overall the performance was comparable with either fuel. This was similar to the nickel catalyst, which showed comparable performance between fuels, whereas the PM showed a lack of performance with iso-octane relative to propane.

In terms of changes between fresh and used catalyst in hydrogen production, the propane tested sample showed very consistent performance, and as already mentioned there was a slight drop in hydrogen production between fresh and used catalyst with the is-octane tested sample, most likely explained by the aforementioned difference in carbon deposition between the two fuels.

Precious Metal Catalyst Performance in the Exhaust Gas Reforming of Iso-octane: Additional Experiments

As discussed previously, the PM catalyst showed an unexplained drop in performance when iso-octane was used as the surrogate fuel. This was especially unexpected because the same effect was not seen with the supposedly less active nickel catalyst. Several possible explanations for this were proposed, and tests carried out to try and establish a cause.

First it was hypothesized that there could be a different mechanism involved in the exhaust gas reforming process between precious metals and base metals.

In order to test this some static temperature tests were carried out on the PM catalyst, with the aim of establishing when carbon deposition occurred. If the deposition occurred at different temperatures between the nickel and PM catalysts, this could be evidence of differing reaction pathways.

However, the tests where the PM was held at 200 °C for two hours, and 300 °C for two hours showed no blackening of the monolith, suggesting no/negligible coking had occurred. This was also the case for the nickel catalyst. Therefore, carbon deposition, for both catalysts, happens simultaneously with the onset of reforming, and therefore is significant at 400 °C or higher.

The above does not conclusively disprove this hypothesis, however in combination with the performance of the prepared 1 % Rh on ceria zirconia catalyst, does suggest that, as would be expected given the lack of evidence to the contrary in the literature, that the reaction mechanisms for precious and base metals for reforming are largely the same.

Since the true nature of the PM is, as previously mentioned, unknown, it is possible that the PM does not contain rhodium, and in which case its lack of performance with iso-octane could be explained by whatever the active precious metals might be. This will be discussed in the final chapter.

It was also suggested that the explanation for the lack of hydrogen was down to experimental or physical reasons, rather than the chemical nature of the catalyst.

Therefore, a further range of tests were carried out. First it was observed that since the PM was tested at a higher total gas flow rate (to match GHSV with the nickel catalyst) there was a higher base pressure in the reactor system, and that this pressure at times could hinder fuel flow. Therefore pressure was eased in the system by opening up a by-pass valve on the GC. The GC was then recalibrated so as to take into account the change, and the PM tested again under conditions of $\lambda = 1.5$ with 5 % iso-octane. Though this did fix the restriction to fuel flow, there was no significant improvement in reforming performance from these changes.

Second, it was hypothesized that the higher total gas flow rate could be effecting the PM either by causing disruptions to the fuel flow after the fuel has exited the nozzle (through turbulence or some similar effect), or that the GHSV associated with the high flow rate was too high, and therefore not permitting the reactants enough residency time on the catalyst surface to carry out the reforming reactions. The possibility of both was therefore simply tested by reducing the total gas flow rate to several different total gas flow rates, previously described. This too had no observable effect on reforming performance.

The final test involved using a slightly fresher PM monolith, in order to see if the age of the catalyst could explain the fall in performance when testing with iso-octane. This second monolith also showed poor performance with iso-octane. It should be noted that this monolith had also been used extensively, if less than the original monolith. So this does not necessarily rule out aging as the cause of the poor performance, but suggests it is not the only reason

Therefore, at this stage it was still unclear as to the root cause of the lack of performance with the PM catalyst when tested with iso-octane under exhaust gas reforming conditions.

Conclusions

The key results from this chapter are summarized below:

- Increasing the quantity of iso-octane in the synthetic exhaust gas mixture had the effect of boosting activity (oxidation and reforming), but also of increasing carbon deposition, most likely through the resulting decrease in H_2O/C ratio.
- Greatly increasing the steam content of the synthetic exhaust gas mixture by a factor of ten depressed coking, but did not eradicate it. It also had the effect of greatly enhancing hydrogen production at higher temperature.
- Exposing the hot catalyst to an oxidizing atmosphere, post-testing with iso-octane as the surrogate fuel, again had the effect of removing carbon from the catalyst surface.
    - Though this had negligible effect on catalyst stability, relative to cooling in an inert atmosphere, it avoided pressure build ups in system from the buildup of carbon.
    - The use of an oxidizing atmosphere during cool down was not found to be totally deactivating when iso-octane was the surrogate fuel, in contrast to when propane was used.
    - This was assigned to the vastly greater quantity of carbon deposited during testing with iso-octane.
- Carbon formation was found, as expected, to be simultaneous with the onset of reforming reactions for iso-octane, for both the PM and nickel catalysts (at temperatures above 300°C).
- The 1% Rh on ceria zirconia catalyst prepared showed consistent performance between fuels.
- The rhodium catalyst showed greater resistance to carbon deposition than the nickel catalyst, with either fuel.
- The rhodium catalyst showed lower light off temperature with propane as the surrogate fuel compared to the nickel catalyst, but higher than the PM (in the latter case, likely due to absence of a second precious metal such as platinum).
- The rhodium catalyst did not display lower performance when iso-octane was the surrogate fuel compared to propane that was seen with the PM, suggesting that the (predicted) presence of rhodium in the PM is not responsible for the PM low performance with iso-octane.
- Carbon deposition during exhaust gas reforming of iso-octane still remained an issue for the powdered catalysts, particularly the nickel catalyst.
- The cause of the lack of performance of the PM catalyst in the exhaust gas reforming of iso-octane was still unclear:
    - It did not seem to be explained by simple experimental causes, the potential presence of rhodium, differing reaction pathways or the age of the monolith.

Unfortunately, due to time constraints, more work on these issues was not possible.

The key points from this work as a whole, as well as suggested further work focusing on these key issues will now be presented in the final chapter.

Chapter 7 - Discussion, Further Work & Conclusions

Introduction

This chapter will aim to bring together the key results presented in the previous chapters, and assess them relative to the aims set out at the beginning of this work and their meaning for the potential application of exhaust gas reforming. Suggestions of further work to build on the findings presented here will also be made.

Discussion

By benchmarking against precious metal catalysts, the aim of this work was to assess the potential of base metal catalysts in the application of exhaust gas reforming, which was done by using gaseous (propane) and liquid (iso-octane) surrogate fuels for gasoline.

The simple base metal catalyst used in this work, specifically 10 % Ni/CeO_2-ZrO_2, showed similar performance when propane was used as a surrogate for gasoline as when iso-octane was used. This is shown in Figure 7.1 below, which shows the average hydrogen content of the product gas for the nickel catalyst across the standard exhaust gas reforming conditions (λ = 1, 1.5 and 2.12) tested in this work, for both propane and iso-octane.

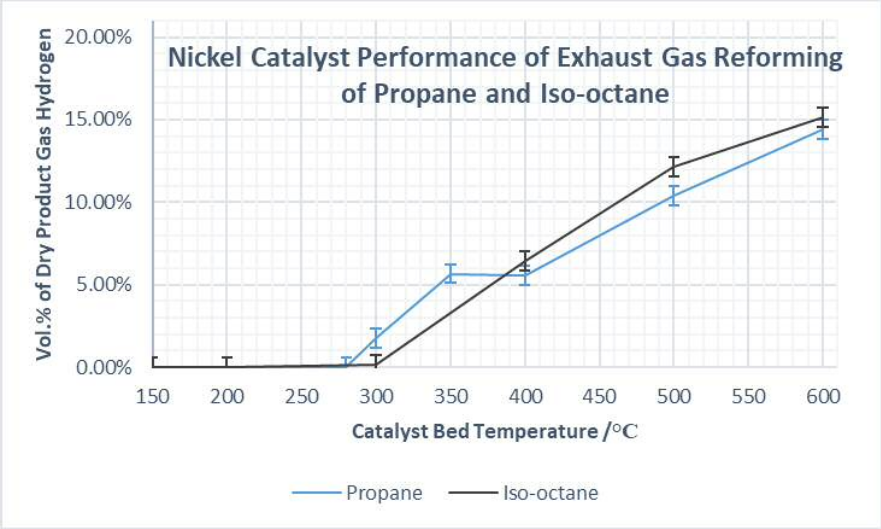

Figure 7.1: Average exhaust gas reforming performance of the 10% Ni/CeO_2-ZrO_2 catalyst with both propane and iso-octane, in terms of hydrogen content of the product gas as a function of catalyst bed temperature

Not only was the performance, in terms of hydrogen content of the product gas, comparable across fuels, but the level of hydrogen produced by the nickel catalyst was indeed in sufficient quantity at typical exhaust gas temperatures (5-20 % by volume of the reformate product gas) to be of benefit if fed back into the engine intake of a real vehicle [41, 43].

In terms of hydrogen yield per mole of fuel in the reactant feed, the nickel catalysts performance was superior to that of propane, as shown below in Figure 7.2. This, as discussed in Chapter 5 is most likely due to the lower activation energy of the heavier hydrocarbon towards the higher yielding steam reforming reactions.

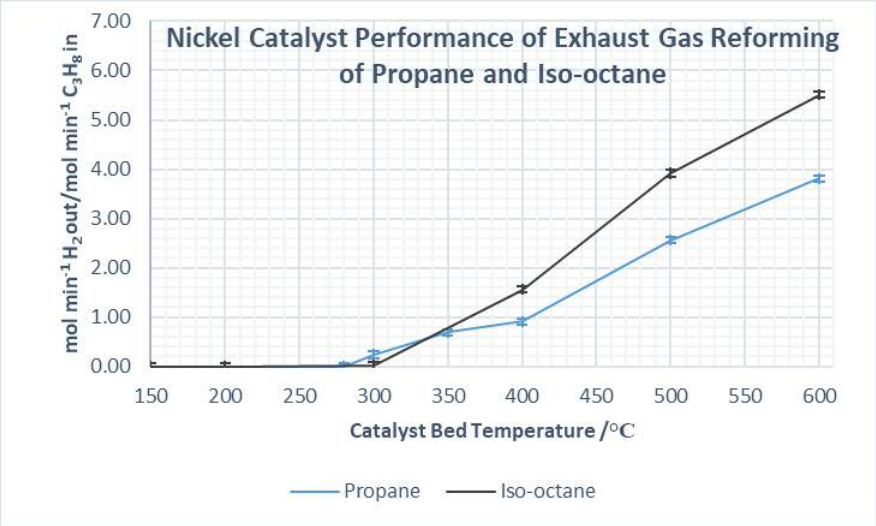

Figure 7.2: Average exhaust gas reforming performance of the 10% Ni/CeO_2-ZrO_2 catalyst with both propane and iso-octane, in terms of hydrogen yield as a function of catalyst bed temperature

It was also found that an exhaust gas containing reasonable quantities of both oxygen and steam was required to achieve the best results. The oxygen helped promote exothermic POx, which while also producing hydrogen, encouraged more endothermic reforming by raising the catalyst bed temperature. However, as discussed previously, an exhaust gas reforming unit is best used as a thermochemical recuperation device, and therefore the hydrogen needs to primarily be produced from endothermic steam reforming reactions, which will help recover waste heat in the exhaust [35].

In this work, the $\lambda = 1$ condition typically showed the highest hydrogen yield per mole of fuel in the reactant stream, but only at high temperature. This was due to the fact that under this condition there is negligible oxygen in the reactant stream and high steam content, therefore fuel conversion takes place primarily via the higher yielding, but endothermic, steam reforming reactions. However, the lack of oxygen in the reactant stream, and hence lack of exothermic POx also meant that the proportion of the reformate containing hydrogen (vol. %) was often significantly lower than at the higher lambda conditions. Therefore intermediate conditions, similar to those at $\lambda = 1.5$ with reasonable proportions of steam and oxygen in the feed, are likely to be the best operating conditions for an exhaust gas reforming unit.

As shown in Chapter 5 and Chapter 6 this level of hydrogen production also compares well with the performance of the two precious metal based reforming catalysts, the commercial-PM and the Rh-only catalysts, tested in this work. There were indeed some differences in performance between the Ni10CZ and PM catalysts. The first of which was the superior hydrogen production of the PM with propane in the region of 100 °C to 400 °C, which was assigned to the superior POx performance of the PM catalyst.

The second of which was that the nickel catalyst was found to significantly outperform the PM catalyst when iso-octane was used as the fuel, at all temperatures and conditions.

The hydrogen production capability of the nickel catalyst, both in terms of absolute quantity, but also relative to the commercial catalyst was therefore promising in terms of its potential use in a real vehicle.

However, other results presented in this work served to highlight remaining issues with all catalysts, particularly when iso-octane was used as the fuel – which have ramifications for using such catalysts in a real vehicle for exhaust gas reforming.

Firstly, all catalysts showed much higher rates of coking when iso-octane was the test fuel relative to propane, and in the case of the nickel catalyst these rates were extremely high. Secondly, as mentioned above, the PM catalyst showed very poor performance with iso-octane, relative to both its own performance with propane, and the nickel catalyst's performance with iso-octane.

The latter of these observations was unexpected, and the various experiments described in Chapter 6 seemed to eliminate experimental artifacts as the cause for the PM catalysts poor performance when iso-octane was used.

It is therefore clear that at a fundamental level there were significant differences between the reactivity of the two hydrocarbon fuels and their interaction with the different catalysts that gave rise to these two aspects. The issues associated with the use of iso-octane as the surrogate fuel are important because it would be expected that, particularly in the case of carbon deposition, that iso-octane would be better model for commercial gasoline than would propane. Hence, the higher rates of coking observed in this work with iso-octane would be expected to also be present with the immediate target application.

Carbon deposition is an unavoidable possibility in steam reforming applications due to its sharing of reaction intermediates and active sites with the reforming reactions. Hence, steps are usually taken with regards to the control of reaction conditions or with the design of the catalyst to minimize the rate of the deposition [76, 134].

Carbon is deposited on catalysts via a number of possible routes and in a number of different forms – often in complex combinations that are determined by the hydrocarbon feedstock, conditions and the catalyst nature.

One route is the thermal cracking of the hydrocarbon feedstock into smaller hydrocarbon units and radicals which can then undergo polymerization. This process is not limited to the catalyst surface and can occur in the gas phase, resulting in the blocking of flow streams. Other possibilities are chemical reactions on the catalyst, but as in thermal cracking involve the dissociative adsorption of the hydrocarbon, again forming various intermediate carbon species that can then act as the seed for further deposition. The buildup of these deposits can occur through various mechanisms such as β-eliminations, cyclisation and hydride transfer type reactions.

The carbon species deposited on the catalyst surface can take a number of forms, including polymeric amorphous carbon films or filaments, metal carbide species, graphitic structures either encapsulating the active catalytic components or growing in whisker like structures through the active metal crystals. Carbon deposition is also possible from carbon monoxide, rather than the hydrocarbon since CO can also dissociate on the metal [69, 76, 134, 135].

Regardless of which pathway is involved, they all involve the formation of an adsorbed reactive carbon intermediate on the catalyst surface, this can be atomic carbon (C_α), a carbon radical, or ions such as a carbenium ion (C^+).

In the case of CO dissociating on the metal to form C_α, this can then form carbon filaments, metal carbide species and polymeric carbon film (C_β) which can then lead to graphitic type carbon being formed. These options are shown below in Figure 7.3, taken from the review of catalyst deactivation by Argyle and Bartholomew [69], describing coking with reference to nickel steam reforming catalysts:

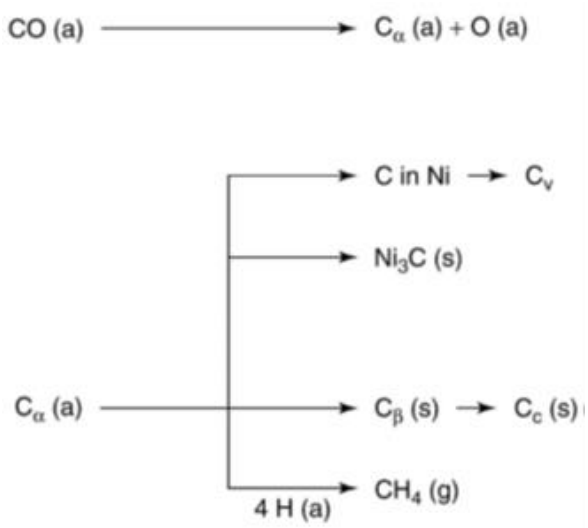

	Structural type	Designation	Temp. formed, °C	Peak temp. for reaction with H_2, °C
1.	Adsorbed, atomic (surface carbide)	C_α	200–400	200
2.	Polymeric, amorphous films or filaments	C_β	250–500	400
3.	Vermicular filaments, fibers, and/or whiskers	C_v	300–1000	400–600
4.	Nickel carbide (bulk)	$C\gamma$	150–250	275
5.	Graphitic (crystalline) platelets or films	C_c	500–550	550–850

Figure 7.3: Pathways to carbon deposition during reforming [69]

In the case of the of the hydrocarbons dissociating on the catalyst, all these intermediate carbon species can be formed, via the routes shown in Figure 7.4 [69].

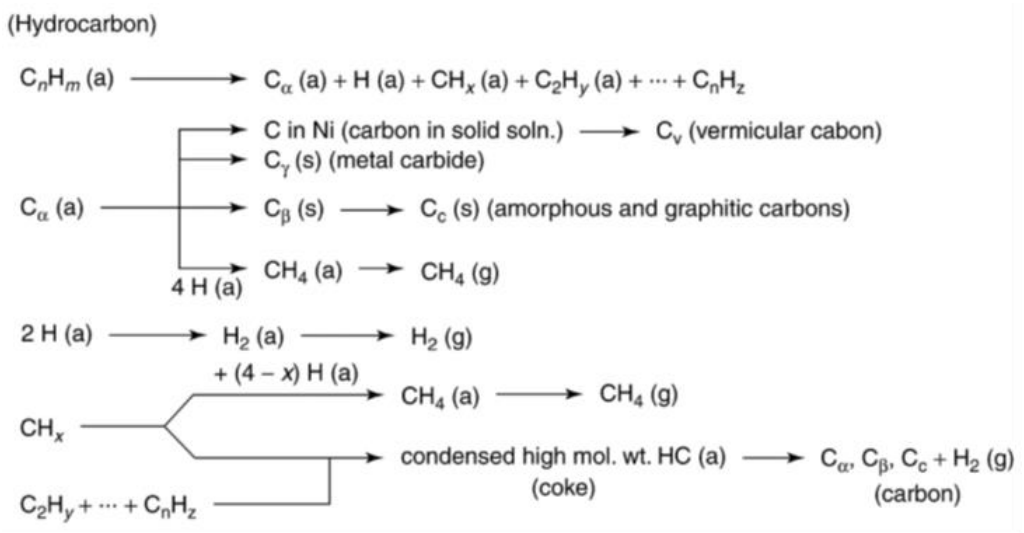

Figure 7.4: Formation of carbon deposits from hydrocarbon dissociation, via carbon intermediates [69]

In this work it was clear that the rate of coking was significantly higher with iso-octane than propane, and significantly higher on the nickel catalyst than both the PM and rhodium catalysts. This was shown by the results in Chapter 5 & Chapter 6.

The difference between the fuels is summarized below in Table 7.1.

Fuel	**Average TGA Maximum % Weight Loss**	**Average Sample % Weight Gain**
Propane	7.22	3.67
Iso-octane	44.20	86.86

Table 7.1: Average maximum TGA weight loss and average sample weight gain of all powdered catalyst samples tested under exhaust gas reforming conditions of propane and iso-octane

The results above show clearly that the weight loss events (from the oxidation of deposited carbon) in the TGA experiments were significantly larger for the samples tested with iso-octane than those with propane. They also show that the samples tested with iso-octane showed significant weight gain after testing. Both point to the much greater carbon deposits left on the catalyst after testing with iso-octane.

The increased propensity of the heavier hydrocarbon towards coking was not unexpected, however the degree to which this was shown was surprising. Propane can be converted to carbon during reforming through unwanted side reactions such as those shown below [136]:

(7.1)

(7.2)

(7.3)

(7.4)

(7.5)

(7.6)

Iso-octane can be converted to carbon through similar reactions, however the rate of carbon deposition, whether through catalytic decomposition of the hydrocarbon, or through pyrolytic (thermal) cracking, is known to be higher [76, 134, 137] with heavier feedstock. This is largely due to the faster dissociative adsorption of the higher hydrocarbons to the active metal. Branched paraffins have also been shown to be very prone to thermal cracking. This has been found to be particularly prevalent with iso-octane in zeolite catalysis [138].

As discussed previously, the H_2O/C ratio under the "standard" λ-condition tests were lower for iso-octane than in the propane tests, due to the selection of the same % of fuel in the reactant feed combined with the higher carbon content per mol of iso-octane. High steam to carbon ratios are an important tactic for the suppressing of the rate of carbon formation [76, 134], therefore this will certainly have contributed to the difference between the two fuels. However as shown in Chapter 6, when the water content in the reactant feed was raised by a factor of ten, the rate of carbon deposition was still not negligible.

There were also differences between the catalysts in terms of the rate of carbon deposition when iso-octane was used. This was shown in Chapter 6 (Figure 6.10 and Table 6.1), where the results clearly show the rhodium catalyst displayed greater resistance to carbon formation than the nickel catalyst.

Again, this was not unexpected, since precious metals such as rhodium have been shown to be more resistant to coking than base metal catalysts like nickel [60, 61]. The pathways to carbon deposition described above are all known possibilities for nickel catalysts in reforming applications, however, these pathways are also known to be different with rhodium catalysts [76, 139, 140]. In the case of nickel, the main problem with coking arises from the formation, diffusion and dissolution of carbon into the metal. Rhodium (and other precious metals) do not dissolve carbon to the same extent.

The buildup of carbon on the nickel catalyst was also shown to be a problem when propane was used as the reforming fuel, though in a different way to high rate of coking described above for iso-octane.

Instead, as shown in Chapter 4, the lower rate of coking with propane exposed the catalyst to a different deactivation route if the hot catalyst was exposed to an oxidizing atmosphere during the shut-down phase of the testing/use cycle.

Chapter 4 detailed the investigation into observed nickel catalyst deactivation, and found that it was associated with a temperature spike in the catalyst bed observed when the hot catalyst was exposed to an oxidizing atmosphere during the shutdown phase of testing. By testing the catalyst under exhaust gas reforming conditions and then exposing it, while still hot, to differing atmospheres during this shut-

down phase, it was shown that this temperature spike occurred when the hot catalyst was exposed to an oxidizing atmosphere (the "Oxygen" and "Air" cool down methods), and that severe catalyst deactivation was observed in subsequent tests. This was in contrast to when the hot catalyst was exposed to an inert atmosphere (the "Nitrogen cool down method") during the shut-down phase after testing, where in fact the catalyst was activated by such an exposure.

This same affect was also observed in Chapter 6 when iso-octane was used as the fuel. However, the deactivation was not observed to be as severe as when propane was used, and given that there was still a significant quantity of carbon deposited on the catalyst with iso-octane, it is unclear how much of the deactivation observed was due to the exposure to an oxidizing atmosphere during the shut-down phase, or simply the buildup of carbon on the catalyst.

In both cases it was proposed that the carbon built up on the catalyst during testing was being oxidized if the catalyst was still hot enough, once exposed to the oxygen/air cool down methods, and that this process, being exothermic caused the temperature spike in the catalyst bed. The measured temperature spike of as much as 150 °C was also thought to be much greater on the catalyst surface itself, since the thermocouple was positioned just below the catalyst bed and was therefore unlikely to be recording the full rise.

We have proposed that the rapid rise in surface temperature of the catalyst caused by the combustion of surface carbon, raises the temperature above the Huttig and Tamman temperatures for the active NiO and Ni(0) species causing the thermal sintering of the active species, along with the conversion of Ni(0) to NiO. These two factors were thought to explain the combination of temporary and permanent loss of active surface area, and the resulting nature of the catalyst deactivation.

The proposed reason for this effect being much more severe when propane was used was due to the lower rate of coking. When iso-octane was used, the quantity of carbon deposited on the catalyst surface was so great that it was thought that this meant there was too much carbon to burn through before reaching the catalyst surface.

Similar types of post-operation catalyst deactivation have been reported in reforming applications [125-128], and is similar to the coke burn off regeneration process utilized in industry. However, such a process is usually operated at lower temperatures to avoid the damage to the catalyst seen here [19, 108].

So, though the deactivation of the nickel catalyst was via the thermal sintering of the active components, this was in effect induced by the buildup of carbon on the surface, and initiated by exposure of the hot catalyst to an oxidizing atmosphere.

This is relevant for two reasons; (1) it is likely that in a real exhaust gas reforming system, when the vehicle is turned off after operation, an oxidizing atmosphere, in the form of air will most likely be able to enter by back-diffusion through the exhaust tail-pipe and hence the catalyst will indeed be exposed to an oxidizing atmosphere. (2) This effect was present with both fuels, however was much more severe with propane, and as discussed previously, though propane may not be the best model for the rate of

carbon deposition with commercial gasoline, it would be expected that it is a better model for other potential automotive fuels such as LPG and possibly natural gas. Short-chain hydrocarbon fuels are viewed as a possibility for meeting ever stricter emissions targets, particularly for heavy duty vehicles [52, 141, 142], therefore this issue would be expected to be present in such applications.

Hence, arguably the key finding in this work is that, though the nickel catalyst showed suitable activity for exhaust gas reforming (in terms of producing sufficient quantities of hydrogen), there were aspects with respect to its durability that would need to be addressed before it would be suitable for a real system – specifically its resistance to coking under exhaust gas reforming, regardless of fuel choice, and its thermal stability. This therefore should be the key focus of any future work, suggestions for which will be made in the next section.

Another key finding was the poor performance of the commercial PM catalyst when tested under exhaust gas reforming conditions with iso-octane as the surrogate fuel. Furthermore, the range of experiments presented in Chapter 6 seemed to rule out experimental artifacts as the cause.

This was surprising because as discussed at length in Chapter 1, precious metals are considered to be stronger candidates for most reforming applications where the reformer is operated under non steady-state conditions (nickel based catalysts are widely used in the large scale synthesis of hydrogen). In this work too, it was found that the PM catalyst displayed superior low-temperature exhaust gas reforming performance when propane was the surrogate fuel, and both the Rh1CZ and PM catalyst showed better resistance to coking with both surrogate fuels.

Furthermore, the Rh1CZ catalyst did not show the same drop in performance when iso-octane was used relative to propane.

Therefore, this suggests that the root cause of the poor performance of the PM catalyst with iso-octane was the specific composition of the commercial catalyst, rather than that it was formulated using precious metals, and that it interacted with iso-octane under exhaust gas reforming conditions in a fundamentally different way to propane.

As stated in Chapter 2, it was thought that the commercial PM catalyst was formulated using reasonably high loadings of rhodium and platinum. Assuming this is correct, and given the performance of the Rh1CZ catalyst, it is clear the presence of Rh would not explain this behavior. Therefore, again assuming the composition of the PM is as thought, then this strongly suggests that the presence of the platinum is the key to explaining the poor performance with iso-octane.

Ambroise et al. [44] simulated exhaust gas reforming using iso-octane as the fuel (under conditions equivalent to the $\lambda = 1$ condition used in this work) , with a range of cobalt only, rhodium only or cobalt-noble metal based bimetallic catalysts. These included Co-Rh and Co-Pt formulations.

Their results show that the Co-Rh formulation was superior to the Co-Pt formulation, however the Co-Pt formulation outperformed a Rh only formulation. However, this does not fully explain why a Rh-Pt

(the PM catalyst) formulation would be worse than a Rh only formulation (the Rh1CZ catalyst) or a nickel catalyst.

An additional piece of evidence to explain the poor performance of the PM catalyst could be found in the manner in which the product gas composition changes as the lambda value is raised between propane and iso-octane. This is shown in the Figures below.

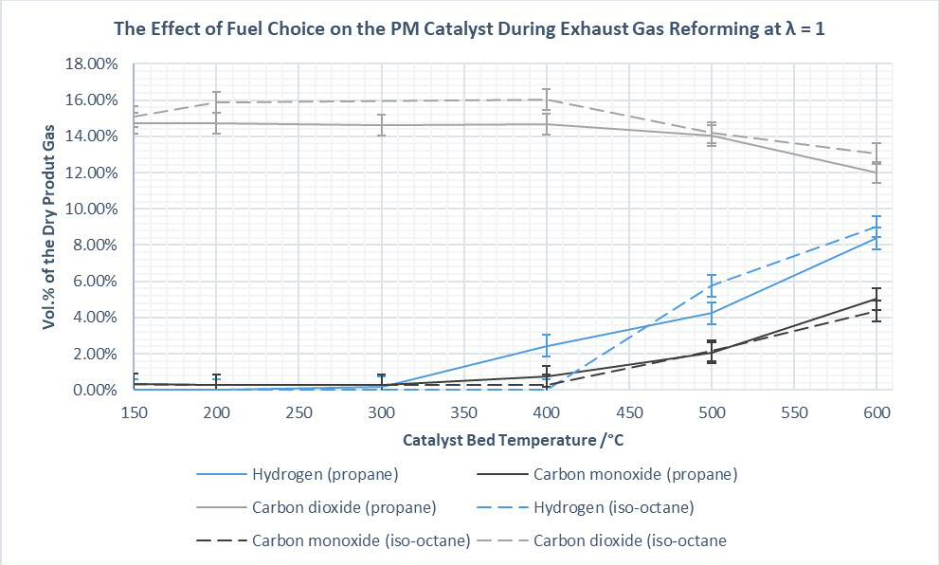

Figure 7.5: Comparing the exhaust gas reforming performance of the PM catalyst with propane and iso-octane, in terms of the composition of the dried product gas composition as a function of bed temperature at λ = 1

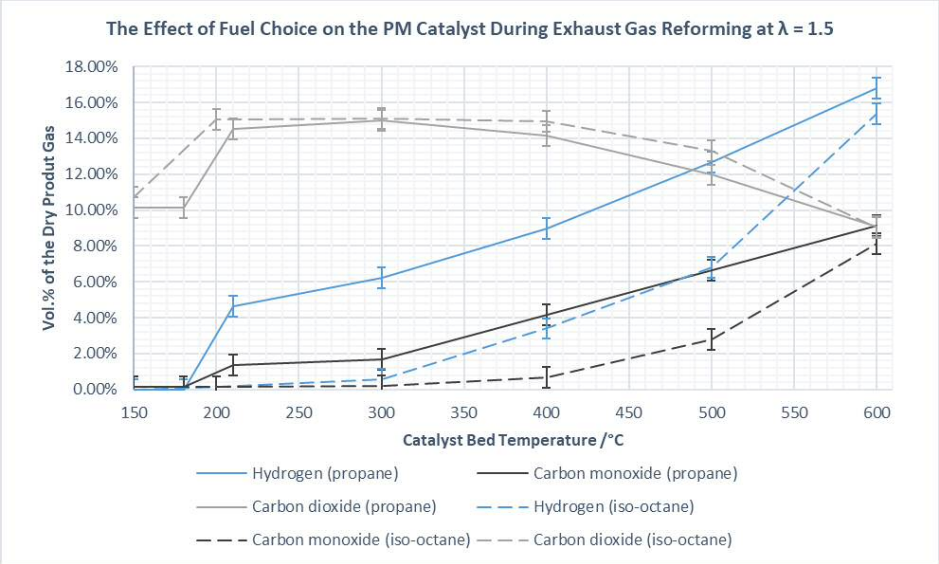

Figure 7.6: Comparing the exhaust gas reforming performance of the PM catalyst with propane and iso-octane, in terms of the composition of the dried product gas composition as a function of bed temperature at λ = 1.5

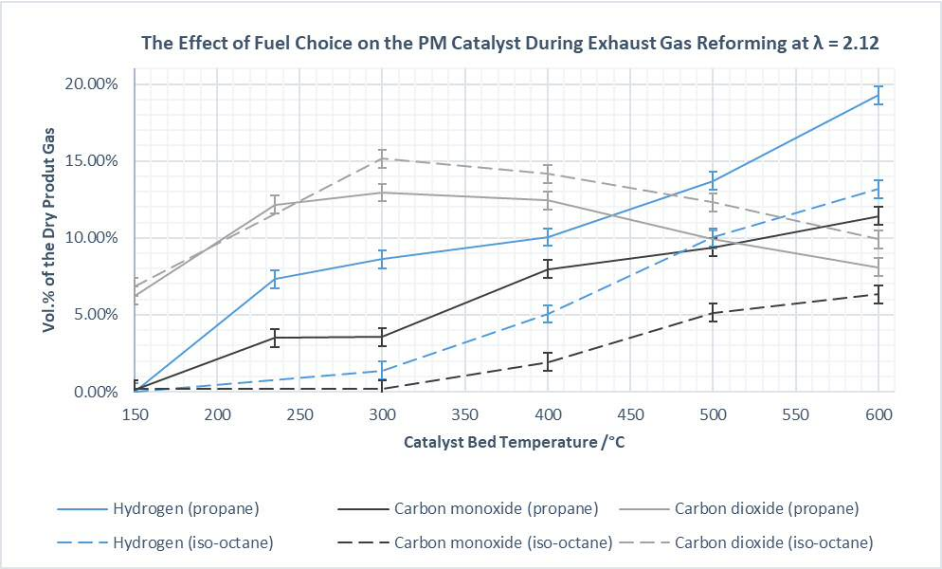

Figure 7.7: Comparing the exhaust gas reforming performance of the PM catalyst with propane and iso-octane, in terms of the composition of the dried product gas composition as a function of bed temperature at λ = 2.12

The results in Figure 7.5 show that the hydrogen and carbon monoxide levels in the product gas were comparable between fuels, while the carbon dioxide levels were higher in the product gas of iso-octane than propane at the λ = 1 condition.

In contrast, a noticeable gap opens up between the hydrogen and carbon monoxide levels in the product gas at λ = 1.5 and λ = 2.12, though the carbon dioxide level relationship between fuels is maintained. Specifically, below 600 °C, the hydrogen content of the product gas was around 5 % higher with propane than iso-octane at λ = 1.5, and was 2-3 % higher for carbon monoxide (Figure 7.6). This was also true of the λ = 2.12 condition below 500 °C (Figure 7.7).

In other words, the PM catalysts performance deficit with iso-octane compared to propane was most distinct at the higher lambda conditions. The significant difference between the λ = 1 condition and the two higher conditions is that in the former, the oxygen content in the reactant stream is negligible (0.4 vol.%), whereas in the latter it is significant (6.8 vol.% and 10.7 vol.% for λ = 1.5 and λ = 2.12 respectively).

Additionally, the increase in carbon dioxide levels during the light off stage can be seen to be greater at both the higher lambda conditions relative to λ = 1, and the increase in CO_2 content of the product gas was also greater with iso-octane than propane in all conditions.

This dependence on the oxygen content of the reactant feed suggests that the lack of performance of the PM catalyst could be due to a greater preference for oxidation reactions, particularly at low temperatures, with iso-octane than with propane.

This preference could be driven by the aforementioned greater ease of auto-ignition with heavier hydrocarbon feedstocks [89], combined with the fact that platinum is known to be an effective oxidation catalyst of hydrocarbons, hence its selection for the role of oxidizing the lighter hydrocarbon fractions

in a three way catalyst/catalytic converter in vehicle exhausts [143] which often consist of Pt-Rh formulations akin to that thought to be present in the PM catalyst.

Similarly, Barbier Jr. and Duprez [144], when studying autothermal (what they term "oxy-steam reforming") of propane (among other reactions such as WGS oxidation, and steam reforming) state that in their Pt-Rh catalyst formulation, the Pt was responsible for promoting the oxidation reactions and the Rh the reforming reactions – yielding a highly active formulation compared to both Pt-only and Rh-only formulations.

The high activity of the supposedly Pt-Rh composed PM catalyst in the exhaust gas reforming of propane in conditions similar to autothermal reforming, in that steam and oxygen present were in the reactant feed, was also observed in this work.

Assessing the carbon balance of the experiments performed in this work also suggest that the selectivity, and/or fuel conversion, were different for the PM relative to the nickel and rhodium catalysts with iso-octane when compared to propane.

Figure 7.8 below shows the average carbon balances for the PM, Ni10CZ and Rh1CZ catalysts in the testing of iso-octane and propane under exhaust gas reforming conditions at $\lambda = 1.5$.

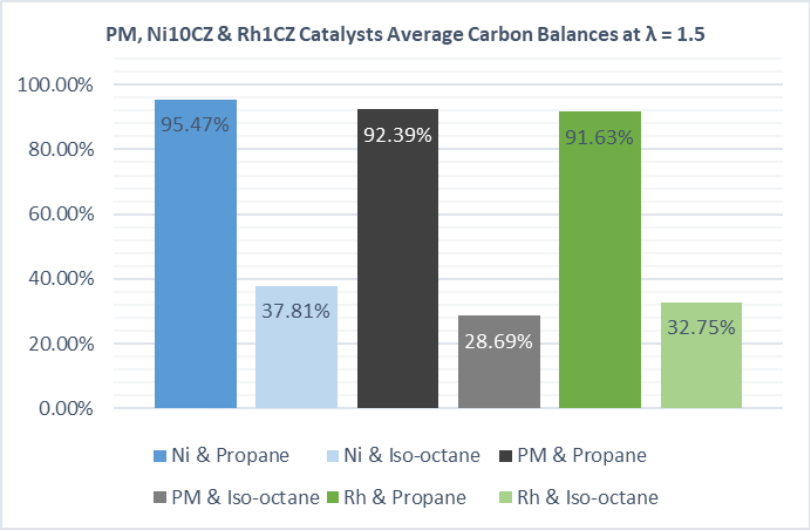

Figure 7.8: Average carbon balances for the PM, nickel and rhodium catalysts at λ = 1.5 with both propane and iso-octane

For all three catalysts, there was a significant reduction in the average carbon balance when iso-octane was used relative to propane. This suggests that under these conditions, (1) iso-octane conversion was significantly lower than that of propane, and/or (2) the iso-octane was being converted to carbon containing species other than carbon dioxide and carbon monoxide. As shown throughout this work, a large contribution to the carbon balance deficit with iso-octane is likely to be down to the much higher rates of coking, since this would certainly not be detected by the GC.

However, this reduction was more significant, in relative and absolute terms, for the PM catalyst compared to both the nickel and rhodium catalysts. This could therefore suggest that (1) the PM catalyst was converting a lower proportion of the iso-octane than the nickel and rhodium catalysts, and/or (2)

the PM catalyst was converting a greater share of the iso-octane to side carbon containing products, both of which could help explain the lower hydrogen producing activity of the PM with iso-octane compared to propane.

Though all three catalysts exhibited much higher selectivity for carbon during testing with iso-octane when compared with propane, this effected the PM catalyst to a much lesser extent than the powder nickel and rhodium catalysts. Therefore, this could mean that the PM shows high selectivity for other carbon containing compounds.

For example, methane is predicted by the thermodynamics (though if not always observed in experiments) to be a major product during exhaust gas reforming of iso-octane [31, 48]. This can be formed by methanation reactions, which would consume hydrogen and produce methane (see reaction equations in Table 1.1 in Chapter 1). Such reactions could therefore be contributing to the low hydrogen yield and low carbon balance of measured during testing of the PM catalyst relative to the nickel and rhodium catalysts.

Therefore, it is proposed that this combination of Pt and Rh is effective for exhaust gas reforming of lighter hydrocarbon fuels, such as propane, since the combination of the oxidation performance of the Pt, with the reforming performance of the Rh, works effectively. However, with the heavier hydrocarbon fuels, the balance shifts unfavorably, with selectivity for hydrogen and or/fuel conversion decreasing. Additional information would be required to prove this conclusively, the details on how to obtain which will be suggested in the next section on suggested further work.

This poorer selectivity for hydrogen of platinum in the autothermal reforming of iso-octane for the purpose of fuel cells, specifically relative to nickel, has also been shown in the work of Krumpelt et al. [145]. They show that Pt shows better iso-octane conversion than nickel at temperatures below 600 °C, while nickel shows the better hydrogen selectivity at these temperatures.

This result serves to highlight how important careful selection of the active components, with reference to the intended application (in this case the target fuel) is in catalyst design. As shown in this work, carbon deposition aside, a nickel based catalyst showed superior performance in the exhaust gas reforming of heavier hydrocarbons

The results also show that the 1% Rh/CeO_2-ZrO_2 formulation, showed similar performance to the nickel catalyst with both fuels while showing significantly lower coking rates and hence was less prone to deactivation. This higher resistance to coking with iso-octane was also observed in the PM catalyst despite its poorer reforming performance. Therefore, as covered in the discussion on carbon deposition, there are still certain advantages to using precious metals even with the heavier feedstock, but that these components still need to be selected carefully.

Further Work

Any future work should build on the key results presented in this work in order to make significant strides towards tackling the remaining issues facing the incorporation of exhaust gas reforming as a technology in real vehicles. It is suggested that such work focus on the following three areas:

1. Further develop an understanding of the underlying chemistry of exhaust gas reforming of hydrocarbon fuels.
2. Optimization of a nickel based catalyst formulation.
3. Testing with potential commercial fuels.

Each of these areas of focus will be discussed in more detail below.

Probing the Chemistry of Exhaust Gas Reforming

Initially the main area of interest in this study was the hydrogen producing ability of the various catalysts under a range of exhaust gas reforming conditions and fuels.

However, there are a number of additional modifications to the reactor set up/testing procedure that would allow greater detail on the product gas composition, temperature profile throughout the reactor/catalyst bed, and characterization of the catalyst.

For example, the single thermocouple positioned in close proximity to the exit of the catalyst bed measured the outlet-gas temperature and not the true temperature of the catalyst bed. Being able to obtain a better reflection of surface temperature would be particularly useful if more clarity on the effect of exposing the catalyst to an oxidizing atmosphere during the shutdown phase of testing was desired. Additionally a more complex array of thermocouples positioned along the length of the reactor/catalyst bed, as often seen in the literature [47, 50, 85-87], would enable a more nuanced understanding of temperature profiles to be established, therefore allowing more accurate inferences to be made regarding the reactions occurring during the testing process and cycle. Such a set up used by Gonzalez et al. [50] indeed provides evidence for the inaccuracy of a single thermocouple positioned close, but not in contact with the foot of the catalyst bed. Their thermocouple array showed the potential for the temperature of the gas stream to drop 30 °C to 40 °C over a distance as short as 80mm in the autothermal reforming of FT-diesel.

More important adaptations would involve modifications to allow more detailed analysis of the product stream. Specifically, the ability to detect and quantify a greater range of gaseous hydrocarbon compounds, along with that of the liquid fractions not analyzed in the GC.

The need for this is demonstrated by Figure 7.9 below with shows the average carbon balances of the experiments conducted with propane as the surrogate fuel, compared to those conducted using iso-octane as the surrogate fuel.

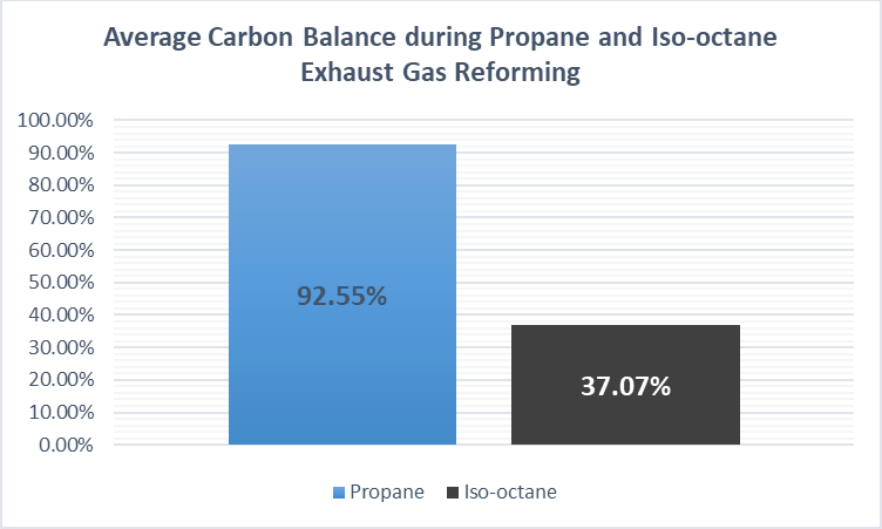

Figure 7.9: Average carbon balance during propane and iso-octane exhaust gas reforming

The significant fall in average carbon balance for the iso-octane experiments, relative to those of propane, will be down to incomplete conversion of iso-octane and/or the formation of other carbon containing products measured by the GC (CO_2, CO and C_3H_8), such as carbon or methane. Carbon in particular was found to be formed in significant quantities during this work when iso-octane was the surrogate fuel, particularly with the nickel catalyst, so this will certainly be contributing.

This would be achieved by calibration of the GC to detect other hydrocarbon compounds aside from propane (e.g. methane, ethane e.t.c). In the case of the liquid fractions (unconverted iso-octane, other liquid hydrocarbons and water) this could involve the inclusion of additional techniques such as Fourier Transform Infra-Red (FTIR), or GC-MS. These latter techniques are often used in the literature for this purpose [46, 50, 51, 54, 109].

Furthermore, the selectivity towards solid carbon, through coking reactions would need to be assessed for each of the catalysts. This would involve further analysis of the TGA data provided in this work in the case of the nickel and rhodium catalysts, but would require post-testing characterization of the PM which was not performed here.

These additions would allow analysis of the full product composition, displayed in higher carbon balances, and hence calculations of conversions, yields and selectivity to be performed with the liquid fuels. Such additions would also be of great use in proving or disproving the hypothesis put forward in this chapter for the poor performance of the PM catalyst with iso-octane, as well as further detail on the differences between the exhaust gas reforming of lighter hydrocarbon fuels relative to heavier feedstock. The latter aspect could therefore shed additional light on the greater coking rate found with the heavier feedstock.

The nature of the carbon deposition across different fuels and catalyst should also be probed through the use of additional characterization techniques on the used catalysts. Specifically, microscopy techniques such as Scanning Electron Microscopy (SEM), which is frequently used in catalysis to provide high-resolution three dimensional images of the catalyst surface, and can provide structural and chemical

information on the catalyst, such as the distribution and location of components on the surface (including contaminants) and particle sizes, for example [146].

SEM is frequently used in the study of reforming applications as a way to characterize carbon deposits on the catalyst surface, providing a straightforward method of distinguishing between say amorphous and whisker type carbon deposits, as was done by Alberton et al. [147] in their work on carbon formation on nickel ethanol steam reforming catalysts. Such information would be beneficial in understanding the processes leading to the coking, and hence assist in suppressing the rate of such deposition – whether from controlling of reaction conditions or by improving catalyst design.

Such a technique may also be useful in confirming the proposed hypothesis as to the cause of the deactivation induced by exposing the hot nickel catalyst to an oxidizing atmosphere during the shutdown phase of testing detailed in Chapter 4.

Further work in this area, particularly if the additional modifications suggested above are incorporated into the testing regime, could involve testing both the base and precious metal formulations under a different range of conditions to determine their activity towards some of the key reactions occurring during exhaust gas reforming. For example, the catalysts could be tested with both liquid and gaseous fuels under steam reforming conditions (no oxygen) and partial oxidation conditions (no steam), among others. These tests would help to reveal differences in the catalysts activity towards the key reactions involved in exhaust gas reforming, and hence shed light on the differences involved under the exhaust gas reforming conditions. Such tests could also yield useful information regarding the PM catalysts poor performance with iso-octane.

Computation of the expected thermodynamic equilibrium composition for each of the λ conditions could also be performed. Such calculations would allow the comparison between the experimentally obtained results and the predicted equilibrium compositions, which could lead to further useful insights relating to how close each of the catalysts were to thermodynamic equilibrium.

Optimizing the Nickel Catalyst

The 10% Ni/CeO_2-ZrO_2 catalyst prepared and tested in this work showed promising performance in terms of hydrogen production, across both fuels and relative to the PM and Rh-based catalysts, however issues remain regarding its durability. Specifically, its resistance to carbon deposition, and thermal stability would need to be improved before it could be considered as a suitable candidate for a lower-cost option for exhaust gas reforming compared to precious metals.

These aspects – resistance to carbon formation, sintering and durability to cope with multiple cycles of exposure to changing conditions is crucial. Three way catalytic converters incorporated into modern vehicles are legislated to have a lifespan of the same order of magnitude as the guaranteed vehicle lifetime, which can be in the range of 160,000km or 100,000 miles of use [53, 56, 57]. These catalysts also have to cope with inconsistent driving conditions resulting in variations in exhaust conditions (contents,

flow and temperature), environmental conditions, and exposure to temperature shocks from startup/shutdown cycles. This therefore should be viewed as the benchmark for the durability of any potential exhaust gas reforming catalyst.

The formulation used in this work was very much a preliminary formulation, intended for early stage testing – which therefore means there is significant scope for these aspects to be improved through optimization of both the catalytic components and the preparation method.

Given the importance of developing lower cost options for exhaust gas reforming catalysts to become eligible for use in real vehicles, this area of work should be the priority. The additional insight achieved through incorporation of the reactor modifications and additionally testing/characterization techniques described in the previous section should steer the development path of the catalyst.

The preparation method used in this study was wet impregnation which offers the dual advantages of being a simple technique and the ability to achieve homogenous deposition of the active metal on the support material. However it does not offer control on other aspects such as optimizing particle size of metal-support interactions [66-68]. Some examples of how these aspects can affect the properties of the resulting catalyst have been discussed previously in the Introduction Chapter. For example the work by Achouri et al. [83] showed how the preparation method could improve both the activity and stability of a nickel catalyst for diesel steam reforming.Work by Ambroise et al. [44, 80] showed how both the use of bimetallic formulations and control of the preparation method could yield catalysts with improved performance for exhaust gas reforming. The latter case showed how a sol-gel prepared catalyst showed superior performance to a simple impregnation prepared catalyst – and this could be a good candidate for a second generation of the nickel on ceria zirconia catalyst formulation.

Another more involved preparation technique would be the preparation of core-shell type catalysts, such as those presented for steam reforming of methane by Zhang et al. [148] and Kim et al. [117]. Such catalyst structures can show improved performance and stability due to the strong metal support interactions.

Zhang and colleagues tested three different methods for production Ni/Al_2O_3-Sil-1 core shell catalysts. The first (the typical method for producing core shell catalysts) involved impregnating the alumina support beads with nickel using incipient wetness impregnation, followed by drying and calcination. Then the Sil-1 zeolite layer was deposited on the catalyst beads by following a “seeding and regrowth” method used to prepare zeolite membranes, before final calcination.

The second approach starts by growing the Sil-1 shell on the alumina beads, followed by impregnation of the nickel.

The final method followed the second method, but added additional steps to remove residual nickel from the Sil-1 shell through repeated water and toluene soakings.

The authors provide a diagrammatic representation of these processes, which is shown below in Figure 7.10. This final method produced the most stable and active catalyst for steam reforming of methane.

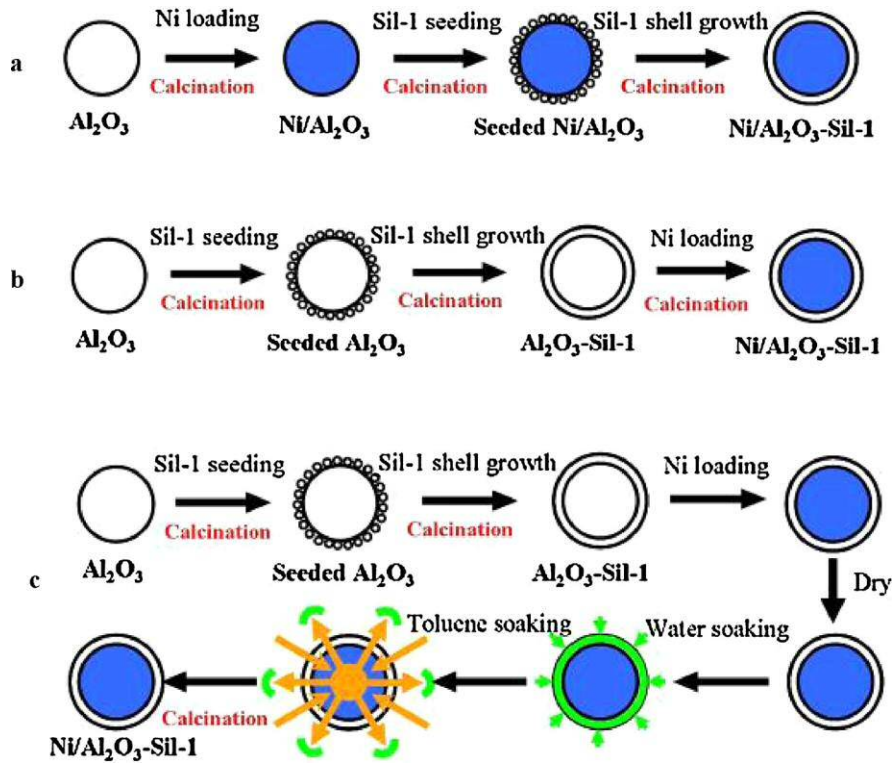

Figure 7.10: Preparation strategies for core-shell nickel reforming catalysts [148]

The work by Kim and colleagues [117] presents core shell nickel reforming catalysts on a range of supports: Ni/Al_2O_3, $Ni/MgO\text{-}Al_2O_3$, Ni/CeO_2 and $Ni/Ce_{0.4}Zr_{0.6}O_2$. The synthesis method used was a specialty technique used for producing nano-materials called multibubble sonoluminescence (MBSL). The resulting alumnina supported catalysts showed high methane conversion during SRM, and good thermal stability, however the authors report the technique was not so successful for the ceria supported catalysts.

Alumina is a high surface area support known for enhancing thermal stability, and therefore could be used in combination with ceria-zirconia, and the more advanced preparation techniques described above to improve catalyst stability.

Further development of the catalyst could involve coating an optimized catalyst formulation onto a monolithic substrate which again can assist in thermal stability, as well as the known benefits from using monolith substrates such as their low pressure drop compared to packed bed catalysts. Furthermore, such a monolithic catalyst would likely be the end form of any exhaust gas reforming catalyst similar to that used in three way catalytic converters [50, 51, 67].

Improvements could also be made to the formulation simply through optimizing the nickel loading. As Han et al. [149] show, both too much and too little active nickel content can be detrimental to catalyst activity and stability. Only one formulation was tested in the present work, containing 15% by weight nickel, which was selected based on their findings. However, given the different applications it is possible that this loading is not optimized for exhaust gas reforming.

The formulation could also be improved by the addition of other metals or dopants, which often yield improved activity and stability over simple single active metal catalysts.

As shown in the work of Liu et al.[150] the dopant can be non-precious metal based such as copper. They present a Ni/Ceo_2-ZrO_2 ethanol steam reforming catalyst which when doped with copper showed improved ethanol conversion and hydrogen selectivity. They assign this to increased dispersion of NiO particles, beneficial modification of the CeO_2 support surface, and enhanced interactions between the Cu-Ni metal species and the support.

The bimetallic formulations could also contain low levels of precious metals, weighted enough to achieve the performance gains, while avoiding the cost associated with high loadings of precious metals.

As discussed in the Introduction, and shown in Chapters 3 and 6 rhodium, is a good reforming catalyst showing greater reducibility (therefore potentially improving low temperature activity) and higher resistance to coking than the nickel catalyst. Hence, a bimetallic rhodium-nickel formulation with low loadings of rhodium could be another candidate for future testing.

Other precious metals could also be considered, especially those that could lower light off temperature such as platinum and palladium through improved reducibility. Such additions could also improve resistance to coking through stabilization of the Ni sites, as found in work by Profeti et al. [151] in the reforming of biofuels. Promotion with 0.3 % by weight loadings with Pt and Pd brought these benefits to a Ni/Ceo_2-Al_2O_3 catalyst. Platinum has also been found to assist in lowering light off temperatures on a rhodium based catalyst for exhaust gas reforming [43].

Similar results were found by Dantas et al. [152] for Pt and Pd. The authors also tested a silver doped $Ni/CeZrO_2$ catalyst, and found that this formulation showed the best performance and stability in the autothermal reforming and partial oxidation of methane, through improved reducibility and improved redox capacity. The loadings of the precious metals in their work was low, at 0.1 %.

However, as discussed in this chapter, particularly when working with heavier hydrocarbon feedstock, the selection of precious metal dopants such as platinum, while potentially bringing some benefits such as improved stability and low temperature activity, may also present some issues.

Though beyond the scope of this work, in the real application, resistance to sulfur poisoning would also be a key requirement since commercial fuels are likely to continue to contain low levels of sulfur compounds. As discussed in the Introduction Chapter, this would be another area where the addition of dopants, particularly low levels of precious metals could help improve catalyst stability.

Also as discussed in the Introduction Chapter, nickel is not the only base metal used in reforming applications, cobalt formulations could also be trialed in order to see if they offer improvements on the nickel catalyst shortcomings, particularly in terms of resistance to coking.

In summary, this should be the key area of focus in any future work. Obtaining a high activity, durable and cheap catalyst is the key to incorporating exhaust gas reforming to real vehicles. On the evidence of this work the nickel catalyst can produce useful levels of hydrogen, however progress is still blocked by a lack of durability, and optimizing the catalyst to this end is critical.

Furthermore, improvement here should be attainable since there is plenty of scope to produce an optimized base metal catalyst, given the simplicity of the formulation/methods used here, that could show similar levels of resistance to coking to that of the PM catalyst. Such an optimized catalyst may not only improve durability, but also the activity of the formulation which would therefore yield a much more effective catalyst.

Testing with Commercial Fuels

One of the recurring themes of this work is the differences between the two surrogate fuels.

For example, if the target application involves heavier fuel feedstocks (e.g gasoline or diesel) then this work shows that propane is likely to significantly underestimate the rate of coking under exhaust gas reforming conditions, and be much more realistic a model for gaseous hydrocarbon fueled applications (such as natural gas or LPG). Furthermore, as in the case of the PM catalyst, testing revealed significant differences in reactivity between propane and iso-octane.

Single component surrogate fuels were used in this work to avoid the complications associated with the vaporization of complex multicomponent commercial fuels and the effect of poisons still present in such fuels such as sulfur compounds. Such a compromise was viewed as appropriate for early stage testing such as that in this work to enable a more controlled study of the chemistry. Furthermore, iso-octane and propane could still be useful during the catalyst development stage to test catalysts resistance to coking and thermal stability as revealed in this work.

If required, future work could look to transition to commercial gasoline by using more complex mixtures of surrogate fuels, such as that proposed by Kang et al. [61], which contained a mixture of paraffinic and aromatic compounds, along with a common gasoline additive: methyl tert-butyl ether (MTBE).

Their mixture consistent of iso-octane (50 % by vol.), hexane (20 % by vol.), toluene (20 % by vol.), and MTBE (10 % by vol.). This mixture was found to yield similar product compositions to commercial gasoline.

However, it is proposed that testing with the target commercial fuels should be carried out as soon as a suitably optimized base metal catalyst formulations have been produced, since at that stage it would be important to assess the performance of the catalysts under more realistic conditions.

As discussed in the introduction, particularly focus should be given to gasoline, since the benefits to spark ignition engines show significant promise [35, 54, 55]. However, other commercial fuels, and potential future commercial fuels, could also be tested such as diesel, natural gas and bio-fuels.

At the same time, it is suggested that a wider range of exhaust gas conditions be tested to provide a much more complete picture as to the ideal operating conditions of an exhaust gas reforming unit when operating with commercial fuels. This could include varying the exhaust gas composition through altering the λ value, or changing the flow conditions through using different flow rates. As discussed previously in this work, it is likely to be that the ideal exhaust gas compositions are those where the

stream contains reasonable quantities of oxygen and steam, so as to yield a reformate with containing a high enough proportion of hydrogen, produced as much as possible via high yielding endothermic steam reforming reactions. This would give the best chance of yielding both improved combustion in the engine when the reformate is recirculated into the engine intake, as well as ensuring the unit acts as a thermochemical recuperation device.

Conclusions

Modifications, including the installation of a specialized ultrasonic spray nozzle, were made to a test rig which had originally been designed for long-term testing of steam-reforming catalysts under fixed operating conditions. The modifications allowed quantities of both gaseous and liquid hydrocarbon fuels to be added to a simulated exhaust gas mixture for the purpose of testing under dynamic exhaust-gas reforming conditions in the lab.

A prototype base metal exhaust gas reforming catalyst, containing 10 % nickel on a ceria-zirconia support, was synthesized using a wet impregnation method. This prototype catalyst was tested against a commercial precious metal based reforming catalyst, and a 1% rhodium on ceria-zirconia catalyst, the latter again synthesized via the wet impregnation method.

All catalysts were tested with both propane and iso-octane as gaseous and liquid surrogates for LPG and gasoline respectively, under exhaust gas reforming conditions.

A range of characterization techniques were used to assist in the analysis of the catalyst both pre- and post- testing, such as TPR, BET surface area, XRD and TGA.

The results in this work showed that the nickel catalyst did not display the durability that would be required for use in a real vehicle. It was both sensitive to the atmosphere it was exposed to during post-operation cool down, and showed very high rates coking with the heavier liquid fuel. Both of which caused deactivation of the catalyst.

The former issue was assigned to the oxidation of surface carbon, deposited during operation, if the hot catalyst was exposed to an oxidizing atmosphere during cool down (e.g air), raising the surface temperature of the catalyst leading to sintering of the active species.

The nickel catalyst did show comparable performance in terms of hydrogen production, with both surrogate fuels, to the precious metal based catalysts tested, yielding hydrogen levels in the product gas of sufficient quantity as to be useful in a real system. However, as per the above, improvements are required in terms of the nickel catalysts resistance to coking and in its thermal stability before such a formulation can be considered a suitable candidate for application in real vehicles. Suggestions for future work focusing on improving these aspects were made.

The commercial precious metal catalyst showed superior performance to the nickel catalyst with propane, but not with iso-octane. A hypothesis to explain this poor performance, centering on the

supposed presence of platinum in the PM catalyst formulation, and the resulting preference for oxidation reactivity over selectivity for hydrogen through reforming was proposed, and future work suggested to prove/disprove this hypothesis.

The three avenues of work suggested focused on yielding greater understanding of the chemistry of exhaust gas reforming (through additional techniques and modifications to the test rig/procedure), the optimization of the nickel catalyst formulation, and the testing with commercial fuels.

It is recommended that particular focus be given to developing an optimized nickel catalyst formulation, and then quickly progressing to testing with commercial fuels.

If it is possible to make significant gains in the resistance of the nickel catalyst to coking, as well as improvements to its thermal stability, then this would represent the overcoming of the largest remaining hurdles to exhaust gas reforming being incorporated as an active technology in vehicles transport. Since as this work has shown, such base metal formulations show sufficient reforming activity to compete with precious metal formulations, at a fraction of the cost, as long as these issues with durability can be overcome.

Appendix 1 – XRD Reference data for the Ceria Zirconia Support

Ceria Zirconia

Name and formula

Reference code:	00-062-0009
Compound name:	Zirconium Cerium Oxide
PDF index name:	Zirconium Cerium Oxide
Empirical formula:	CeO_4Zr
Chemical formula:	$ZrCeO_4$

Crystallographic parameters

Crystal system:	Tetragonal
Space group:	P42/nmc
Space group number:	137
a (Å):	3.7347
b (Å):	3.7347
c (Å):	5.2877
Alpha (°):	90.0000
Beta (°):	90.0000
Gamma (°):	90.0000
Volume of cell (10^6 pm^3):	73.75
Z:	1.00
RIR:	-

Subfiles and quality

Subfiles:	Ceramic
	Inorganic
	Pigment/Dye
Quality:	Indexed (I)

Comments

Creation Date:	9/1/2012
Modification Date:	1/1/1970

Sample Preparation:	Prepared by mixing and heating "Zr O Cl2 ·8 H2 O", "Ce (N O3)3 ·6 H2 O" along with citric acid monohydrate. The redox reaction yields 1000-1800 K of exothermic heat
Temperature of Data Collection:	Pattern taken at 298 K
Warning:	Lower quality mark was set by the editor.

References

Primary reference: Chandini Sam, S., Dept. of Physics, Univ. College, Kerala, India., *Private Communication*, (2011)

Peak list

No.	h	k	l	d [A]	2Theta[deg]	I [%]
1	1	0	1	3.05210	29.237	100.0
2	0	0	2	2.64440	33.871	20.0
3	1	1	2	1.86900	48.679	38.0
4	1	0	3	1.59370	57.808	24.0
5	2	0	2	1.52500	60.678	3.0

Stick Pattern

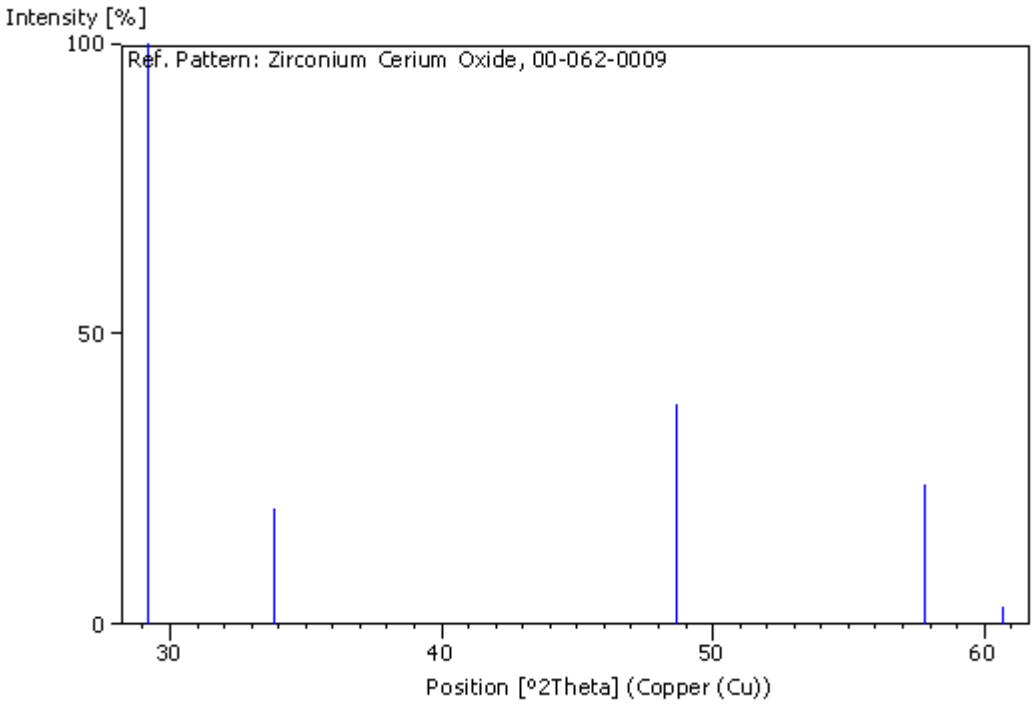

Appendix 2 – XRD Reference Data for the Ni10CZ Catalyst

Nickel Oxide

Name and formula

Reference code:	00-047-1049
Mineral name:	Bunsenite, syn
Compound name:	Nickel Oxide
PDF index name:	Nickel Oxide
Empirical formula:	NiO
Chemical formula:	NiO

Crystallographic parameters

Crystal system:	Cubic
Space group:	Fm-3m
Space group number:	225
a (Å):	4.1771
b (Å):	4.1771
c (Å):	4.1771
Alpha (°):	90.0000
Beta (°):	90.0000
Gamma (°):	90.0000
Calculated density (g/cm^3):	6.81
Volume of cell (10^6 pm^3):	72.88
Z:	4.00
RIR:	6.15

Subfiles and quality

Subfiles:	Alloy, metal or intermetalic
	Common Phase
	Forensic
	Inorganic
	Mineral
Quality:	Star (S)

Comments

Color:	Green
Creation Date:	1/1/1970
Modification Date:	1/1/1970
Additional Patterns:	To replace 00-004-0835
Color:	Green. Average relative standard deviation in intensity of the 5 strongest reflections for 3 specimen mounts = 1.1%. Validated by calculated pattern
Sample Preparation:	Sample annealed for 72 hours at 1100 C
Sample Source or Locality:	Sample obtained from J.T. Baker Chemical Corporation
Source of Unit Cell Data:	Powder Diffraction
CAS Number:	1313-99-1.

References

Primary reference:	Martin, K., McCarthy, G., North Dakota State Univ., Fargo, ND, USA., (1991)
Optical data:	Winchell, Winchell., 58, (1964)

Peak list

No.	h	k	l	d [A]	2Theta[deg]	I [%]
1	1	1	1	2.41200	37.249	61.0
2	2	0	0	2.08900	43.276	100.0
3	2	2	0	1.47680	62.879	35.0
4	3	1	1	1.25940	75.416	13.0
5	2	2	2	1.20580	79.409	8.0
6	4	0	0	1.04430	95.059	4.0
7	3	3	1	0.95830	106.993	3.0
8	4	2	0	0.93400	111.123	7.0

Stick Pattern

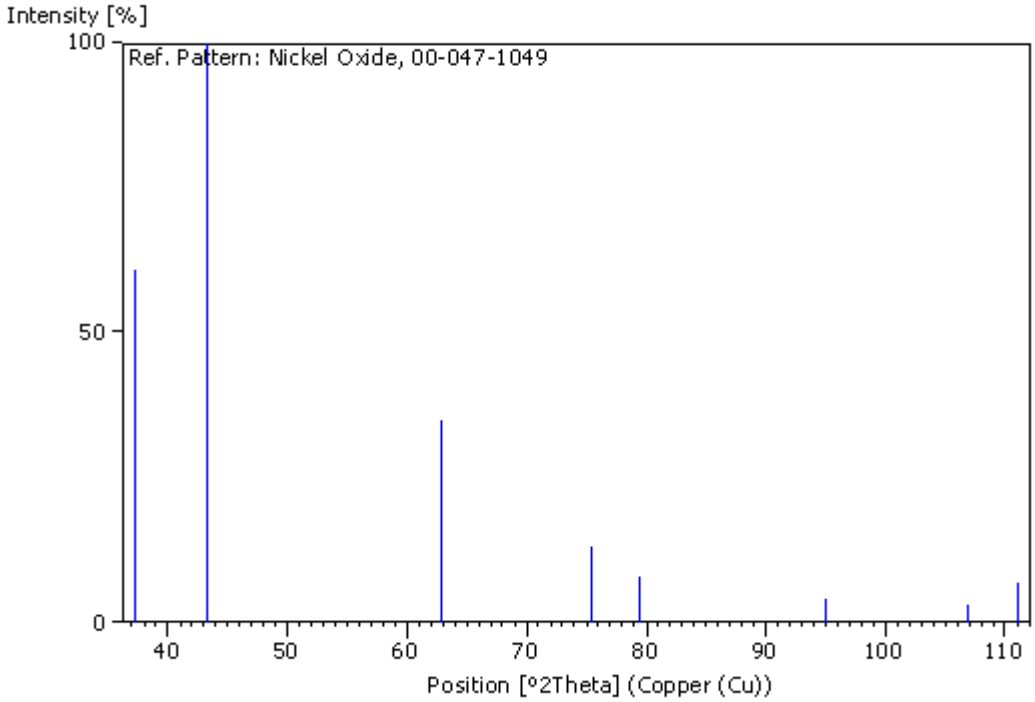

Ceria Zirconia

Name and formula

Reference code:	00-062-0009
Compound name:	Zirconium Cerium Oxide
PDF index name:	Zirconium Cerium Oxide
Empirical formula:	CeO_4Zr
Chemical formula:	$ZrCeO_4$

Crystallographic parameters

Crystal system:	Tetragonal
Space group:	P42/nmc
Space group number:	137
a (Å):	3.7347
b (Å):	3.7347
c (Å):	5.2877
Alpha (°):	90.0000
Beta (°):	90.0000
Gamma (°):	90.0000

Volume of cell (10^6 pm^3):	73.75
Z:	1.00
RIR:	-

Subfiles and quality

Subfiles:	Ceramic
	Inorganic
	Pigment/Dye
Quality:	Indexed (I)

Comments

Creation Date:	9/1/2012
Modification Date:	1/1/1970
Sample Preparation:	Prepared by mixing and heating "Zr O Cl2 ·8 H2 O", "Ce (N O3)3 ·6 H2 O" along with citric acid monohydrate. The redox reaction yields 1000-1800 K of exothermic heat
Temperature of Data Collection:	Pattern taken at 298 K
Warning:	Lower quality mark was set by the editor.

References

Primary reference:	Chandini Sam, S., Dept. of Physics, Univ. College, Kerala, India., *Private Communication*, (2011)

Peak list

No.	h	k	l	d [A]	2Theta[deg]	I [%]
1	1	0	1	3.05210	29.237	100.0
2	0	0	2	2.64440	33.871	20.0
3	1	1	2	1.86900	48.679	38.0
4	1	0	3	1.59370	57.808	24.0
5	2	0	2	1.52500	60.678	3.0

Stick Pattern

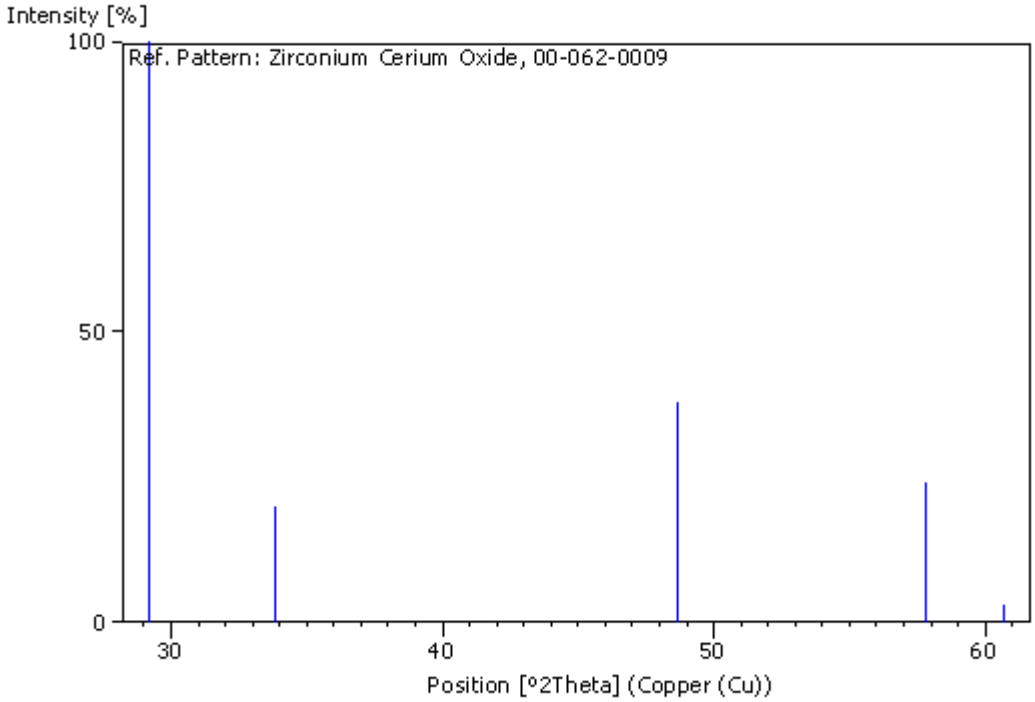
Intensity [%]
100
50
0
Ref. Pattern: Zirconium Cerium Oxide, 00-062-0009
30
40
50
60
Position [°2Theta] (Copper (Cu))

Appendix 3 – XRD Reference Data for the Rh1CZ Catalyst

Rhodium Oxide

Name and formula

Reference code:	00-043-0009
Compound name:	Rhodium Oxide
Common name:	β-Rh2 O3
PDF index name:	Rhodium Oxide
Empirical formula:	O_3Rh_2
Chemical formula:	Rh_2O_3

Crystallographic parameters

Crystal system:	Orthorhombic
Space group:	Pbca
Space group number:	61
a (Å):	5.1472
b (Å):	5.4379
c (Å):	14.6910
Alpha (°):	90.0000
Beta (°):	90.0000
Gamma (°):	90.0000
Calculated density (g/cm^3):	8.20
Volume of cell (10^6 pm^3):	411.20
Z:	8.00
RIR:	4.03

Subfiles and quality

Subfiles:	Alloy, metal or intermetalic
	Inorganic
Quality:	Star (S)

Comments

Color:	Dark gray
Creation Date:	1/1/1970
Modification Date:	1/1/1970
Additional Patterns:	To replace 00-016-0311
Color:	Dark gray. Pattern contains five unidentified weak reflections at d=3.7318, 1.9926, 1.3124, 1.2203 and 1.2014. High temperature form
Sample Preparation:	Sample obtained by annealing "Rh2 O3" (anhydrous, 81.1% Rh, Heraeus) at 1273 L for 1 week in a corundum crucible, subsequently quenched
Temperature of Data Collection:	Pattern taken at 293 K.

References

Primary reference:	Renkenberger, C., Eysel, W., Mineral.-Petrogr. Institut der Universitaet Heidelberg, Germany., (1991)
Structure:	Biesterbos, J., Hornstra, J., **30**, 121, (1973)

Peak list

No.	h	k	l	d [A]	2Theta[deg]	I [%]
1	0	0	4	3.67100	24.225	10.0
2	1	1	1	3.62100	24.565	8.0
3	0	2	0	2.71600	32.952	30.0
4	0	2	1	2.67300	33.498	2.0
5	1	1	4	2.61900	34.210	100.0
6	2	0	0	2.57300	34.841	50.0
7	0	2	3	2.37800	37.801	1.0
8	2	1	1	2.29900	39.152	1.0
9	1	2	2	2.28400	39.420	1.0
10	2	1	2	2.21800	40.644	1.0
11	1	0	6	2.21000	40.798	2.0
12	0	2	4	2.18600	41.266	1.0
13	2	0	4	2.10800	42.867	3.0
14	2	2	0	1.86900	48.679	35.0
15	2	2	1	1.85450	49.085	2.0
16	0	0	8	1.83570	49.621	9.0
17	2	2	3	1.74680	52.333	4.0
18	1	3	1	1.69780	53.963	6.0
19	1	3	2	1.66590	55.083	4.0
20	1	1	8	1.64860	55.711	8.0
21	3	1	1	1.62580	56.562	1.0

22	2	2	5	1.57730	58.467	1.0
23	1	3	4	1.54970	59.612	7.0
24	0	2	8	1.52190	60.815	4.0
25	2	0	8	1.49420	62.065	40.0
26	1	3	5	1.47800	62.823	1.0
27	3	1	5	1.42930	65.222	1.0
28	0	2	9	1.40000	66.763	1.0
29	2	1	9	1.33610	70.414	1.0
30	1	3	7	1.32580	71.043	1.0
31	0	4	3	1.30980	72.045	4.0
32	4	0	0	1.28690	73.535	4.0
33	3	3	1	1.24120	76.721	1.0
34	3	3	2	1.22840	77.669	1.0
35	0	0	12	1.22440	77.971	1.0
36	3	1	8	1.22210	78.146	2.0
37	4	0	4	1.21440	78.737	1.0
38	0	4	6	1.18850	80.801	1.0
39	2	4	2	1.18630	80.982	1.0
40	3	3	4	1.18000	81.506	2.0
41	1	2	11	1.16730	82.584	1.0
42	1	1	12	1.16320	82.940	7.0
43	3	3	5	1.14740	84.342	1.0
44	4	2	3	1.13170	85.790	1.0
45	0	2	12	1.11650	87.248	1.0
46	2	0	12	1.10560	88.330	2.0

Stick Pattern

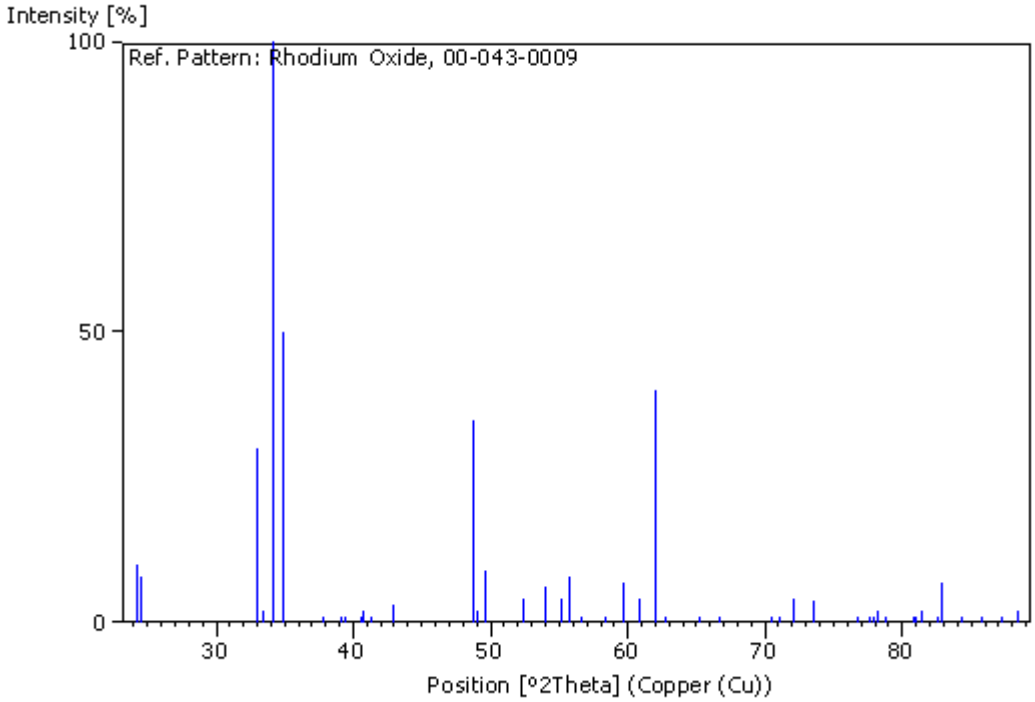

Ceria Zirconia Support

Name and formula

Reference code:	00-062-0009
Compound name:	Zirconium Cerium Oxide
Empirical formula:	CeO_4Zr
Chemical formula:	$ZrCeO_4$

Crystallographic parameters

Crystal system:	Tetragonal
Space group:	P42/nmc
Space group number:	137
a (Å):	3.7347
b (Å):	3.7347
c (Å):	5.2877
Alpha (°):	90.0000
Beta (°):	90.0000
Gamma (°):	90.0000
Volume of cell (10^6 pm^3):	73.75

Z:	1.00
RIR:	-

Subfiles and quality

Subfiles:	Ceramic
	Inorganic
	Pigment/Dye
Quality:	Indexed (I)

Comments

Creation Date:	9/1/2012
Modification Date:	1/1/1970
Sample Preparation:	Prepared by mixing and heating "Zr O Cl2 ·8 H2 O", "Ce (N O3)3 ·6 H2 O" along with citric acid monohydrate. The redox reaction yields 1000-1800 K of exothermic heat
Temperature of Data Collection:	Pattern taken at 298 K
Warning:	Lower quality mark was set by the editor.

References

Primary reference:	Chandini Sam, S., Dept. of Physics, Univ. College, Kerala, India., *Private Communication*, (2011)

Peak list

No.	h	k	l	d [A]	2Theta[deg]	I [%]
1	1	0	1	3.05210	29.237	100.0
2	0	0	2	2.64440	33.871	20.0
3	1	1	2	1.86900	48.679	38.0
4	1	0	3	1.59370	57.808	24.0
5	2	0	2	1.52500	60.678	3.0

Stick Pattern

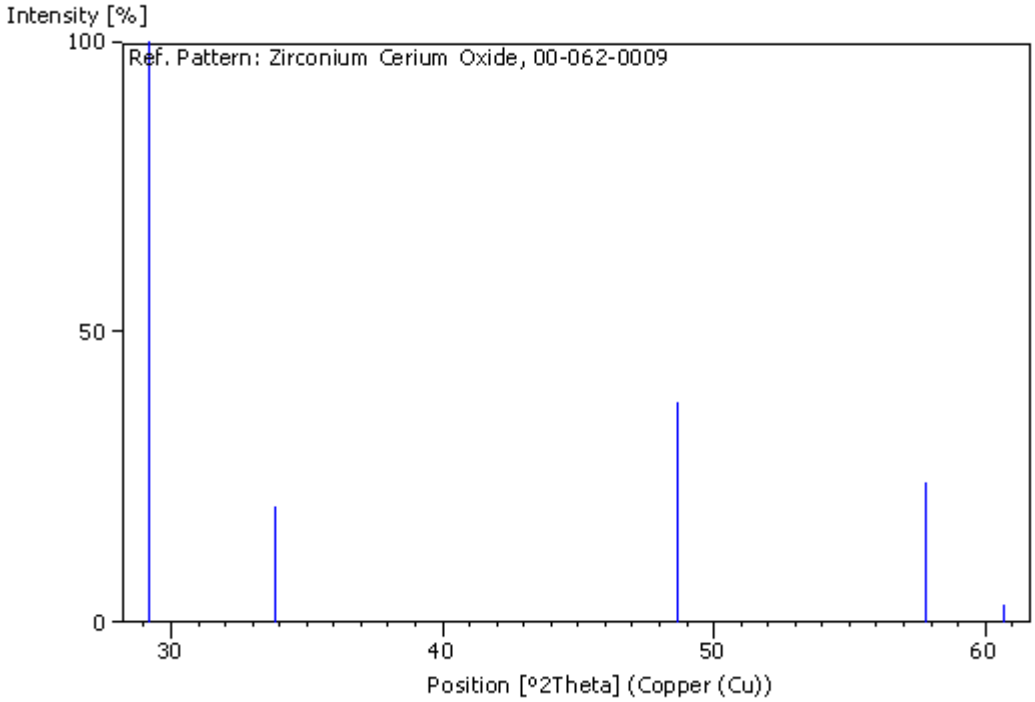
Intensity [%]
100
50
0
Ref. Pattern: Zirconium Cerium Oxide, 00-062-0009
30
40
50
60
Position [°2Theta] (Copper (Cu))

Appendix 4 – XRD Reference Data for nitrogen cooled Ni10CZ

Nickel Metal

Name and formula

Reference code:	01-071-4655
Mineral name:	Nickel
PDF index name:	Nickel
Empirical formula:	Ni
Chemical formula:	Ni

Crystallographic parameters

Crystal system:	Cubic
Space group:	Fm-3m
Space group number:	225
a (Å):	3.5060
b (Å):	3.5060
c (Å):	3.5060
Alpha (°):	90.0000
Beta (°):	90.0000
Gamma (°):	90.0000
Volume of cell (10^6 pm^3):	43.10
Z:	4.00
RIR:	7.41

Status, subfiles and quality

Status:	Alternate Pattern
Subfiles:	Inorganic
	Mineral
	Alloy, metal or intermetalic
	ICSD Pattern
Quality:	Indexed (I)

Comments

ANX:	N.
Wyckoff Sequence:	a (FM3-M).

ICSD collection code: 53809.

References

Primary reference: *Calculated from ICSD using POWD-12++*

Structure: Davey, W.P., *Ann. Phys. (Weinheim, Ger.)*, **79**, 35, (1926)

Peak list

No.	h	k	l	d [A]	2Theta[deg]	I [%]
1	1	1	1	2.02419	44.735	100.0
2	2	0	0	1.75300	52.134	41.9
3	2	2	0	1.23956	76.841	16.2
4	3	1	1	1.05710	93.554	14.3
5	2	2	2	1.01209	99.122	3.9
6	4	0	0	0.87650	123.005	1.7
7	3	3	1	0.80433	146.547	5.4

Stick Pattern

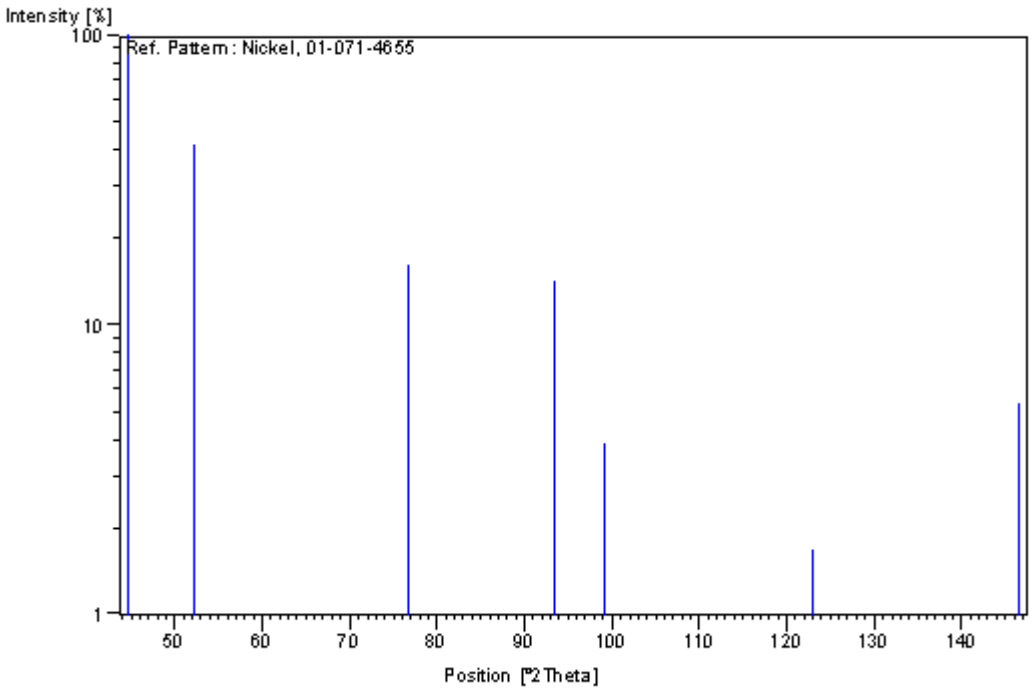

Nickel Oxide

Name and formula

Reference code:	01-089-3080
PDF index name:	Nickel Oxide
Empirical formula:	NiO
Chemical formula:	NiO

Crystallographic parameters

Crystal system:	Rhombohedral
Space group:	R-3m
Space group number:	166
a (Å):	5.9108
b (Å):	5.9108
c (Å):	7.2259
Alpha (°):	90.0000
Beta (°):	90.0000
Gamma (°):	120.0000
Volume of cell (10^6 pm^3):	218.63
Z:	12.00
RIR:	4.74

Subfiles and Quality

Subfiles:	Inorganic
	Corrosion
	ICSD Pattern
Quality:	Indexed (I)

Comments

ANX:	AX.
Wyckoff Sequence:	e d b a (R3-MR).
Analysis:	Ni1 O1. Formula from original source: Ni O.
Additional pattern:	See PDF 01-089-7101.

Temperature: 297 K. Minor Warning: No R value given in the paper. No e.s.d. reported/abstracted on the cell dimension.

ICSD collection code: 43740. Other Cell: 4.177 4.177 4.177 90.07 90.07 90.07.

References

Primary reference: *Calculated from ICSD using POWD-12++*, (2004)

Structure: Slack, G.A., *J. Appl. Phys.*, **31**, 1571, (1960)

Peak list

No.	h	k	l	d [A]	2Theta[deg]	I [%]
1	1	0	1	4.17699	21.254	0.1
2	1	1	0	2.95178	30.254	0.1
3	0	2	1	2.41257	37.240	55.8
4	0	0	3	2.40864	37.303	43.5
5	2	0	2	2.08850	43.287	100.0
6	2	1	1	1.86892	48.682	0.1
7	1	2	2	1.70560	53.697	0.1
8	2	2	0	1.47769	62.837	25.8
9	0	2	4	1.47589	62.923	27.0
10	0	3	3	1.39082	67.263	0.1
11	3	1	2	1.32137	71.317	0.1
12	2	2	3	1.25955	75.406	10.3
13	0	4	2	1.20629	79.370	8.0
14	0	0	6	1.20432	79.526	4.0
15	3	2	1	1.15914	83.295	0.1
16	2	3	2	1.11684	87.215	0.1
17	4	0	4	1.04425	95.065	3.7
18	4	1	3	1.01336	98.954	0.1
19	3	3	0	0.98513	102.875	0.1
20	2	4	1	0.95882	106.908	2.1
21	0	4	5	0.95808	107.028	1.5
22	0	2	7	0.95734	107.148	1.3
23	4	2	2	0.93446	111.040	5.2
24	2	2	6	0.93355	111.204	5.2
25	2	3	5	0.91075	115.512	0.1
26	0	5	4	0.89098	119.663	0.1
27	0	1	8	0.88950	119.992	0.1
28	6	0	0	0.85280	129.180	4.3
29	2	0	8	0.85176	129.476	2.1
30	4	3	1	0.83540	134.463	0.1

31	1	3	7	0.83491	134.623	0.1
32	5	2	0	0.81968	140.023	0.1
33	1	4	6	0.81898	140.291	0.1
34	4	2	5	0.80390	146.753	1.7

Stick Pattern

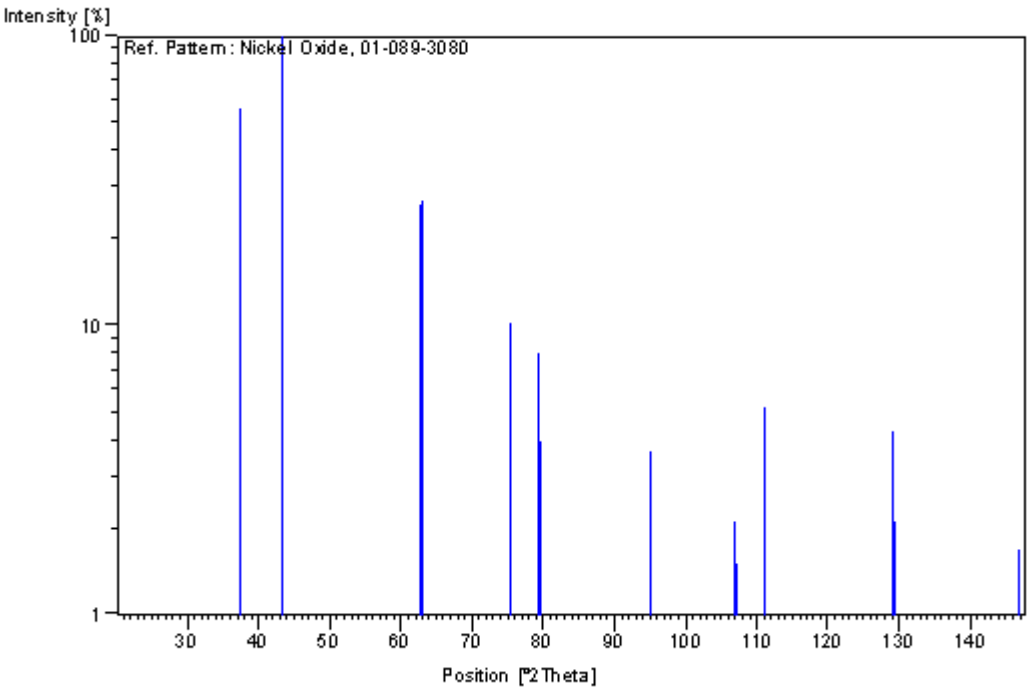

Ceria Zirconia Support

Name and formula

Reference code:	00-038-1436
PDF index name:	Cerium Zirconium Oxide
Empirical formula:	$Ce_{0.5}O_2Zr_{0.5}$
Chemical formula:	$Zr_{0.5}Ce_{0.5}O_2$

Crystallographic parameters

Crystal system:	Tetragonal
Space group:	P42/nmc
Space group number:	137
a (Å):	3.7205

b (Å):	3.7205
c (Å):	5.3039
Alpha (°):	90.0000
Beta (°):	90.0000
Gamma (°):	90.0000
Calculated density (g/cm^3):	6.68
Volume of cell (10^6 pm^3):	73.42
RIR:	-

Status, subfiles and quality

Status:	Marked as deleted by ICDD
Subfiles:	Inorganic
	Corrosion
Quality:	Indexed (I)

Comments

Deleted by:	Deleted by 00-055-0997, more complete, higher FN, LRB 8/04.
General comments:	This phase is metastable, made by "non equilibrium" cooling conditions.

References

Primary reference:	Meriani, S., Spinolo, G., *Powder Diffraction*, **2**, 255, (1987)

Peak list

No.	h	k	l	d [A]	2Theta[deg]	I [%]
1	1	0	1	3.05100	29.248	100.0
2	0	0	2	2.65200	33.771	11.0
3	1	1	0	2.63200	34.035	18.0
4	1	1	2	1.86730	48.727	22.0
5	2	0	0	1.86120	48.897	24.0
6	1	0	3	1.59720	57.669	6.0
7	2	1	1	1.58840	58.019	12.0
8	2	0	2	1.52290	60.770	3.0
9	0	0	4	1.32620	71.018	2.0
10	2	2	0	1.31570	71.672	3.0
11	2	1	3	1.21140	78.970	5.0
12	3	0	1	1.20820	79.220	6.0
13	1	1	4	1.18400	81.172	2.0

14	3	1	0	1.17750	81.715	2.0
15	2	0	4	1.07930	91.074	2.0
16	3	1	2	1.07520	91.520	4.0
17	1	0	5	1.02010	98.072	1.0
18	3	0	3	1.01530	98.698	1.0
19	3	2	1	1.01270	99.041	3.0
20	2	2	4	0.93370	111.176	1.0
21	4	0	0	0.93100	111.663	1.0
22	2	1	5	0.89440	118.914	2.0
23	3	2	3	0.89130	119.593	3.0
24	4	1	1	0.88960	119.970	4.0
25	3	1	4	0.88000	122.171	2.0
26	4	0	2	0.87770	122.717	2.0
27	1	1	6	0.83810	133.591	1.0
28	4	2	0	0.83220	135.524	2.0

Stick Pattern

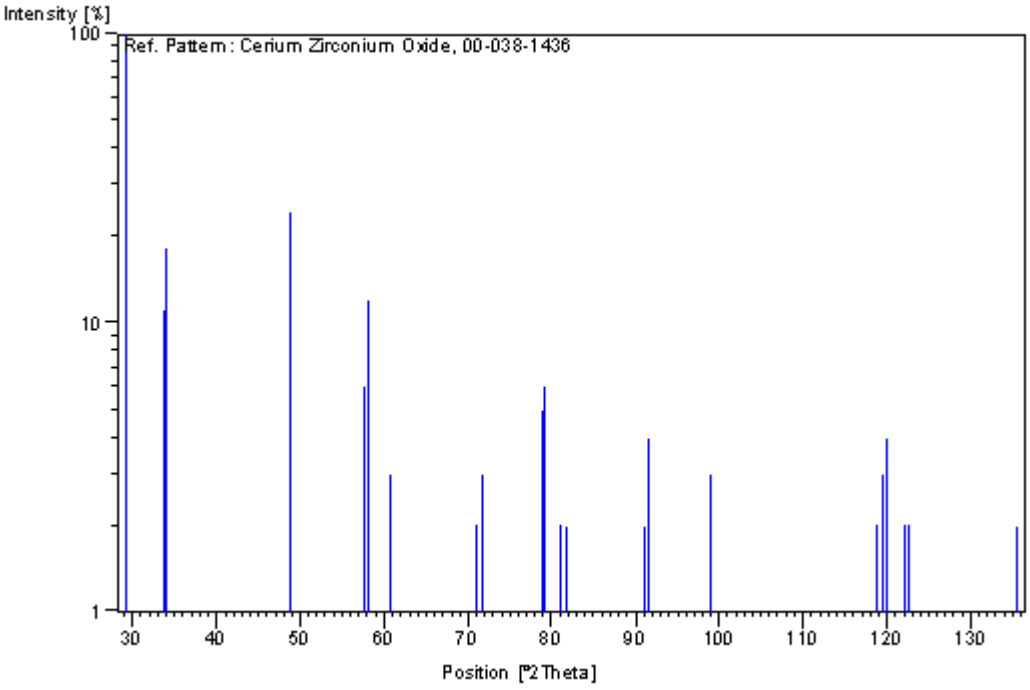

Appendix 5 – Appearance of the Samples Tested in Chapter 4

Fresh 10% Nickel on Ceria Zirconia

Used 10% Nickel on Ceria Zirconia Cooled in a Nitrogen Atmosphere

Used 10% Nickel on Ceria Zirconia Cooled in a “Air” Atmosphere

Used 10% Nickel on Ceria Zirconia Cooled in a Oxygen Atmosphere

Used 10% Nickel on Ceria Zirconia Cooled initially in an oxygen atmosphere, followed by a nitrogen atmosphere (the “reversed” sample)

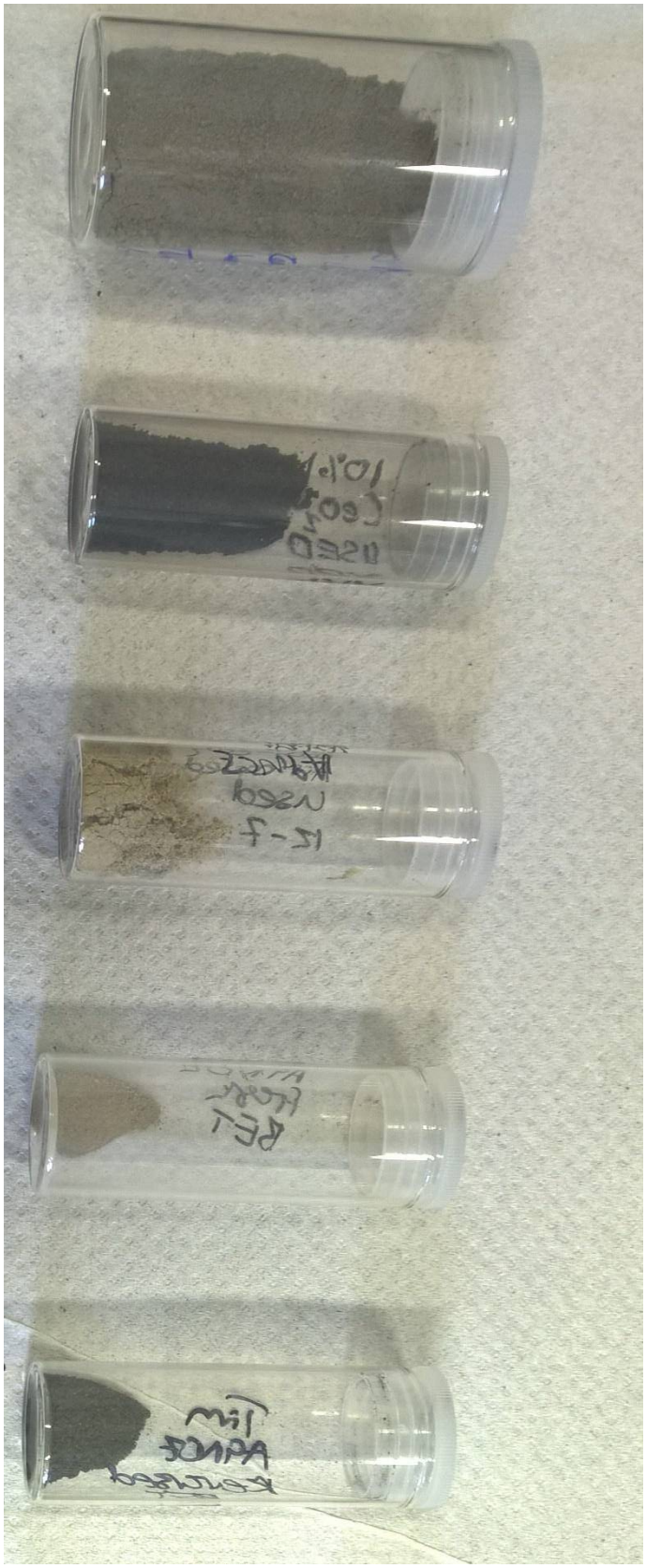

References

1. IPCC, in *Climate Change 2014: Synthesis Report. Contribution of Working Groups I, II and III to the Fifth Assessment Report of the Intergovernmental Panel on Climate Change*, eds. R. K. Pachauri and L. A. Meyer, IPCC, Geneva, Switzerland, 2014.
2. UNFCC, United Nations Framework Convention on Climate Change, The Paris Agreement, http://unfccc.int/paris_agreement/items/9485.php, (accessed 13th October, 2017).
3. N. Stern, *Why Are We Waiting?: The Logic, Urgency, and Promise of Tackling Climate Change*, MIT Press, 2015.
4. IPCC, *Summary for Policymakers, In: Climate Change 2014: Mitigation of Climate Change. Contribution of Working Group III to the Fifth Assessment Report of the Intergovernmental Panel on Climate Change*, Cambridge University Press, Cambridge, United Kingdom and New York, NY, USA., 2014.
5. IPCC, in *Climate Change 2014: Mitigation of Climate Change. Contribution of Working Group III to the Fifth Assessment Report on the Intergovernmental Panel on Climate Change*, eds. R. S. Sims R., F. Creutzig, X. Cruz-Núñez, M. D'Agosto, D. Dimitriu, M. J. Figueroa Meza, L. Fulton, S. Kobayashi, O. and A. M. Lah, P. Newman, M. Ouyang, J. J. Schauer, D. Sperling, and G. Tiwari, Cambridge University Press, Cambridge, United Kingdom and New York, NY, USA., 2014.
6. USEPA, Light-Duty Vehicle CO2 and Fuel Economy Trends, https://www.epa.gov/fuel-economy-trends/trends-report, (accessed 13th October, 2017).
7. USEPA, History of Reducing Air Pollution from Transportation in the United States, https://www.epa.gov/air-pollution-transportation/accomplishments-and-success-air-pollution-transportation#road, (accessed 13th October, 2017).
8. EU, European Comission, Reducing CO2 Emissions From Passenger Cars, https://ec.europa.eu/clima/policies/transport/vehicles/cars_en, (accessed 13th October, 2017).
9. *Journal*, 12th August, 2017.
10. *Journal*, 18th February, 2017.
11. National Geographic, Biofuels, http://www.nationalgeographic.com/environment/global-warming/biofuel/, (accessed 13th October, 2017).
12. D. A. J. Rand, R. Dell and R. S. o. Chemistry, *Hydrogen Energy: Challenges and Prospects*, Royal Society of Chemistry, 2008.
13. R. J. Press, K. S. V. Santhanam, M. J. Miri, A. V. Bailey and G. A. Takacs, *Introduction to Hydrogen Technology*, Wiley, 2008.
14. Q. Ming, T. Healey, L. Allen and P. Irving, *Catalysis Today*, 2002, **77**, 51-64.
15. D. R. Crow, Taylor & Francis, 1994, ch. 11, pp. 248-249.
16. H. L. MacLean and L. B. Lave, *Progress in energy and combustion science*, 2003, **29**, 1-69.
17. H. L. MacLean, L. B. Lave, R. Lankey and S. Joshi, *Journal of the air & waste management association*, 2000, **50**, 1769-1779.
18. Y. Jamal and M. Wyszynski, *International Journal of Hydrogen Energy*, 1994, **19**, 557-572.
19. O. Deutschmann, H. Knözinger, K. Kochloefl and T. Turek, in *Ullmann's Encyclopedia of Industrial Chemistry*, Wiley-VCH Verlag GmbH & Co. KGaA, 2000, DOI: 10.1002/14356007.a05_313.pub2.
20. U. Gov, Hydrogen Production: Natural Gas Reforming, https://energy.gov/eere/fuelcells/hydrogen-production-natural-gas-reforming, (accessed 7th October, 2017).
21. T. Ralph and M. Hogarth, *Platinum Metals Review*, 2002, **46**, 117-135.

22. F. Zhou, S. J. Andreasen, S. K. Kær and J. O. Park, *International Journal of Hydrogen Energy*, 2015, **40**, 14932-14941.

23. M. S. Newkirk and J. L. Abel, 1972.

24. in *Catalysis: Volume 19*, eds. J. J. Spivey and K. M. Dooley, The Royal Society of Chemistry, 2006, vol. 19, pp. 184-254.

25. P. K. Cheekatamarla and C. M. Finnerty, *Journal of Power Sources*, 2006, **160**, 490-499.

26. S. Ahmed and M. Krumpelt, *International Journal of Hydrogen Energy*, 2001, **26**, 291-301.

27. J. Jenkins and E. Shutt, *Platinum Metals Review*, 1989, **33**, 118-127.

28. S. Golunski, *Energy & Environmental Science*, 2010, **3**, 1918-1923.

29. P. Leung, A. Tsolakis, J. Rodriguez-Fernandez and S. Golunski, *Energy & Environmental Science*, 2010, **3**, 780-788.

30. D. Fennell, J. Herreros and A. Tsolakis, *International Journal of Hydrogen Energy*, 2014, **39**, 5153-5162.

31. S. R. Gomes, N. Bion, G. Blanchard, S. Rousseau, V. Bellière-Baca, V. Harlé, D. Duprez and F. Epron, *Applied Catalysis B: Environmental*, 2011, **102**, 44-53.

32. S. O. Akansu, Z. Dulger, N. Kahraman and T. N. Veziroğlu, *International Journal of Hydrogen Energy*, 2004, **29**, 1527-1539.

33. T. I. Energy, in *The Institute of Energy's Second International Conference on COMBUSTION & EMISSIONS CONTROL: Proceedings of The Institute of Energy Conference Held in London, UK, on 4-5 December 1995*, eds. M. L. Wyszynski and T. Wagner, Elsevier Science, 2013, ch. Concept of On-board Fuel Reforming, pp. 375-384.

34. J. Jadhao and D. Thombare, *International Journal of Engineering and Innovative Technology (IJEIT)*, 2013, **2**.

35. P. Leung, A. Tsolakis, J. M. Herreros, M. L. Wyszynski and S. E. Golunski, *Johnson Matthey Technology Review*, 2018, **62**, 407-416.

36. I. Sen and A. K. Avci, *International Journal of Hydrogen Energy*, 2014, **39**, 844-852.

37. B. O. Lindstrom, *Journal*, 1975.

38. Y. Jamal, T. Wagner and M. L. Wyszynski, *International Journal of Hydrogen Energy*, 1996, **21**, 507-519.

39. M. R. Jones, J. W. Dunn and M. L. Wyszynski, presented in part at the IMechE International Conference: Automotive Power Systems - Environment and Conservation, Paper No. C394/014, Chester, U.K, 1&2 September, 1990.

40. M. R. Jones and M. L. Wyszynski, 1993.

41. A. Tsolakis, A. Megaritis and M. L. Wyszynski, *Energy & Fuels*, 2003, **17**, 1464-1473.

42. A. Tsolakis and A. Megaritis, *International Journal of Hydrogen Energy*, 2004, **29**, 1409-1419.

43. S. Peucheret, M. Feaviour and S. Golunski, *Applied Catalysis B: Environmental*, 2006, **65**, 201-206.

44. E. Ambroise, C. Courson, A. Kiennemann, A.-C. Roger, O. Pajot, E. Samson and G. Blanchard, *Topics in Catalysis*, 2009, **52**, 2101-2107.

45. J. D. Holladay, J. Hu, D. L. King and Y. Wang, *Catalysis Today*, 2009, **139**, 244-260.

46. R. K. Kaila and A. O. I. Krause, *International Journal of Hydrogen Energy*, 2006, **31**, 1934-1941.

47. S. Rabe, F. Vogel, T.-B. Truong, T. Shimazu, T. Wakasugi, H. Aoki and H. Sobukawa, *International Journal of Hydrogen Energy*, 2009, **34**, 8023-8033.

48. S. R. Gomes, N. Bion, G. Blanchard, S. Rousseau, D. Duprez and F. Epron, *RSC Advances*, 2011, **1**, 109-116.

49. A. Tsolakis and S. E. Golunski, *Chemical Engineering Journal*, 2006, **117**, 131-136.

50. A. V. González, X. Karatzas and L. J. Pettersson, *Fuel*, 2013, **107**, 162-169.

51. A. V. González and L. J. Pettersson, *Catalysis Today*, 2013, **210**, 19-25.

52. T. Korakianitis, A. Namasivayam and R. Crookes, *Progress in Energy and Combustion Science*, 2011, **37**, 89-112.

53. T. J. Meurig, in *Handbook Of Heterogeneous Catalysis*, ed. H. K. G. Ertl, F. Schüth, and J. Weitkamp, Wiley-VCH Verlag GmbH & Co. KGaA, Weinheim, 2nd edn., 2009, vol. 5, ch. 11, pp. 2274-2343.

54. Y. Chang, J. P. Szybist, J. A. Pihl and D. W. Brookshear, *Energy & Fuels*, 2018, **32**, 2245-2256.

55. Y. Chang, J. P. Szybist, J. A. Pihl and D. W. Brookshear, *Energy & Fuels*, 2018, **32**, 2257-2266.

56. J. Kašpar, P. Fornasiero and N. Hickey, *Catalysis Today*, 2003, **77**, 419-449.

57. W. Amatayakul and O. Ramnäs, *Journal of Cleaner Production*, 2001, **9**, 395-403.

58. D. J. Moon, *Catalysis surveys from Asia*, 2011, **15**, 25-36.

59. J. R. Rostrup-Nielsen, in *Catalysis: Science and Technology*, eds. J. R. Anderson and M. Boudart, Springer Berlin Heidelberg, Berlin, Heidelberg, 1984, DOI: 10.1007/978-3-642-93247-2_1, pp. 1-117.

60. J. Xuan, M. K. H. Leung, D. Y. C. Leung and M. Ni, *Renewable and Sustainable Energy Reviews*, 2009, **13**, 1301-1313.

61. I. Kang, J. Bae and G. Bae, *Journal of Power Sources*, 2006, **163**, 538-546.

62. M. Ni, D. Y. C. Leung and M. K. H. Leung, *International Journal of Hydrogen Energy*, 2007, **32**, 3238-3247.

63. I. Mine, Rhodium Prices and Rhodium Price Charts, http://www.infomine.com/investment/metal-prices/rhodium/, (accessed 3rd November, 2018).

64. I. Mine, Nickel Prices and Nickel Price Charts, http://www.infomine.com/investment/metal-prices/nickel/, (accessed 3rd November, 2018).

65. J. A. Moulijn, A. E. van Diepen and F. Kapteijn, *Applied Catalysis A: General*, 2001, **212**, 3-16.

66. F. Pinna, *Catalysis Today*, 1998, **41**, 129-137.

67. M. Campanati, G. Fornasari and A. Vaccari, *Catalysis Today*, 2003, **77**, 299-314.

68. C. Perego and P. Villa, *Catalysis Today*, 1997, **34**, 281-305.

69. M. D. Argyle and C. H. Bartholomew, *Catalysts*, 2015, **5**, 145-269.

70. Praharso, A. A. Adesina, D. L. Trimm and N. W. Cant, *Chemical Engineering Journal*, 2004, **99**, 131-136.

71. G. Rothenberg, in *Catalysis*, Wiley-VCH Verlag GmbH & Co. KGaA, 2008, DOI: 10.1002/9783527621866.ch4, ch. 4, p. 130.

72. K. Hou and R. Hughes, *Chemical Engineering Journal*, 2001, **82**, 311-328.

73. W. Xu, Z. Liu, A. C. Johnston-Peck, S. D. Senanayake, G. Zhou, D. Stacchiola, E. A. Stach and J. A. Rodriguez, *ACS Catalysis*, 2013, **3**, 975-984.

74. J. Zhang, Z. Zhong, X. M. Cao, P. Hu, M. B. Sullivan and L. Chen, *ACS Catalysis*, 2013, **4**, 448-456.

75. C. H. Bartholomew, *Catalysis Reviews*, 1982, **24**, 67-112.

76. D. L. Trimm, *Catalysis Today*, 1997, **37**, 233-238.

77. R. D. Parmar, A. Kundu and K. Karan, *Journal of Power Sources*, 2009, **194**, 1007-1020.

78. R. K. Kaila, A. Gutiérrez and A. O. I. Krause, *Applied Catalysis B: Environmental*, 2008, **84**, 324-331.

79. P. K. Cheekatamarla and A. M. Lane, *Journal of Power Sources*, 2006, **154**, 223-231.

80. E. Ambroise, C. Courson, A.-C. Roger, A. Kiennemann, G. Blanchard, S. Rousseau, X. Carrier, E. Marceau, C. La Fontaine and F. Villain, *Catalysis Today*, 2010, **154**, 133-141.

81. F. Frusteri, S. Freni, L. Spadaro, V. Chiodo, G. Bonura, S. Donato and S. Cavallaro, *Catalysis Communications*, 2004, **5**, 611-615.

82. M. C. Sánchez-Sánchez, R. M. Navarro and J. L. G. Fierro, *International Journal of Hydrogen Energy*, 2007, **32**, 1462-1471.

83. I. E. Achouri, N. Abatzoglou, C. Fauteux-Lefebvre and N. Braidy, *Catalysis Today*, 2013, **207**, 13-20.

84. M. Nilsson, X. Karatzas, B. Lindström and L. J. Pettersson, *Chemical Engineering Journal*, 2008, **142**, 309-317.

85. A. Qi, S. Wang, C. Ni and D. Wu, *International journal of hydrogen energy*, 2007, **32**, 981-991.

86. P. K. Cheekatamarla and A. M. Lane, *Journal of Power Sources*, 2005, **152**, 256-263.

87. J. Boon, E. van Dijk, S. de Munck and R. van den Brink, *Journal of Power Sources*, 2011, **196**, 5928-5935.

88. G. Hill, ed. J. S. Holman, Cheltenham : Nelson Thornes, Cheltenham, 6th ed. edn., 2011, ch. 14, pp. 247-250.

89. G. Veser, M. Ziauddin and L. D. Schmidt, *Catalysis Today*, 1999, **47**, 219-228.

90. C. Palm, P. Cremer, R. Peters and D. Stolten, *Journal of Power Sources*, 2002, **106**, 231-237.

91. A. Avcı, Z. İ. Önsan and D. Trimm, *Topics in Catalysis*, 2003, **22**, 359-367.

92. K. W. Kolasinski, *Surface Science; Foundations of Catalysis and Nanoscience*, Wiley, Chichester, 2nd edn., 2008.

93. F. Rouquerol, J. Rouquerol and K. Sing, in *Adsorption by Powders and Porous Solids*, eds. F. Rouquerol, J. Rouquerol and K. Sing, Academic Press, London, 1999, DOI: https://doi.org/10.1016/B978-012598920-6/50002-6, pp. 1-26.

94. F. Rouquerol, J. Rouquerol and K. Sing, in *Adsorption by Powders and Porous Solids*, eds. F. Rouquerol, J. Rouquerol and K. Sing, Academic Press, London, 1999, DOI: https://doi.org/10.1016/B978-012598920-6/50007-5, pp. 165-189.

95. B. Cornils, W. A. Harrmann, R. Schlogl and C. H. Wong, *Catalysis: From A to Z*, Wiley-VCH, Wienheim, 2nd edn., 2003.

96. H. Knözinger, in *Handbook of Heterogeneous Catalysis*, Wiley-VCH Verlag GmbH & Co. KGaA, 2008, DOI: 10.1002/9783527610044.hetcat0056.

97. R. C. D. J. Mendham, J. D. Barnes and M. Thomas, *Vogel's Textbook of Quantitative Chemical Analysis*, Prentice Hall, New Jersey, 6th edn., 2000.

98. J. W. Robinson, eds. E. M. S. Frame and G. M. Frame, New York : Marcel Dekker, New York, 6th ed. edn., 2005, ch. 8, pp. 546-558.

99. in *Analytical chemistry: a modern approach to analytical science*, eds. J. M. Mermet, M. Otto, R. Kellner, M. V. Cases and H. M. Widmer, Wiley-VCH, 2nd edn., 2004, ch. 28, pp. 952-964.

100. J. A. Anderson, M. Fernández-García and A. Martínez-Arias, in *Supported Metals in Catalysis*, DOI: 10.1142/9781848166783_0002, pp. 41-79.

101. J. Grebenkemper, Powder X-ray Diffraction, https://chem.libretexts.org/Core/Analytical_Chemistry/Instrumental_Analysis/Diffraction_Scattering_Techniques/Powder_X-ray_Diffraction, (accessed 18th October, 2017).

102. Sono-Tek, How Ultrasonic Nozzles Work, http://www.sono-tek.com/how-ultrasonic-nozzles-work/, (accessed 23rd October, 2017).

103. ChemSpider, 2,2,4-Trimethylpentane, http://www.chemspider.com/Chemical-Structure.10445.html?rid=5448844a-1566-47e3-abbe-f10bedb92051, (accessed 23rd October, 2017).

104. ChemSpider, Propane, http://www.chemspider.com/Chemical-Structure.6094.html?rid=66b98c1c-4104-4802-9357-e6917963af07, (accessed 24th October, 2017).

105. G. Hill and J. Holman, *Chemistry in Context*, Nelson Thornes Limited, 2000.

106. ChemSpider, Water, http://www.chemspider.com/Chemical-Structure.937.html?rid=74aa616b-033b-40a6-815d-10317ec71ac0, (accessed 23rd October, 2017).

107. D. Phoenix, in *Introductory Mathematics for the Life Sciences*, CRC Press, 2002, ch. 11, pp. 179-203.

108. J. A. Moulijn, A. E. van Diepen and F. Kapteijn, in *Handbook of Heterogeneous Catalysis*, Wiley-VCH Verlag GmbH & Co. KGaA, 2008, DOI: 10.1002/9783527610044.hetcat0098, pp. 1829-1845.

109. V. Palma, F. Castaldo, P. Ciambelli, G. Iaquaniello and G. Capitani, *International Journal of Hydrogen Energy*, 2013, **38**, 6633-6645.

110. M. Patel, T. K. Jindal and K. K. Pant, *Industrial & Engineering Chemistry Research*, 2013, **52**, 15763-15771.

111. H. Yao and Y. F. Yao, *Journal of Catalysis*, 1984, **86**, 254-265.

112. I. I. Soykal, H. Sohn, D. Singh, J. T. Miller and U. S. Ozkan, *ACS Catalysis*, 2014, **4**, 585-592.

113. T. Masui, T. Ozaki, K.-i. Machida and G.-y. Adachi, *Journal of Alloys and Compounds*, 2000, **303–304**, 49-55.

114. E. Rocchini, M. Vicario, J. Llorca, C. de Leitenburg, G. Dolcetti and A. Trovarelli, *Journal of Catalysis*, 2002, **211**, 407-421.

115. C. Diagne, H. Idriss and A. Kiennemann, *Catalysis Communications*, 2002, **3**, 565-571.

116. F. Frusteri, S. Freni, V. Chiodo, S. Donato, G. Bonura and S. Cavallaro, *International Journal of Hydrogen Energy*, 2006, **31**, 2193-2199.

117. H.-W. Kim, K.-M. Kang, H.-Y. Kwak and J. H. Kim, *Chemical Engineering Journal*, 2011, **168**, 775-783.

118. R. K. Singha, A. Shukla, A. Yadav, L. N. Sivakumar Konathala and R. Bal, *Applied Catalysis B: Environmental*, 2017, **202**, 473-488.

119. R. K. Singha, S. Ghosh, S. S. Acharyya, A. Yadav, A. Shukla, T. Sasaki, A. M. Venezia, C. Pendem and R. Bal, *Catalysis Science & Technology*, 2016, **6**, 4601-4615.

120. B. Cornils, W. A. Herrmann, C. H. Wong and H. W. Zanthoff, *Catalysis from A to Z: a Concise Encyclopedia*, Wiley-VCH Verlag GmbH, 2003.

121. J. H. Jeong, J. W. Lee, D. J. Seo, Y. Seo, W. L. Yoon, D. K. Lee and D. H. Kim, *Applied Catalysis A: General*, 2006, **302**, 151-156.

122. J.-H. Kim, D. J. Suh, T.-J. Park and K.-L. Kim, *Applied Catalysis A: General*, 2000, **197**, 191-200.

123. Q. Shi, C. Liu and W. Chen, *Journal of Rare Earths*, 2009, **27**, 948-954.

124. X. Zhai, S. Ding, Z. Liu, Y. Jin and Y. Cheng, *International Journal of Hydrogen Energy*, 2011, **36**, 482-489.

125. D. Li, I. Atake, T. Shishido, Y. Oumi, T. Sano and K. Takehira, *Journal of Catalysis*, 2007, **250**, 299-312.

126. D. Li, K. Nishida, Y. Zhan, T. Shishido, Y. Oumi, T. Sano and K. Takehira, *Applied Catalysis A: General*, 2008, **350**, 225-236.

127. P. Guo, L. Chen, Q. Yang, M. Qiao, H. Li, H. Li, H. Xu and K. Fan, *International Journal of Hydrogen Energy*, 2009, **34**, 2361-2368.

128. P.-J. Guo, L.-F. Chen, G.-B. Yu, Y. Zhu, M.-H. Qiao, H.-L. Xu and K.-N. Fan, *Catalysis Communications*, 2009, **10**, 1252-1256.

129. O. Yamazaki, K. Tomishige and K. Fujimoto, *Applied Catalysis A: General*, 1996, **136**, 49-56.

130. D. L. Trimm and Z. I. Önsan, *Catalysis Reviews*, 2001, **43**, 31-84.

131. S. Li and J. Gong, *Chemical Society Reviews*, 2014, **43**, 7245-7256.

132. B. Whittington, C. Jiang and D. Trimm, *Catalysis today*, 1995, **26**, 41-45.

133. R. Seiser and K. Seshadri, *Proceedings of the Combustion Institute*, 2005, **30**, 407-414.

134. D. L. Trimm, *Catalysis Today*, 1999, **49**, 3-10.

135. G. Ertl, H. Knözinger and J. Weitkamp, Wiley-VCH, 2008, vol. 3, ch. 5, pp. 1624-1636.

136. G. Zeng, Y. Tian and Y. Li, *International Journal of Hydrogen Energy*, 2010, **35**, 6726-6737.

137. J. Abbot and P. R. Dunstan, *Industrial & Engineering Chemistry Research*, 1997, **36**, 76-82.

138. J. Abbot and B. W. Wojciechowski, *Journal of Catalysis*, 1988, **113**, 353-366.

139. H. E. Curry-Hyde and R. Howe, *Natural Gas Conversion II*, Elsevier, 1994.

140. J. Rostrup-Nielsen and D. L. Trimm, *Journal of Catalysis*, 1977, **48**, 155-165.

141. A. Arnberger, S. Golini, D. Mumford and G. Hasenbichler, in *Internationaler Motorenkongress 2018*, Springer, 2018, pp. 315-338.

142. A. Ozbilen, I. Dincer and M. Hosseini, in *Exergetic, Energetic and Environmental Dimensions*, Elsevier, 2018, pp. 913-934.

143. D. Chatterjee, O. Deutschmann and J. Warnatz, *Faraday Discussions*, 2002, **119**, 371-384.

144. J. Barbier Jr and D. Duprez, *Applied Catalysis B: Environmental*, 1993, **3**, 61-83.

145. M. Krumpelt, T. R. Krause, J. D. Carter, J. P. Kopasz and S. Ahmed, *Catalysis Today*, 2002, **77**, 3-16.

146. C. B. Faust, *Modern chemical techniques*, London : Royal Society of Chemistry, London], 1992.

147. A. L. Alberton, M. M. V. M. Souza and M. Schmal, *Catalysis Today*, 2007, **123**, 257-264.

148. J. Zhang, T. Zhang, X. Zhang, W. Liu, H. Liu, J. Qiu and K. L. Yeung, *Catalysis Today*, 2014, **236, Part A**, 34-40.

149. S. J. Han, Y. Bang, J. Yoo, J. G. Seo and I. K. Song, *International Journal of Hydrogen Energy*, 2013, **38**, 8285-8292.

150. Q. Liu, Z. Liu, X. Zhou, C. Li and J. Ding, *Journal of Rare Earths*, 2011, **29**, 872-877.

151. L. P. R. Profeti, E. A. Ticianelli and E. M. Assaf, *International Journal of Hydrogen Energy*, 2009, **34**, 5049-5060.

152. S. C. Dantas, J. C. Escritori, R. R. Soares and C. E. Hori, *Chemical Engineering Journal*, 2010, **156**, 380-387.